Étude de l'activité électrocatalytique des biofilms microbiens en fonction des forces d'adhésion pour l'optimisation des performances des biopiles microbiennes

Alexiane Godain

N°d'ordre NNT : xxx

THESE de DOCTORAT DE L'UNIVERSITE DE LYON

opérée au sein de
l'Université Claude Bernard Lyon 1

Ecole Doctorale N° 160
(Électronique, Électrotechnique et Automatique)

Spécialité de doctorat : Bioingénierie

Soutenue publiquement le 06/04/2018, par :
Alexiane Godain

Etude de l'activité électrocatalytique des biofilms microbiens en fonction des forces d'adhésion pour l'optimisation des performances des biopiles microbiennes.

Devant le jury composé de :

Achouak, Wafa, Directrice de Recherche CNRS, CEA Cadarache	Rapporteure
Head, Ian, Professeur, Newcastle university	Rapporteur
Basséguy, Régine, Directrice de Recherche CNRS, Université de Toulouse III	Examinatrice
Simonet, Pascal, Directeur de Recherche CNRS, Ecole centrale de Lyon	Examinateur
Vogel, Timothy M., Professeur des Universités Université Lyon1	Directeur de thèse
Haddour, Naoufel, Maître de conférences, Ecole Centrale de Lyon	Invité
Fongarland, Pascal, Professeur des Universités, Université Lyon 1	Invité

UNIVERSITE CLAUDE BERNARD - LYON 1

Président de l'Université	**M. le Professeur Frédéric FLEURY**
Président du Conseil Académique	M. le Professeur Hamda BEN HADID
Vice-président du Conseil d'Administration	M. le Professeur Didier REVEL
Vice-président du Conseil Formation et Vie Universitaire	M. le Professeur Philippe CHEVALIER
Vice-président de la Commission Recherche	M. Fabrice VALLÉE
Directrice Générale des Services	Mme Dominique MARCHAND

COMPOSANTES SANTE

Faculté de Médecine Lyon Est – Claude Bernard	Directeur : M. le Professeur G.RODE
Faculté de Médecine et de Maïeutique Lyon Sud – Charles Mérieux	Directeur : Mme la Professeure C. BURILLON
Faculté d'Odontologie	Directeur : M. le Professeur D. BOURGEOIS
Institut des Sciences Pharmaceutiques et Biologiques	Directeur : Mme la Professeure C. VINCIGUERRA
Institut des Sciences et Techniques de la Réadaptation	Directeur : M. X. PERROT
Département de formation et Centre de Recherche en Biologie Humaine	Directeur : Mme la Professeure A-M. SCHOTT

COMPOSANTES ET DEPARTEMENTS DE SCIENCES ET TECHNOLOGIE

Faculté des Sciences et Technologies	Directeur : M. F. DE MARCHI
Département Biologie	Directeur : M. le Professeur F. THEVENARD
Département Chimie Biochimie	Directeur : Mme C. FELIX
Département GEP	Directeur : M. Hassan HAMMOURI
Département Informatique	Directeur : M. le Professeur S. AKKOUCHE
Département Mathématiques	Directeur : M. le Professeur G. TOMANOV
Département Mécanique	Directeur : M. le Professeur H. BEN HADID
Département Physique	Directeur : M. le Professeur J-C PLENET
UFR Sciences et Techniques des Activités Physiques et Sportives	Directeur : M. Y.VANPOULLE
Observatoire des Sciences de l'Univers de Lyon	Directeur : M. B. GUIDERDONI
Polytech Lyon	Directeur : M. le Professeur E.PERRIN
Ecole Supérieure de Chimie Physique Electronique	Directeur : M. G. PIGNAULT
Institut Universitaire de Technologie de Lyon 1	Directeur : M. le Professeur C. VITON
Ecole Supérieure du Professorat et de l'Education	Directeur : M. le Professeur A. MOUGNIOTTE
Institut de Science Financière et d'Assurances	Directeur : M. N. LEBOISNE

Abstract

Microbial fuel cells (MFCs), as a potentially sustainable biotechnology, can directly convert organic matter into electricity by using bacterial biofilms as biocatalysts. In a political context where European legislation favors and imposes the revalorization of organic waste from industries, MFC seems an inexpensive and promising technology to meet this need. The aim of this thesis is to improve knowledge of the formation of electroactive biofilms on the anodic surface, and to understand the mechanisms involved in the competition between electroactive bacteria (EAB) and other bacteria. Special attention will be paid to shear force as a tool to control the formation of anodic biofilms. First, bacterial successions have been studied under stationary conditions and in standard laboratory configurations. The results show that the formation of the biofilm is divided in two stages. At first, non-specific EAB grow in all MFCs, producing or not electricity. Then, specific EAB become predominant only in MFCs producing electricity and is associated to an exponential increase of electricity. From these results, we hypothesize that inhibition of the first step should decrease the competition between nonspecific and specific EAB. We propose to use the shear stress to select specific EAB during the adhesion. First, MFCs with a shear stress flow chamber configuration were designed, constructed and set up. The results show that the proportion of specific EAB such as *Geobacter* was higher, up to 30.14% as opposed to a lower shear stress (less than 1%). Then, the effect of shear stress on microbial selection during biofilm growth was studied. These results confirm the previous conclusions: specific EAB are selected when shear stress is higher. This work demonstrates the major role of shear stress in biofilm formation and could be a way to control the selection of EAB. This factor should be taken into account in the architecture and implementation of the reactors.

Résumé court

Les piles à combustible microbiennes, en tant que biotechnologie potentiellement durable, peuvent assurer la conversion directe de la matière organique en électricité en utilisant des biofilms bactériens comme biocatalyseurs. Dans un context politique où les législations françaises et européennes favorisent et imposent la revalorisation des déchets organiques provenant des industries ou des collectivités territoriales, les biopiles microbiennes semblent un moyen peu couteux et prometteur pour répondre à ce besoin. Cette thèse a pour objectif d'améliorer les connaissances sur la formation des biofilms électroactifs à la surface de l'anode, et de comprendre les mécanismes impliqués dans la compétition entre les bactéries électroactives et les autres communautés bactériennes dans le but d'améliorer la sélection des bactéries électroactives dans le biofilm anodique. Une attention particulière sera portée sur les forces de cisaillement comme un outil de control de la formation des biofilms anodiques. Ces recherches ont pour but à long terme d'améliorer la production d'électricité produite par les biopiles microbiennes, et plus particulièrement d'améliorer les performances du compartiment anodique, en vue d'appliquer cette technologie dans les stations d'épurations pour la réduction du coût énergétique du traitement des eaux usées.

A travers cette thèse, différents points sur la dynamique des communautés bactériennes lors de la formation du biofilm ont été mis en évidence. La formation du biofilm est divisée en deux étapes. Dans un premier temps, les bactéries électroactives (EAB) non spécifiques se développent dans toutes les biopiles, produisant ou non de l'électricité et dans le milieu liquide comme sur l'anode. Les EAB spécifiques deviennent ensuite plus compétitives et prédominantes mais seulement dans les biopiles produisant de l'électricité et seulement dans le biofilm anodique. Cette deuxième étape correspond à une augmentation exponentielle de la production d'électricité. A partir de ces résultats, nous émettons l'hypothèse qu'une inhibition de la première étape devrait diminuer la compétition entre les EAB non spécifiques et spécifiques au cours de la colonisation anodique, et favoriser la croissance des EAB spécifiques dans le biofilm. Nous proposons d'utiliser la contrainte de cisaillement pour sélectionner les EAB spécifiques pendant l'étape d'adhésion en détachant les EAB non spécifiques. Dans un premier temps, pour cette étude, des biopiles avec une configuration de chambre à écoulement de cisaillement ont été conçues, construites et mises en place. Les résultats démontrent que sous une contrainte de cisaillement élevée, l'abondance des EAB spécifiques telle que *Geobacter* était très élevée, jusqu'à 30,14% en opposition à une contrainte de cisaillement faible où l'abondance relative était inférieure à 1%. En outre, la contrainte de cisaillement diminue le pourcentage de couverture de la surface anodique, ce qui montre que la sélection des EAB spécifiques se produit en détachant d'autres bactéries. Ainsi, la contrainte de cisaillement pourrait être utilisée pour sélectionner les EAB spécifiques durant les premières étapes d'adhésion. Enfin, l'effet de la contrainte de cisaillement sur la sélection microbienne au cours de la croissance du biofilm a été étudié. Ces résultats confirment les conclusions précédentes: les EAB spécifiques sont sélectionnées lorsque les contraintes de cisaillement sont plus élevées. Ce travail démontre le rôle majeur des contraintes de cisaillement dans la formation du biofilm L'utilisation de contraintes de cisaillement pourrait être un moyen de contrôler la sélection des EAB et la quantité de matières mortes dans les biofilms anodiques. C'est un facteur qui devrait être pris en compte dans l'architecture et la mise en place des réacteurs.

Résumé long

Les piles à combustible microbiennes, en tant que biotechnologie potentiellement durable, peuvent assurer la conversion directe de la matière organique en électricité en utilisant des biofilms bactériens comme biocatalyseurs. Dans un contexte politique où les législations françaises et européennes favorisent et imposent la revalorisation des déchets organiques provenant des industries ou des collectivités territoriales, les biopiles microbiennes semblent un moyen peu couteux et prometteur pour répondre à ce besoin. En effet, depuis les années 2000, les recherches scientifiques sur ce sujet ont augmenté, et permis des progrès remarquables, augmentant la production d'électricité de seulement 10µW.m^{-2} avant les années 2000 à environ 1W.m^{-2} actuellement.

Les biopiles microbiennes sont classiquement composées d'un compartiment anodique contenant les eaux chargées de matières organiques et de microorganismes.. Un biofilm se développe progressivement sur l'anode (souvent une anode de carbone) et oxyde la matière organique en CO_2. Seuls certains microorganismes spécifiques appelés bactéries électroactives (EAB) sont capables de transférer les électrons issus de cette oxydation à une électrode (l'anode). Ces électrons circulent ensuite dans le circuit externe à travers une résistance jusqu'à la cathode qui est classiquement une électrode de carbone dopée en platine catalysant la réduction du dioxygène en eau.

Cette thèse a pour objectif d'améliorer les connaissances sur la formation des biofilms électroactifs à la surface de l'anode, et de comprendre les mécanismes impliqués dans la compétition entre les bactéries électroactives et les autres communautés bactériennes dans le but d'améliorer la sélection des bactéries électroactives dans le biofilm anodique. Une attention particulière sera portée sur les forces de cisaillement comme un outil de control de la formation des biofilms anodiques. Ces recherches ont pour but à long terme d'améliorer la production d'électricité produite par les biopiles microbiennes, et plus particulièrement d'améliorer les performances du compartiment anodique, en vue d'appliquer cette technologie dans les stations d'épurations pour la réduction du coût énergétique du traitement des eaux usées.

Les bactéries électroactives appartiennent à une grande diversité de taxons et peuvent être séparées en deux groupes. Un premier groupe, qu'on nommera ici EAB spécifiques, présente une adaptation très spécifique aux transferts extracellulaires d'électrons, utilisant un transfert d'électrons direct, vivant dans un environnement anoxique et capable d'utiliser seulement une gamme réduite d'accepteurs d'électrons et de substrats. Le deuxième groupe, qu'on appellera ici EAB non spécifiques, comprend des bactéries avec un métabolisme plus versatile, vivant dans un environnement aérobie ou anoxique, capables d'utiliser une large gamme d'accepteurs d'électrons et de substrats et utilisant des transferts d'électrons extracellulaires indirects.

La densité de courant produite par les biopiles pourrait être fortement améliorée par une augmentation de la densité de bactéries électroactives dans le biofilm anodique. A travers cette thèse, différents points sur la dynamique des communautés bactériennes lors de la formation du biofilm ont été mis en évidence. Premièrement, les successions bactériennes ont été étudiées dans des conditions stationnaires et dans des configurations de laboratoire classiques. Deux résultats principaux ont été

montrés. (i) La formation du biofilm est divisée en deux étapes. Dans un premier temps, les EAB non spécifiques se développent dans toutes les biopiles, produisant ou non de l'électricité et dans le milieu liquide comme sur l'anode. Les EAB spécifiques deviennent ensuite plus compétitives et prédominantes mais seulement dans les biopiles produisant de l'électricité et seulement dans le biofilm anodique. Cette deuxième étape correspond à une augmentation exponentielle de la production d'électricité. Il en résulte que l'abondance relative des EAB spécifiques était positivement corrélée à la densité de puissance maximale, tandis que l'abondance relative des EAB non spécifiques était corrélée négativement à la densité de puissance maximale. (ii) Les résultats ne montrent pas seulement une compétition pour la colonisation de l'anode entre EAB spécifiques et non spécifiques mais également une compétition au sein des EAB spécifiques, en particulier entre *Geobacter* et *Desulfuromonas* lors de la deuxième étape. Mais la domination de l'une ou de l'autre n'a pas entraîné une production d'électricité meilleure ou moindre.

A partir de ces résultats, nous émettons l'hypothèse qu'une inhibition de la première étape devrait diminuer la compétition entre les EAB non spécifiques et spécifiques au cours de la colonisation anodique, et favoriser la croissance des EAB spécifiques dans le biofilm. Nous proposons d'utiliser la contrainte de cisaillement pour sélectionner les EAB spécifiques pendant l'étape d'adhérence en détachant les EAB non spécifiques. De plus, plusieurs études dans la littérature montrent une augmentation de la production d'électricité lorsque le biofilm se développe sous contraintes de cisaillement. Mais la compréhension de ces effets sur les biofilms anodiques reste absente. Dans un premier temps, pour cette étude, des biopiles avec une configuration de chambre à écoulement de cisaillement ont été conçues, construites et mises en place. Les résultats démontrent que sous une contrainte de cisaillement élevée, l'abondance des EAB spécifiques telle que *Geobacter* était très élevée, jusqu'à 30,14% en opposition à une contrainte de cisaillement faible où l'abondance relative était inférieure à 1%. En outre, la contrainte de cisaillement diminue le pourcentage de couverture de la surface anodique, ce qui montre que la sélection des EAB spécifiques se produit en détachant d'autres bactéries. Ainsi, la contrainte de cisaillement pourrait être utilisée pour sélectionner les EAB spécifiques durant les premières étapes d'adhésion.

Enfin, l'effet de la contrainte de cisaillement sur la sélection microbienne au cours de la croissance du biofilm a été étudiée. Ces résultats confirment les conclusions précédentes: les EAB spécifiques sont sélectionnées lorsque les contraintes de cisaillement sont plus élevées. Les biofilms anodiques développés sous 10mPa présentaient une abondance relative plus élevée de EAB spécifiques (35,78 ± 6,70%) dominée par *Geobacteriaceae*, à l'inverse des biofilms anodiques développés sous 1mPa (16,20 ± 3,14%). De plus, la contrainte de cisaillement ralentit la cinétique de développement des biofilms. Mais après 10 jours, aucune différence de pourcentage de recouvrement ou d'épaisseur n'a été observée. Cette étude montre également que la contrainte de cisaillement modifie la proportion de bactéries vivantes et mortes dans le biofilm. Les biofilms développés sous une contrainte de cisaillement de 5 mPa présentaient la plus faible proportion de bactéries mortes. Il est probable qu'une contrainte de cisaillement inférieure ne permettait pas le détachement de matière morte et qu'une contrainte de cisaillement plus élevée était certainement nuisible aux bactéries. Ce travail démontre le rôle majeur des contraintes de cisaillement dans la formation du biofilm L'utilisation de contraintes de cisaillement pourrait être un moyen de contrôler la sélection des EAB et la quantité de matière morte dans les biofilms anodiques. C'est un facteur qui devrait être pris en compte dans l'architecture et la mise en place des réacteurs.

Remerciements

Je tiens tout d'abord à remercier mes directeurs de thèse, Timothy M. Vogel, Naoufel Haddour et Pascal Fongarland pour m'avoir fait confiance et donner l'opportunité de travailler avec une grande liberté sur ce sujet de recherche. Merci pour leurs nombreux conseils, leur patience et leur disponibilité durant ces 3 années.

Je remercie également l'Université de Lyon pour avoir acceptée de financer cette thèse. Ce travail a été financé par le LABEX iMUST (ANR-10-LABX-0064) de l'Université de Lyon au sein du programme « Investissement d'Avenir » (ANR-11-IDEX-0007 opéré par l'Agence Nationale de Recherche (ANR).

Je souhaite particulièrement remercier Richard Barthollet, Frédéric Bornette et Fabrice Campoli pour leurs conseils, leur rigueur et leur aide dans la fabrication et la mise en place des réacteurs.

Je remercie l'ensemble des membres (et anciens membres) de l'équipe Bioingénierie du laboratoire Ampère. Un grand merci à Sébastien Cecillon pour m'avoir fait découvrir tous les recoins du laboratoire, pour sa disponibilité et pour m'avoir souvent conseillé pendant ces trois années. Je remercie également Sandrine Demanèche et Laure Franqueville pour leur gestion du laboratoire, des stocks et surtout leur temps et leur disponibilité.

Je remercie aussi l'ensemble des membres (et anciens membres) du Laboratoire de Génie des Procédés Catalytiques (LGPC). Je remercie particulièrement Alain Favre-Réguillon, Laurent Vanoye et Régis Philippe pour leur temps, leurs conseils et pour m'avoir accueilli dans le laboratoire. Je remercie également Edouard Rebmann pour le temps qu'il a investi et son travail sur la modélisation des biopiles.

Enfin je remercie l'ensemble des membres du laboratoire Ampère de l'Ecole Centrale de Lyon et les membres de l'Ecole Doctorale EEA.

Table contents

Thesis objectives

The goal of this thesis is to improve knowledges on the formation of an electroactive biofilm on the anodic surface, and to understand the mechanisms involved in the competition between electroactive bacteria and other bacterial communities, in order to improve the selection of electroactive bacteria in the anodic biofilm. A special attention will be put on shear forces as a tool to control the formation of anodic biofilms. The long-term objective of this research is to improve the electrical production of microbial fuel cells, and more particularly the anodic compartment performances, for wastewater treatment plant station, to reduce the energy cost of wastewater treatment.

Societal challenges of MFC

Microbial Fuel Cell (MFC) is a sustainable technology capable of converting the organic matter into electricity using a biofilm to catalyze the reaction (Figure 1). The power generated by MFC is about 1W/m² of anodic surface. The anodic compartment contains water with organic matter and microorganisms. A biofilm grows on the anode (often a carbon anode) and oxides organic matter into CO_2. Some specific microorganisms called Electroactive Bacteria (EAB) are capable to transfer their electrons from this oxidation to an electrode (the anode). The electrons from this oxidation circulate in the external circuit through an external resistance to the cathode. The cathode is classically a carbon electrode with platinum as catalyzer. The dioxygen is reduced into water on the cathode. This technology is capable to produce electricity from organic matter as glucose. Even if historically the main application of MFC is for waste water treatment, this technology could have different applications in bioremediation, biosensors or bioproduction [1].

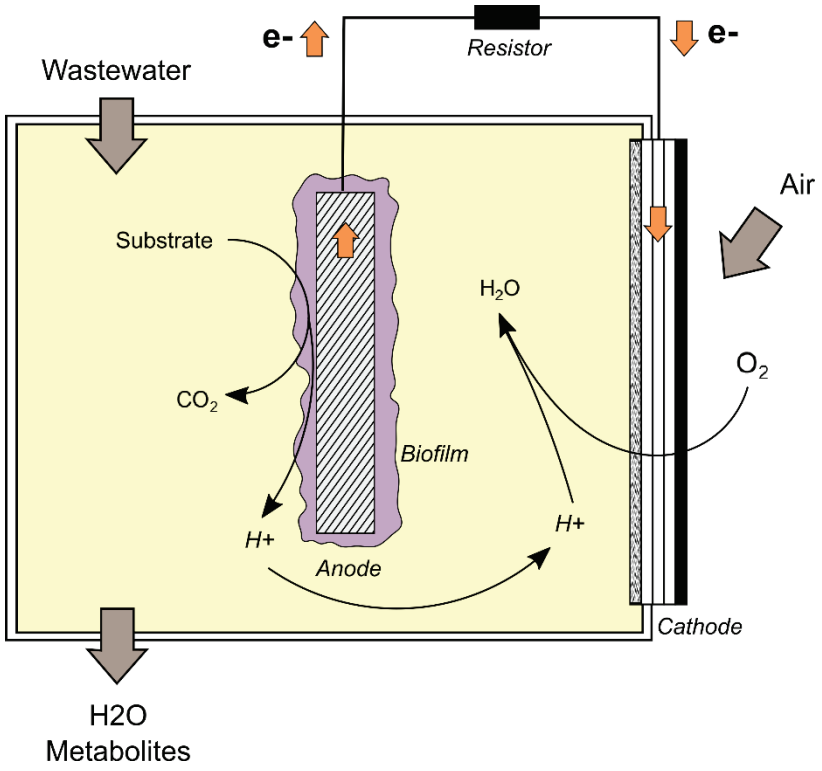

Figure 1. Schematic of a Microbial Fuel Cell

Bioproduction

Recently, the production of useful compounds from renewable resources attracted a lot of interest among research world [2]. The hydrogen and methane production occupy a large part of studies. The other molecules produced can be hydrogen peroxide or acetic acid for example.

Biosensors

The biofilm on the electrode can be used as a bioreceptor for the detection of Biological Oxidation Demand in carbon (BOD) or specific toxic compounds. The electricity production being proportional to the BOD, MFC seems to be an ideal biosensor [3], [4]. The chemical toxicants can inhibit the metabolic activity of anodic microbial population and decrease the electricity production. For this reasons, MFCs are proposed as a biosensor for toxic compound detection as plumb or phenol for example [5].

Power source

Autonomous robot are being increasingly employed in industry. In this context, the incorporation of energy source is needed for sustained operation. So, the MFCs can provide viable options [6]. For example, Gastrobots [7] or EcoBotare [8] autonomous robots employ MFCs as an energy source. MFC can be a power source for implantable medical devices as glucose sensing and cardiac pacing [9].

Bioremediation

MFC was used to remove a large scale of pollutants. Several studies have shown that MFC can produce a value-addition for the treatment of persistent organic pollutants as terephthalic acid, diesel organics, aromatic hydrocarbons or chlorinated compounds[10]–[13]. Another major application in bioremediation is to remove heavy metal as Chromium, Arsenic, or Uranium[14]–[16]. Also it is possible to use heavy metals as electron acceptors in the cathodic chamber.

Waste water treatment

Potentially, MFCs can generate the power needed in a conventional treatment process involving aerating of the activated sludge. Several studies have shown that MFC are capable to remove organic matter from a large diversity of effluent [17]–[19], and the efficiency of MFC can be very high (90%). It is a stable and not expensive system which can be implanted in a waste water treatment plant station[20].

Since the 2000s years, the researches in MFC have increased and allowed progress in this technology. The generated power density was about $10\mu W.m^{-2}$ before 2000s and is today about $1W.m^{-2}$ [21]. Moreover, the French and European legislations favor and impose the revalorization of organic waste from industries or regional collectivities [22]. MFC is a way to meet this need.

Synthèse en français

Objectifs de cette thèse

Cette thèse a pour objectif d'améliorer les connaissances sur la formation des biofilms électroactifs à la surface de l'anode, et de comprendre les mécanismes impliqués dans la compétition entre les bactéries électroactives et les autres communautés bactériennes dans le but d'améliorer la sélection des bactéries électroactives dans le biofilm anodique. Une attention particulière sera portée aux forces de cisaillement comme un outil de contrôle de la formation des biofilms anodiques. Ces recherches ont pour objectif à long terme d'améliorer la production d'électricité produite par les biopiles microbiennes, et plus particulièrement d'améliorer les performances du compartiment anodique, afin que les biopiles microbiennes puissent être utilisées pour réduire le coût énergétique du traitement des eaux usées dans les stations d'épurations.

Enjeux sociétaux des biopiles microbiennes

Les biopiles microbiennes permettent de convertir la matière organique en électricité en utilisant un biofilm pour catalyser la réaction (Figure 1). La puissance générée par les biopiles microbiennes est d'environ 1W/m² de surface anodique. Le compartiment anodique contient une solution aqueuse, de la matière organique et des micro-organismes. Un biofilm se développe sur l'anode (souvent une anode de carbone) et oxyde la matière organique en CO_2. Certains micro-organismes appelés bactéries électroactives (EAB) sont capables de transférer les électrons issus de cette oxydation à une électrode (l'anode). Ces électrons circulent ensuite dans le circuit électrique externe à travers une résistance jusqu'à la cathode qui catalyse la réduction du dioxygène en eau. Cette technologie est capable de produire de l'électricité à partir de matière organique sous forme de glucose par exemple, et en fait donc une source d'énergie renouvelable prometteuse. Même si historiquement l'application principale des biopiles microbiennes est le traitement des eaux usées, cette technologie pourrait avoir différentes applications dont la bioremédiation, les biocapteurs ou la bioproduction [1].

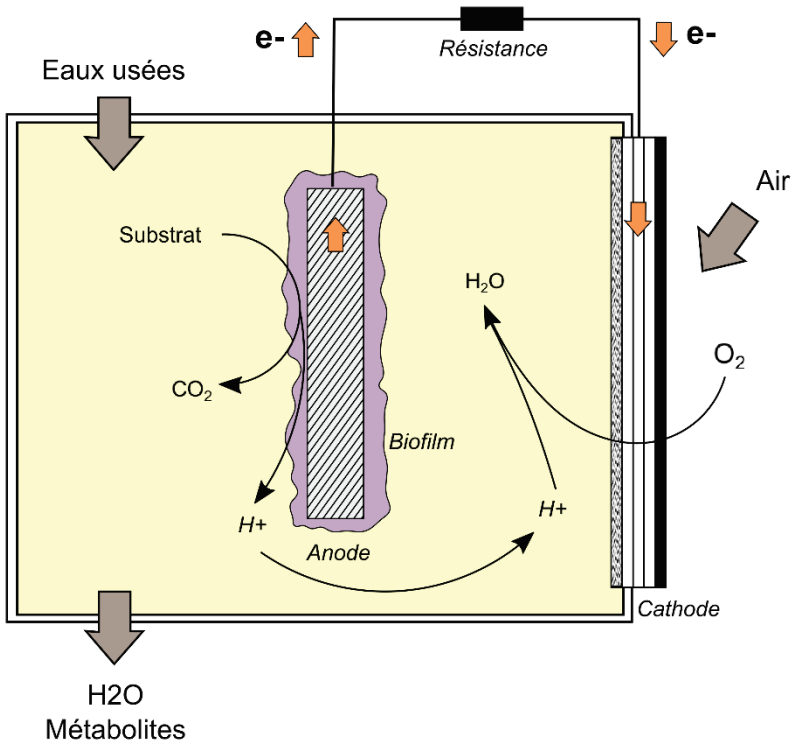

Figure 1. Schéma d'une biopile à combustible microbienne.

La bioproduction

Récemment, la production de composés utiles à partir de ressources renouvelables a suscité beaucoup d'intérêts [2]. La production d'hydrogène et de méthane occupe une grande partie des études. Les autres molécules produites peuvent être du peroxyde d'hydrogène ou de l'acide acétique par exemple.

Les biocapteurs

Le biofilm sur l'électrode peut être utilisé comme un biocapteur pour la détection de la demande biologique en oxygène pour l'oxydation de la matière carbonée (DBO), ou pour la détection de composés toxiques. La production d'électricité étant proportionnelle à la DBO, les biopiles microbiennes semblent être un biocapteur idéal [3], [4]. Les produits chimiques toxiques peuvent inhiber l'activité métabolique de la population microbienne anodique et diminuer la production d'électricité. Pour ces raisons, les biopiles sont aussi proposées comme biocapteurs de composés toxiques comme le plomb ou le phénol [5].

Une source d'énergie

Les robots autonomes sont de plus en plus employés dans l'industrie. Dans ce contexte, l'incorporation de la source d'énergie est nécessaire pour un fonctionnement permanent. Il a été montré que les biopiles microbiennes peuvent fournir des options viables [6]. Par exemple, les robots autonomes Gastrobots [7] ou EcoBotare [8] utilisent des biopiles microbiennes comme source d'énergie. Les biopiles peuvent également être une source d'énergie pour les dispositifs médicaux implantables comme la détection de glucose et la stimulation cardiaque.

La bioremediation

Les biopiles microbiennes ont été utilisées pour dépolluer une large gamme de polluants. Plusieurs études ont montré que les biopiles peuvent être une valeur ajoutée pour le traitement des polluants organiques persistants tels que l'acide téréphtalique, les composés organiques du diesel, les hydrocarbures aromatiques ou les composés chlorés [10]–[13]. Une autre application majeure de la bioremédiation consiste à éliminer les métaux lourds comme le chrome, l'arsenic ou l'uranium [14]–[16]. Il est alors possible d'utiliser des métaux lourds comme accepteurs d'électrons dans la chambre cathodique.

Le traitement des eaux usées

Les biopiles microbiennes peuvent potentiellement générer une puissance électrique suffisante pour alimenter les différents processus de traitement des eaux impliquant l'aération des bassins. Plusieurs études ont montré que les biopiles sont capables d'éliminer les matières organiques d'une grande diversité d'effluents [17]–[19]. Il a également été montré que l'efficacité coulombique peut être très élevée (90%). C'est un système stable et peu coûteux qui peut être implanté dans une station d'épuration des eaux usées [20].

Depuis les années 2000, les recherches sur les biopiles microbiennes ont augmenté et permis des progrès remarquables dans cette technologie. La densité de puissance générée était d'environ $10\mu W.m^{-2}$ avant les années 2000 et est aujourd'hui d'environ $1W.m^{-2}$ [21]. De plus, les législations françaises et européennes favorisent et imposent la revalorisation des déchets organiques provenant des industries ou des collectivités territoriales [22]. Dans ce contexte, les biopiles microbiennes sont un moyen de répondre à ce besoin.

Introduction générale

1.1 Evolution historique des recherches sur les biopiles à combustible microbiennes

1.1.1. Les premiers pas de la recherche sur les biopiles à combustible microbiennes

Les biopiles à combustible microbiennes (BPCMs) est un sujet relativement récent qui est né il y a un siècle. Les premières recherches proposant d'utiliser des micro-organismes pour produire de l'électricité sont attribuées à Potter en 1911 [23]. Il a observé une augmentation de l'électricité lors de la décomposition de la matière organique par fermentation en utilisant la levure *Saccharomyces*. Jusqu'aux années 1960, l'intérêt pour les BPCMs était très faible et les progrès dans ce domaine restaient mineurs.

En 1962, Davis a été l'un des pionniers à utiliser l'expression "Microbial Fuel Cell" [24]. Il a confirmé une conversion de la matière organique en électricité grâce au métabolisme bactérien et a conclu dans ce travail que *"microbial metabolism as a source of measurable electrical energy is established, but as far as we know, no one has made a serious attempt to employ this energy"* (« *le métabolisme microbien en tant que source d'énergie électrique mesurable est établi, mais pour autant que nous sachions, personne n'a fait de tentative sérieuse d'employer cette énergie* »). Bientôt, en 1963, la NASA veut recycler les déchets organiques produits par les astronautes en électricité [25], [26]. L'intérêt pour les BPCMs a été relancé mais l'électricité générée par les micro-organismes restait encore faible et les progrès encore limités.

Au début des années 1980, le travail de Bennetto et de ses collaborateurs sur les médiateurs synthétiques a été un développement important pour les recherches sur les BPCMs [27]–[30]. Des médiateurs synthétiques ajoutés au milieu permettent d'augmenter la production d'électricité. La compréhension du transfert extracellulaire d'électrons (EET) vers l'anode, associée à un grand nombre de publications a permis de relancer et vulgariser ces recherches. Malgré cela, les applications des BPCMs semblent encore loin. En effet, l'ajout de médiateurs dans le milieu est une barrière économique et écologique pour l'utilisation des BPCMs à grande échelle. Pour cela, les recherches sur les BPCMs étaient plus considérées comme une curiosité qu'une réelle et utile technologie.

1.1.2. **Des avancées en microbiologie fondamentale**

L'essor des BPCMs a commencé au début des années 2000, comme le montre la Figure 1.1 par l'augmentation du nombre de publications (A) et du nombre de citations par publications (B). Des travaux fondamentaux en microbiologie ont permis une meilleure compréhension des BPCMs. Grâce à l'identification de bactéries électroactives (EAB), les stratégies de sélection des EAB ont pu être mises en œuvre. Les études de Kim *et al.* en 1999 [31], [32] ont permis d'identifier *Shewanella putrefaciens* comme EAB, puis *Clostridum butyricum* dans les travaux de Park *et al.* en 2001 [33]. La découverte de *Geobacter sulfurreducens* comme EAB par Bond *et al.* en 2003 a marqué un tournant important [34]. Ces découvertes ont conduit à l'étude de BPCMs sans médiateurs redox synthétiques.

En 2002, Kim *et al.* ont rapporté l'utilisation d'une BPCM sans médiateur en utilisant *Shewanella putrefaciens* comme EAB [35]. Son travail suggère que *"the electron transfer from bacterial cells to the electrode also depends on physical contact between the cells and the electrode" (*« le transfert d'électrons des cellules bactériennes à l'électrode dépend aussi du contact physique entre les cellules et l'électrode »). L'hypothèse que les bactéries peuvent transférer leurs électrons directement à l'anode via des cytochromes sans utiliser de médiateurs s'était répandue.

La découverte de nano-filaments par Gorby *et al.* en 2006 [36] et Reguera *et al.* en 2006 [37] a mis en évidence les mécanismes mis en œuvre par les bactéries pour transférer leurs électrons et a offert de nouvelles perspectives pour la recherche sur les BPCMs. Parallèlement, différents mutants de *Geobacter* et *Shewanella* ont été construits pour déterminer les gènes impliqués dans les Transferts Extracellulaires d'Electrons (TEEs) [36]–[40]. Ces avancées fondamentales ont rendu les applications des BPCMs plus concrètes. L'utilisation de BPCMs pour réduire le coût énergétique devient plus réaliste. Aujourd'hui, la découverte de nouvelles EAB et la compréhension des mécanismes impliqués dans les TEEs sont toujours un enjeu majeur de la recherche sur les BPCMs.

1.1.3. **Les BPCMs comme une nouvelle biotechnologie**

Avant le milieu des années 2000, la recherche portait essentiellement sur le compartiment anodique et la microbiologie du biofilm. Après cela, la recherche s'est diversifiée et d'autres disciplines comme les sciences de l'ingénieur, les sciences des matériaux ou la chimie verte sont devenues une partie plus importante de la recherche sur les BPCMs (Figure 1.1 (C)). En 2004, Liu et Logan construisent une BPCM avec une cathode à air, permettant de doubler la densité de puissance de la BPCM [19]. Les BPCMs étaient jusqu'alors construites avec deux compartiments (un compartiment anodique et un cathodique) séparés par une membrane échangeuse de protons (MEP). La cathode à air a permis de supprimer la MEP, permettant de créer une BPCM à un seul compartiment. La densité de puissance a alors augmenté grâce à une diminution de la résistance interne, due à l'absence de MEP et à une concentration plus élevée de dioxygène à la cathode. Cette découverte a conduit à une augmentation exponentielle du nombre d'articles: 13 articles contenant l'expression «Microbial Fuel Cell» ou «Electroactive bacteria» dans le titre, le résumé ou les mots-clés de la base de données Scopus en 2000, 57 en 2005 et 767 en 2015 (Figure 1.1 (A)).

La recherche sur les performances cathodiques s'est poursuivie. En 2006, He a écrit une revue sur les biocathodes suggérant que la biocathode dans les BPCMs pourrait améliorer la cinétique à la cathode [41] (jusqu'à présent, la réaction à la cathode était abiotique, et catalysée par le platine). Deux ans plus tard, en 2008, Rabaey *et al.* ont développé une biocathode dans une BPCM capable de réduire directement le dioxygène en eau [42]. L'optimisation des biocathodes et la compréhension des

communautés bactériennes cathodiques sont toujours une partie importante de la recherche sur les BPCMs. Une autre partie de la recherche sur le compartiment cathodique porte sur le choix de l'accepteur d'électrons: par exemple, les composés de chrome [43], de fer [44] ou de chlorure [45] peuvent être utilisés comme accepteur d'électrons. Plusieurs études tentent d'augmenter le courant cathodique en utilisant un autre accepteur d'électrons que le dioxygène ou en utilisant un biofilm microbien comme catalyseur.

D'autres études ont pour objectif d'optimiser la membrane [46], [47], la structure de l'électrode (anode ou cathode) [48], [49], l'architecture des BPCMs [50], [51], ou les propriétés physico-chimiques telles que le pH, la température, ou la force ionique [52]. Ces avancées sont couplées avec des études sur les applications de BPCMs. Plusieurs études ont testé l'utilisation de BPCMs avec différents types d'effluents: eaux usées d'origines domestiques, agricoles ou industrielles [17], [19], [53]–[55].

Le 15 septembre 2011, la Société internationale d'électrochimie et de technologie microbienne (ISMET) (www.is-met.org) a été fondée: *"The goal of ISMET is to link researchers from various areas of science and engineering towards studying the complex interactions of microorganisms and electrodes, while finding novel ways to use them for sustainability applications." (*«ISMET a pour objectif de mettre en relation des chercheurs de diverses domaines scientifiques étudiant les interactions complexes des micro-organismes avec une électrode, tout en trouvant de nouvelles façons de les utiliser pour des applications de durabilité. »). L'électrochimie microbienne est alors devenue une discipline distincte.

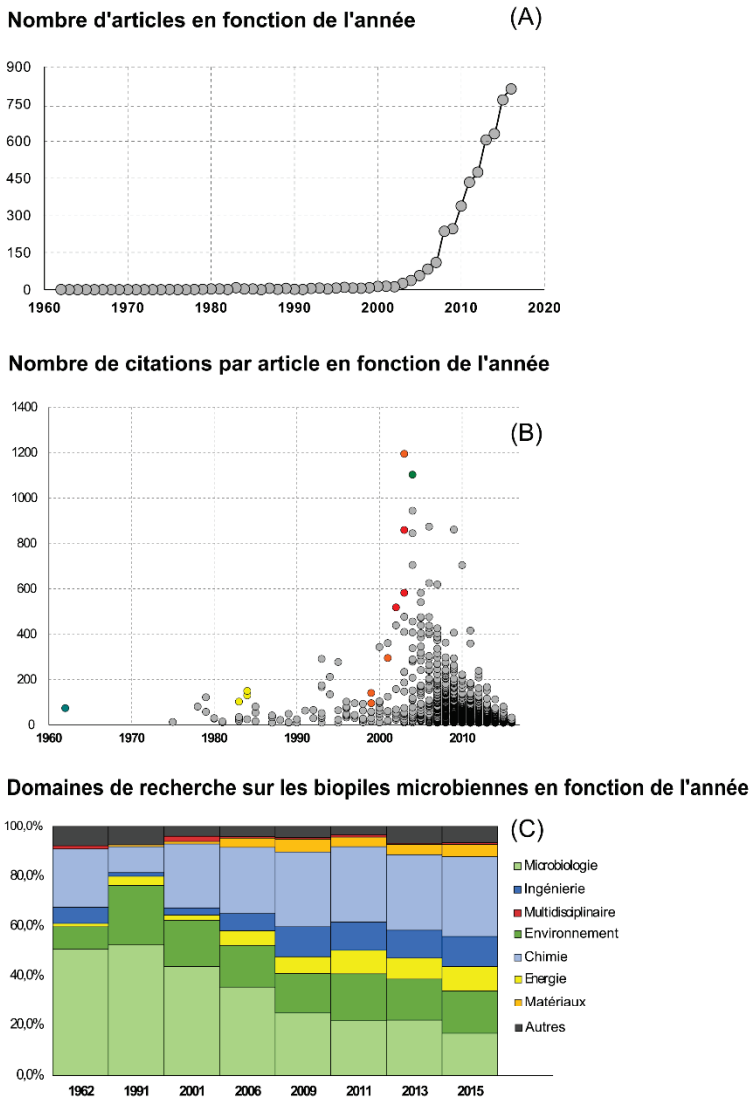

Figure 1.1. Evolution des recherches sur les biopiles microbiennes.

(A) Nombre d'articles publiés en fonction des années.

(B) Nombre de citations par article en fonction des années: le point bleu est l'article de Davis J.B. *et al.* en 1962, les points jaunes représentent les articles de Bennetto *et al.* sur les médiateurs en 1983 et 1984, les points oranges représentent les articles majeurs sur la découverte des EAB et des TEEs, les points rouges sont les premiers articles sur les BPCMs sans médiateurs. Le point vert est l'utilisation de la cathode à air.

(C) Evolution des domaines de recherché dans les BPCMs en fonction des années. La classification des sujets a été faite en fonction du journal de publication.

Les données proviennent de la base de données Scopus par recherche de l'expression "Microbial Fuel Cell" ou "Electroactive bacteria" dans le titre, les mots-clés et l'abstract des articles.

1.2 Les pertes énergétiques dans les BPCMs

Dans le but d'améliorer la production d'électricité des BPCMs, il est important d'identifier les différents types de pertes énergétiques. Ce chapitre a pour objectif de décrire les paramètres utilisés pour caractériser la production d'électricité, d'identifier les puissances maximales théoriques que pourrait produire une BPCM, et de décrire les pertes énergétiques possibles.

1.2.1. Puissance maximale théorique générée par une BPCM

La puissance générée par une BPCM est définie par l'équation *(1.1)*:

$$P = U.I \qquad (1.1)$$

avec P la densité de puissance en W/m², U la tension de la BPCM en V, et I la densité de courant en A/m². Pour augmenter la puissance générée par la BPCM, il est donc possible d'augmenter soit la tension de la biopile soit la densité de courant.

Tension maximale d'une BPCM

La tension maximale d'une BPCM est fixée par le potentiel redox d'équilibre de chacune des réactions à l'anode et à la cathode *(1.2)*:

$$U_{max} = E_{eq,c} - E_{eq,a} \quad (1.2)$$

avec U_{max} la tension maximale d'une BPCM en V, $E_{eq,c}$ le potentiel d'équilibre à la cathode en V et $E_{eq,a}$ le potentiel d'équilibre à l'anode en V. La tension maximale d'une BPCM spécifique est mesurée en circuit ouvert lorsque le courant est égal à zéro. Le potentiel d'équilibre d'une électrode est donné par l'équation de Nernst *(1.3)*:

$$E_{eq} = E^0 + \left(\frac{RT}{nF}\right) \ln\left(\frac{[Ox]}{[Red]}\right) \qquad (1.3)$$

avec E_{eq} le potentiel d'équilibre de l'électrode en V, E^0 le potentiel standard du couple Ox/Red en V, [Ox] et [Red] la concentration respective de l'oxydant et du réducteur en mol/L, R la constante des gaz parfaits de 8.31 $J.mol^{-1}.K^{-1}$, T la température en K, *n* le nombre d'électrons échangés et F la constante de Faraday de 96485.33 C. L'exemple décrit par Logan est reproduit ici [56]. Si la réaction à la cathode est la réduction du dioxygène en eau, le potentiel d'équilibre de la cathode devrait être de 0.805V/ENH (Electrode Normale à Hydrogène avec un potentiel standard de 1.229V/ENH, une pression partielle en O_2 de 0.2 et un pH de 7 *(1.4)*. Si la réaction à l'anode est l'oxydation de l'acétate en HCO_3^-, le potentiel d'équilibre à l'anode devrait être -0.296V/ENH avec un potentiel standard de 0.187V/ENH, une concentration d'acétate et d'HCO_3^- de 5mM, et un pH de 7 *(1.5)*. La tension maximale de la BPCM devrait alors être de 1.101V.

$$O_2 + 4H^+ + 4e^- \rightarrow 2H_2O \qquad E^0 = 1.229V/ENH \qquad (1.4)$$

$$2HCO_3^- + 9H^+ + 8e^- \rightarrow CH_3COO^- + 4H_2O \qquad E^0 = 0.187V/ENH \qquad (1.5)$$

Courant anodique maximale d'une BPCM

Les réactions à l'anode sont considérées ici comme le facteur limitant de l'intensité maximale. Le courant maximal est alors dépendant du métabolisme bactérien et de la densité cellulaire sur l'anode *(1.6)*:

$$I_{\max} = r_{max} XnF \qquad (1.6)$$

avec I_{max} la densité de courant maximale en A/m², X la densité bactérienne en cel/m² et r_{max} la vitesse maximale d'utilisation du substrat en $mol.cell^{-1}.s^{-1}$. La densité maximale de courant d'une BPCM spécifique est mesurée en circuit fermé lorsque la tension de la BPCM est nulle. La vitesse maximale de consommation de l'acétate par une bactérie est d'environ $2.30\ 10^{-13}$ $mol.cel^{-1}.j^{-1}$ [57]. Dans le cas d'une situation idéale, sans aucune perte énergétique, cela correspondrait à un courant de $2.06\ 10^{-12}$ A produit par une bactérie. La densité cellulaire d'un biofilm peut énormément varier. Par exemple, dans le cas d'une monocouche de EAB (en considérant qu'une bactérie a une surface de 2µm²), la densité serait de $5.00\ 10^{11}$ cel/m², ce qui correspond à un courant de 1.03 A/m². Un biofilm peut potentiellement croître jusqu'à plusieurs centaines de micromètres.

À partir d'une tension et d'un courant maximal, la puissance théorique maximale est entre 1 (dans le cas d'une monocouche parfaite de EAB) et plusieurs centaines de W/m² (pour un biofilm de plusieurs centaines de micromètres d'épaisseur). La densité des EAB joue un rôle majeur dans la puissance générée. De meilleures connaissances sur les mécanismes impliqués dans la sélection des EAB et sur la structure physique du biofilm anodique permettraient d'améliorer la densité des EAB sur l'anode.

1.2.2. Définition des pertes énergétiques dans les BPCMs.

Dans le but de déterminer la puissance réelle maximale générée par une BPCM, la tension de la BPCM est mesurée en fonction de l'intensité pour tracer une courbe de polarisation (Figure1.2). La courbe de polarisation était initialement utilisée pour étudier les systèmes électrochimiques (et non bioélectrochimiques) [58], [59]. Cela permet d'observer les pertes d'énergie associées à une baisse progressive de la tension de la BPCM en fonction de l'intensité électrique. Les différences entre la tension maximale de la cellule électrochimique et la tension mesurée pour une intensité donnée est appelée surtension η *(1.7)*:

$$\eta = U_{max} - U \quad (1.7)$$

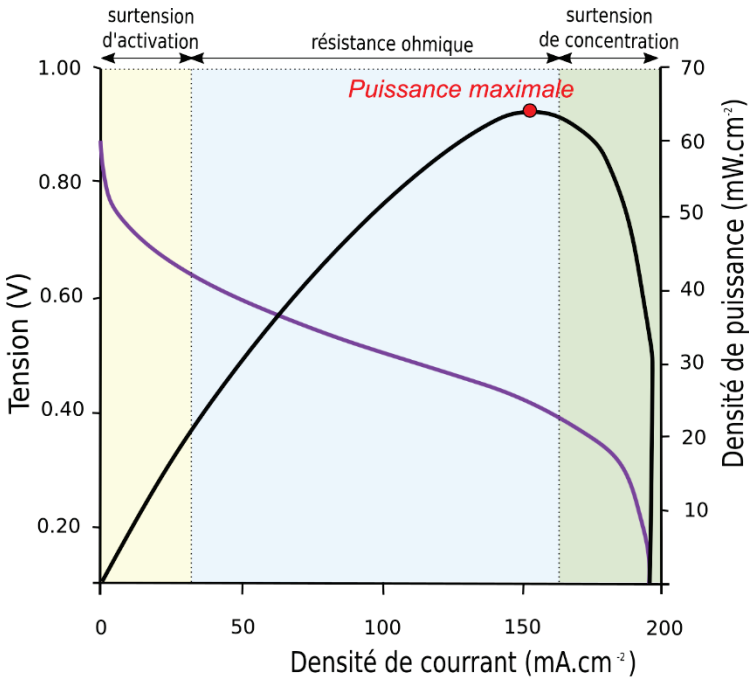

Figure1.2. Courbe de polarisation et de puissance. La courbe violette représente la tension de la pile en fonction de l'intensité. La courbe noire représente la densité de puissance en fonction de l'intensité.

La surtension η est la somme des surtensions anodiques et cathodiques, respectivement η_a et η_c, définies par l'équation *(1.8)*:

$$\eta_a = E_a - E_{eq,a} \quad et \quad \eta_c = E_c - E_{eq,c} \qquad (1.8)$$

À chaque valeur d'une densité de courant corresponds une certaine surtension. Trois types de surtensions sont habituellement définies : la surtension d'activation, la résistance ohmique et la surtension de concentration. Chaque perte énergétique est associée à différentes étapes dans le transport des électrons (Figure 1.3). Les réactions aux électrodes peuvent être représentées par une résistance, composée d'une série de résistances représentant les différentes étapes (Figure1.4).

La surtension d'activation

La surtension d'activation est due à l'énergie d'activation nécessaire à la réaction. La surtension d'activation est prédominante lorsque le transfert de masse n'est pas limitant, donc lorsque la cinétique est lente. L'énergie d'activation est le facteur limitant de la production d'électricité pour un courant faible. Il correspond à la perte d'énergie associée à une réaction et au transfert d'électrons vers une électrode. La surtension d'activation à l'anode est notée $\eta_{act,a}$ et la surtension d'activation à la cathode est notée $\eta_{act,c}$.

La résistance ohmique

La résistance ohmique, notée η_{ohmic}, correspond à la résistance des connections et à la résistance du milieu entre l'anode et la cathode. La résistance ohmique dépend de la conductivité du milieu et de la distance entre l'anode et la cathode. La qualité de la membrane ou du pont salin entre l'anode et la

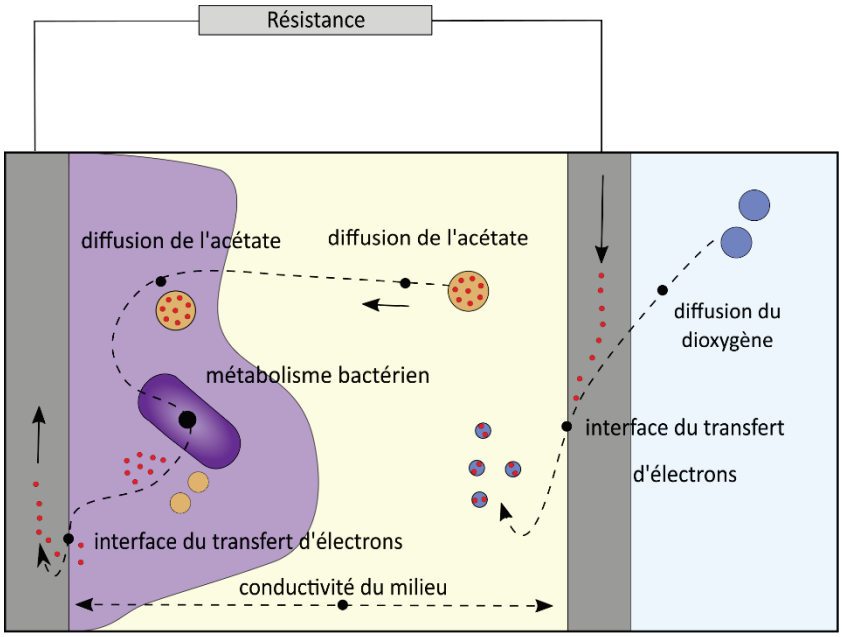

Figure 1.3. Schéma du flux d'électrons et des mécanismes associés aux pertes énergétiques.

cathode peut également modifier la résistance ohmique. Le courant est relié à la résistance ohmique, notée R_{ohm}, par la loi d'ohms.

La surtension de concentration

La surtension de concentration correspond à la résistance associée au transport des substrats vers l'électrode. S'il n'y a pas de convection dans le milieu, le transport de masse est seulement dû à la diffusion. Sur la Figure 1.3, la surtension anodique de concentration, notée $\eta_{conc,a}$, est associée à la diffusion de l'acétate à l'anode, et la surtension cathodique de concentration, notée $\eta_{conc,c}$, est associée à la diffusion du dioxygène à la cathode. Pour une espèce redox Ox/Red, le courant est lié à la concentration d'*Ox* et *Red* à la surface de l'électrode (x = 0), par l'équation (1.9):

$$\frac{I}{nF} = D_{ox}\left[\frac{\partial C_{Ox}(x,t)}{\partial x}\right]_{x=0} = -D_{Red}\left[\frac{\partial C_{Red}(x,t)}{\partial x}\right]_{x=0} \qquad (1.9)$$

avec Cox et Cred la concentration respectivement de l'oxydant et du réducteur en mol/L, Dox et Dred les coefficients de diffusion respectif de l'oxydant et du réducteur *m²/s.*

Les autres pertes d'énergie

D'autres pertes d'énergie doivent être prises en compte dans les BPCMs contrairement au système électrochimique classique. Les autres pertes d'énergie sont représentées dans le circuit électrique de la Figure1.4, et sont dues aux mécanismes suivants. (i) La présence d'un biofilm sur l'électrode crée une seconde barrière de diffusion pour les substrats, notée $\eta_{conc,b,a}$. Cette barrière de diffusion dépend de la densité du biofilm, de la nature des exopolysaccharides extracellulaires et de l'épaisseur du biofilm. (ii) La consommation du substrat pour la croissance bactérienne conduit à une perte d'électrons, notée $\eta_{growth,b,a}$. Si l'acétate n'est pas consommé pour la respiration mais pour la croissance, une partie des molécules d'acétate n'est pas oxydée en CO_2 et un pourcentage d'électrons

est perdu. (iii) Une autre perte d'énergie est due au métabolisme bactérien: c'est l'énergie du substrat utilisée par les bactéries et qui est notée $\eta_{energie,b,a}$. La cascade d'oxydoréduction dans la chaîne respiratoire entraîne une baisse successive de potentiel. Le résultat est que le potentiel des protéines membranaires ou des molécules des navettes est plus faible que celui du substrat d'origine. (iv) Enfin, une autre résistance est due au TEE ou au transfert de charge de la membrane bactérienne vers l'électrode, notée $\eta_{TEE,b,a}$. Si des navettes redox sont utilisées, la diffusion de ces navettes à l'intérieur du biofilm entraîne également une résistance non négligeable. En revanche, si le TEE est direct via une protéine membranaire ou via des nanofilaments, la résistance serait très faible. Les mécanismes de transfert d'électrons sont décrits plus précisément dans les sections 1.3 et 1.4 de ce chapitre.

1.2.3. **Les capacitances dans les BPCMs**

Dans tout système électrochimique, l'interface électrode/solution peut être comparée à un condensateur. La capacitance d'un condensateur est définie par l'équation suivante *(1.10)*:

$$C = \frac{q}{U_c} \quad (1.10)$$

avec C la capacitance en F, q la charge stockée sur le condensateur en C et U_c la différence de potentiels à travers le condensateur en V. La charge sur l'électrode notée q_M, est compensée par le charge présente en solution, notée q_S, telle que *(1.11)*:

$$q_M = -q_S \quad (1.11)$$

La distribution de l'ensemble des charges à l'interface électrode/solution forme la double couche électrique (Figure 1.5). La double couche est composée d'une couche interne appelée la couche de Stern et dont le plan central est appelé le plan interne d'Helmholtz (PIH), et d'une couche externe appelée couche de diffusion dont le plan centrale est appelé le plan externe d'Helmholtz (PEH). La couche de Stern est formée d'ions spécifiques adsorbés et la couche de diffusion est formée d'ions non spécifiques adsorbés. L'épaisseur de la couche de diffusion dépend de la concentration ionique de la solution. La double couche peut affecter la densité de courant si les espèces électronégatives sont adsorbées de manière non spécifique et ne peuvent donc approcher l'électrode que jusqu'au PEH.

Dans un système biotique, la présence d'un biofilm avec sa matrice extracellulaire constituée de polysaccharides peut être associée à un condensateur. Les protéines membranaires telles que les c-cytochromes peuvent stocker une grande quantité d'électrons. En fonction des espèces bactériennes présentes dans le biofilm, de l'expression de leurs gènes et de la composition de la matrix extracellulaire, la capacité anodique peut être très élevée. Le travail de Malvankar *et al.* [60] reporte une capacitance de 620 µF/cm² de biofilms de *Geobacter sulfurreducens* due aux cytochromes membranaires. Les auteurs comparent *G. sulfurreducens* à un supercondensateur: *"En traitant les hèmes de cytochromes comme des matériaux actifs, la capacitance spécifique calculée du biofilm DL-1 est de 111 F.g^{-1}, ce qui est comparable aux supercapacitance synthétiques."* (*"Treating cytochrome hemes as active materials, the computed specific capacitance of DL-1 biofilm is 111 F.g^{-1}, which is comparable to synthetic supercapacitors.").*

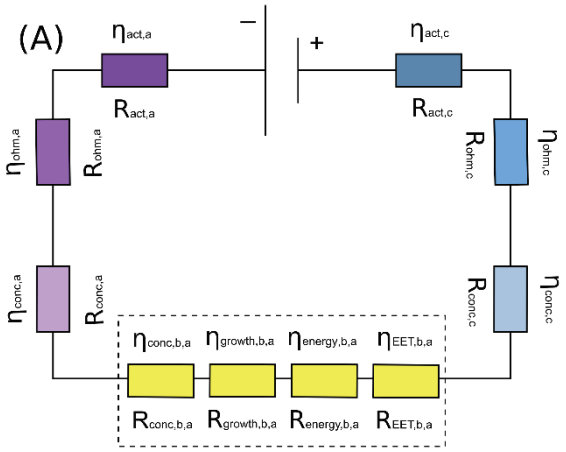

Figure1.5. Circuit électrique équivalent d'une BPCM. Circuit électrique équivalent d'une BPCM composée d'une bioanode et d'une cathode abiotique telle que représentée dans la Figure 1.3. Chaque surtension est associée à une résistance. Les résistances violettes et bleues correspondent respectivement aux mécanismes abiotiques du compartiment anodique et cathodique. Les résistances jaunes correspondent aux mécanismes biotiques du biofilm anodique.

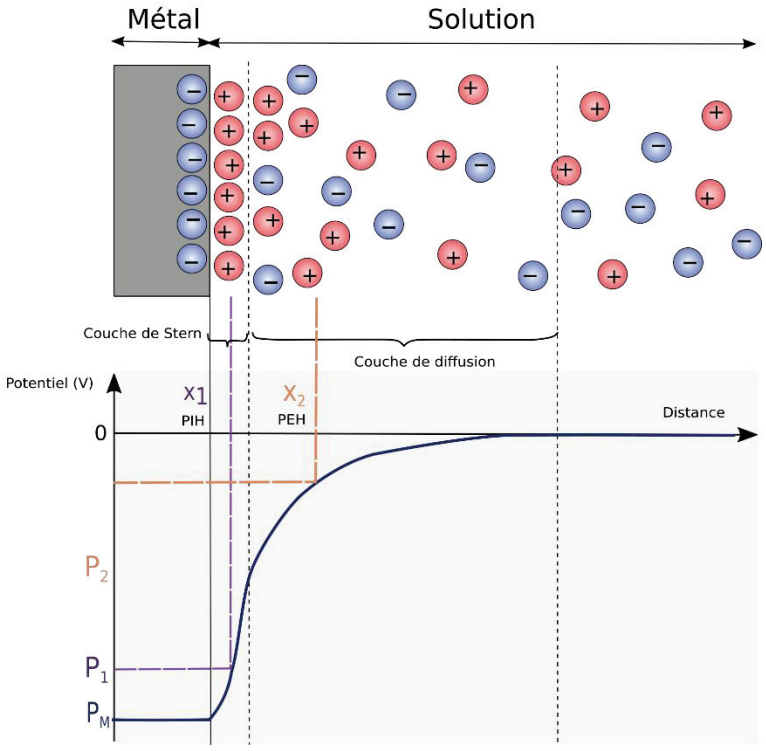

Figure 1.4. La double couche électrique. Ce schéma représente la distribution des charges à l'interface électrode/solution et l'évolution du potentiel de l'électrode à la solution.

1.3 Identité des bactéries électroactives

1.3.1. Diversité phylogénétique

Concept de phylogénie en microbiologie

La vie est divisée en trois domaines: *bacteria* (procaryotes), *archeae* (procaryotes) et *eucaryota*. La taxonomie regroupe les organismes en taxons d'un rang donné. Les groupes d'un rang peuvent être agrégés pour former un groupe d'un rang supérieur, créant ainsi une hiérarchie taxonomique. Les différents rangs du niveau supérieur au niveau inférieur sont le domaine, le phylum, la classe, l'ordre, la famille, le genre, l'espèce et la souche. Actuellement, la classification phylogénétique des bactéries est faite en comparant la séquence du gène de l'ARN ribosomique 16S qui est un composant du ribosome procaryote. Il est utilisé pour la phylogénie en raison de sa faible vitesse d'évolution. Les différences dans les séquences du gène de l'ARNr 16S sont des marqueurs de la distance phylogénétique entre les bactéries. Pour cette raison, il est considéré que les bactéries appartenant à la même espèce ont 97% de similarité sur leur séquence du gène de l'ARNr 16S, mais il n'y a pas de règle de similarité pour les autres niveaux taxonomiques. Enfin, les bactéries ayant 100% de similarité sur l'ensemble de leur génome appartiennent à la même souche. Compte tenu de ces caractéristiques, il est possible d'identifier les bactéries au niveau de l'espèce en comparant la séquence du gène de l'ARNr 16S à des séquences de bases de données comme SILVA ou RDP.

La diversité bactérienne dans les BPCMs

Les EAB appartiennent à une grande diversité de taxons (Figure1.6) [61], [62]. Les travaux de Koch *et al* répertorient 69 espèces ayant la capacité de transférer des électrons à l'anode, et appartenant à 37 genres différents [41]. Ils sont présents dans 9 sous-classes: *Alphaproteobacteria*, *Betaproteobacteria*, *Deltaproteobacteria*, *Gammaproteobacteria*, *Acidobacteria*, *Cyanobacteria*, *Actinobacteria*, *Bacilli* et *Clostridia*. Les groupes, *Deltaproteobacteria* et *Gammaproteobacteria*, sont les groupes les plus importants contenant respectivement 6 et 10 genres bactériens de EAB. L'identification de nouvelles EAB est une étape critique en raison du manque de marqueur génétique de l'électroactivité. Pour identifier une nouvelle EAB, il est nécessaire de passer par une étape d'enrichissement, de culture et d'isolement. Pour ces raisons, le nombre de EAB est certainement sous-estimé. Aujourd'hui, aucun lien entre la phylogénie et l'électroactivité des bactéries n'est observé. La démocratisation du séquençage du gène de l'ARNr 16S a permis d'étudier la diversité taxonomique des biofilms anodiques. Les BPCMs avec une abondance relative plus élevée de *Geobacter* ont souvent les meilleures performances électriques [17]. Cependant, les cultures mixtes ont souvent généré une puissance supérieure à celle des cultures pures. Récemment, certaines études ont étudié la diversité taxonomique et la structure de biofilms anodiques mixtes [17], [63]–[68]. Les principaux taxons varient d'une étude à l'autre : les *Deltaproteobacteria* [67] [68], *Betaproteobacteria* [17] et *Bacteroidetes* [65] ont toutes été détectées comme les principales bactéries présentes dans un biofilm anodique.

Stratford *et al.* [66] ont étudié la relation entre différents paramètres de diversité et la production d'énergie. La diversité peut être divisée en deux composantes: la richesse et la régularité. La richesse est le nombre de taxons dans un environnement et la régularité est la proportion de chaque taxon et la façon dont les proportions de ces taxons sont similaires. Ils ont montré que l'indice de Shannon, défini par l'équation (1.12), (représentatif à la fois de la richesse et de la régularité) était positivement

corrélé avec la production d'énergie. Mais dans d'autres études, les BPCMs avec une production d'énergie plus élevée avaient un indice de Shannon inférieur [67].

$$H = \sum_{i=1}^{m} p_i . \ln(p_i) \quad (1.12)$$

avec *H* l'indice de Shannon, *m* le nombre total de taxons, p_i la proportion du taxon *i*. Ces résultats contradictoires sont représentatifs du manque de connaissances sur l'écologie des biofilms anodiques.

Le rôle de chaque taxon dans la production d'électricité ou encore dans la formation de biofilm est encore mal connu. La plupart des études sur la communauté anodique sont souvent des études à un instant donné. Peu d'études ont observé l'évolution et la formation du biofilm permettant une meilleure compréhension des successions bactériennes au cours de la colonisation de l'anode [69], [70]. Hodgson *et al.* étudient les communautés microbiennes anodiques dans une BPCM en cascade à différents instants. Ils ont mis en évidence la relation entre les populations fermentaires et anodiques dans les BPCMs. A. Paitier *et al.* [70] montrent l'intérêt de s'intéresser aux changements précoces des communautés microbiennes et à la compétition entre EAB qui semble être importante lors de la colonisation de l'anode. Plus d'investigations sur la dynamique de la formation de biofilms devraient permettre une meilleure compréhension du rôle des communautés bactériennes et de leurs interactions dans le biofilm anodique.

1.3.2. **Le métabolisme énergétique des bactéries électroactives**

La vie cellulaire dépend d'une source d'énergie stockée sous forme chimique, l'ATP (Adenosine Triphosphate) qui est synthétisée par la respiration ou la fermentation. La Figure 1.7 décrit le métabolisme bactérien en général et la respiration bactérienne en particulier. Le donneur d'électrons qui est souvent (mais pas toujours) la source de carbone est oxydé en CO_2. Les électrons issus de cette oxydation circulent vers la chaîne respiratoire via des molécules redox navettes comme le NADH. Une fois dans la chaîne respiratoire, les électrons entrent dans une cascade de réactions d'oxydoréduction jusqu'à un accepteur d'électrons tel que le dioxygène (en milieu aérobie), le nitrate, le fer ou une électrode dans le cas d'une BPCM. Au cours de cette cascade d'oxydoréduction, des protons sont produits et sécrétés dans le compartiment extracellulaire, établissant un gradient de protons à travers la membrane. Cette différence de potentiel électrique à travers la membrane est ensuite convertie en énergie chimique pour la cellule: les protons sont utilisés par l'ATPase pour produire de l'ATP. Le gain d'énergie pour les bactéries dépend de la différence de potentiel entre le couple donneur d'électrons et le couple accepteur d'électrons. L'énergie libre, notée *G*, en $J.mol^{-1}$ est la fonction thermodynamique utilisée pour décrire ce gain d'énergie et est définie à l'équilibre par l'équation suivante (1.13):

$$\Delta G^{0'} = -nF(E^{0'}_{acceptor} - E^{0'}_{donor}) \quad (1.13)$$

Par exemple, le potentiel d'équilibre du couple donneur d'électrons CO_2/acétate est de -0.290 V/ENH [71], et ceux des couples accepteurs d'électrons O_2/H_2O et citrate de Fe(III)/citrate de Fe(II) sont respectivement de 0.800 et 0.372 V/ENH. L'énergie libre pour l'oxydation de l'acétate par O_2 et par le citrate de Fe(III) sont alors respectivement de -841,35 $kJ.mol^{-1}$ et -330,36 $kJ.mol^{-1}$. La croissance bactérienne est affectée par ce gain énergétique. Il en découle que les bactéries aérobies se développent plus rapidement que les bactéries anaérobies. Par exemple, le temps de doublement d'*Escherichia coli* dans des conditions aérobies est d'environ 20 min [72]. Cependant, le temps de doublement de *Geobacter uraniireducens* a été déterminé à 18,5 heures avec de l'oxyde de Fe(III) comme accepteur d'électrons et 50,1 heures dans des environnements complexes tels que les sédiments [73].

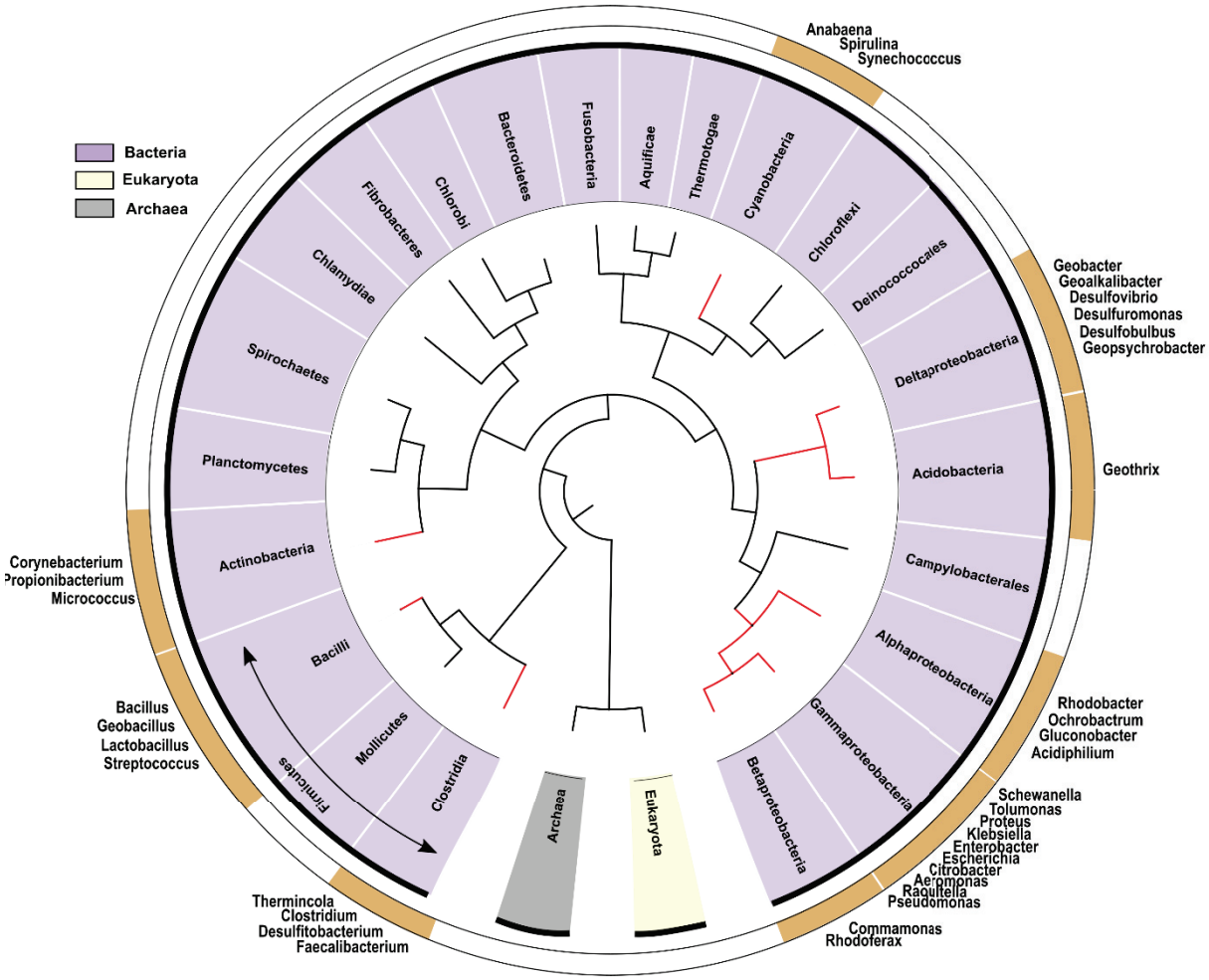

Figure1.6. Arbre phylogénétique des bactéries électroactives. La figure représente l'arbre phylogénétique de la vie. Les classes des bactéries sont représentées en violet. Dans le cercle extérieur, la présence des EAB est représentée en rouge. Le genre des EAB est écrit à l'extérieur du second cercle. La figure a été réalisée à partir de l'inventaire des EAB anodiques réalisé dans le travail de [41].

Dans le cas des BPCMs, l'accepteur d'électrons est l'anode: c'est une respiration anodique. Du point de vue thermodynamique, un fort potentiel anodique favorise la croissance des bactéries, mais entraîne une perte d'énergie importante dans la production d'électricité [74]. Le travail de Wei *et al.* [75] met en évidence le rôle du potentiel anodique sur le métabolisme bactérien. Une culture pure de *G. sulfurreducens* est utilisée dans des BPCMs sous différents potentiels anodiques (-160, 0 et +400 mV). Plus le potentiel anodique était faible et plus la quantité de biomasse était faible, mais plus l'intensité du courant de la BPCM était élevée. Plus le potentiel de l'anode est proche du potentiel du donneur d'électrons, moins il y a de pertes d'énergie dans la BPCM mais moins la croissance bactérienne est rapide.

Différents types de métabolismes peuvent être observés chez les EAB Kracke *et al.* étudient le métabolisme de 8 bactéries issues de systèmes bioélectrochimiques dont 5 bactéries capables de transférer leurs électrons à l'anode [76] (Figure 1.8.). Dans cette étude, trois bactéries sont capables de se développer dans des conditions aérobies: *E. coli*, *S. oneidensis* et *P. aeruginosa*. *E. coli* et *P. aeruginosa* sont capables d'utiliser une large gamme d'accepteurs d'électrons qui peuvent être des

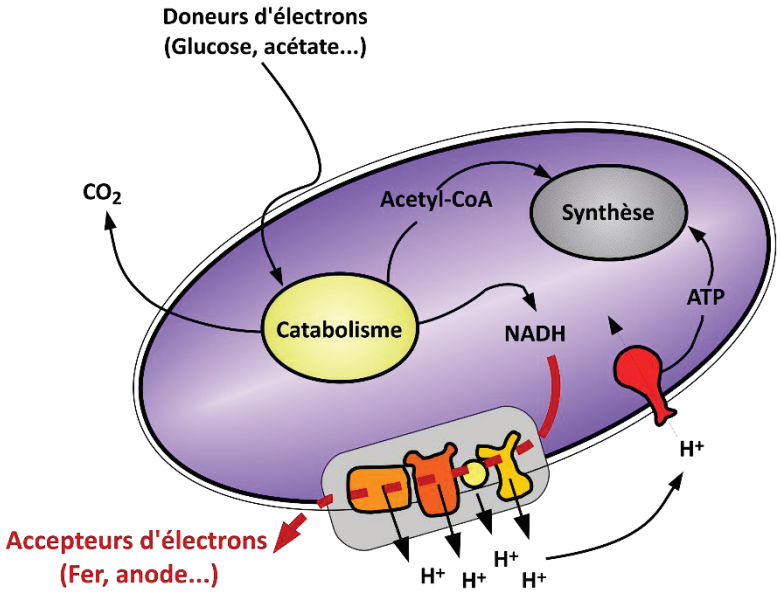

12

Figure1.7. Métabolisme bactérien. Schéma adapté de C.I. Torres *et al.* [74]

composés inorganiques ou organiques à l'exception des accepteurs d'électrons insolubles qui sont sous forme de particules de manganèse ou de fer. Ils ne sont pas non plus capables d'utiliser des accepteurs d'électrons à faible potentiel redox tels que les sulfates. Contrairement à eux, *S. oneidensis* peut utiliser une plus large gamme d'accepteurs d'électrons: solubles ou non, à faible potentiel redox ou non, accepteurs d'électrons organiques ou inorganiques. Le second groupe est moins flexible: *C. lijungdahlii* et *G. sulfurreducens*. *G. sulfurreducens* ne peut pas utiliser un accepteur d'électrons solubles inorganique classique tel que les nitrates ou les sulfates, mais peut utiliser différents accepteurs d'électrons insolubles. *C. lijungdahlii* ne peut utiliser que des accepteurs d'électrons à très faible potentiel redox (environ moins de -300 mV/ENH).

1.3.3. Diversité fonctionnelle impliquée dans le transfert extracellulaire d'électrons (TEE)

Plusieurs mécanismes peuvent être utilisés par les bactéries pour transférer leurs électrons vers un accepteur d'électrons insoluble : le transfert peut être direct ou indirect. Dans le cas d'un TEE indirect, les bactéries utilisent des navettes redox endogènes ou exogènes. De nombreuses bactéries peuvent utiliser des navettes redox qui peuvent être des molécules de la famille des phénazines (*Pseudomonas*) ou des flavines (*Shewanella*). Dans le cas d'un TEE direct, les bactéries peuvent transférer leurs électrons directement des cytochromes de type c qui sont des protéines membranaires, à l'anode, ou via des pili conducteurs appelés nanofilaments. Seuls quelques individus ont été étudiés en détails pour identifier les protéines impliquées dans le TEE, telles que *Shewanella oneidensis* et *Geobacter sulfurreducens*. Pour ces deux bactéries, les cytochromes c de la membrane externe jouent un rôle clé. La Figure 1.9. illustre les modèles proposés de la respiration anodique chez ces deux bactéries.

Geobacter sulfurreducens

Les voies métaboliques impliquées dans la respiration ne sont pas encore bien comprises, même si des avancées importantes ont été réalisées ces dernières années [76]–[82]. La circulation des électrons chez *G. sulfurreducens* est particulièrement complexe et diverse. Les voies métaboliques sont différentes en fonction (i) du potentiel redox de l'accepteur d'électrons, et (ii) du type d'accepteur d'électrons (fumarate soluble, Fe(III) insoluble, électrode ...). Mais certains modèles émergent. Les cytochromes de la membrane interne ImcH et CbcL sont impliqués dans le transfert d'électrons hors du pool de quinones [79], [83], [84]. L'implication de ImcH ou CbcL dépend du potentiel de l'accepteur d'électrons: CbcL est capable de transférer des électrons à une électrode (ou oxydes de Fe(III)) ayant un potentiel inférieur à -100mV et ImcH à une électrode ayant un potentiel supérieur à -100mV. Les mutants ΔimcHΔcbcL (qui ne possèdent donc pas les protéines ImcH et CbcL) ne sont pas capables de réduire l'électrode ou l'oxyde de Fe(III) [81]. Ainsi, leur rôle est indispensable au TEE.

Le travail de Lloyd *et al* suggère que 5 cytochromes-c périplasmiques de la famille PcpA sont également impliqués dans le transfert d'électrons à travers le périplasme [77], [85]. Enfin, les électrons circulent vers le milieu extérieur par des conduits de porine-cytochromes. Plusieurs groupes de ces conduits sont identifiés dans le génome de *G. sulfurreducens*, mais un seul a récemment été identifié comme impliqué dans le TEE vers une électrode de -100mV [81]: le cluster ExtABCD.

Plusieurs cytochromes putatifs de la membrane externe avec des multihèmes ont été annotés dans la séquence du génome, dont un est particulièrement bien étudié le cytochrome OmcZ qui est indispensable pour produire de l'électricité: le mutant ΔOmcZ ne peut pas croître avec une électrode comme accepteur d'électrons mais peut croître avec Fe(III) comme accepteur d'électrons. De plus, OmcZ est insoluble et peut être sécrété dans l'environnement extracellulaire. Il peut alors former une matrice conductrice en association avec des polysaccharides extracellulaires.

Un dernier moyen possible de transférer des électrons à des accepteurs d'électrons insolubles consiste à utiliser des pili ayant une conductivité élevée [36], [86], [87]. La conductivité des nanofilaments chez *G. sulfurreducens* est due à l'arrangement des protéines PilA constituant les pili, donnant une conductivité similaire à celle du métal. Le travail de Leang *et al.* a montré la présence de plusieurs cytochromes OmcS sur les pili [88]. La délétion du gène *omcS* élimine la capacité de réduction du Fe(III) insoluble mais pas l'électroactivité. Cependant il semble nécessaire au transfert d'électrons à une autre bactérie et à la formation de biofilms plus épais [39], [89]. D'autres travaux ont mis en évidence la diversité du potentiel des multihèmes des cytochromes : entre -180 et + 200mV. Ceci est en accord avec le fait que *G. sulfurreducens* pourrait utiliser différentes voies en fonction des potentiels des accepteurs d'électrons. Tous ces résultats ont mis en évidence la complexité et la flexibilité du métabolisme de *G. sulfurreducens*. Une grande diversité de cytochromes associés à une large gamme d'hèmes avec des potentiels différents permet à *G. sulfurreducens* d'utiliser différents accepteurs d'électrons insolubles, montrant une adaptation spécifique au TEE.

Shewanella oneidensis

La voie respiratoire de *Shewanella oneidensis* est relativement bien comprise [90]. Les électrons sont envoyés dans le compartiment périplasmique par l'intermédiaire d'une quinol oxydase CymA, impliquée dans la respiration des accepteurs d'électrons solubles et insolubles. Puis les électrons traversent un conduit de cytochromes c multihémiques: le complexe MtrCAB. MtrC est une réductase terminale impliquée dans la réduction des accepteurs d'électrons insolubles et des flavines [91]–[93]. Un deuxième cytochrome de la membrane externe, OmcA, a été trouvé pour être impliqué dans le TEE.

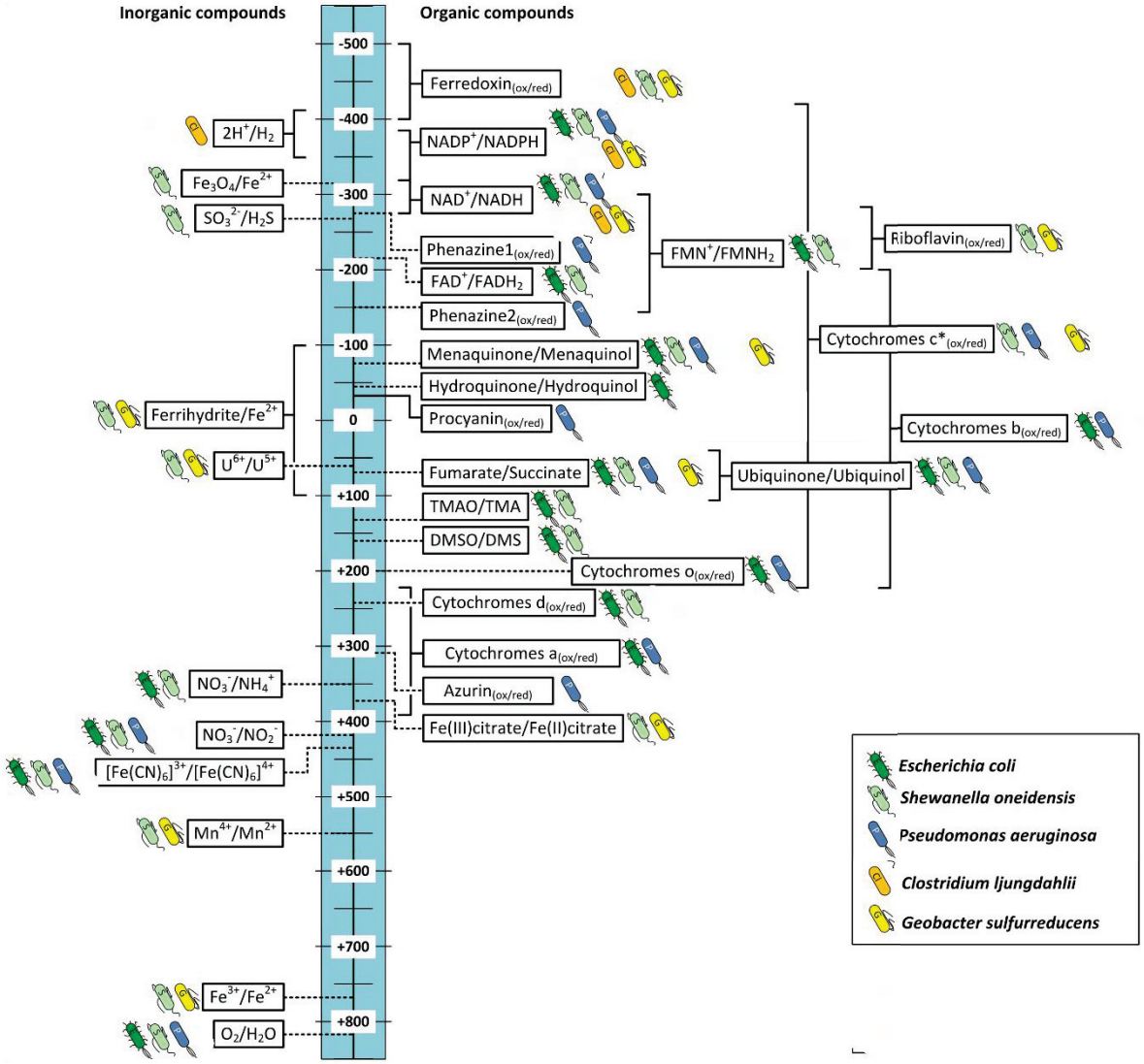

Figure1.8. Potentiels redox des accepteurs d'électrons ou des réactions redox importantes dans la chaine de transport des électrons catalysés par 5 EAB anodiques. Les potentiels redox standard sont indiqués par des lignes en pointillées. Les potentiels redox dans les conditions physiologiques ou environnementales sont indiqués par une ligne continue. La figure est adaptée du travail de Kracke *et al.* [76].

S. oneidensis peut également produire des nanofilaments mais qui sont fondamentalement différents des nanofilaments de *G. sulfurreducens*. Les nanofilaments de *S. oneidensis* sont des extensions de la membrane externe et du périplasme plutôt que des structures faites de piline. Ces extensions contiennent des cytochromes dans la membrane externe permettant un TEE entre ces cytochromes [94]. Si *Shewanella* est capable de TEE direct, elle utilise principalement des molécules redox navettes de la famille des flavines telles que les riboflavines et les flavomononucléotides (FMN). Le travail de Kotloski *et al.* ont démontré que le TEE indirect représentait environ 75% de la capacité des TEEs de *Shewanella oneidensis* [95].

Les autres bactéries

Chez les autres bactéries, les gènes impliqués dans les TEEs sont moins bien compris. En outre, « on pourrait supposer que, quand on les amène au voisinage d'une électrode et en présence d'un produit chimique redox-actif qui interagit avec des navettes redox intracellulaires (par exemple NADH ou quinones), presque tous les micro-organismes conduisent à certain courant électrique » (“it might be assumed that, when brought in the vicinity of an electrode and in presence of a redox-active chemical that interacts with intracellular redox-carriers (e.g. NADH or quinones), almost every microorganism will lead to a certain current flow”) [61]. Un marqueur génétique serait donc utile pour détecter les EAB dans un environnement complexe.

Geobacter et *Shewanella* ont en commun un nombre élevé de gènes codant pour des cytochromes c, laissant supposer que ces gènes pourraient être utilisés comme marqueurs. Sturn *et al.* [62] ont analysé le nombre de cytochromes c de 483 génomes bactériens. Le nombre moyen était de 13 alors que celui de *S. oneidensis* MR-1 est de 41 cytochromes c putatifs et celui de *Geobacter sulfurreducens* est de plus de cent [96]. Leur travail montre une certaine corrélation entre le nombre de cytochromes et la capacité des bactéries aux TEEs. Par exemple, *Shewanella denitrificans* n'a que 14 cytochromes c et est incapable de TEE. Cependant, certaines bactéries ont un plus grand nombre de cytochromes, mais sont incapables de TEE comme *Bradyrhizobium japonicum.* D'autres bactéries ont un nombre plus faible de cytochromes c mais sont capables de TEE tels que *Escherichia coli*.

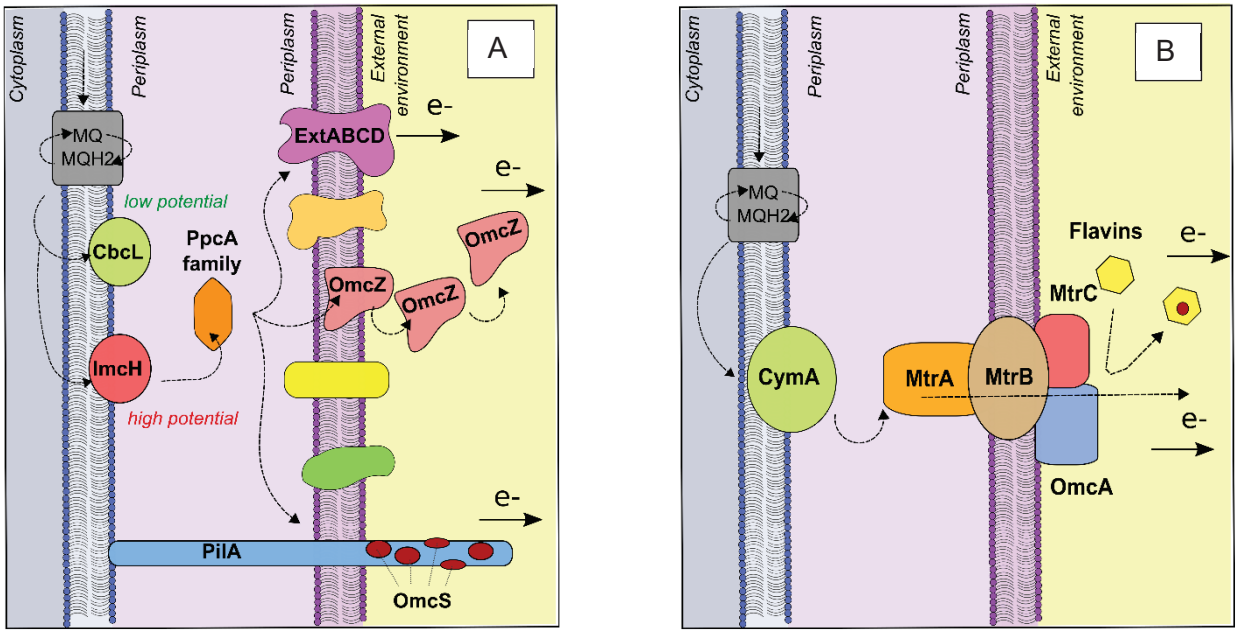

Figure1.9. Proposition de schéma pour le TEE. (A) Modèle de *G. sulfurreducens*. (B) Modèle de *S. oneidensis*

En conclusion, il n'y a pas une seule adaptation écologique des EAB mais deux modes de vie existent: un groupe vivant dans une niche écologique dont les conditions peuvent énormément varier (aérobie ou anoxique), qui sont capable d'utiliser une large gamme d'accepteurs d'électrons et de substrats, et qui utilisent principalement les TEE indirects (représenté par *Shewanella oneidensis)*, et un autre groupe vivant dans une niche écologique plus spécifique, dans un environnement anoxique capable d'utiliser une gamme limitée d'accepteurs d'électrons et de substrats, et utilisant principalement les TEE directs (représenté par *Geobacter sulfurreducens*).

1.4 Conditions hydrodynamiques et formation de biofilms

1.4.1. Formation des biofilms

La dynamique de la formation de biofilms est un processus majeur qui conduit à un biofilm mature, très résistant et résilient. Cinq étapes interviennent dans la formation des biofilms: l'adhésion réversible, l'adhésion irréversible, la formation de microcolonies, la maturation et la dispersion (Figure1.10). Dans un premier temps, les macromolécules présentes dans la solution sont adsorbées à la surface et modifient les conditions de surface et donc la fixation bactérienne. Les bactéries sont amenées à la surface par les mouvements du milieu liquide ou simplement grâce à la mobilité bactérienne. Lors de la première étape, l'adsorption bactérienne est réversible et les bactéries peuvent être facilement détachées de la surface par le flux, puis l'adsorption devient irréversible. L'adhésion n'est pas seulement une adsorption lorsque les bactéries commencent à produire des organelles extracellulaires comme des pili ou des flagelles pour avoir une adhérence physique avec la surface. Par la suite, les bactéries adhérant à la surface se développent et forment des microcolonies. Le biofilm s'étend et les bactéries commencent à sécréter une matrice extracellulaire constituée de polysaccharides: c'est l'étape de maturation. Les polysaccharides extracellulaires (EPS) jouent différents rôles dans (i) l'adhésion, (ii) la cohésion et la structuration du biofilm, (iii) la protection contre les antibiotiques et (iv) comme réservoir d'enzymes, de substrats ou de molécules redox navettes. Dans les BPCMs, la matrice extracellulaire peut considérablement influencer la conductivité du biofilm. Après cela, certaines parties du biofilm se détachent pour coloniser d'autres surfaces. Les bactéries sont dispersées dans l'environnement: c'est l'étape de dispersion

1.4.2. L'adhésion bactérienne

La fixation de bactéries à une surface est souvent considérée comme une étape critique pour la formation de biofilm. Cette étape peut être une étape clé pour la sélection des EAB. Il est nécessaire de comprendre quels paramètres influencent l'adsorption des bactéries sur l'anode. Le modèle DLVO (Derjaguin-Landau-Verwey-Overbeek) [97] est un modèle fréquemment utilisé pour déterminer l'adsorption d'une particule sur une surface. Ce modèle décrit deux types de forces: les forces de Van

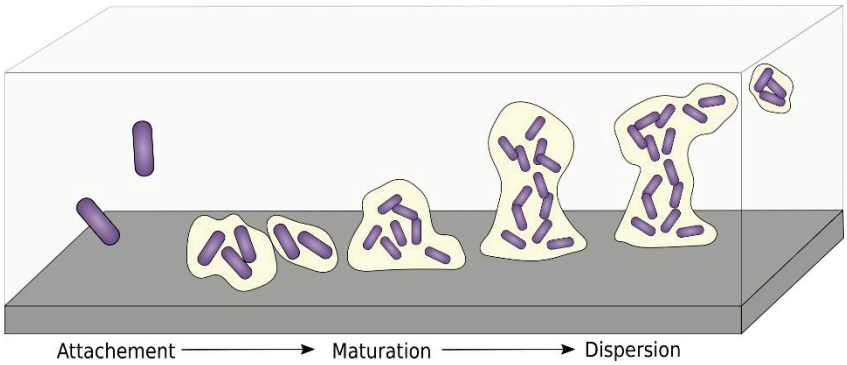

Figure1.10. Schéma de la formation d'un biofilm.

der Waals et les forces électrostatiques. Les forces de Van der Waals sont des forces appliquées entre dipôles. Dans l'eau, ces forces sont toujours attractives et agissent sur de longues distances (plus de 10nm). L'énergie libre due à ces forces entre une surface plane et une sphère est donnée par l'équation (1.14):

$$G_{vdw} = \frac{-Ar}{6d} \quad (1.14)$$

avec G_{vdw} l'énergie libre entre les bactéries et l'anode en J, A la constante de Haymaker en J, r le rayon des bactéries en m, et d la distance entre les bactéries et l'anode en m. La deuxième force, la force électrostatique, est appliquée entre deux surfaces chargées dans un milieu ionique. Les forces sont attractives si les surfaces ont des charges opposées, et répulsives si les surfaces ont les mêmes charges. L'énergie libre de ces forces est donnée par l'équation (1.15):

$$G_{elect.} = \varepsilon r\pi \left(2.P_b.P_s.ln\left(\frac{1+e^{-kd}}{1-e^{-kd}}\right) + (P_b^2 + P_s^2).ln(1-e^{-2kd}\right) \quad (1.15)$$

avec P_b le potentiel de surface des bactéries en V, P_s le potentiel de surface de l'anode en V, k l'inverse de l'épaisseur de la double couche en m^{-1} et ε la permittivité absolue du milieu en F/m. L'épaisseur de la double couche, également appelée longueur de Debye, dépend de la force ionique (1.16):

$$k^{-1} = \left(\frac{\varepsilon k_B T}{2e^2 N_A F_I}\right)^{1/2} \quad (1.16)$$

avec N_A la constante d'Avogadro de 6,022 10^{23} mol^{-1}, e la charge élémentaire de 1,602 10^{-19} C, k_B la constante de Boltzmann de 1,381 10^{-23} $m^2.kg.s^{-2}.K^{-1}$ et FI la force ionique en mol/L défini par l'équation (1.17):

$$F_I = \frac{1}{2}\sum_i C_i z_i^2 \quad (1.17)$$

avec C_i la concentration en ions i en mol/L et z le nombre de charges de l'ion i. L'équation (1.16) montre que l'augmentation de la force ionique diminue l'épaisseur de la double couche, en diminuant la distance à laquelle la force électrostatique s'applique (qui peut varier de plusieurs nanomètres à plusieurs centaines de nanomètres). La force totale, résultant des forces de Van der Waals et des forces électrostatiques est établie en fonction de la distance à l'anode dans la Figure1.11. Deux minimums sont observés: un minimum secondaire correspondant à une adhérence réversible et un minimum primaire correspondant à une adhésion irréversible. Les bactéries doivent traverser la barrière d'énergie, créée par la force électrostatique pour s'approcher de l'anode et tomber dans le minimum primaire. Les forces de Van der Waals étant toujours attractives, les forces électrostatiques sont critiques pour l'adhésion bactérienne. La théorie DLVO est souvent élargie aux forces acide/bases de Lewis qui considèrent les caractéristiques hydrophobes et hydrophiles des deux surfaces [98].

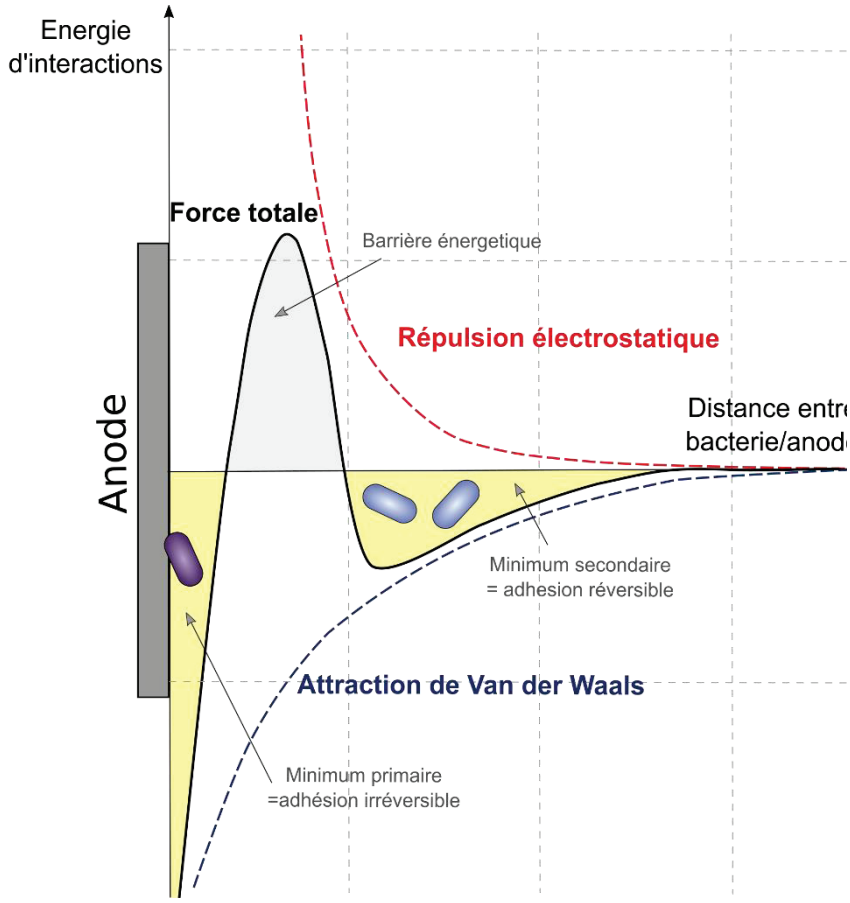

Figure1.11. Forces impliquées dans la théorie DLVO. Energie d'interaction des forces électrostatiques (en rouge), des forces de Van der Waals (en violet) et des forces totals (en noir) en fonction de la distance à l'électrode.

En résumé, l'adhésion bactérienne dépend d'abord de la probabilité de contact de la bactérie avec la surface. Ce processus est influencé par le flux de la solution, la concentration bactérienne et la mobilité bactérienne. Deuxièmement, les bactéries doivent être adsorbées à la surface. Ce processus dépend des caractéristiques physico-chimiques de la surface inerte et de la surface bactérienne: de leurs charges de surface (elles-mêmes dépendante de la force ionique du milieu) et de leurs caractéristiques hydrophiles et hydrophobes. Enfin, l'expression des protéines de la membrane externe et des organites extracellulaires a un impact sur l'adhésion bactérienne au cours de l'étape d'adhésion irréversible. Les rugosités des deux surfaces sont également un paramètre influençant l'adhésion bactérienne.

1.4.3. **La croissance du biofilm**

Après l'adhésion, le développement du biofilm est principalement dépendant de la croissance bactérienne. Dans les études sur les BPCMs, la croissance bactérienne à l'intérieur du biofilm est souvent exprimée comme une équation de Monod avec double limitation en substrats (1.18) [99]–[102]:

$$\rho = q_{max} X \frac{S_D}{S_D + Ks_D} \frac{S_A}{S_A + Ks_A} \qquad (1.18)$$

avec ρ le taux d'utilisation du donneur d'électrons en mol.cm^{-3}.day^{-1}, q_{max} le taux maximal spécifique d'utilisation du donneurs d'électrons en mol.cell^{-1}.day^{-1}, S_D la concentration du donneur d'électrons en mol/L, S_A la concentration d'accepteur d'électrons en mol/L, Ks_D le coefficient de demi-saturation de Monod du donneur d'électrons en mol/L, Ks_A le coefficient de demi-saturation de l'accepteur d'électrons en mol/L et X la densité bactérienne en cell.cm^{-3}. Les donneurs d'électrons sont des molécules carbonatées sous forme d'acétate ou de lactate [103], [104]. L'accepteur d'électrons peut être l'anode [99], ou la forme oxydée des médiateurs redox [100]–[102] si le TEE est indirect. Deux modèles prennent en compte l'effet du potentiel anodique sur la consommation du donneur d'électrons. Marcus *et al.* [99] ont lié le potentiel anodique aux cinétiques d'utilisation du donneur d'électrons par l'équation de Nernst-Monod tandis que Hamelers *et al.* [100] ont utilisé l'équation de Butler-Volmer-Monod. Le potentiel anodique modifie la cinétique d'utilisation du substrat et donc la densité de courant [74], mais modifie aussi la cinétique de croissance des différentes communautés de EAB et la compétition entre les communautés anodiques. Le travail de Torres *et al.* a rapporté une sélection de *Geobacter,* utilisant un TEE direct, avec un potentiel négatif et une plus grande diversité bactérienne, utilisant des médiateurs comme TEE, avec un potentiel positif [105].

La cinétique d'utilisation du substrat associée aux paramètres de transport de masse à l'intérieur du biofilm influence la croissance du biofilm. La concentration de substrat diminue de la solution à la surface et les produits s'accumulent à l'intérieur du biofilm (Figure1.12). Certaines études modélisent l'effet de l'accumulation de protons sur la croissance du biofilm limitant la production d'électricité [104], [106]. La diminution du pH sur la surface anodique diminue l'activité bactérienne. Expérimentalement, il est difficile de mesurer un pH local dans le biofilm. Franks *et al.* [107] ont utilisé une sonde fluorescente sensible au pH couplée à la microscopie confocale à balayage laser pour construire une carte 3D des valeurs de pH dans le biofilm. Ils mesurent un pH de 7 à l'extérieur du biofilm et seulement de 6,1 à l'intérieur. Ce gradient de concentration peut conduire à une stratification du biofilm avec une couche de bactéries mortes en surface et une couche de bactéries actives en contact avec la solution [99]. Dans une communauté complexe, ces gradients peuvent conduire à une sélection spatiale différentielle des taxons bactériens. La nature de la matrice extracellulaire et la densité bactérienne influencent le processus de transport de masse à l'intérieur du biofilm, en modifiant la constante de diffusion.

Un autre paramètre influençant la croissance du biofilm est la conductivité du biofilm due notamment à la densité des nanofilaments, mais aussi à la concentration et à la diffusion des médiateurs redox. Malvankar *et al.* [108] ont rapporté une conductivité élevée dans un biofilm de *Geobacter sulfurreducens* et une diminution du courant associée à une diminution du biofilm. Ils ont fait l'expérience avec un inoculum complexe et observé une conductivité du biofilm comparable à la culture pure de *Geobacter* [109].

1.4.4. **Rôle des contraintes de cisaillement sur la structure du biofilm**

Les forces hydrodynamiques, plus précisément les contraintes de cisaillement, influencent fortement le développement du biofilm que ce soit sur la structure physique ou biologique du biofilm. La contrainte de cisaillement est définie par l'équation (1.19). Cela dépend du gradient de vitesse de l'écoulement et de la viscosité du fluide:

$$\tau = \mu \frac{\partial V}{\partial y} \qquad (1.19)$$

avec τ la contrainte de cisaillement en Pa, μ la viscosité dynamique en Pa.s (environ 1.10^{-3} pour l'eau à 20 °C), v la vitesse du fluide à la distance y de la surface en m/s, et y la distance à la surface en m. Dans un canal soumis à des conditions laminaires, la contrainte de cisaillement dépend de l'écoulement du fluide et des dimensions du canal (1.20):

$$\tau = \frac{6\mu Q}{wh^2} (1.20)$$

avec w la demi largeur et h la demi hauteur du canal en m et Q le débit du fluide en $m^3.s^{-1}$. Les forces et couples appliqués sur une particule sont (i) la traînée hydrodynamique F_p, (ii) le couple hydrodynamique M_t et (iii) la portance F_t (Figure 1.13). La force de traînée est définie par l'équation suivante (1.21):

$$F_p = \tau A_b \qquad (1.21)$$

où A_b est la surface de la bactérie en contact avec le fluide en m^2 et F_p la force de traînée en N.

Effets des contraintes de cisaillement sur la formation des biofilms

La contrainte de cisaillement impacte différents paramètres de la structure du biofilm: (i) l'épaisseur, (ii) la densité, (iii) le pourcentage de bactéries mortes et (iv) l'homogénéité spatiale des biofilms. Pendant l'étape d'adhésion, la force de traînée est opposée à la force d'adhésion. La force d'adhésion peut varier de quelques pN à plusieurs centaines de pN [110]. Une contrainte de cisaillement élevée peut induire un ralentissement de la colonisation anodique en empêchant l'adhésion bactérienne [111]. Peu de bactéries adhérentes peuvent alors se développer rapidement et coloniser toute la surface. Thomen *et al. [91]* ont observé une augmentation du temps de latence en fonction de la contrainte de cisaillement pour une valeur comprise entre 0,42 et 10 mPa mais aucun effet n'a été observé sur le taux de croissance.

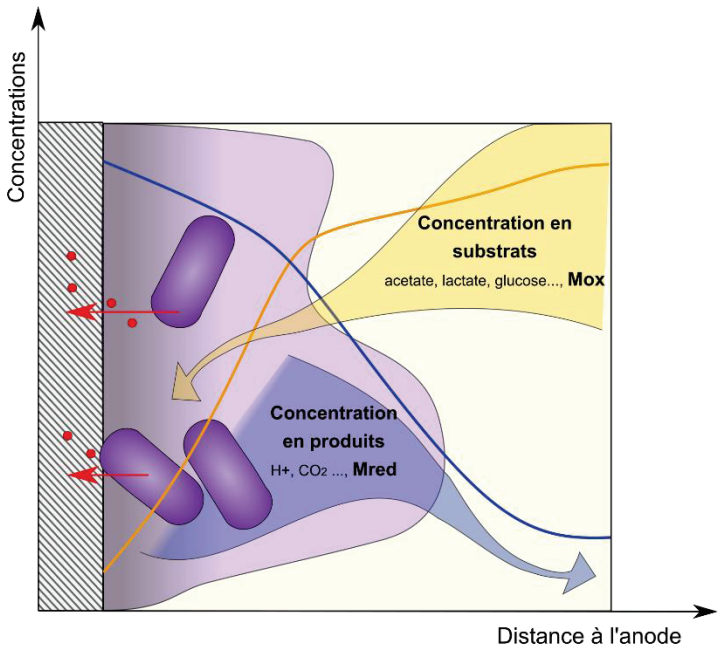

Figure1.12. Schéma du transport de matière au sein du biofilm.

A plus grande échelle, la contrainte de cisaillement modifie la structure du biofilm: sous une contrainte de cisaillement plus élevée, l'épaisseur du biofilm diminue et la densité augmente [110], [112], [113]. Lemos *et al.* [112] étudient l'effet de la contrainte de cisaillement sur la formation de biofilms de *Bacillus cereus* et observent une diminution de l'épaisseur (respectivement 298, 220 et 108 µm pour une contrainte de cisaillement de 20, 120 et 170 mPa) et une augmentation de la densité volumétrique (respectivement 12.9, 28.4 et 66.8 $mg.cm^{-2}$). Cependant, plusieurs études ont observé une épaisseur de biofilm plus élevée dans des conditions de contraintes de cisaillement plus élevées [114], [115]. En effet, la contrainte de cisaillement est d'abord favorable à la formation de biofilms en raison d'une plus grande probabilité de contact entre les bactéries et la surface et d'un meilleur transport du substrat à la surface du biofilm et à l'intérieur du biofilm [116]. Si elle augmente trop, la contrainte de cisaillement devient défavorable, ce qui diminue la croissance bactérienne et augmente la vitesse de détachement. A. Park *et al.* [117] ont observé une contrainte de cisaillement optimale de 0.170 dyn s.cm pour le recouvrement de surface d'un biofilm de *Pseudomonas aeruginosa* PAO1. Aujourd'hui, il n'est pas possible de donner une valeur spécifique de contrainte de cisaillement pour déterminer la gamme de contrainte de cisaillement séparant ces deux situations.

Peu de travaux étudient l'impact de la contrainte de cisaillement sur les communautés bactériennes [114], [118], [119]. Rochex *et al.* [114] ont observé une diminution de la diversité après une semaine lorsque la contrainte de cisaillement augmente (de 55 à 270 mPa). Mais l'analyse de la composition bactérienne a été faite en utilisant la technique SSCP (PCR-single strand conformation polymorphism) qui ne permet pas une bonne identification des bactéries. Des résultats opposés ont été trouvés pour des contraintes de cisaillement plus faibles. Fang *et al.* [119] ont observé que la diversité augmente lorsque la contrainte de cisaillement augmente (de 2.79 à 21.2 mPa). L'analyse du gène de l'ARNr 16S a révélé une composition bactérienne différente dans différentes conditions de contrainte de cisaillement. En plus du fait que la contrainte de cisaillement modifie la communauté bactérienne du biofilm en sélectionnant des bactéries plus résistantes, la contrainte de cisaillement modifie la régulation de l'activité [120]. Par exemple, l'analyse du protéome de *Staphylococcus aureus* a révélé des expressions protéiques différentielles sous une contrainte de cisaillement comprise entre 50 et 1000 mPa.

Effets des contraintes de cisaillement sur les BPCMs

Peu d'études étudient l'effet des contraintes de cisaillement sur les performances des BPCMs [115], [121]–[123]. Pham *et al* [115] ont observé une augmentation de la production d'énergie sous un taux de cisaillement de 120 s^{-1} (environ 120 m Pa) par rapport à un taux de cisaillement de 0.3 s^{-1} (environ 0.3 mPa). L'épaisseur et la densité du biofilm étaient plus élevées sous une contrainte de cisaillement élevée qu'une contrainte de cisaillement faible. Les études de Oliveira *et al.* [121] et Ajayi *et al.* [122] utilisent le nombre de Reynolds comme indicateur de la vitesse de rotation et donc de la force hydrodynamique. Ils montrent une augmentation de la production d'électricité pour un nombre de Reynolds plus élevé: Ajayi *et al.* ont observé un courant électrique plus élevé pour Re = 4900 que pour Re = 900, et Oliveira *et al.* montrent une densité de puissance plus élevée pour Re = 22317 que Re = 2236 ou Re = 11152. Cependant, ces observations conduisent à plus d'interrogations sur l'effet de la contrainte de cisaillement sur la composition bactérienne et sur la structure physique: (i) y a-t-il plus d'interactions et donc plus de transferts d'électrons entre bactéries sous contrainte de cisaillement? , (ii) l'épaisseur du biofilm est-elle plus dense sous contrainte de cisaillement conduisant à une densité de courant plus élevée?, (iii) la proportion de biomasse active est-elle plus élevée en raison du détachement préférentiel de la biomasse morte sous contrainte de cisaillement? y a-t-il une sélection

des EAB sous contrainte de cisaillement ?, (v) les contraintes de cisaillement modifient-t-elles les interactions entre les différentes populations?

En conclusion, peu d'études mettent en évidence le rôle des contraintes de cisaillement sur la composition bactérienne fonctionnelle et taxonomique dans un environnement complexe. Dans le cas des BPCMs, certaines études ont observé une production d'électricité plus élevée en fonction du débit mais la contrainte de cisaillement n'est pas précisément contrôlée et aucune étude n'examine l'effet de la contrainte de cisaillement sur la composition bactérienne ou la structure physique du biofilm.

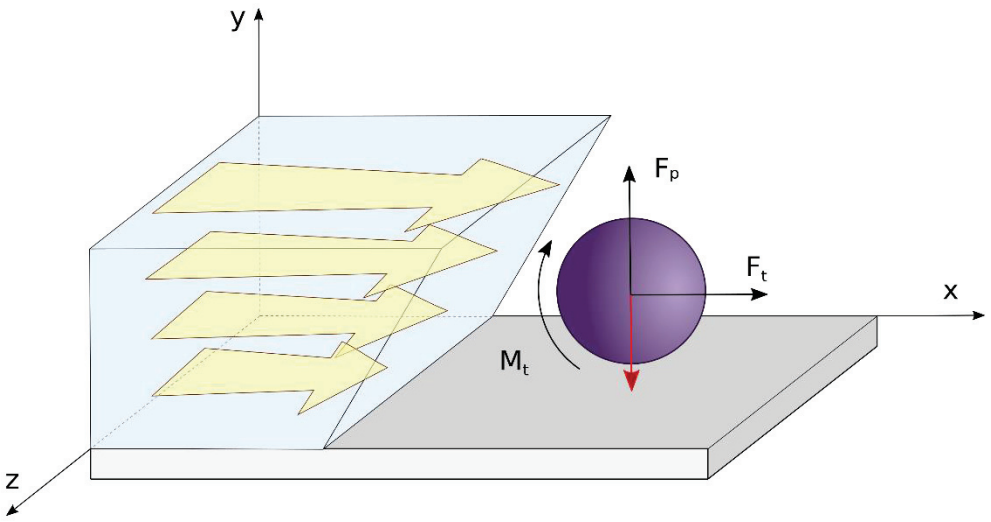

Figure1.13. Forces appliquées sur une particule en conditions laminaires. La flèche rouge symbolise la force d'adhésion. Mt est le moment hydrodynamique, Fp est la force de portance et Ft est la force de traînée.

Résultats expérimentaux

1.1 Competition bactérienne pour la colonization de l'anode en conditions stationnaires.

Depuis quelques années les bactéries électroactives (EAB), capables de réduire les particules magnétiques ou les électrodes, suscitent un vif intérêt. Plusieurs applications découlant de cette particularité semblent de plus en plus réalisables notamment dans les stations d'épuration : les biopiles microbiennes pourraient être utilisées comme source d'énergie durable couplée au traitement des eaux usées ou comme biocapteurs de charges en carbone oxydable dissous. Cependant, le développement de ces applications nécessite plus d'investigations sur les successions de communautés bactériennes et sur la sélection des EAB, lors de la spécialisation du biofilm électroactif à partir des bactéries présentes dans les eaux usées. Le but de cette étude est de comprendre comment se déroule la sélection des EAB, en suivant la compétition ou la synthrophie entre les communautés bactérienne durant la formation du biofilm. Pour cela, les biopiles microbiennes ont été mises en place avec différentes résistances externes, aidant ou bloquant le flux d'électrons. Les formations de biofilms ont été suivies par microscopie à épifluorescence, l'activité électrocatalytique par mesures de puissances maximales et par voltammétries cycliques, et les communautés bactériennes ont été identifiées en fonction du temps par séquençage du gène de l'ARNr 16S. Les principaux résultats montrent deux étapes dans la formation du biofilm: d'abord les EAB non spécifiques avec un métabolisme très flexible et utilisant un transfert extracellulaire d'électrons indirect se développent dans toutes les biopiles, produisant ou non de l'électricité, puis les EAB spécifiques adaptées à un transfert extracellulaire direct deviennent plus compétitives et prédominantes dans le biofilm. La deuxième étape ne s'est produite que dans les biopiles produisant de l'électricité et correspondait à une augmentation exponentielle de la production d'électricité. Les résultats montrent également une compétition entre les EAB spécifiques, en particulier entre *Geobacter* et *Desulfuromonas* au cours de la deuxième étape, mais cela n'a pas conduit à une production d'électricité meilleure ou moindre. Ces résultats donnent plus d'informations pour comprendre et contrôler les formations de biofilms.

1.2 Adhésion des bactéries électroactives sous flux laminaires

L'adhésion des bactéries sur une surface est souvent considérée comme une étape critique pour la formation de biofilm, ce qui peut être une étape clé pour la sélection de EAB. De plus, les forces hydrodynamiques, plus précisément les forces de cisaillement, influent fortement sur l'adhésion bactérienne. Dans cette étude, nous émettons l'hypothèse que les contraintes de cisaillement peuvent sélectionner les EAB sur l'anode durant la phase d'adhésion en détachant les bactéries non électroactives. Les EAB pourraient alors croître et coloniser l'anode sans compétition avec les autres bactéries. Tout d'abord, des biopiles microbiennes avec une configuration en chambre à écoulement de cisaillement, afin d'imposer une contrainte de cisaillement spécifique sur l'anode, ont été conçues et fabriquées. L'évolution de l'adhésion sous différentes conditions de cisaillement (1, 10 et 50 mPa) a ensuite été comparée. Le contrôle utilisé était une biopile classique sans contrainte de cisaillement. La structure microbiologique a été étudiée par séquençage du gène de l'ARN 16S (*rrs*), et le pourcentage de recouvrement a été étudié par fluorescence. Cette étude montre que sous une contrainte de cisaillement élevée, l'abondance relative des EAB spécifiques telle que *Geobacter* était très élevée, jusqu'à 30,14%, en opposition aux contraintes de cisaillement faible où l'abondance relative était inférieure à 1%. En outre, la contrainte de cisaillement diminue le pourcentage de recouvrement de la surface de l'anode, ce qui montre que la sélection des EAB spécifiques se produit par détachement des autres bactéries. La contrainte de cisaillement pourrait donc être utilisée pour sélectionner les EAB spécifiques afin d'augmenter l'électroactivité des biofilms anodiques. Plus d'investigations sont nécessaires pour comprendre l'effet des contraintes de cisaillement sur les biofilms matures.

1.3 Développement de biofilms électroactifs sous flux laminaires

Dans l'environnement comme dans les procédés industriels, les biofilms microbiens sont structurés par les forces hydrodynamiques. Ces forces et plus précisément les forces de cisaillement impactent fortement la structure microbienne mais aussi physique des biofilms. Nous formulons l'hypothèse que les contraintes de cisaillement pourraient être un moyen de contrôler la formation de biofilms à la surface des électrodes des biopiles microbiennes. L'objectif de ce travail est donc d'étudier l'effet de ces contraintes sur la composition biologique du biofilm durant son développement. L'hypothèse principale étant que sous contraintes de cisaillement, les bactéries avec les plus fortes interactions avec l'anode seront sélectionnées, entraînant la sélection de EAB capable de TEE direct avec l'anode. Dans un premier temps, des réacteurs permettant de contrôler les contraintes de cisaillement ont été conçus et construits. Puis l'évolution de la croissance des biofilms sous trois contraintes de cisaillement (1, 5 et 10 mPa) ont été comparés. La structure taxonomique et fonctionnelle a été étudiée par séquençage métagénomique, et la structure physique a été analysée par microscopie à fluorescence.

Ces résultats confirment les conclusions du précédent: les EAB spécifiques ont été sélectionnées sous contraintes de cisaillement. Les biofilms anodiques développés sous 10 mPa présentaient une plus grande abondance relative de EAB spécifiques (35.78±6.70%) dominées par *Geobacteriaceae* que ceux développés sous 1 mPa (16.20±3.14%). A cela s'ajoute le fait que les contraintes de cisaillement ralentissent les cinétiques de croissance des biofilms. Mais après 10 jours, aucune différence sur le pourcentage de recouvrement ou l'épaisseur n'était observée. Ceci est probablement dû à la relative faible gamme de contraintes utilisée. Les contraintes modifient également la proportion de bactéries vivantes et mortes dans le biofilm. Les biofilms formés sous 5 mPa avaient les plus faibles proportions de matière mortes: de plus faibles contraintes de cisaillement ne permettaient peut-être pas de les détacher, et de plus fortes contraintes de cisaillement étaient certainement délétères pour les bactéries. Ce travail démontre le rôle majeur des contraintes de cisaillement dans la formation des biofilms. Ce paramètre devrait être pris en compte dans la conception des réacteurs. L'application de contraintes de cisaillement adaptées pendant le développement de biofilms sur l'anode pourrait être un moyen de contrôler la sélection des EAB mais aussi de conserver un biofilm vivant avec peu de cellules mortes.

1.4 Etude d'une biopile en configuration de réacteur de Taylor

Les conditions hydrodynamiques jouent un rôle majeur dans la formation des biofilms. Ils influencent la composition bactérienne, leurs activités et la structure physique du biofilm, en contrôlant le transport des substrats et des produits à l'extérieur et à l'intérieur du biofilm. Ils contrôlent également les forces de cisaillement appliquées à une surface qui influent la formation du biofilm en termes de densité, d'épaisseur ou de proportion de biomasse morte. Le transport de masse et les contraintes de cisaillement dépendent tous deux des vitesses du fluide. Pour ces raisons, il est difficile d'étudier l'effet de la contrainte de cisaillement indépendamment du transport de masse et du temps de séjour. Afin de résoudre ce problème, une biopile microbienne avec une configuration de réacteur de Taylor a été conçue et construite. Les réacteurs de Taylor ont l'avantage d'être étudiés dans différents domaines, de sorte que les conditions hydrodynamiques sont bien connues. Ils sont composés de deux cylindres: un cylindre interne rotatif et un cylindre externe fixe. Le milieu liquide est présent entre ces deux cylindres. Différents types d'écoulement peuvent être observés en fonction des dimensions du réacteur et de la vitesse de rotation du cylindre interne. A partir d'un nombre de Reynolds critique, les vortex de Taylor peuvent être observés entre les cylindres. Ce travail présente les caractéristiques hydrodynamiques de cette biopile et les expériences préliminaires pour tester la production d'électricité de cette biopile microbienne.

Le réacteur était composé de deux cylindres: un cylindre interne rotatif (ø160x380mm) sur lequel était fixée une anode en tissu de carbone recouvrant toute la surface (1909,12 cm²) et un cylindre externe fixe (ø 189x380 mm) sur lequel 12 cathodes à air (ø 40mm) ont été insérées (surface cathodique: 150.80 cm²). Le volume entre les cylindres était de 3,02 L. La distance entre les cylindres, et donc entre les électrodes était de 14,5 mm. Dans cette configuration, les contraintes de cisaillement ne sont pas

homogènes sur la surface anodique. Ces variations ont été décrites et devraient être prise en compte dans le choix de la vitesse de rotation et de la stratégie d'échantillonnage. Sous une contrainte de cisaillement comprise entre 76,9 et 131,8 mPa, correspondant à une vitesse de rotation de 80 rpm, la biopile avait une puissance maximale de 4,52 mW/m² après 25 jours et un débit en DOB de 1,29 $g.L^{-1}.jour^{-1}$. La biopile était capable de dégrader 63% de la D0B, soit une activité de 0,32 $g.L^{-1}.jour^{-1}$. Les résistances de la biopile après 25 jours étaient de 14,97 ± 0,38 ohms pour la résistance ohmique, de 5,85 ± 0,35 ohms pour la résistance liée à la cathode et de 12,04 ohms pour la résistance liée à l'anode. La croissance du biofilm a été très longue, due d'une part à une limite en substrat et peut-être à une contrainte de cisaillement trop élevée.

La configuration en réacteur de Taylor semble être une bonne solution pour étudier indépendamment la contrainte de cisaillement et le transport de masse dans les biopiles microbiennes, qui sont des paramètres majeurs pour la mise à l'échelle de cette technologie. Davantage d'expériences à différentes contraintes de cisaillement et différents temps de séjour sont nécessaires et devraient fournir plus d'informations sur l'optimisation des paramètres hydrodynamiques pour la mise à l'échelle des biopiles microbiennes.

Conclusion

À travers cette thèse, différents aspects de la dynamique des communautés bactériennes lors de la formation du biofilm ont été mis en évidence. Basé sur le travail de C. Koch *et al.* [[61]], une attention particulière a été accordée aux EAB spécifiques et non spécifiques. Les EAB spécifiques comprennent des bactéries vivant dans un environnement aérobie ou anoxique, capables d'utiliser une large gamme d'accepteurs d'électrons et de substrats et capables d'utiliser des TEE indirects telles que *Shewanella oneidensis*. En revanche, les EAB non spécifiques comprennent des bactéries vivant dans un environnement anoxique, capables d'utiliser une gamme réduite d'accepteurs d'électrons et de substrats, et capables d'utiliser des TEEs directs, telles que *Geobacter sulfurreducens*. Les mécanismes impliqués dans la sélection des EAB ont été également une partie importante de ce travail.

Premièrement, les successions bactériennes ont été étudiées dans des conditions stationnaires et dans des configurations de laboratoire classiques. Trois résultats principaux ont été montrés:

• la formation du biofilm est divisée en deux étapes: une première où les EAB non spécifiques avec un métabolisme très flexible et utilisant un TEE indirect se développent dans toutes les biopiles produisant ou non de l'électricité, puis les EAB spécifiques adaptées aux TEEs directs deviennent plus compétitives et prédominantes dans le biofilm. La deuxième étape ne se produit que dans les biopiles produisant de l'électricité et elle est associée à une augmentation exponentielle de la production d'électricité. De plus, l'abondance relative des EAB spécifiques était positivement corrélée à la densité de puissance maximale, tandis que l'abondance relative des EAB non spécifiques était corrélée négativement à la densité de puissance maximale.

• Les résultats montrent également une compétition au sein des EAB spécifiques, en particulier entre *Geobacter* et *Desulfuromonas* lors de la deuxième étape, mais cela n'a pas conduit à une production d'électricité meilleure ou moindre.

• La sélection des EAB spécifiques s'est produite uniquement dans le biofilm anodique et non dans le milieu liquide contrairement à celle des EAB non spécifiques.

A partir de ces résultats, nous émettons l'hypothèse qu'une inhibition de la première étape devrait diminuer la compétition entre EAB non spécifiques et spécifiques au cours de la colonisation anodique, et favoriser la croissance des EAB spécifiques dans le biofilm. Nous proposons d'utiliser la contrainte de cisaillement pour sélectionner les EAB spécifiques pendant l'étape d'adhérence en détachant les EAB non spécifiques et les bactéries non électroactives. Pour cela, des biopiles avec une configuration en chambre à écoulement de cisaillement ont été conçues, construites et mises en place. Les résultats démontrent que sous une contrainte de cisaillement élevée, l'abondance relative des EAB spécifiques telles que *Geobacter* était plus élevée, jusqu'à 30,14% en opposition à une contrainte de cisaillement faible où l'abondance relative était inférieure à 1%. En outre, la contrainte de cisaillement diminue le pourcentage de recouvrement de la surface anodique, ce qui montre que la sélection de EAB spécifiques se produit en détachant les autres bactéries. Ainsi, la contrainte de cisaillement pourrait être utilisée pour sélectionner les EAB spécifiques dans le but d'augmenter l'électroactivité des biofilms anodiques.

Enfin, l'effet de la contrainte de cisaillement sur la sélection microbienne au cours de la croissance du biofilm a été étudié. Ces résultats confirment les conclusions précédentes: les EAB spécifiques sont sélectionnés sous contraintes de cisaillement. Les biofilms anodiques développés sous 10mPa présentaient une abondance relative plus élevée de EAB spécifiques (35,78 ± 6,70%) dominée par *Geobacteriaceae*, à l'inverse des biofilms anodiques développés sous 1mPa (16,20 ± 3,14%). De plus, la contrainte de cisaillement ralentit la cinétique de développement des biofilms. Mais après 10 jours, aucune différence de pourcentage de recouvrement ou d'épaisseur n'a été observée. La contrainte de cisaillement modifie également la proportion de bactéries vivantes et mortes dans le biofilm. Les biofilms développés sous une contrainte de cisaillement de 5 mPa présentaient la plus faible proportion de bactéries mortes: une contrainte de cisaillement plus faible ne permettait probablement pas le détachement de matière morte, et une contrainte de cisaillement plus élevée était certainement nuisible aux bactéries. Ce travail démontre le rôle majeur de la contrainte de cisaillement dans la formation du biofilm, et devrait être pris en compte dans l'architecture des réacteurs. L'application d'une contrainte de cisaillement pourrait être un moyen de contrôler la sélection des EAB et la quantité de matière morte dans les biofilms anodiques.

Abstract: Chapter 1

The goal of this chapter is to present the fundamental knowledge concerning microbial fuel cells (MFCs) and the basis of this work. The objectives are (i) to summarize the historic evolution of MFCs, (ii) to explain the thermodynamic aspects at the scale of MFCs and at the scale of bacteria, (iii) to present the different limits and the energy losses in MFCs, (iv) to identify the electroactive bacteria (EAB) from a taxonomic, functional and ecological point of view, (v) to present the different steps of biofilm formation, and (vi) to highlight the effects of shear stress during the steps of biofilm formation on the bacterial communities and the physical structure of a biofilm.

The rise in MFCs started in the beginning of 2000s, with the identification of first EAB that became the EAB models, *Shewanella* and *Geobacter*. Today MFC science is divided into two groups: fundamental microbiology that continues to identify EAB and the mechanisms of electron transfer and engineering sciences that regroups the large part of current research. Secondly, the energy losses are not only the classical energy losses in corrosion system but must also to consider the bacterial energy metabolism losses. Moreover, the maximal power density can be strongly increased by increasing current density that can be increased by increasing EAB density on the anode, in opposite to the decrease of the different overvoltages of the MFC that cannot theoretically increase in the same way the electricity production. (iii) Thirdly, two different EAB groups can be identified: one with a specific adaptation of electron transfer using a direct electron transfer, and another with a more versatile metabolism, able to use indirect electron transfer. (iv) Finally, the last chapter presents experiments showing an increase of electricity production under shear stress conditions in MFC, but highlights also the lack of knowledges of the effect of shear stress on anodic biofilms.

Chapter 1.

General Introduction

1.1 History of the Research in MFC

1.1.1. The first steps of MFC research

MFC is a relatively recent topic that was born one century ago. The first research proposing to use microorganisms to produce electricity is attributed to Potter in 1911 [23]. He observed an increase of electricity during the decomposition of organic matter by fermentation using the yeast *Saccharomyces*. Until the 1960s, the interest for MFC was low and there were only minor advances. In 1962, Davis was one of the pioneers to use the expression "Microbial Fuel Cell" [24]. He confirmed a conversion of organic matter into electricity due to the bacterial metabolism and concluded that *"microbial metabolism as a source of measurable electrical energy is established, but as far as we know, no one has made a serious attempt to employ this energy"*. Soon afterwards, in 1963, the NASA wanted to recycle organic waste produced by astronauts into electricity [25], [26]. The interest for MFCs had been revived but electricity generated by microorganisms was still low. In the beginning of 1980s, the work of Bennetto and his collaborators on synthetic mediators was an important development for MFC research [27]–[30]. Synthetic mediators added to the medium increased the electricity production. The comprehension of extracellular electron transfers (EETs) to the anode associated to a large number of publications allowed to revive and popularize the research. Despite that, MFC applications seem still away because the addition of mediators in the medium is an economic and ecologic barrier to large scale and the research on MFC were more considered as a curiosity that a real and useful technology.

1.1.2. The advances in fundamental microbiology

The rise of MFC started really in the beginning of 2000s, as showed in the Figure 1.1 by the increase of the number of publications (A) and the number of citations per publications (B). Fundamental works in microbiology allowed a better comprehension of MFC. Due to the EAB identification, the strategies to select EAB could be implemented. The studies of Kim *et al.* in 1999 [31], [32] allowed to identify *Shewanella putrefaciens* as EAB, then *Clostridum butyricum* in the work of Park *et al.* in 2001 [33]. The discovery of *Geobacter sulfurreducens* as EAB by Bond *et al.* in 2003 marked a turning point [34]. These discoveries led to the study of MFC without synthetic mediators. In 2002, Kim *et al.*, reported the utilization of a mediator less MFC with *Shewanella putrefaciens* as EAB [35]. His work suggested that *"the electron transfer from bacterial cells to the electrode also depends on physical contact between the cells and the electrode"*. The hypothesis that bacteria can transfer their electrons directly to the anode via cytochromes without used mediator was widespread. The discovery of nanowires by Gorby *et al.* in 2006 [36] and Reguera *et al.* in 2006 [37] highlighted the mechanisms employed by bacteria to transfer their electrons and offered new perspectives for MFC research. In parallel, different mutants of *Geobacter* and *Shewanella* were built to determine the genes involved in EET [36]–[40]. This fundamental advances made MFC applications more concrete. The use of MFC to reduce the energetic cost becomes more realistic. Today, the discovery of new EAB and the comprehension of mechanisms involved in EET is still a major issue of MFC research.

1.1.3. MFC as a new technology

Before the middle of 2000s, the research was manly on the anodic compartment and the microbiology of the biofilm. After that, research became more diverse and other disciplines as engineering sciences, material sciences, or green chemistry became more important in MFC research (Figure 1.1 (C)). In 2004, Liu and Logan reported that they had built a MFC with an air cathode [57]. Before their work, MFCs were built with two compartments (the anodic and cathodic compartments) separated by a proton exchange membrane (PEM). The air cathode eliminated the need for the PEM, resulting in a MFC with one compartment. The power density increased due to a decrease of the internal resistance due to a lack of PEM, and a higher molecular oxygen concentration at the cathode because of a higher O_2 concentration in air than in water. In the work of Liu and Logan, the air cathode allowed to double the power density of the MFC. This innovation led to an exponential increase in the number of papers: 13 papers containing the expression "Microbial fuel cell" or "Electroactive bacteria" in the title, the abstract or the keywords in the Scopus database in 2000, 57 in 2005 and 767 in 2015 (Figure 1. (A)). The research on cathodic performances continued. In 2006, He wrote a review on biocathodes suggesting that biocathodes in MFCs could improve the kinetics of the cathode [41] (up until then, the reaction on the cathode was abiotic, and catalyzed by platinum). Two years later, in 2008, Rabaey K. *et al.* developed a biocathode in a MFC capable to reduce O_2 directly [42]. The optimization of biocathodes and the comprehension of bacterial cathodic communities are still an important part of the MFC research. Another part of the research about cathodic compartment was the choice of the electron acceptor: for example, chromium [43], iron [44], or chloride compounds [45] can be used as electron acceptor. Several studies tried to increase the cathodic current by using another electron acceptor than molecular oxygen or by using a microbial biofilm as catalyst. The goal of other studies was to optimize the membrane [46], [47], the electrode structure (anode or cathode) [48], [49], the architecture of MFC [50], [51], and the physico-chemical proprieties as pH, temperature, ionic force… [52]. These improvements were coupled with studies on the applications of MFCs. There are several studies testing the use of MFCs with different types of effluent: domestic, agricultural or industrial wastewater [17], [19], [53]–[55].

The 15th September 2011, The International Society for Microbial Electrochemistry and Technology (ISMET) (*www.is-met.org*) was founded: *"The goal of ISMET is to link researchers from various areas of science and engineering towards studying the complex interactions of microorganisms and electrodes, while finding novel ways to use them for sustainability applications."* Microbial electrochemistry became a distinct disciplinary.

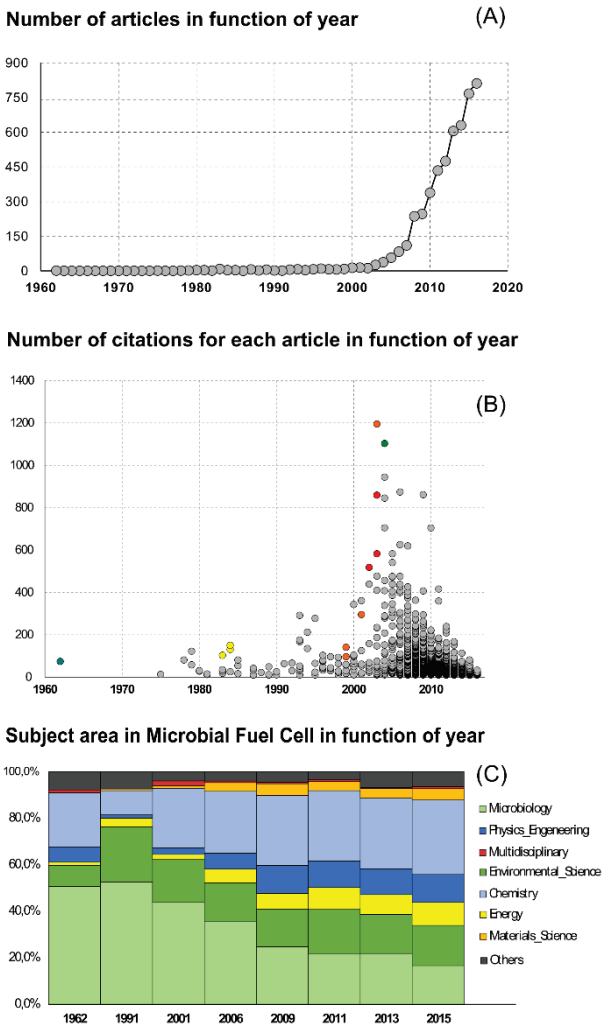

Figure1.1. Evolution of MFC research.

(A) Number of published articles as a function of the publication year.
(B) Number of citations per article as a function of the publication year: blue point is the article of Davis J.B. *et al.* in 1962, yellow points represent the articles of Bennetto *et al.* on mediators in 1983 and 1984, orange points represent the major articles on the discovery of EAB and EET, red points are the first articles about MFC without mediator. Green point is the utilization of air cathode.
(C) Evolution of the subject area in MFC as a function of the publication year. The classification of the subject was done as a function of the journal.
Data come from Scopus database with the research of expression "Microbial Fuel Cell" or "Electroactive bacteria" in the title, keywords or abstract of articles.

1.2 Energy losses in MFC

In order to improve the electricity production, it is important to identify the different energy losses. This chapter describes the parameters used in the electricity production characterization, and identifies the theoretical maximal power of a MFC and the possible energy losses.

1.2.1. Theoretical maximal power generated by a MFC

The power generated by a MFC can be defined by the equation *(1.1)*:

$$P = U.I \qquad (1.1)$$

with P the power density in Watts/m² of anode, U the voltage of MFC in Volts, and I the current density in Ampere/m². To increase the power generated by MFCs, the voltage or the current density of the MFC must be increased.

Maximal voltage of a MFC

The maximal voltage of MFC is fixed by the redox equilibrium potential for each reaction at the anode and the cathode *(1.2)*:

$$U_{max} = E_{eq,c} - E_{eq,a} \quad (1.2)$$

with U_{max} the maximal voltage of the MFC in V, $E_{eq,c}$ the equilibrium potential at the cathode in V and $E_{eq,a}$ the equilibrium potential at the anode in V. The maximal voltage of a specific MFC is measured in open circuit when the current is zero. The equilibrium potential of an electrode is given by the Nernst equation *(1.3)*:

$$E_{eq} = E^0 + \left(\frac{RT}{nF}\right) \ln\left(\frac{[Ox]}{[Red]}\right) \qquad (1.3)$$

with E_{eq} the equilibrium potential of the electrode in V, E^0 the standard potential of the couple Ox/Red in V, $[Ox]$ and $[Red]$ the respective concentration of the oxidant and the reducer in mol/L, R the universal gas constant of 8.31 J.mol^{-1}.K^{-1}, T the temperature in K, *n* the number of exchanged electrons and F the Faraday constant of 96485.33 C. The example described by Logan is reproduced here [56]. If the reaction at the cathode is the reduction of molecular oxygen to water, the equilibrium potential of the cathode would be 0.805 V with a standard potential of 1.229V, a O_2 partial pressure of 0.2 and a pH of 7 *(1.4)*. If the reaction at the anode was the oxidation of acetate into bicarbonate (HCO_3^-), the equilibrium potential of the anode would be -0.296V with a standard potential of 0.187V, a concentration of acetate and HCO_3^- of 5mM, and a pH of 7 *(1.5)*. The maximal voltage of this MFC would be 1.101V.

$$O_2 + 4H^+ + 4e^- \rightarrow 2H_2O \qquad E^{0'} = 1.229V \qquad (1.4)$$

$$2HCO_3^- + 9H^+ + 8e^- \rightarrow CH_3COO^- + 4H_2O \qquad E^{0'} = 0.187V \qquad (1.5)$$

Maximal anodic current of a MFC

The reactions on the anode are considered here as the limiting factors of maximal intensity. So the maximal current would be dependent of the bacterial metabolism and the bacterial density on the anode *(1.6)*:

$$I_{\max} = r_{max} XnF \qquad (1.6)$$

with I_{max} the maximal current density in A/m², X the bacterial density in cell/m² and r_{max} the maximal rate of substrate utilization in mol.cell^{-1}.s^{-1}. The maximal current density of a specific MFC is measured in closed circuit when the voltage of the MFC is null. The maximal rate of acetate consumption by a bacteria is about 2.30 10^{-13} mol.cell^{-1}.day^{-1} [57]. In a perfect situation, without any energy losses, it corresponds to a current of 2.06 10^{-12} A produced by one bacteria. The bacterial density in a biofilm can have very large variation. For example, for a monolayer of EAB (considering that one cell has a surface of 2µm²), the density would be 5.00 10^{11} cell/m², corresponding to a current of 1.03 A/m². A biofilm can grow up to several hundred of micrometers thick.

From the maximal voltage and the maximal intensity, the theoretical maximal power is between 1 (for a perfect monolayer of EAB) and several hundred of W/m² (for a biofilm thickness of several hundred micrometers). The density of EAB plays a major role in the generated power. A better knowledge about the EAB selection on the anode and the physical structure of the anodic biofilm would improve the EAB density on the anode.

1.2.2. **Energy losses**

In the order to determine the real maximal power generated by the MFC, the voltage of the MFC is measured as a function of the intensity to draw a polarization curve (Figure1.2). The polarization curve was initially used to study chemical corrosion [58], [59]. It measures energy losses associated with a progressive decrease in the MFC voltage as a function of the electrical intensity. The difference between the maximal voltage of the cell and the measured voltage for a given intensity is termed "overpotential" η *(1.7)*:

$$\eta = U_{max} - U \quad (1.7)$$

The overpotential η is the sum of the anodic and cathodic overpotential, respectively η_a and η_c, defined by the equation *(1.8)*:

$$\eta_a = E_a - E_{eq,a} \quad and \quad \eta_c = E_c - E_{eq,c} \quad (1.8)$$

Each value of a current density is driven by a certain overpotential. Three types of overpotential are usually identified in corrosion studies: the overpotential of activation, the ohmic resistance and the overpotential of concentration. Each energy loss is associated with a different reaction step of the charge transfer (Figure 1.3). The electrode reactions can be represented by a circuit, which is composed of a series of the resistances representing the different steps (Figure1.4).

Activation overpotential

The activation overpotential is due to the energy activation of the reaction. The activation overpotential is the major overpotential when the mass transfer is not limiting, so when the kinetics are slow. The energy activation is the limiting factor of electricity production for a low current. It

corresponds to the energy loss associated to a reaction and the electron transfer to an electrode. The anodic overpotential of activation is noted $\eta_{act,a}$ and the cathodic overpotential of activation is noted $\eta_{act,c}$.

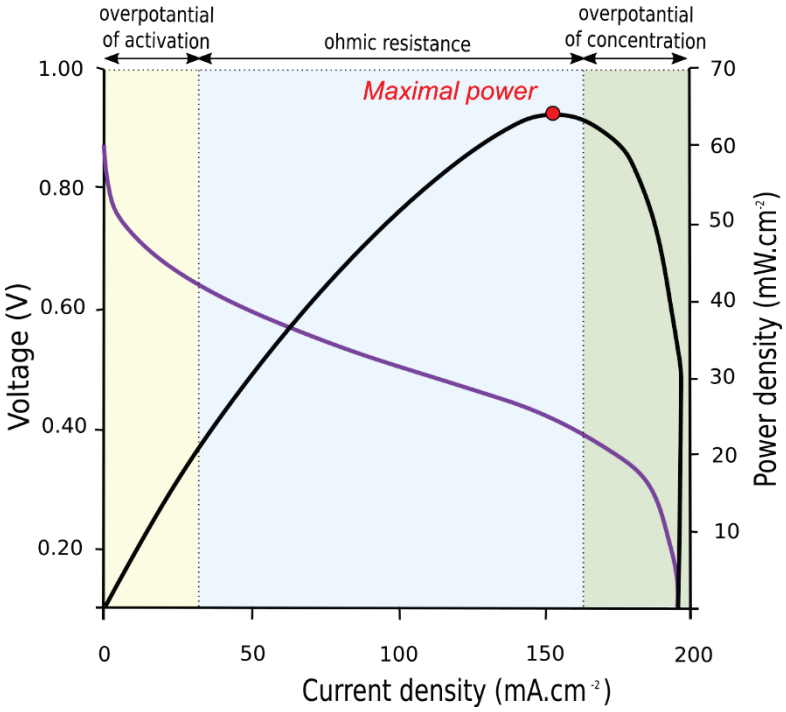

Figure1.2. Polarization curve and power curve. The voltage in function of the intensity is the purple line. The power density in function of the intensity is the dark line.

Ohmic resistance

The ohmic resistance, noted η_{ohmic}, corresponds to the resistance of the connections and the resistance of the medium between anode and cathode. The ohmic resistance is dependent of the medium conductivity and the distance between the anode and the cathode. The quality of the membrane or the salt bridge between the anode and the cathode can also modify the ohmic resistance. The current is related to the ohmic resistance, noted R_{ohm}, by the Ohm's low.

Concentration overpotential

The concentration overpotential corresponds to the resistance associated to the mass transport of the substrate to the electrode. If there is no convection in the medium, the mass transport is only due to the diffusion. In the Figure 1.3, the anodic overpotential of concentration, noted $\eta_{conc,a}$, is associated to the diffusion of acetate to the anode, and the cathodic overpotential of concentration, noted $\eta_{conc,c}$, is associated to the diffusion of O_2 to the cathode. For a redox species Ox/Red, the current is related to the concentration of Ox and Red at the electrode surface (x=0), by the equation (1.9):

$$\frac{I}{nF} = D_{ox}\left[\frac{\partial C_{Ox}(x,t)}{\partial x}\right]_{x=0} = -D_{Red}\left[\frac{\partial C_{Red}(x,t)}{\partial x}\right]_{x=0} \qquad (1.9)$$

with Cox and $Cred$ the concentration of the oxidant and the reducer respectively in mol/L, and Dox and $Dred$ the respective diffusion coefficient of the oxidant and the reducer in m²/s.

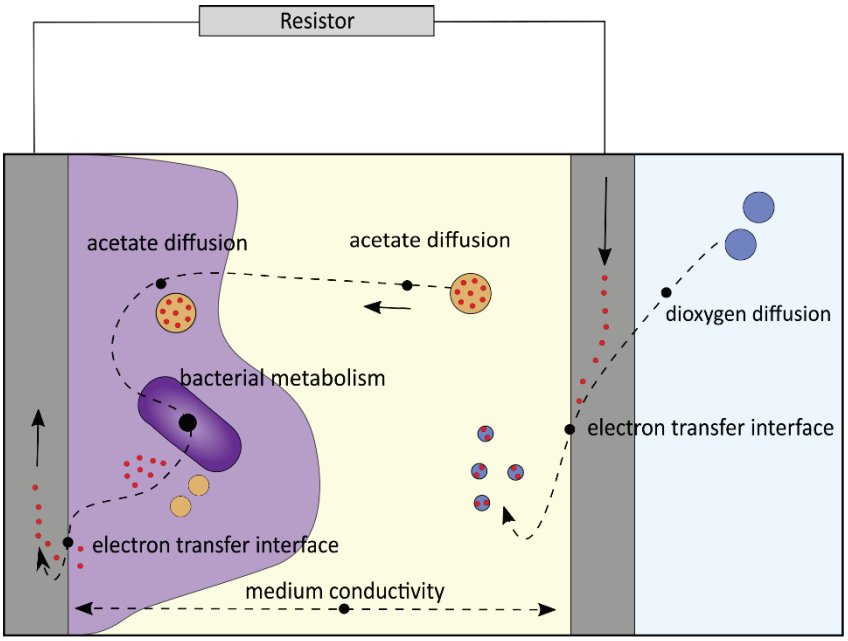

Figure1.4. Schematic of the electron flow and mechanisms associated to energy losses

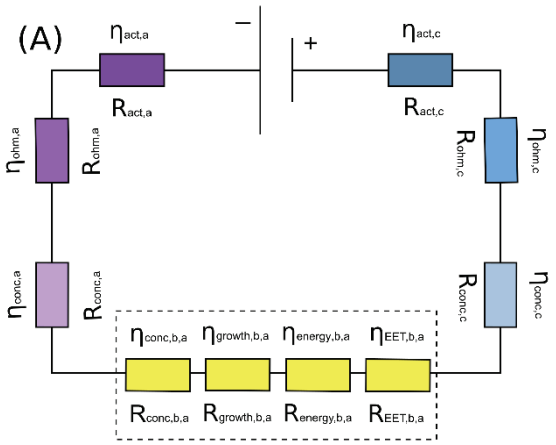

Figure 1.3. Equivalent electrical circuit of a MFC. Equivalent electrical circuit of a MFC with a bioanode and an abiotic cathode such as the MFC represented in the Figure 1.3. Each overpotential is associated to a resistance. Purple and blue resistances correspond respectively to the abiotic steps in the anodic and cathodic compartment. Yellow resistances corresponding to the biotic steps of the anodic biofilm.

Other energy losses

Other energy losses need to be considered in MFC in opposite of classical electrochemical system. The other energy losses are represented in the electrical circuit in the Figure1.4, and are due to the following mechanisms: (i) The presence of a biofilm on the electrode creates a second diffusion barrier

for the substrates, noted $\eta_{conc,b,a}$. This diffusion barrier is dependent on the biofilm density, the nature of extracellular exopolysaccharide and the thickness of the biofilm. (ii) The consumption of the substrate during bacterial growth leads to a loss of electrons, noted $\eta_{growth,b,a}$. If the acetate is not consumed for respiration but for growth, part of the acetate is not oxidized to CO_2 and a percentage of the electrons is lost. (iii) Another energy loss is due to the bacterial metabolism: it is the energy used by bacteria from the substrate, noted $\eta_{energy,b,a}$. The oxido-reduction cascade in the respiratory chain drives a decrease in potential. The result is that the potential of the membrane proteins or the shuttles molecules is lower than the original substrate. (iv) Finally, another resistance is due to the EET or the charge transfer from the bacterial membrane to the electrode, noted $\eta_{EET,b,a}$. If shuttles are used, the diffusion of these shuttles inside the biofilm leads to a non-negligible resistance. If the EET is direct via a membrane protein or via nanowires, the resistance would be lower. The mechanisms of electrons transfer will be described in the section 1.3 and 1.4 of this chapter.

1.2.3. **Capacitance in the MFC**

In any electrochemical system, the electrode/solution interface is analogous to a capacitor. The capacitance of a capacitor is defined by the following equation *(1.10)*:

$$C = \frac{q}{U_c} \quad (1.10)$$

with C the capacitance in F, q the charged stored on the capacitor in C and U_c the potential across the capacitor in V. There is a charge on the electrode, noted q_M, and a charge in the solution, noted q_S, such as *(1.11)*:

$$q_M = -q_S \quad (1.11)$$

The distribution of the whole charges at the electrode/solution interface forms the electrical double layer (Figure 1.5). The double layer is composed of an inner layer called the Stern layer and the locus of the electrical center is called the Inner Helmholtz Plane (IHP), and an outer layer called the diffusion layer with an electrical center called Outer Helmholtz Plane (OHP). The Stern layer is formed of specific adsorbed ions and the diffusion layer is formed of nonspecific adsorbed ions. The thickness of the diffusion layer is dependent of the ionic concentration of the solution. The double layer can affect the current density if the electronegative species are nonspecifically adsorbed and so can approach the electrode only until OHP.

In a biotic system, the presence of a biofilm with his extracellular matrix constituted of polysaccharides can be associated to a capacitor. The membrane proteins such as c-cytochromes can stock a high quantity of electrons. Dependent of bacterial species present in the biofilm, their gene expression, and the composition of the extracellular matrix, the anodic capacitance can be very high. The work of Malvankar *et al.* [60] reported a capacitance of 620µF/cm² of *Geobacter sulfurreducens* biofilm due to the membrane cytochromes. The authors compare the *G. sulfurreducens* to a supercondensators: *"Treating cytochrome hemes as active materials, the computed specific capacitance of DL-1 biofilm is 111 F.g^{-1}, which is comparable to synthetic supercapacitors."*

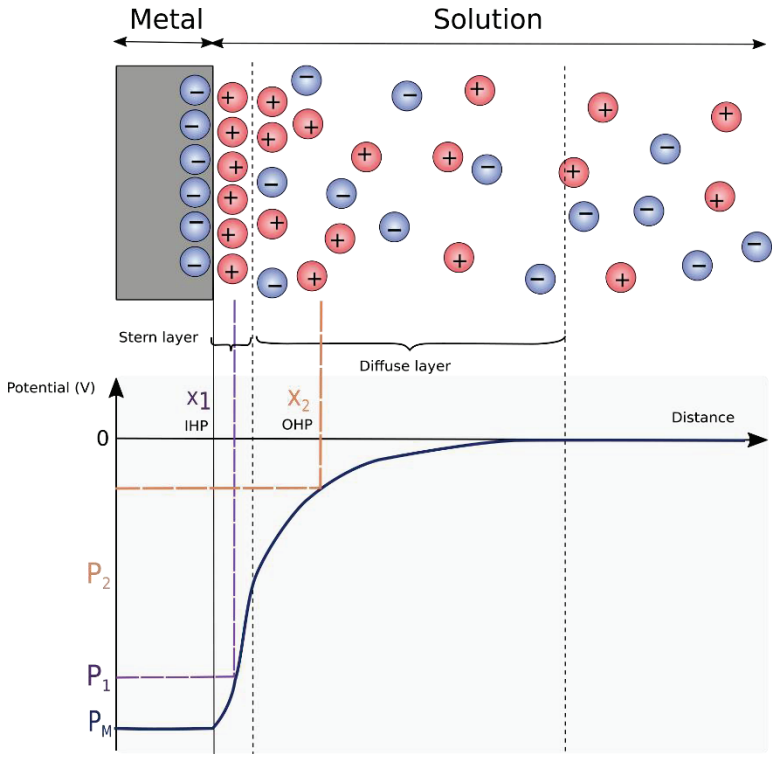

Figure1.5. The electrical double layer. The schematic represents the charge distribution at the electrode/solution interface and the evolution of the potential from the electrode to the solution.

1.3 Identity of Electroactive bacteria

1.3.1. Phylogenetic diversity

Concepts of phylogeny in microbiology

The life is considered to be divided into three domains: *bacteria* (prokaryotes), *archaea* (prokaryotes) and *eukaryota* domains. The taxonomy groups are organized into taxa of a taxonomic rank. Groups of a given rank can be aggregated to form a group of a higher rank, thus creating a taxonomic hierarchy. The different ranks from the higher level to the lower level are domain, phylum, class, order, family, genus, species and strain. Currently, the phylogenetic classification of bacteria is usually done by comparing the 16S ribosomal RNA gene sequence which is a component of a prokaryotic ribosome and is used for phylogeny due to its slow rate of evolution. The dissimilarities in the 16S rRNA gene sequences are markers of the phylogenetic distance between bacteria. For this reason, we assume that bacteria belonging to different species have less than 97% of similarity on their 16S rRNA gene sequence , but there is no accepted rule of similarity for the other higher taxonomic levels. Finally, bacteria with 99% of similarity on their whole genome belong to the same strain. Considering these characteristics, the comparison of the 16S rRNA gene sequence to sequences in databases as SILVA and RDP could provide putative taxonomic identification.

Bacterial diversity in MFCs

EAB belong to a large diversity of taxa (Figure1.6) [61], [62]. The work of C. Koch *et al* inventories 69 species with the capacity for anodic electron transfer, belonging to 37 genus [61]. They are present in 9 subclasses: *Alphaproteobacteria*, *Betaproteobacteria*, *Deltaproteobacteria*, *Gammaproteobacteria*, *Acidobacteria*, *Cyanobacteria*, *Actinobacteria*, *Bacilli*, and *Clostridia*. The two groups, *Deltaproteobacteria* and *Gammaproteobacteria*, are the biggest groups containing respectively 6 and 10 bacterial genus of EAB. The identification of new EAB is a difficult step because of the lack of genetic marker of the electroactivity. To identify a new EAB, it is necessary to enrich, culture and isolate them. For this reason, the current known number of EAB is underestimated. Today, no link between phylogeny and the electroactivity of bacteria has been observed. The democratization of 16S rRNA gene sequencing has led to investigating the taxonomic diversity of the anodic biofilm. The MFCs with a higher relative abundance of *Geobacter* often have the best electrical performances [17]. However, mixed-cultures often generated higher power than pure cultures. Recently, some studies investigated the taxonomic diversity and structure of mixed-species anodic biofilms [17], [63]–[68]. The major taxa varied from one study to another as *Deltaproteobacteria* [67] [68], *Betaproteobacteria* [17], and *Bacteroidetes* [65] were all observed to be the major bacteria present. Stratford *et al.* [66] investigated the relation between different parameters of diversity and power production. Diversity consists of two components: richness and evenness. Richness is the number of taxa in an environment and evenness is the proportion of each taxon and how the abundances of these taxa are equal. They showed that

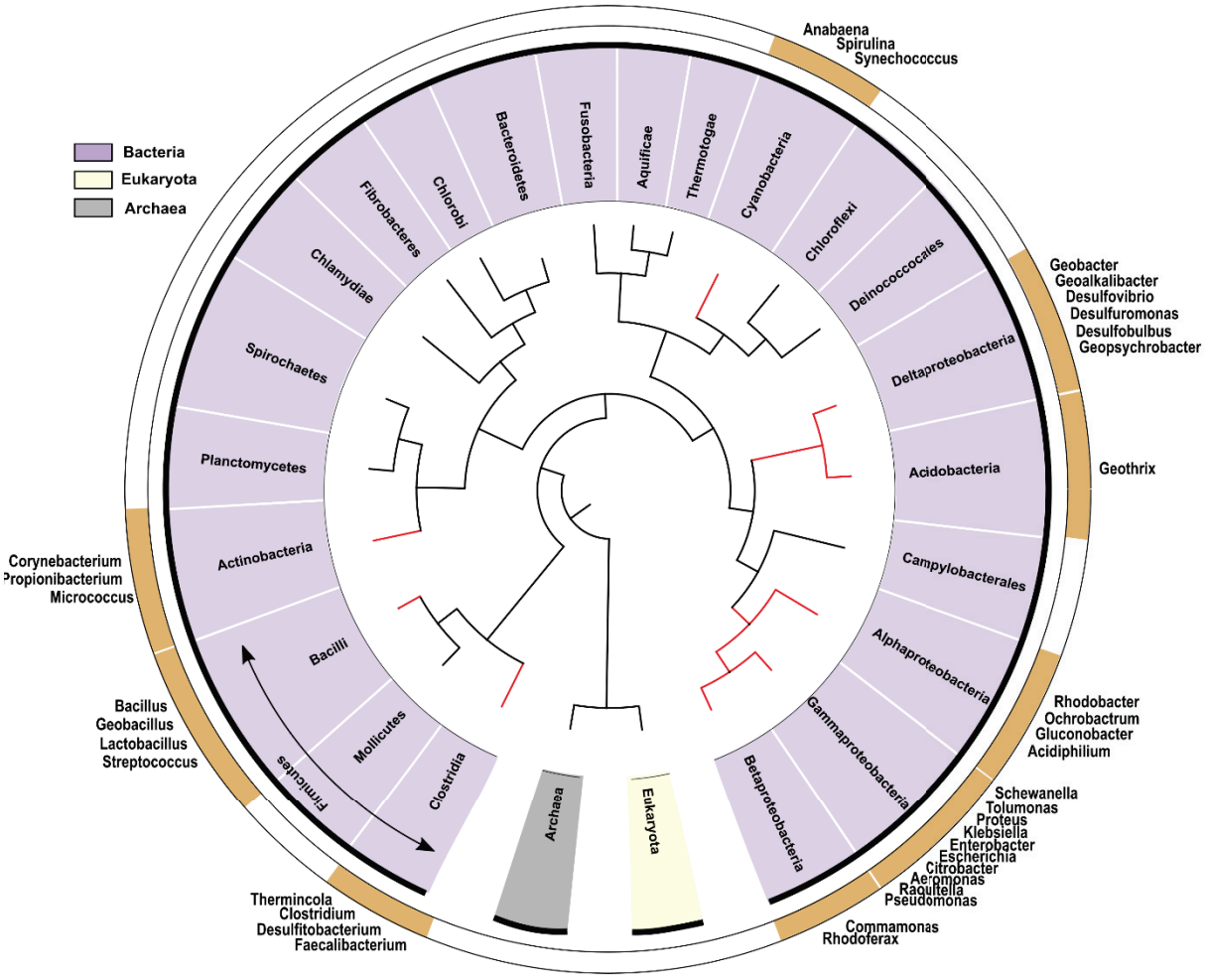

Figure1.6. Phylogeny tree of electroactive bacteria. The figure represents the phylogeny tree of the life. The class taxon of bacteria are represented in purple. In the second circle, the presence of EAB in the corresponding class is represented in red. The genus of EAB are written at the outside of the second circle. The figure was realized from the inventory of anodic EAB in the work of Koch *et al.* [41].

the Shannon index, defined by the equation (1.12), (representative of both richness and evenness) was positively correlated with power production. While in other studies, MFCs with a higher power production had a lower Shannon index [67].

$$H = \sum_{i=1}^{m} p_i . \ln(p_i) \quad (1.12)$$

H is the Shannon index, m the total number of taxa, p_i the proportion of the taxon i. These contrary results represent the lack of knowledge about the ecology of anodic biofilm.

The role of each taxon in electroactivity and biofilm formation is still not well known. Most of the anodic community studies study the biofilm at one point in time. Few studies observed the evolution and the formation of the biofilm, although this would help understand the different bacterial successions during the colonization of the anode [69], [70]. Hodgson *et al.* studied the anodic microbial communities in a MFC cascade at different times. They highlighted the relationship between the fermentative and anodophilic populations in a MFC. Paitier *et al.* showed the interest of looking at early microbial community shifts and that the competition between EAB seemed to be important

during the colonization of the anode. More investigations about biofilm formation kinetics would help understanding of the role of bacterial communities and their interactions in anodic biofilm.

1.3.2. **Energy metabolism of electroactive bacteria.**

Cellular life depends on an energy source, which is stored in chemical form as adenosine triphosphate (ATP). ATP is synthetized by respiration or fermentation. Figure 1.7 describes the bacterial metabolism in general and the bacterial respiration in particular. The electron donor, which is often (but not always) the carbon source, is oxidized to CO_2. The electrons from this oxidation move to the respiratory chain by shuttle molecules such as NADH. In the respiratory chain, there is a cascade of oxidoreduction reactions until an terminal electron acceptor such as molecular oxygen (in aerobic environment), nitrate, iron or an electrode in the case of a MFC (in anaerobic environments). During this cascade of oxidoreduction, protons are produced and secreted in the extracellular compartment, establishing an ion gradient across the membrane. Then, this difference of electrical potential and proton gradient across the membrane is converted into chemical energy for the cell: protons are used by the ATPase to produce ATP. The energy gain for bacteria is dependent to the difference of potential between the couple of electron donor and the couple of electron acceptor. The free energy, G, in $J.mol^{-1}$ is the thermodynamic function used to describe this energy gain and is defined at the equilibrium by the following equation (1.13):

$$\Delta G^{0'} = -nF(E^{0'}_{acceptor} - E^{0'}_{donor}) \quad (1.13)$$

For example, the equilibrium potential of electron donor couple CO_2/acetate is -0.290 V [71], and of electron acceptor couple O_2/H_2O and Fe(III)citrate/Fe(II)citrate are respectively 0.800 and 0.372 V. The Gibbs free energy for the acetate oxidation by O_2 and Fe(III)citrate is also respectively -841.35 $kJ.mol^{-1}$ and -330.36 $kJ.mol^{-1}$. The bacterial growth is affected by this energy gain, resulting in aerobic bacteria growing faster than anaerobic bacteria. For example, the doubling time of *Escherichia coli* under aerobic conditions is about 20 min [72]. However, the doubling time of *Geobacter uraniireducens* was determined to be 18.5 hours with Fe(III)oxide as electron acceptor and 50.1 hours in complex

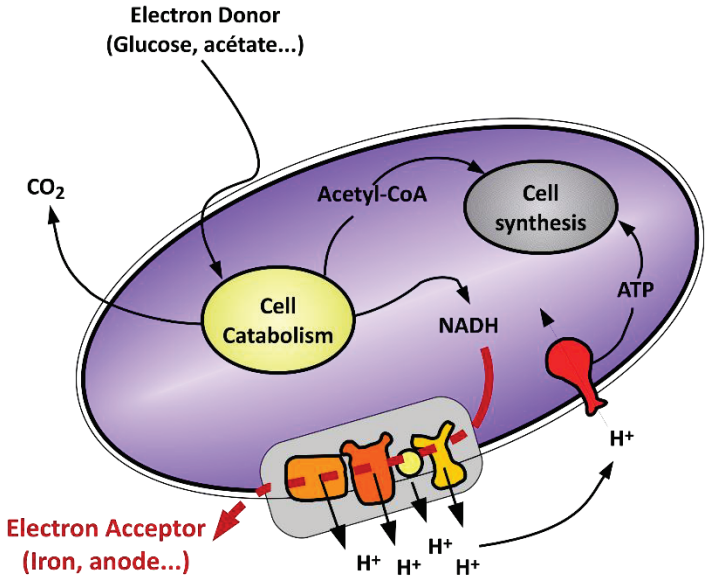

Figure1.7. Bacterial metabolism. Schematic adapted to C.I. Torres *et al.* [54]

environments such as in sediments [73]. In MFCs, the electron acceptor is the anode: anodic respiration. Thermodynamically, a high anodic potential favors the growth of bacteria, but creates a high energy loss in electricity production [74]. The work of Wei *et al.* [75] highlighted the role of anodic potential on the bacterial metabolism. A pure culture of *G. sulfurreducens* grew in MFCs under different anodic potentials (-160, 0 and +400 mV). The lower the anodic potential and the lower the biomass quantity was too, but the higher the current intensity of the MFC was. The closer the anode potential of the anode is to the potential of the electron donor, the lower the energy loss is in MFC and the lower the bacterial growth is.

Different types of metabolisms can be observed among EAB. Kracke *et al.* studies the metabolism of 8 bacteria founded in bioelectrochemical systems including 5 bacteria capable to transfer their electrons to the anode [76] (Figure 1.8.). In their study, three bacteria were capable of growing under aerobic conditions: *E. coli, S. oneidensis* and *P. aeruginosa. E. coli* and *P. aeruginosa* were able to use a large range of electron acceptors such as inorganic and organic compounds except insoluble electron acceptors such as manganese or iron particles. They were also not able to use low redox potential electron acceptors such as sulfates. On the other hand, *S. oneidensis* could use a larger range of electron acceptors: soluble or not, with a low redox potential or not, both organic and inorganic electron acceptors. The second group iwas less flexible: *C. lijungdahlii* and *G. sulfurreducens. G. sulfurreducens* could not use classical inorganic soluble electron acceptor such as nitrates or sulfates, but could use different insoluble electron acceptors. *C. lijungdahlii* could only use low redox potential electron acceptors (less than -300 mV).

1.3.3. **Functional diversity involved in the Extracellular Electron Transfer (EET)**

Several mechanisms can be used by bacteria to transfer their electrons to an insoluble electron acceptor. The transfer can be direct or indirect. During an indirect EET, bacteria used endogenous or exogenous shuttles to transfer their electrons. Many bacteria can use redox shuttles, such as phenazine (*Pseudomonas*) and the flavin (*Shewanella*) family. During a direct EET, bacteria can transfer their electrons directly from outer membrane c-cytochrome proteins to the anode or via the conductive pili named nanowires. Only a few EAB were studied in depth to know the way electrons flow through membrane proteins such as those in *Shewanella oneidensis* and *Geobacter sulfurreducens*. For both species, outer membrane c-cytochromes play a key role in EET. Figure 1.9. shows a model for the respiratory chain of these bacteria

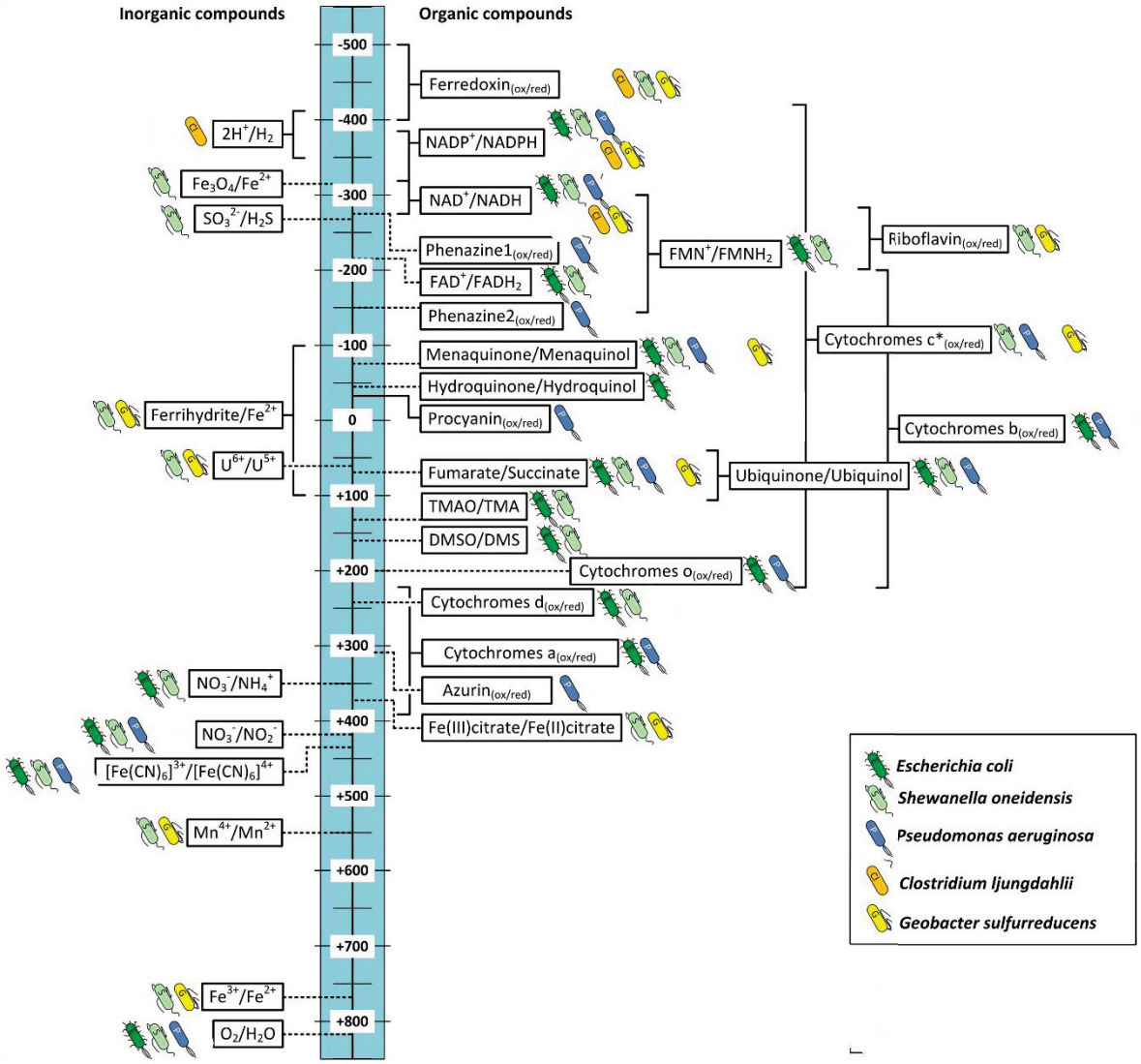

Figure1.8. Redox potentials of electron acceptors or important redox reactions in electron transport chain catalyzed by 5 anodic EAB. Standard redox potentials are indicated by dashed lines. Redox potential in physiological or environmental conditions are indicated by solid line. The figure was adapted from Kracke *et al.* [76].

Geobacter sulfurreducens model

The metabolic pathway in *G. sulfurreducens* is not yet completely understood, even if important progress has been done over the last few years [76]–[82]. The electron transfer pathways in *G. sulfurreducens* are particularly complex and diverse. Pathways differ as a function of the redox potential of the electron acceptor and the type of electron acceptor (soluble fumarate, insoluble Fe(III), electrode…). But some patterns have emerged. The inner membrane cytochromes ImcH and CbcL are involved in the electron transfer out of the quinone pool [79], [83], [84]. The implication of ImcH and CbcL is dependent on the electron acceptor potential: CbcL is able to reduce poised electrode (or Fe(III)oxides) with a low potential less than -100mV and ImcH is able to reduce poised electrode with a high potential more than -100mV. Mutant *ΔimcHΔcbcL* are not able to reduce poised electrode nor Fe(III)oxide [81]. So, their role is indispensable to the EET. The work of Lloyd *et al* suggested that five periplasmic c-cytochromes of PcpA family are also involved in the electron transfer across the periplasm [77], [85]. Finally, electrons are released to the external environment by porin-cytochrome conduit clusters. Several clusters have been identified in the *G. sulfurreducens* genome, but only one was recently identified as involved in the EET to a -100mV poised electrode [81]: the cluster ExtABCD. Several putative outer membrane cytochromes with multihemes were annotated in the genome sequence. One particularly well studied protein, OmcZ, is indispensable for the production of electricity; mutant ΔOmcZ cannot grow with an electrode as electron acceptor, but it can grow with Fe(III) as electron acceptor. In addition, insoluble OmcZ can be secreted in the extracellular environment forming a conductive matrix by association with extracellular polysaccharides. A last possible way to transfer electrons to insoluble electron acceptors is to use pili with high conductivity [36], [86], [87]. The conductivity of nanowires in *G. sulfurreducens* is due to the arrangement of the protein pilA constituting the pili and provides part of the metal-like conductivity to nanowires. The work of Leang *et al.* showed the presence of several cytochromes OmcS in pili [88]. The deletion of the *omcS* gene eliminates the capacity of reduction of insoluble Fe(III) but not the electroactivity, so it seems necessary to transfer the electrons to another bacteria and to form thicker biofilms [39], [89]. Other work has highlighted the diversity of multiheme cytochromes potentials between -180 and +200mV that enables *G. sulfurreducens* to use different pathways as a function of different electron acceptor potentials. These results highlight the complexity and flexibility of the *G. sulfurreducens* metabolism.

Shewanella oneidensis model

The respiratory pathways of *Shewanella oneidensis* are relatively well understood [90]. Electrons are released into the periplasmic compartment via a quinol oxidase CymA that is involved in the respiration of soluble and insoluble electron acceptors. Then, electrons go through a multiheme c-cytochrome conduit: the complex MtrCAB. MtrC is a terminal reductase involved in the reduction of insoluble electron acceptors and the flavin family [91]–[93]. A second outer membrane cytochrome, OmcA, was found to be involved in EET. *S. oneidensis* can also produce nanowires but they are fundamentally different than the nanowires of *G. sulfurreducens*. Nanowires of *S. oneidensis* are outer-membrane and periplasmic extensions rather pilin-based structures. These extensions contain outer-membrane cytochromes that mediate a multistep redox hopping EET [94]. While *Shewanella* is able to use direct EET, it mainly uses shuttle molecules of flavin family such as riboflavins and flavin mononucleotides (FMN). The work of Kotloski *et al.* demonstrated that electron shuttling accounts for about 75% of EET capacity in *Shewanella oneidensis* [95].

Other bacteria

In other bacteria, genes involved in EET are less understood. In addition, “it might be assumed that, when brought in the vicinity of an electrode and in presence of a redox-active chemical that interacts with intracellular redox-carriers (e.g. NADH or quinones), almost every microorganism will lead to a certain current flow” [61]. A genetic marker would be useful to detect EAB in complex environments. Both *Geobacter* and *Shewanella* have a high number of c-cytochrome genes. Sturn *et al.* [62] analyzed the number of c-cytochromes of 483 proteobacterial genomes. The average number was 13 whereas *S. oneidensis* MR-1 has 41 putative c-type cytochromes and *Geobacter sulfurreducens* has more than one hundred [96]. EAB would be adapted to large insoluble electron acceptors with large surface potentials by using a large diversity of c-cytochromes with different redox catalytic sites. Their work [96] shows some correlation between the number of cytochromes and the ability to mediate EET. For example, *Shewanella denitrificans* has only 14 c-cytochromes and is unable to EET. However some other bacteria, such as *Bradyrhizobium japonicum*, have a higher number of cytochromes, but are unable to mediate EET. Other bacteria, such as *Escherichia coli*, have a lower number of c-cytochromes but are able to mediate EET.

In conclusion, there is not one ecological adaptation of EAB but two life-style modes inside EAB: one group, represented by *Shewanella oneidensis*, living in the large ecological niche in an aerobic or anoxic environment and capable of using a large range of electron acceptors and substrates and able to mediate indirect EET, and another group, represented by *Geobacter sulfurreducens*, living in specific ecological niche in an anoxic environment and capable of using a small range of electron acceptors and substrates and able to mediate direct EET.

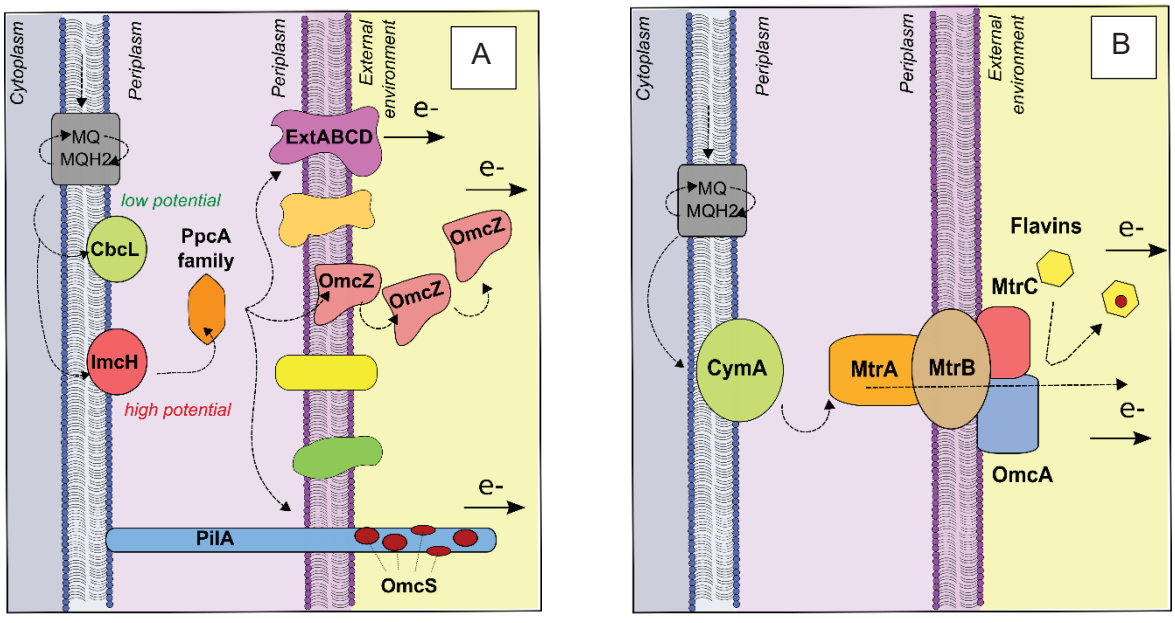

Figure 1.9. Schematic proposition of EET. (A) Model of *G. sulfurreducens*. (B) Model of *S. oneidensis*

1.4 Hydrodynamic and biofilm formation

1.4.1. Biofilm formation

The dynamic of the biofilm formation is a major process that leads to a stable, resistant and resilient mature biofilm. Five stages have been described for biofilm formation: reversible adhesion, irreversible adhesion, microcolony formation, maturation and dispersion (Figure1.10). First, macromolecules present in the solution are adsorbed to the surface and modify the surface conditions and so that the bacteria can attach. Bacteria reach the surface by hydrodynamic flow and/or bacterial mobility. During the first stage, the bacterial adsorption is reversible and they can be detached easily by the hydrodynamic forces. The next step is irreversible adhesion. The adhesion is not just adsorption since the bacteria start to produce extracellular organelles such as pili or flagella that physically adhere to the surface. During the third step, bacteria adhering to the surface grow and form microcolonies. During the fourth step, the biofilm expands and bacteria begin to secret an extracellular matrix constituted of polysaccharides. The extracellular polysaccharides (EPS) play different roles in (i) bacterial adhesion, (ii) cohesion and structuration of the biofilm, (iii) antibiotic protection, and (iv) storage of enzymes, substrates and shuttle molecules. In MFCs, the extracellular matrix can considerably influence biofilm conductivity. Finally during the fifth step, part of the biofilm detaches to colonize other surfaces.

1.4.2. Bacterial adhesion

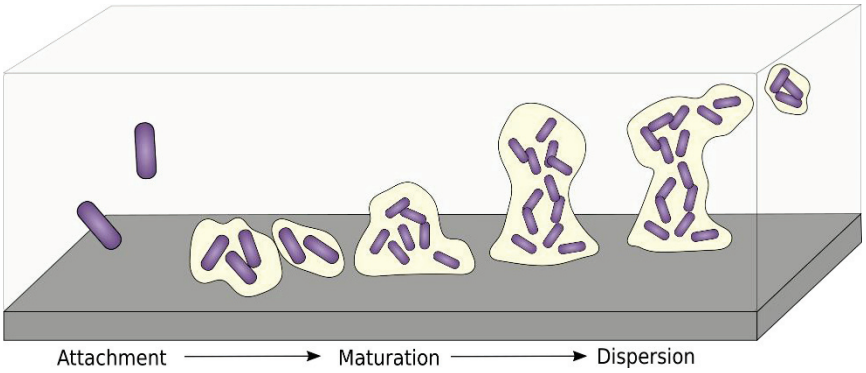

Figure1.10. Schematic of biofilm formation

Bacterial attachment to a surface is often considered as a critical step for biofilm formation. This step can be a key step for the selection of EAB. The parameters that influence the adsorption of bacteria on the anode need to be understood. The Derjaguin-Landau-Verwey-Overbeek (DLVO) model [97] is a model frequently used to determine the adsorption of one particle to a surface. This model describes two types of forces: Van der Waals forces and electrostatic forces. The Van der Waals forces are forces applied between dipoles. In water, these forces are always attractive and act at relatively long distances (more than 10nm). The free energy due to these forces between a plane surface and a sphere is given by the equation (1.14):

$$G_{vdw} = \frac{-Ar}{6d} \quad (1.14)$$

with G_{vdw} the free energy between the bacteria and the anode in Joules, A the Haymaker constant in Joules, r the radius of the bacteria in meters, and d the distance between the bacteria and the anode in meters. The second type of forces, electrostatic forces, are applied between two charged surfaces in an ionic medium. The forces are attractive if the surfaces have opposite charges, and repulsive if the surfaces have the same charge. The free energy of these forces is given by the equation (1.15):

$$G_{elect.} = \varepsilon r\pi \left(2.P_b.P_s.ln\left(\frac{1+e^{-kd}}{1-e^{-kd}}\right) + (P_b^2 + P_s^2).ln(1-e^{-2kd}\right) \quad (1.15)$$

with Pb the surface potential of the bacteria in Volts, Ps the surface potential of the anode in Volts, k the inverse of the double layer thickness in meters^{-1} and ε the absolute permittivity of the medium in F/meter. The double layer thickness, also called the Debye length, is dependent of the ionic force (1.16):

$$k^{-1} = \left(\frac{\varepsilon k_B T}{2e^2 N_A F_I}\right)^{1/2} \quad (1.16)$$

with N_A the Avogadro constant of 6.022 10^{23} molecules . mol^{-1}, e the elementary charge of 1.602 10^{-19} C, k_B the Boltzmann constant of 1.381 10^{-23} m².kg.s^{-2}.K^{-1}and F_I the ionic force in moles/L defined by the equation (1.17):

$$F_I = \frac{1}{2}\sum_i C_i z_i^2 \quad (1.17)$$

with C_i the concentration in ions i in moles/L and z the number of charge of the ion i. The equation (1.16) shows that the increase of ionic force decreases the thickness of the double layer, decreasing the range of electrostatic force (which can vary from several nanometers to one hundred nanometers). The total force resulting from both Van der Waals and electrostatic forces is drawn as a function of the distance to the anode in Figure1.11. Two minima are observed: a secondary minimum considered as a reversible adhesion and a primary minimum considered as an irreversible adhesion. Bacteria need to cross the energy barrier created by the electrostatic force to approach the anode and enter the primary minimum. As the Van der Waals forces are always attractive, the electrostatic forces are critical for bacterial adhesion. The DLVO theory is often extended to Lewis acid/base forces that include the hydrophobic and hydrophilic characteristics of bacterial and anodic surfaces [98].

In summary, bacterial adhesion depends first on the (stochastic) contact with the surface. This process is influenced by the flux of the solution, the bacterial concentration and bacterial mobility. Secondly, bacteria have to be adsorbed to the surface. This process is dependent of the physico-chemical characteristics of the inert surface and the bacterial surface: the surface charge (itself dependent of the ionic force of the medium) and the hydrophilic and hydrophobic characteristics. Finally, the expression of outer membrane proteins and extracellular organelles influences the bacterial adhesion during the irreversible adhesion stage. The roughness of both surfaces is also a parameter influencing bacterial adhesion.

1.4.3. **Biofilm growth**

After the adhesion stages, the biofilm development is more related to the bacterial growth. In MFC studies, the bacterial growth inside the biofilm is often expressed as a double Monod limitation kinetic equation (1.18) [99]–[102]:

$$\rho = q_{max} X \frac{S_D}{S_D + Ks_D} \frac{S_A}{S_A + Ks_A} \qquad (1.18)$$

with ρ the rate of electron donors utilization in mol.cm^{-3}.day^{-1}, q_{max} the specific maximal rate of electron donor utilization in mol.cell^{-1}.day^{-1}, S_D the electron donor concentration in mol/L, S_A the electron acceptor concentration in mol/L, Ks_D the Monod half saturation coefficient of the electron donor concentration in mol/L, Ks_A Monod half saturation coefficient of the electron acceptor concentration in mol/L and X the bacterial density in cell.cm^{-3}. The electron donor is the concentration of organic molecules such as acetate or lactate [103], [104]. The electron acceptor can be the anode [99] or the oxide form of mediators [100]–[102] if the EET is indirect via mediator utilization. Two models take into account the effect of anodic potential on the rate of the electron donor. Marcus *et al.* [99] linked the anodic potential to the electron donor rate by the Nernst-Monod equation while Hamelers *et al.* [100] used the Butler-Volmer-Monod equation. The anodic potential modifies the rate of utilization of the substrate and thus the current density [74], but it also modifies the growth kinetics of the different EAB populations and the competition between the anodic communities. Torres *et al.*

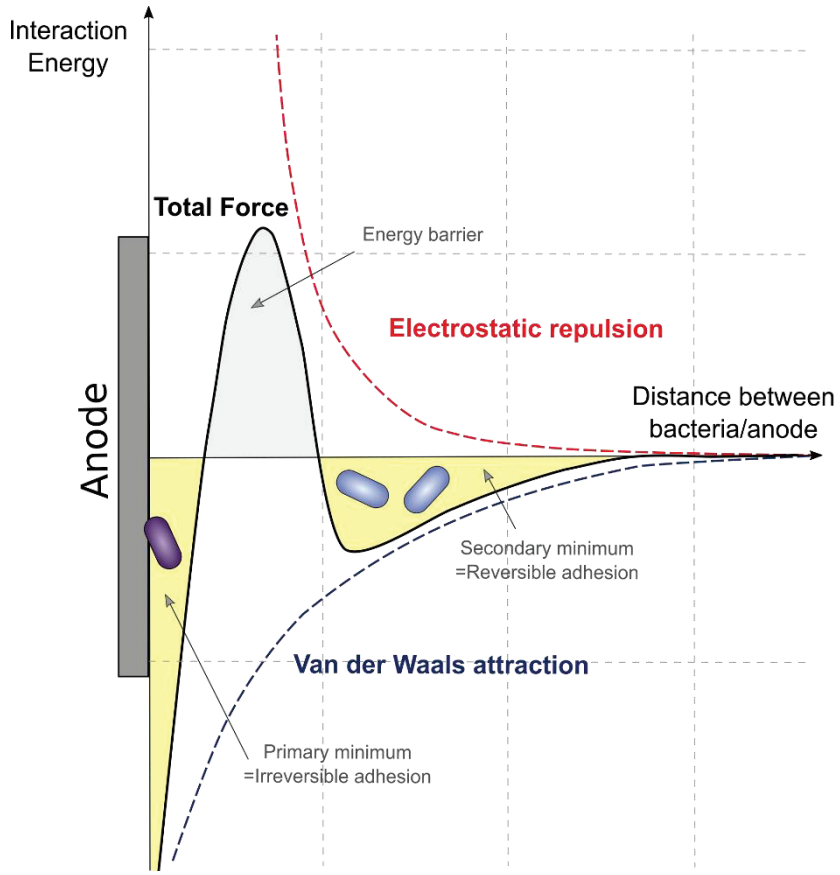

Figure 1.11. Forces involved in the DLVO theory. The interaction energy in function of the distance to the electrode for the electrostatic force (in red), the Van der Waals force (in purple), and the total force (in black).

reported *Geobacter* selection by using a direct EET with a negative potential and a higher bacterial diversity using mediators for EET with a positive potential [105].

The kinetics of substrate utilization associated with the mass transport parameters inside the biofilm influence biofilm growth. The concentration of substrate decreases from the bulk solution to the surface and the products accumulate inside the biofilm (Figure1.12). For example, some studies model the effect of proton accumulation on biofilm growth that limits electricity production [104], [106]. The decrease in pH on the anodic surface decreases bacterial activity. Experimentally, pH is difficult to measure locally in the biofilm. Franks *et al.* [107] used a pH-sensitive fluoroprobe and confocal scanning laser microscopy to build a 3D map of pH in the biofilm. They measure a pH of 7 at the exterior of the biofilm and only 6.1 at the interior. This pH gradient might lead to a stratification of the biofilm with a layer of dead bacteria on the surface and a layer of active bacteria in contact with the solution [99]. In a complex community, these gradients could lead to a spatial selection of bacterial taxa. The nature of the extracellular matrix and the bacterial density influences the process of mass transport inside the biofilm and modifies the diffusion constant.

Another parameter influencing biofilm growth is the conductivity of the biofilm due to the density of nanowires and to the concentration and the diffusion of mediators. Malvankar *et al.* [108] reported a high conductivity in the biofilm composed in part of *Geobacter sulfurreducens* and a decrease in the current associated to a decrease in the biofilm. They did the experiment with a complex inoculum and observed biofilm conductivity comparable to pure culture of *Geobacter* [109].

1.4.4. **Role of shear stress on biofilm structure**

Hydrodynamic forces, especially shear forces, strongly influence development of the physical and the biological structure of the biofilm. Shear stress can be defined by the equation (1.19). This force is dependent on the flow velocity gradient and the fluid viscosity:

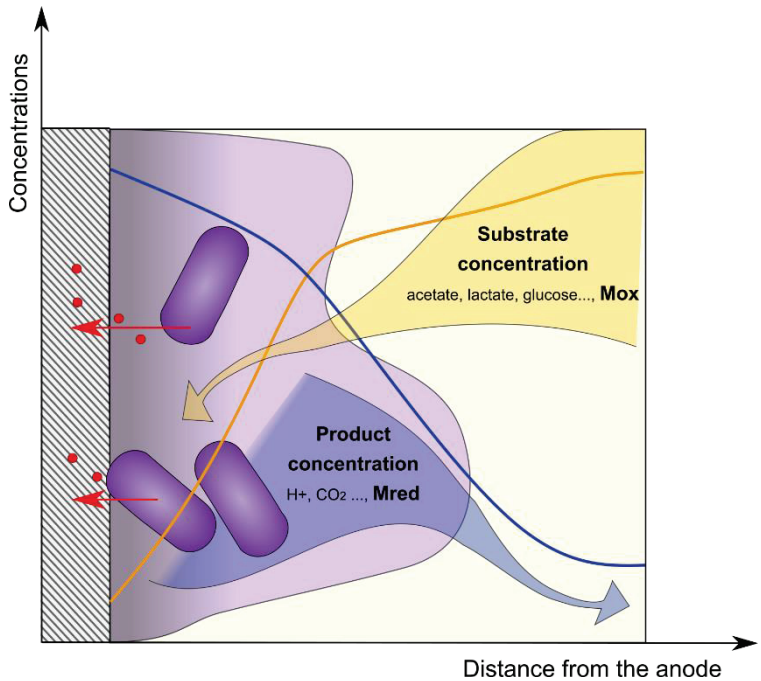

Figure1.12. Mass transport inside the biofilm

$$\tau = \mu \frac{\partial V}{\partial y} \qquad (1.19)$$

with τ the shear stress in Pa, μ the dynamic viscosity in Pa.s (about 1.10^{-3} for water at 20°C), v the velocity of the fluid at the distance y of the surface in meter per second, and y the distance to the surface in meters. In a channel under laminar conditions, the shear stress can be expressed as a function of the fluid flow and the channel dimensions by the equation (1.20):

$$\tau = \frac{6\mu Q}{wh^2} (1.20)$$

with w the half width and h the half height of the channel in meters and Q the fluid flow in cubic meters per second. The forces and torques applied on a particle are (i) the hydrodynamic drag F_p, (ii) the hydrodynamic torque M_t, and (iii) the lift F_t (Figure 1.13). The drag force can be defined by the following equation (1.21):

$$F_p = \tau A_b \qquad (1.21)$$

where A_b is the area of the bacteria in contact with the fluid in square meters and F_p the drag force in Newtons.

Effect of shear stress on biofilm formation

The shear stress influences different parameters of the biofilm structure: (i) the thickness, (ii) the density, (iii) the percentage of dead bacteria and (iv) the spatial homogeneity of biofilm. During the adhesion step, the drag force is opposite to adhesion force. The adhesion force can vary from few to hundreds picoNewton [110]. During reversible adhesion, adhesion is due to the adsorption of bacteria onto the surface and the force is lower than during irreversible adhesion, when bacterial EPS are linked by proteins to the surface. A high shear stress can induce a slow-down of the anode colonization process by preventing bacterial adhesion [111]. Then, the few adhered bacteria could grow quickly and colonize the entire surface. Thomen *et al.* [111] observed an increase in the lag time as a function of the shear stress for values between 0.42 and 10 mPa although no effect was observed on the growth rate.

Under higher shear stress, the biofilm thickness decreases and the density increases [110], [112], [113]. Lemos *et al.* [112] study the effect of shear stress on *Bacillus cereus* biofilm formation and observe a decrease in the thickness (respectively 298, 220 and 108 µm for a shear stress of 20, 120 and 170 mPa) and an increase in volumetric density (respectively 12.9, 28.4 and 66.8 $mg.cm^{-2}$). However, several studies observed an increased biofilm thickness under higher shear stress conditions [114], [115]. In fact, shear stress is at first favorable for biofilm formation due to a higher probability of contact between bacteria and the surface and due to a better substrate transport to the surface of the biofilm and thus within the biofilm [116], but then shear stress becomes unfavorable, decreasing bacterial growth and increasing the rate of detachment. Park *et al.* [117] observed an optimal shear stress of 0.170 dyn s.cm for the surface coverage of a *Pseudomonas aeruginosa* PAO1 biofilm.

Few papers study the impact of the shear stress on bacterial communities [114], [118], [119]. Rochex *et al.* [114] observed a decrease in microbial diversity after one week when the shear stress was increased (from 55 to 270 mPa). On the other hand, for the microbial community analysis, PCR-single strand conformation polymorphism (SSCP) technique, which does not identify the bacteria, was used. Conflicting results were found at smaller shear stress. Fang *et al.* [119] observed that the bacterial diversity increased when the shear stress increased (from 2.79 to 21.2 mPa). Their 16S rRNA gene analysis revealed different bacterial communities under different shear stress conditions. In addition

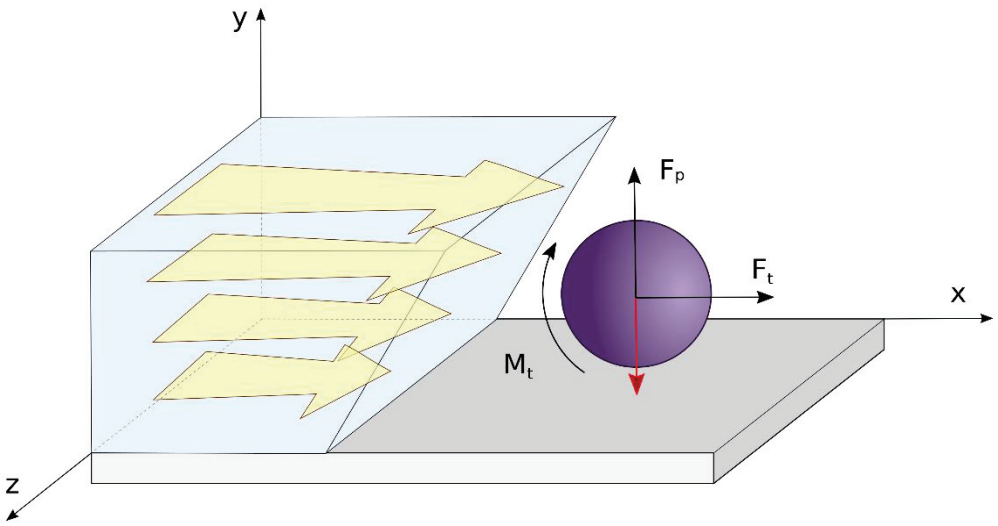

Figure 1.13. Forces applied on a particle under laminar conditions. The red arrow symbolizes the adhesion force. Mt is the hydrodynamic moment, Fp is the hydrodynamic drag and Ft is the hydrodynamic lift.

to shear stress modifying the biofilm bacterial community by selecting more bacteria that are resistant the physical force, shear stress also appears to modify gene expression [120]. For example, the analysis of the *Staphylococcus aureus* proteome revealed differential protein expression under shear stresses between 50 and 1000 mPa [120]. But it is difficult to know if this differential expression is due to a shear stress or a mass transport change.

Effect of shear stress on MFC

Few studies investigate the effect of the shear stress on MFC performances [115], [121]–[123]. Pham *et al* [115] observed an increase in power production under a shear stress of about 120m Pa (120 s^{-1}) in comparison to a shear stress of about 0.3 mPa (0.3 s^{-1}). The thickness and the density biofilm were higher under a high shear stress than a low shear stress. Oliveira *at al.* [121] and Ajayi *et al.* [122] used the Reynolds number as an indicator of the rotation speed and thus the hydrodynamic force. They showed an increase in electricity production at higher Reynolds numbers: Ajayi *et al.* observed a higher electrical current for Re=4900 than for Re=900, and Oliveira *et al.* show a higher power density for Re=22317 than Re=2236 or Re=11152. However, these observations lead to more questions than answers about the effect of shear stress on the bacterial composition and on physical structure: (i) are there more interactions and so more electron transfer between bacteria under shear stress than static conditions? (ii) is the biofilm thickness more dense under increased shear stress conditions leading to a higher current density? (iii) is the proportion of the active biomass higher due to the preferential detachment of dead biomass under increased shear stress conditions? (iv) is there a selection of EAB under increased shear stress conditions? and (v) does shear stress modify the interactions between different bacterial populations?

In conclusion, few studies highlight the role of shear stress on functional and taxonomic bacterial composition in complex environment. In MFCs, some studies observed a higher electricity production as a function of fluid flow but the shear stress was not correctly controlled and no study investigated the effect of shear stress on electroactive anodic biofilms, on bacterial composition, or physical structure.

Abstract: Chapter 2

This chapter aims to define the principle of the methods used throughout this thesis. As MFCs are a recent and multidisciplinary subject, young researchers often have to learn experimental methods outside their field of expertise. In this context, this chapter aims to define the principles and the limits of the different experimental methods used such as electrochemical analysis, microscopy or sequencing. In addition, the design, manufacture and implementation of microbial biopiles is on the one hand an important step in this work and research on MFCs in general, and on the other hand is a work often overlooked in scientific publications. This chapter describes this approach in more detail.

Chapter 2.

Methodology

2.1 Reactor conception

2.1.1. MFC bottles

MFCs with a “classical” configuration were used (Figure 2.1). The cathode was an air cathode created by following the procedure of Cheng *et al*. [124]. It contains one catalytic slide (the inner side) and one diffusion side (the outer side). The catalytic side is composed of carbon powder with 5% platinum powder. The diffusion side is composed of 4 layers of PTFE (Polytetrafluoroethylene). Two different types of anodes were used: carbon cloth and graphite rod (without platinum). The carbon cloth has a high resistivity in comparison of graphite rod (respectively about 50 ohms/cm and 2 ohms/cm). The microscopic surface is very different: the active surface of the carbon cloth is much higher than the active surface of graphite rod.

2.1.2. Inoculum

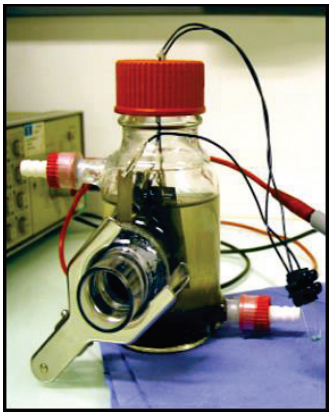

Figure 2.1. MFC bottle with an air cathode.

The samples of wastewater or sludge come from the wastewater plant station of Feyssine (69120 Vaux-en-Velin). Wastewater upstream of the plant station was used as medium. Dehydrated active sludge was

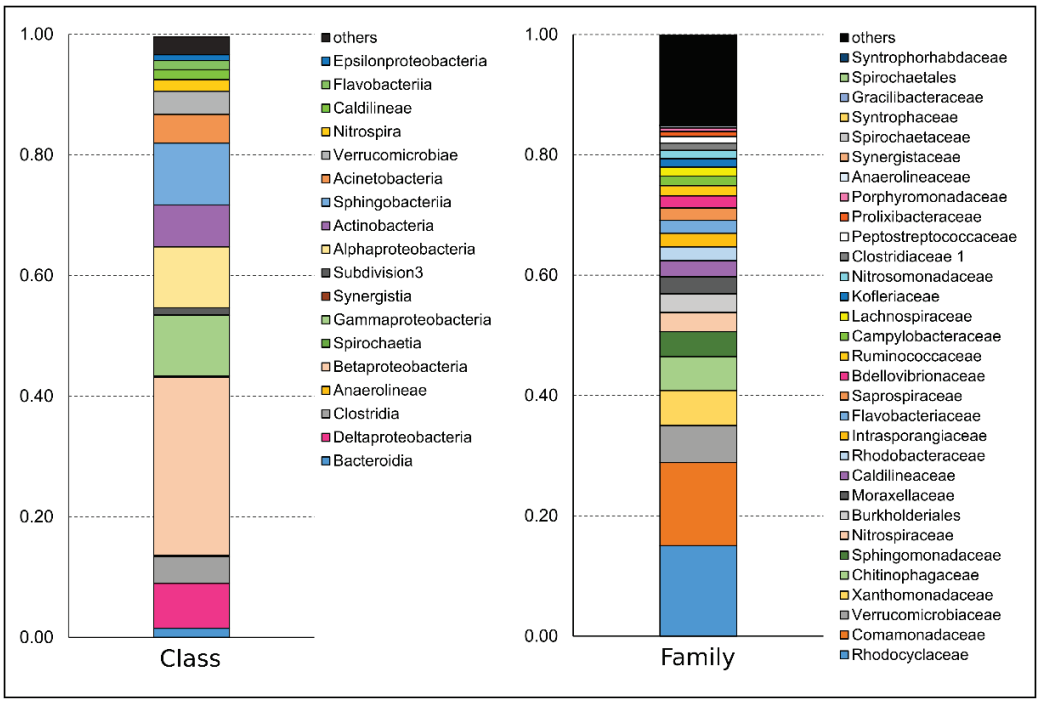

Figure 2.2. Bacterial community composition at class and family levels in active sludge.

added at 4g/L. The medium was amended by 1g/L of acetate sodium. The Figure 2.2 shows the bacterial composition of active sludge. The major class was *Betaproteobacteria* and the major families were *Rhodocyclaceae* and *Comamonadaceae*. The Shannon index was 4.15 (based on the number of genus) and 368.20 genus were detected (mean after 100 replicates on sampling of 26000 sequences).

2.1.3. **Microfluidic multichannel MFCs**

Reactor design

In the Chapter 4 and 5, the biofilm formation was studied as a function of the time for different shear stress. First, MFCs with a shear stress flow chamber configuration was designed and built. The goal was to control shear stress applied on the anodic surface, so the reactor should fit different constraints: (i) a homogenous shear stress over space and time on the anodic surface, (ii) an easy control of shear stress, (iii) an anodic surface large enough to extract DNA after an hour, (iv) an easily removable anode for sampling. The configuration of a shear stress flow chamber was chosen for the quality control and the homogeneity of the shear stress. The characterized hydrodynamics of this configuration was done previously by S. Lorthois *et al.* [125], [126], and the forces applied on a particle wit this configuration were given by M.E. O'Neil [127]. The dimensions were adapted to have a higher anodic surface. The electrodes were added to the configuration. Three multichannel reactors were built (Figure 2.3). Each reactor consisted of (i) one upper PMMA plate B (500x240x20 mm), (ii) one bottom PMMA plate A (500x240x20

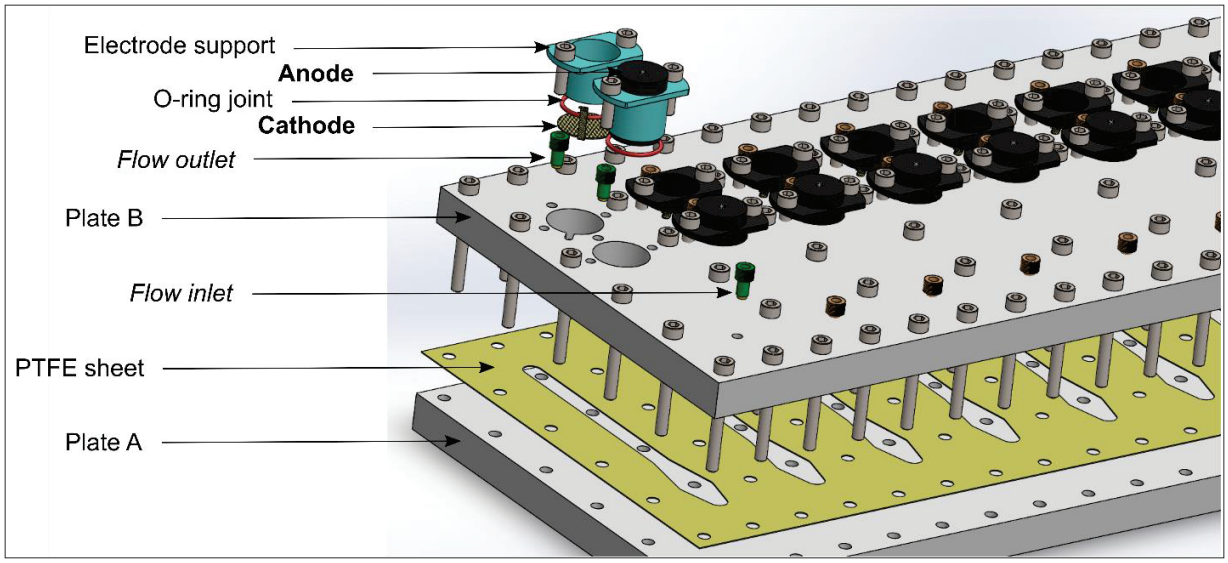

Figure 2.3. Schematic of a multichannel MFC configuration

mm) with different openings for fluid entrance and exit, and for the electrodes, (iii) one hollowed PTFE plate shim (500x240x0.5 mm) to channel the fluid flow. The plates were held together by 70 screws and bolts. The electrodes were a graphite rod (ø24x50mm) for the anode and an air cathode (ø24mm). A plastic piece held each electrode and is easily removable by removing the two screws. An O-ring maintains seal of the reactor.

Hydrodynamic of reactors

In order to ensure uniform flow, the Reynolds number should to be very low (less than 1). It is defined by the following equation (2.1):

$$Re = \frac{vL\rho}{\mu} \qquad (2.1)$$

were *Re* is the Reynolds number, *L* the characteristic length in m, *ρ* the volume mass in $kg.m^{-3}$, and *v* the characteristic velocity of the fluid in $m.s^{-1}$. A diverging-converging channel at the entrance of the fluid ensured a homogenous shear stress in the channel. The thickness of the channel was small (0.5 mm) in comparison to the width of the channel (10 mm). In such a channel, the flow is theoretically a two dimensional Poiseuille flow. The shear stress was uniform except near a very confined part near the channel side walls. With this configuration, the shear stress could be expressed by the following equation (2.2):

$$\tau = \frac{3\mu Q}{4w^2 t} \qquad (2.2)$$

where *w* is the half width of the channel in m and *t* the half thickness of the channel in m. The drag force *D* applied on an isolated bacteria on a surface can be expressed as a function of the shear stress by the equation (2.3):

$$D = 32\tau r^2 \qquad (2.3)$$

with *r* the bacterial radius in m (about 1.10^{-6} m). The table summarizes the different values of Reynolds number, shear stress and drag force as a function of the fluid flow.

τ (mPa)	Q (mL.h^{-1})	Re	D (pN)
1.0	0.75	0.021	0.032
5.0	3.75	0.104	0.160
10.0	7.50	0.208	0.320
50.0	37.50	1.042	1.600

Experimental set up

The experimental set up is illustrated by the Figure (2.4). An external resistance of 1000 ohms was used for all the channels. The voltage of each channel was recorded every 20 min. A phosphate buffer was used as medium amended with 1g/L of sodium acetate. Dehydrated active sludge from wastewater treatment plant was added to the medium at a concentration of 4g/L. The pumps were syringe pumps or HPLC pumps for higher fluid flow. Contrary to other types of pumps, these pumps ensure a homogenous fluid flow as a function of the time. A loss of load was added at the outlet to ensure an equal fluid flow in each channel.

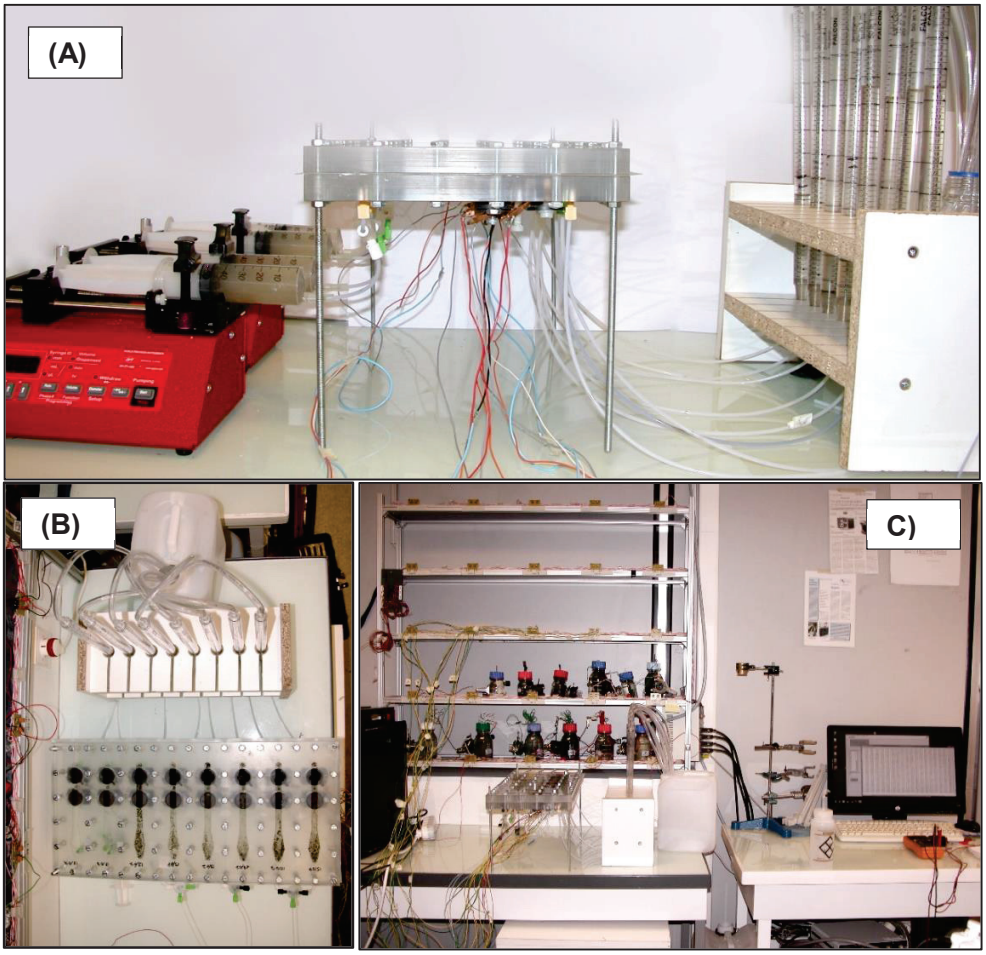

Figure 2.4. Photography of the experimental set up. (A) and (B) Images of the reactors. (c) Image of the reactor connected to a voltammeter and a computer to recorder the cell voltage as a function of the time.

2.2 Electrochemical analysis

2.2.1. Potentiostat operation

A potentiostat OrigaFlex OGF500 from Origalys using a range of current between 5nA and 500mA was to characterize the extracellular electron transfer by cyclic voltammetry and to measure the maximal power by linear voltammetry. A potentiostat controlled a three electrode cell by maintaining the potential of the working electrode at a constant level with respect to the reference electrode by adjusting the current at an auxiliary electrode. By convention, a positive current is due to an oxidation reaction and a negative current due to a reduction reaction. The Figure (2.5) (A) described a potentiostat. The working electrode (the electrode where the studied reaction occurred) was the anode in MFC, the auxiliary electrode (or counter electrode) was the cathode and a silver chloride electrode was used as reference electrode. The silver chloride electrode is a redox electrode. The redox couple is the silver metal (Ag) and the silver chloride (AgCl). A schematic of the silver chloride electrode is shown in the Figure (2.5) (B). The silver wire was coated with a layer of silver chloride. A porous plug provided contact with the solution. The electrode body contained a saturated solution of potassium chloride to stabilize the silver chloride concentration. The potential of a silver chloride electrode in a saturated potassium chloride solution at 25°C with respect

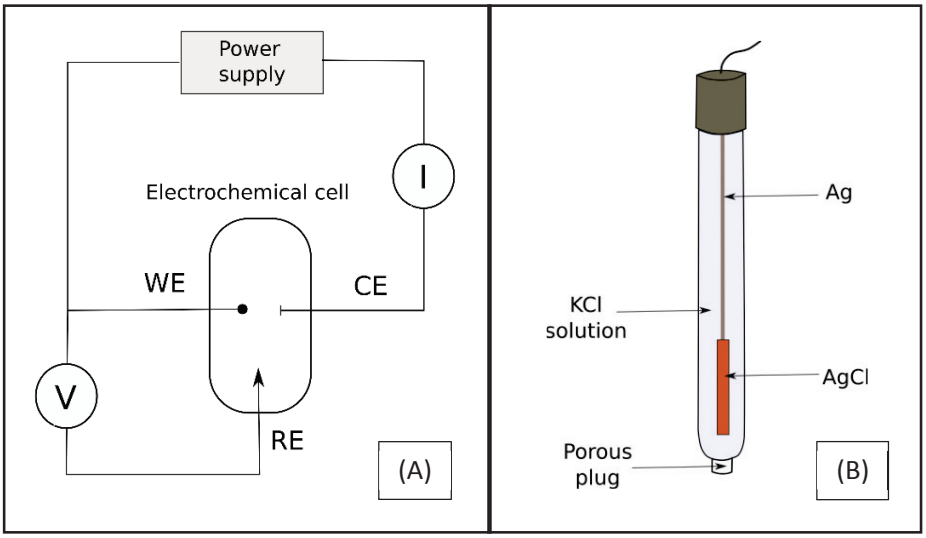

Figure 2. 5. (A) A schematic of a potentiostat representing the counter electrode (CE), the working electrode (WE), the reference electrode (RE), an ammeter (I) and a voltammeter (V). **(B) A schematic of a silver chloride electrode.**

to the standard hydrogen electrode is + 0.197 V. No current circulated in the reference electrode, so the electrochemical potential of the reference stayed stable.

2.2.2. **Polarization curves**

The polarization curves (the voltage of the MFC as a function of the current) were used to determine the different overvoltages in the MFC and to calculate the power curves and the maximal power of the MFC. Two methods were used to do this measurement. The simpler method consisted of modifying the external resistance and measured the voltage of the MFC (Fig. 2.6. (A)). From the voltage as a function of the external resistance, the voltage as a function of the intensity was calculated using the Ohm's law (Fig. 2.6. (B)). The second method used was linear voltammetry. Linear voltammetry consists of applying a linear range of potential and measuring the current (Fig. 2.6. (C)). The linear range applied to the anode was from the anodic equilibrium potential of the MFC in open circuit to that when the anodic potential was equal to the cathodic potential. At the same time, the voltage of the MFC was recorded. This method measured the voltage as a function of the current and observed the compartment of the anode and the cathode separately (Fig. 2.6. (D)).

2.2.3. **Cyclic voltammetry**

During a cyclic voltammetry (CV) measurement, a linear ramp of potential is applied on the working electrode, then the potential is ramped in the opposite direction to return to the initial value (Fig. 2.7.). The cycle is repeated until the stability of electrochemical response. The figure (2.7.) represents the cyclic voltammetry of a molecule redox in its reduced form. In the beginning (the yellow part), the reaction was thermodynamically unfavorable for an oxidation and no current was observed. Then the molecules are oxidized at a potential about -100mV and the current increased. In the second part (in red), the current decreases due to limits of mass transfer. When the potential decreases (the green part), the oxided molecules on the electrode surface are reduced and the current decreases. When all the molecules are reduced (the purple part), the current increases until 0. In this example of voltammogram, an oxidation peak (positive current) is observed at a potential of 20 mV and a reduction peak (negative current) at a potential of -20mV. The equilibrium potential of this reaction is 0mV. The height and the area of the peaks give also some information about the velocity of the reaction.

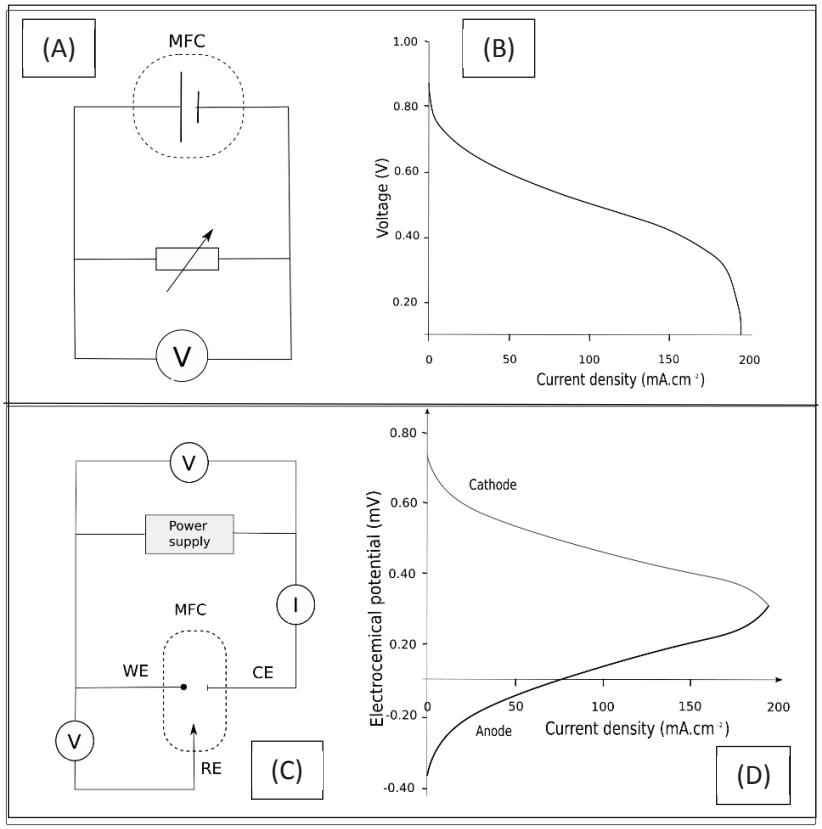

Figure 2.6. Polarization curves. (A) Method of measure with an adjustable resistance. (B) Voltage as a function of the current obtained by the method (B) or deduced from the curves (D). (C) Method of measure by linear voltammetry. (D) Potential of the anode and the cathode as a function of the current obtained by the method (C).

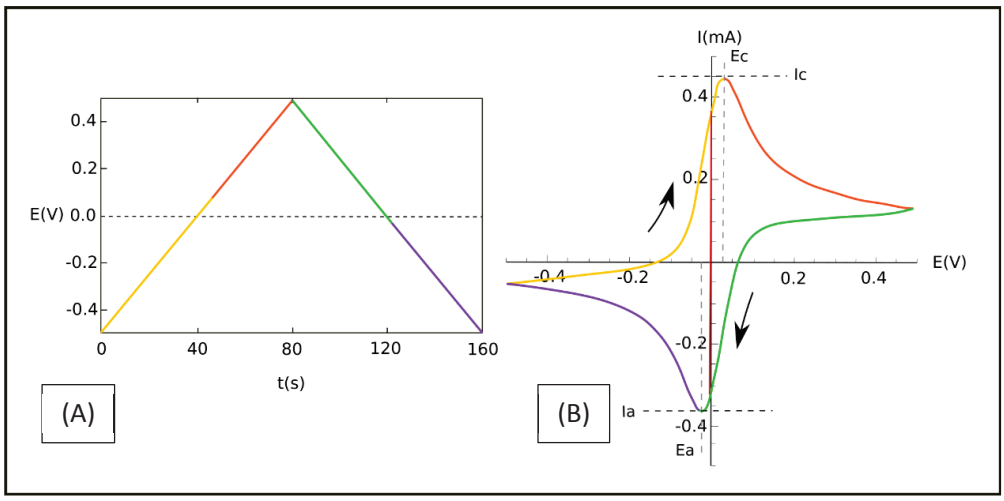

Figure 2.7. Cyclic voltammetry. (A) Potential applied at the anode as a function of the time for one cycle. (B) Current as a function of the anodic potential.

2.3 Microscopy and image analysis

2.3.1. Anodic biofilm observation by epifluorescence microscopy

An epifluorescence microscope was used to observe the biofilms. The biofilms were labelled using the LIVE/DEAD BacLight Bacterial Viability kit (ref. L7007). This kit is composed of two acid nucleic stains: SYTO 9 and propidium iodide. These stains differ both in their spectral characteristics and in their ability to penetrate healthy bacteria. Bacteria with a damaged membrane are considered as dead as opposed to bacteria with an undamaged membrane, which are considered as healthy bacteria. SYTO 9 is a green fluorescent stain that can penetrate all bacteria whether their membrane is intact or not and the propidium iodide, which is a red fluorescent stain, can penetrate only bacteria with a damaged membrane causing a reduction in the SYTO 9 stain fluorescence. The biofilms were observed at magnification x200 and x500. A z-stack acquisition was used by stepping (every 1µm) through the thickness of a sample using a focal drive. The figure (2.8) shows an example of an image acquisition. For each sample, two series of images were performed. Each series was composed of two images for each stain (green and red) multiplied by the number of z-stacks.

2.3.2. Image analysis with image J

The images were analyzed by using the image J software. The green channel and the red channel were treated separately. In the order to remove the out-of-focus signal recorded for each individual image, different filters were applied. First, a 3D median filter was applied, then the background was subtracted (Fig. 2.8). The green channel and the red channel were then grouped together to form a composite image. Finally, the maximal intensity z-projection was used to quantify the percentage of coverage or to have a general view of the image. The maximal intensity z-projection built an image from the maximal intensity of each pixel as a function of the thickness z. The orthogonal view was used to observe the general structure of the biofilm and to measure the thickness of the biofilm.

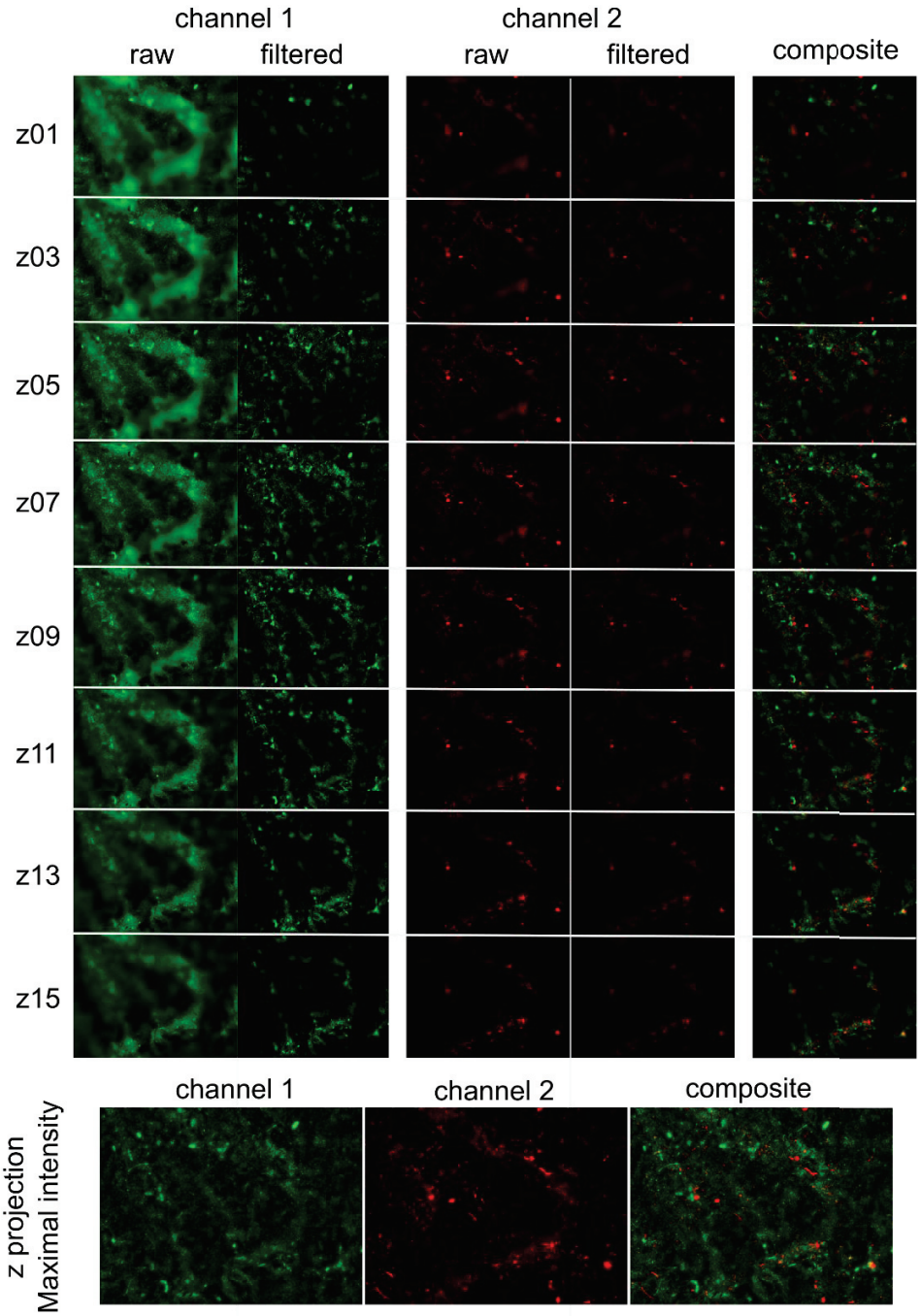

Figure 2.8. Representation of a multidimensional stack. The channel 1 corresponds to the live cell labelled by SYTO 9, and the channel 2 corresponds to the dead cell labelled by propidium iodide. The thickness between each z-stack was 1µm (only one stack every 2µm is represented here to facilitate the observations). The background was subtracted in the filtered images. The composite image is the sum of the filtered channel 1 and 2 images.

2.4 Sequencing

2.4.1. **MiSeq Illumina technology**

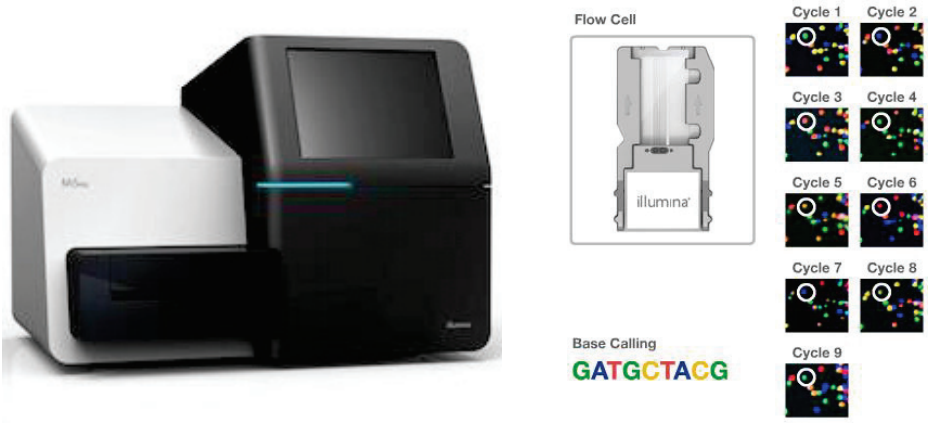

Figure 2.9. MiSeq Illumina technology *(adapted from www.Illumina.com).* (A) Image of a MiSeq. (B) Image of a flow cell and the images taken at each cycle to detect the fluorescent signal to identify the bases.

The Illumina MiSeq technology is a new generation sequencing (NGS) which sequences several millions of small fragments (about 300bp) at the same time (Fig. (2.9.) (A)). The technology consists of a DNA fragment amplification on a flow cell and a sequencing of these clusters by chemical synthesis (Fig. (2.9.) (B)). The sequencing by chemical synthesis consists of the synthesis of the second DNA strand by incorporation of fluorescent nucleic acid. Each base has a specific fluorescent, and at each incorporation an image is taken to identify the base. The principal steps of sequencing are described in the Figure (2.10). The library preparation obtained DNA fragments with the adapters which interact with the flow cell, the index to recognize fragments from a same sample and the sequencing primer binding. Then DNA fragment are loaded in the flow cell. The fragments are linked on the surface flow cell by adapters. The fragments are amplified generating a cluster of identical DNA fragments. Finally, the fragments are sequenced: one base is incorporated per cycle. Each cluster emits the same fluorescent signal allowing to identify the base. It is possible to do pair-end sequencing which allows to sequence both ends of a fragment (2x300 bp) to obtain

a longer sequence (about 550 bp). For example, for a DNA fragment of 550bp, it is possible to sequence one end and generated a read of 300bp (read1), to sequence the other end and to have another read of 300bp (read2). Read 1 and read 2 are pair-end sequences. There is a coverage of 50 bp in the central region which can be used to assemble both reads to generate a longer sequence of about 550bp. More information is available in the Illumina website in the rubric Support >> Training (here).

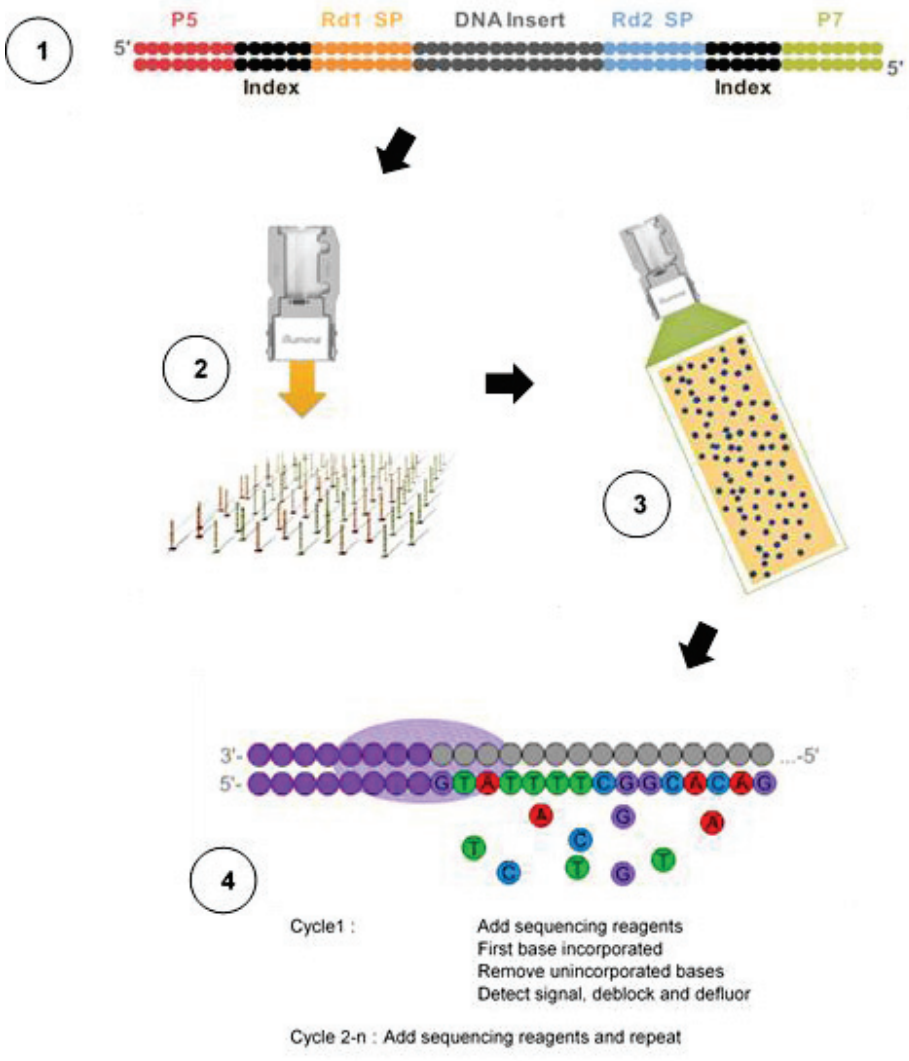

Figure 2.10. Schematic of the different steps for sequencing *(adapted from www.Illumina.com)*. (1) Library preparation. (2) Sample load in the flow cell. (3) Cluster generation. (4) Sequencing by chemical synthesis.

2.4.2. Bacterial identification

The bacterial identification was performed with the sequences of the 16S rRNA gene, which is the molecular clock of evolution (see Chapitre 1 for more explanations). The 16S rRNA gene has about 1500 bp (which is too long to sequence by MiSeq) and contains nine hypervariable regions from about 30 to 100bp. These hypervariable regions can be used to identify bacteria. In this work, the region V3-V4 was amplified (creating an amplicon of about 460bp) and sequenced using the Illumina protocol "16S Metagenomic Sequencing Library Preparation" [128]. The library preparation was performed using the Nextera XT kit. 4x96 samples were loaded in a version V3 flow cell generating about 25 000 reads per samples. After obtaining the sequences, they were compared to a database to identify bacteria. Two major databases exist for 16S rRNA gene: SILVA and RDP databases. The difference between these databases is the way they have been curated. In SILVA database, environmental sequences are accepted but not in the RDP database. In this work, the RDP database was used. The alignment of the sequences against the database was performed using the RDP classifier software. As the DNA fragments were from just one region of the 16S rRNA gene, the taxonomic assignation was not performed at the species level but at the genus or higher level (two bacteria belong to different species if there is less than 97% of homology between their entire 16S rRNA gene)

2.4.3. Functional identification

In this work, metagenomics analysis was done to identify the potential function involved in the EET. The library preparation was done using the Nextera XT kit, and following the protocol of Illumina "Nextera XT DNA Library Prep Kit". The protocol consists of a fragmentation of DNA sample into small fragment size and to tag DNA with adapter sequences. This step is done by an enzyme. For this reason, the size of the fragment was not still centered on 500bp and the standard error around this mean was more or less high dependent of samples. Then, the DNA fragments were loaded in a version V3 flow cell and sequenced. As the DNA fragment sizes were large (often more than 550bp), the sequences were not paired. The sequences of the read 1 and the read 2 were considered as technical replicates. The sequences were then identified by comparison to a database. The database used was the non-redundant protein database (nr) from NCBI (National Center for Biotechnology Information). This database contains a high quantity of sequences from curated (RefSeq, SwissProt, PDB databases) and non-curated databases (Genbank, GenPept, trEMBL databases). This alignment was done to obtain a general view of the potential functions present in the samples. A second alignment was done against more precise databases containing only protein sequences coding for a function involved in the EET. These databases were created from the non-redundant curated protein database, RefSeq.

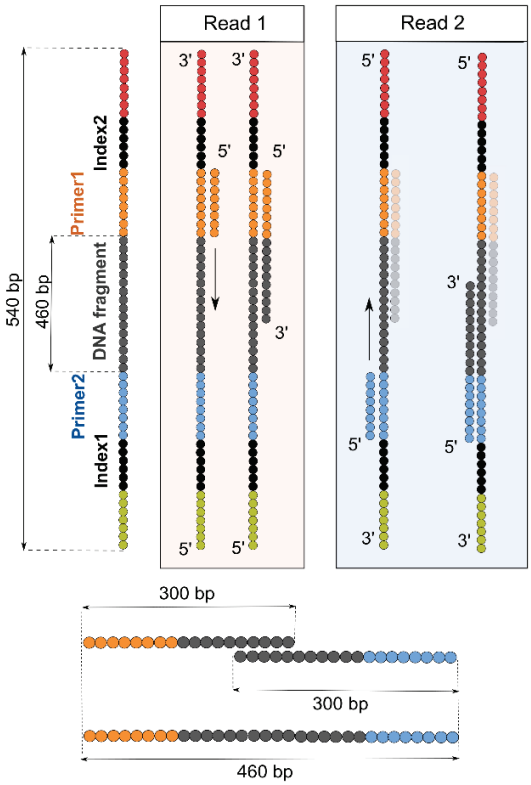

Figure 2.11. Pair-end sequencing. Sequencing of the read 1 and 2 (2x300bp) which are paired to generated a fragment size of 460 bp. *Schematic adapted to www.illumina.com*

Abstract: Chapitre 3

Recently, electroactive bacteria (EAB), which are capable of reducing magnetic iron oxide particles or electrodes, created a strong interest in their capacity to produce electricity. Several applications of this capacity, such as sustainable energy production and biosensors for dissolved organic carbon (DOC) have been studied especially in wastewater treatment plants. However, the application development needs more investigations about bacterial community succession and selection of EAB during the specialization of the electroactive biofilm from original bacterial communities of wastewater. The goal of this study was to understand how EAB selection takes place by following bacterial competition or synthrophy in microbial succession during electroactive biofilm formation. MFCs were set up in duplicate under different external resistances in order to aid or hinder electron flow. Biofilm formation was followed by fluorescence microscopy. The electrocatalytical activity was measured by maximal power measurements and cyclic voltammetry. Bacteria were identified by 16S rRNA gene sequencing over time. Major results show two steps in biofilm formation: first, nonspecific EAB with flexible metabolisms and using indirect EET grow in all MFCs whether they are producing electricity or not, then specific EAB adapted to direct EET become more competitive and dominant in the biofilm. The second step happened only in MFCs producing electricity and corresponded to an exponential increase of electricity production. The results show a competition between different specific EAB, especially between *Geobacter* and *Desulfuromonas*, during the second step, but this did not lead to differences in electricity production. These results help us understand biofilm competition and could improve our control of biofilm formation. An inhibition of the first step should decrease the competition between nonspecific and specific EAB during anode colonization and increase final electricity production.

Chapter 3.

Bacterial Competition for the Anode Colonization under Static Conditions

3.1 Introduction

Bacteria that are capable to reduce metal oxides, such as ferric or manganese particles, created strong interest in both their metabolism and their potential industrial applications. These bacteria, called electroactive bacteria (EAB), can use an electrical electrode as electron acceptor. Several applications of this capacity were considered, such as sustainable energy production for wastewater treatment and biosensors for the dissolved organic carbon (DOC). Unfortunately, the development of EAB applications for wastewater treatment has slowed since electricity production has not reached hoped for levels. These low levels could be due in part to the number and activity of EAB in the anodic biofilm. The biofilm formation on the electrode is a crucial step for the selection of EAB in the biofilm. However, the technological development needs better control of the bacterial community succession and selection of EAB during the development of the electroactive biofilm from the original wastewater bacterial inoculum.

While EAB are mainly represented by *Geobacter sulfurreducens* [34] and *Shewanella oneidensis* [31], [32], they can belong to a large diversity of taxa [61], [62]. They are present in nine classes: *Alphaproteobacteria*, *Betaproteobacteria*, *Deltaproteobacteria*, *Gammaproteobacteria*, *Acidobacteria*, *Cyanobacteria*, *Actinobacteria*, *Bacilli*, and *Clostridia*. The two classes, *Deltaproteobacteria* and *Gammaproteobacteria*, contain the largest numbers of EAB genus, six and ten, respectively [61]. Several mechanisms can be used by EAB to transfer their electrons onto an insoluble electron acceptor. The transfer (EET) can be direct or indirect. In indirect EET, bacteria used endogenous or exogenous shuttles to transfer their electrons. Many bacteria can use redox shuttles such as phenazine (*Pseudomonas*) [129] or members of the flavin (*Shewanella*) family [90], [95], [130], [131]. These bacteria are often facultative aerobic bacteria that are capable of using a large diversity of soluble and insoluble electron acceptors [61]. Shuttle molecules can play other roles than EET, such as intercellular communication, which has been well studied in *Pseudomonas* [132]–[134]. In direct EET, EAB can transfer their electrons directly either from outer membrane c-cytochrome proteins to the anode or via conductive pili named nanowires [36], [37]. These bacteria are often strict anaerobes (*e.g.*, *Geobacter sulfurreducens*) that are only capable of using a limited number of electron acceptors (which are often insoluble). Most environmentally inoculated systems (such as with bacteria from wastewater treatment plants) have a potential diversity of EAB in the subsequent electroactive biofilm. The taxonomic diversity of these anodic biofilms can be determined through 16S rRNA gene sequencing. The MFCs with a higher relative abundance of *Geobacter* often have the best electrical performances [17]. However, mixed-cultures often generated higher power than pure cultures. Recently, some studies investigated the taxonomic diversity and structure of mixed-species anodic biofilms [17], [63]–[68]. The major taxa varied from one study to another as *Deltaproteobacteria* [67] [68], *Betaproteobacteria* [17], and *Bacteroidetes* [65] were all observed to be the major bacteria present in one study or another. Stratford *et al.* [66] investigated the relation between different parameters on bacterial diversity and electrical power production. They showed that the Shannon index was positively correlated with power production. In other studies, MFCs with a higher power

production had lower Shannon indexes [67]. The role of each taxon in electroactivity and the biofilm formation is still not well known. Most of the anodic community studies are often a study at one point in time. Few studies observed the evolution and the formation of the biofilm during the colonization of the anode [69], [70]. Hodgson *et al.* studied the anodic microbial communities in a MFC cascade at different times during biofilm formation. They highlighted the relationship between the fermentative and anodophilic populations in MFC. Paitier *et al.* showed the interest in examining early microbial community shifts and that the competition between EAB seemed to be critical during the colonization of the anode. More investigations about the dynamic behavior of biofilm formation would help our understanding of the role of bacterial communities and their interactions in anodic biofilm.

The goal of this study was to understand how EAB selection takes place by following bacterial competition or synthrophy in microbial succession during electroactive biofilm formation. MFCs were set up in duplicate under different external resistances in order to aid or hinder electron flow. Biofilm formation was followed by fluorescence microscopy. The electrocatalytical activity was measured by maximal power measurements and cyclic voltammetry. Bacteria were identified by 16S rRNA gene sequencing over time.

3.2 Materials and methods

3.2.1. MFC setup and sampling

Single-chamber batch MFCs were set up in in 250mL Wheaton bottles in the laboratory at ambient temperature. The anode consisted of one 10 x 15 cm piece of carbon cloth. The carbon cloth would be cut during sampling to have 25 0.5 x 8 cm pieces as shown in the Figure 3.1. The cathode was prepared with PTFE coating and 5% of platinum catalyst as described by Cheng *et al.* [124]. The MFCs were filled with 250mL of primary effluent and 1g of dehydrated sludge from a Grand Lyon domestic wastewater treatment plant (Lyon, France) and fed with 1g/L of sodium acetate. The experiment was done in duplicate (a and b) separated by a period of 3 months. 2x4 MFCs were started with different external resistances: 1000 ohms (M1000a and M1000b), 330 ohms (M330a, M330b), without resistance (M0a and M0b) and two with an open circuit simulating an infinite resistant (Minfa, Minfb). The MFC voltage was recorded every 5 minutes with a precision of 1µV.

For each time point (0.5, 1, 4, 8, 24, 48, 72, 96, 168, 240 and 360 hours), two samples of 800µL were taken from liquid medium and two anodic samples of 0.5 x 8 cm were taken in each MFC. One part of the anode (0.5 x 6 cm) was used for DNA extraction and one part (0.5 x 2 cm) was used for microscopic observations. In order to compare the evolution of electroactivity, the maximal power was determined by polarization curve analysis and cyclic voltammetry for the time points 48, 96, 168, 240, and 360 hours.

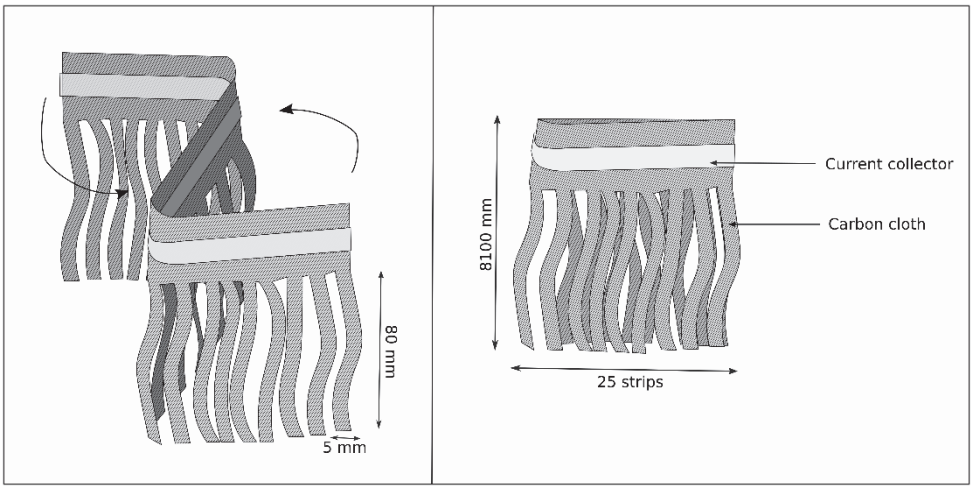

Figure 3.1. Schematic of the anodes. The anode was constituted of 25 carbon cloth strips of 80 x 5 mm. A titanium strip was use as the collector.

3.2.2. Electrochemical measurements

The polarization curves of MFCs were measured at different time points by linear voltammetry with a rate of either 1 mV/s or 0.5 mV/s in a three electrode system. The anode was used as the working electrode, the cathode as the auxiliary electrode and an Ag/AgCl electrode was used as the reference electrode. The potential of the reference electrode Ag/AgCl was +198mV *versus* a standard hydrogen

electrode. All electrochemical potentials were expressed *versus* Ag/AgCl. A voltammeter was added to measure the cell voltage during the linear voltammetry measurements. Under these conditions, the voltage of the cell, and the anodic and cathodic potential could be determined as a function of the current density. The cyclic voltammetry (CV) of the anodes was performed using the same three electrode system. The CV experiments scanned the potential range from -0.6V to 0.8V *vs* Ag/AgCl with a rate of 10mV/s.

3.2.3. **Microscopic observations and image analyses**

The anodic biofilms were observed by fluorescence microscopy. The samples were labelled using a LIVE/DEAD *BacLight* Bacterial viability kit (Invitrogen). An aliquot (1.5µL) of SYTO9 and 1.5µL of propidium iodide were mixed in 2mL of sterile NaCl 0.8%. Then, 200µL were deposed on each sample anodic biofilm. Samples were incubated for 15 min in the dark before observations. Four images were taken per sample using a z-stack of one image per 10 µm and a focus of x 200. The image size was 1388 x 1040 pixels with a resolution of 150 ppp.

The coverage percentage and the proportion of active and inactive bacteria were determined using the ImageJ software [135]–[137]. The green and red channels were treated separately. In the order to remove the out-of-focus signal recorded for each individual image, different filters were applied. First, a 3D median filter was applied and then the background was subtracted with a rolling ball radius of 50 pixels. After which, the maximal intensity z-projection was applied. Finally, a threshold was applied for each channel. The number of white pixels of each channel divided by the total number of pixels was calculated for the coverage percentage of active and inactive bacteria.

3.2.4. **Sequencing analyses**

For each sample (0.5 x 6 cm^2), DNA was extracted using the Nucleospin Soil kit. The solution SL1 was used for the cell lysis and DNA was eluted using 2 x 25µL of the elution solution. Then, the V3-V4 region of 16S rRNA gene was amplified using Platinum Taq DNA Polymerase of ThermoFisher Scientific. The forward primer sequence was:
5' TCGTCGGCAGCGTCAGATGTGTATAAGAGACAGCCTACGGGNGGCWGCAG 3',
and the reverse primer sequence was:

5’ GTCTCGTGGGCTCGGAGATGTGTATAAGAGACAGGACTACHVGGGTATCTAATCC. The PCR program was 95°C for 3 minutes, 25 cycles of 95°C for 30 seconds, 55°C for 30 seconds and 72°C for 30 seconds, then a final step of 72°C for 5 minutes. The resulting amplicon size was about 550 bp. The library preparation was performed following the Illumina protocol [128]. The amplicons were sequenced by a paired-end MiSeq sequencing using the technology V3 of Illumina with 2 x 300 cycles. The adapter sequences were removed by internal Illumina software at the end of the sequencing (forward overhang 5’TCGTCGGCAGCGTCAGATGTGTATAAGAGACAG and reverse overhang 5’GTCTCGTGGGCTCGGAGATGTGTATAAGAGACAG). Due to bad base quality at the end of the read 2, the read 2 sequences were cut at the 200th base using the command *–fastq_filter* and the option *–fastq_trunclen* of USEARCH [138]. Pandaseq [139] was used to linked the read 1 and 2 using a minimal and maximal length of 430 and 490bp, a minimal and maximal overlap of 30 and 60bp, and a quality threshold of 0.9. Other parameters were left at the default values. The mean and the median of the paired sequence percentage were respectively 90.59% (standard error 6.00%) and 90.62%. The repartition of the sequence number after paired-end assembling is shown in the Figure 3.2. (mean = 51446 ± 18240 sequences per sample). The resulting sequences (length mean: 460bp) were annotated by the RDP classifier [140] using the RDP database and an assignment confidence cutoff of 0.8. The statistical data of the annotated percentage as a function of the taxonomic rank are shown in the Figure 3.3. The annotated percentage median decreases in respect of the hierarchical taxonomic group: 99.95% of sequences were annotated at the domain level, 95.07% at the phylum level, 89.00% at the class level, 82.84% at the order level, 78.61% at the family level, and only 56.01% at the genus level. In the bacterial community analysis, family rank was chosen as a good compromise between the precision of the taxonomic rank and the annotated percentage. Two bacterial communities were particularly examined: the nonspecific adapted EAB (composed of *Pseudomonadaceae*, *Comamonadaceae*, and *Moraxellaceae*), and specific adapted EAB (composed of *Geobacteraceae*, *Desulfuromonadaceae*, *Clostridiaceae*, and *Desulfovibrionaceae*).

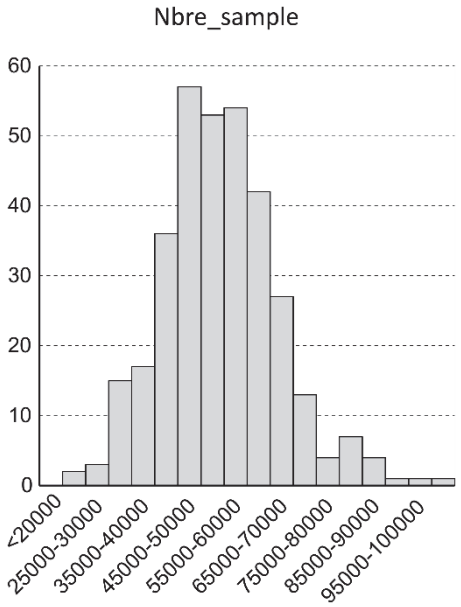

Figure 3.2. Histogram of the repartition of the number of samples in function of the number of sequences

3.2.5. **Statistical analysis**

The diversity analysis was done at the genus level using R software [141] and the R package vegan [142]. Two hundred random subsamples of 10000 sequences each were repetitively taken in each sample in order to compare the diversity between samples. The mean of the number of genus and the mean of the Shannon index was calculated for each sample from these 200 subsamples. Statistical tests were done using R software. Normal distribution of data was tested using the function *shapiro.test*. If the data followed a normal distribution, parametric tests were privileged. Otherwise, non-parametric tests were used.

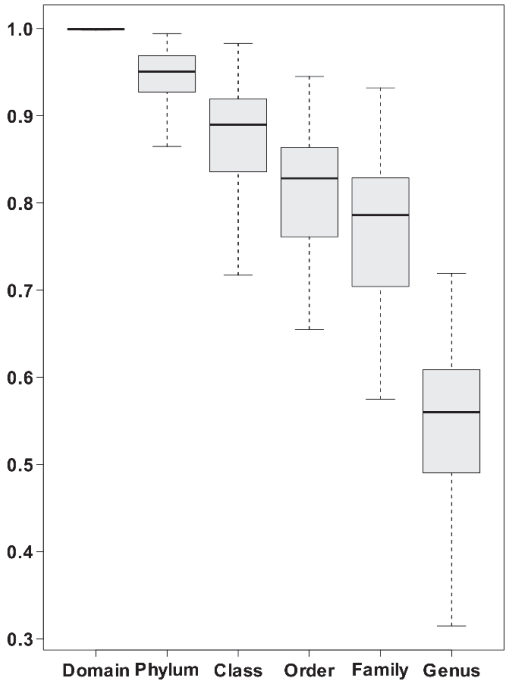

Figure 3.3. Boxplot of the annotated percentage in function of the hierarchical taxonomic group.

3.3 Results

3.3.1. Evolution of the electroactivity function of the anodic biofilms

Electricity production

The cell voltage was recorded as a function of the time during the experiments (Figure 3.4). The open circuit MFC (MFCinfa and MFCinfb) increased quickly from the first day, until an equilibrium voltage of 700mV. But no current could circulated in the external circuit. The electricity production of MFCs operating with an external resistance of 330 or 1000 ohms started to increase at the same time: the 3rd day of the experiment "a" and the 5th day of the experiment "b". The electricity became stable after 5 and 7 days in the experiments a and b, respectively. In both experiments, the electricity production was similar under the same conditions: a cell voltage of about 200mV (corresponding to a current density of about 20mA/m²) for MFC330a and MFC330b, and about 350mV (corresponding to a current density of about 23mA/m²) for MFC1000a and MFC1000b. The cell voltage of the MFCs without external resistance stayed low at about 600µV after 2 weeks. The current density started to increase on the 4th day and the 6th for MFC0a and MFC0b, respectively. The current density became stable on the 5th and 8th day (corresponding to a current density of 26 and 20 mA/m²) for MFC0a and MFC0b, respectively.

The maximal power density was measured at different times in order to compare the electroactivity activity of biofilms (Figure 3.5). After 2 days, the maximal power density was similar for the eight MFCs (3.74 ±1.33 mW/m²). The maximal power density was calculated for a current density of 15.54 ± 7.26 mA/m². In the experiment a, the maximal power density increased quickly for MFC0a, MFC330a and MFC1000a until reaching a similar power density of 50.21 ± 10.83 (for a current density of 173.06 ± 31.61 mA/m²). MFCinf stayed low even after 2 weeks in both experiments. The maximal power densities increased faster in the experiment a than in the experiment b. While the maximal power densities were higher in the experiment b than a for MFC0, MFC330 and MFC1000, the current densities for these MFCs were more similar between the experiments. In both experiments, MFC330 produced the best maximal power density of 58.82 ±.5.45 mW/m² (corresponding to a current density of 208.99 ± 3.41 mA/m²).

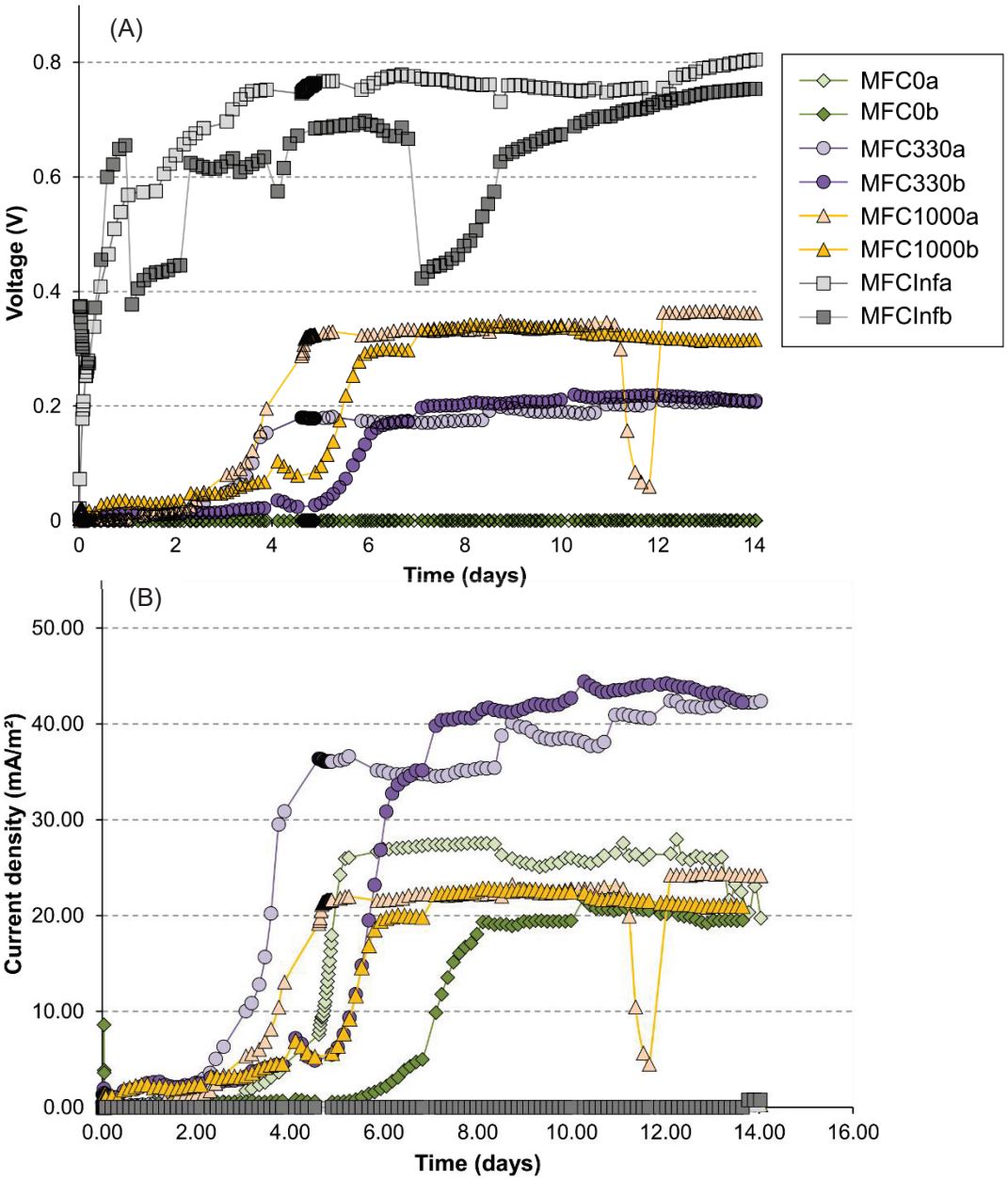

Figure 3.4. Electricity production as a function of time of MFCs. The experiment was performed in duplicate (a and b). The MFCs were set up with different external resistance: 1000 ohms (purple), 330 ohms (yellow), 0 ohms (green) and an infinite resistance (electrode are disconnected) (gray).
(A) Voltage of the MFCs as a function of time. The voltage of MFC with different external resistance was measured as a function of time during two weeks.
(B) Current density as a function of time, calculated by the equation I=U/R. The resistances for MFC0a and b was considered of 2 ohms (the cable resistance).

Cyclic voltammetry

In order to characterize the EET of biofilms, cyclic voltammetry was performed at different times (Figure 3.6). No catalytic activity was observed in MFCinf a and b. In the experiment a, an oxidative peak was observed after two days at around a potential of -100mV *versus* Ag/AgCl and a reductive peak at around -550mV *versus* Ag/AgCl in MFC0a, MFC330a, and MFC1000a. This profile was similar to profile from redox molecules with an equilibrium potential of -300mV *versus* Ag/AgCl. After 10 days,

the profiles were no longer similar to those of redox molecules. An oxidative peak was observed at around a potential of -450mV in MFC0a, MFC330a and MFC1000a. This peak was still observed after 15 days in MFC0a and MFC330a. A second oxidative peak at -300mV *versus* Ag/AgCl was present after 10 and 15 days in MFC330a and MFC1000a, respectively. A third peak at -250mV was observed in MFC1000a after 15 days. The number of catalytic sites seemed to increase over time. In the experiment b, an oxidative peak at around -100mV *versus* Ag/AgCl was also detected after 2 days, but only in MFC0b and MFC330b. After 10 days, an oxidative peak was observed at -350mV in MFC0b, MFC330b, MFC1000b. A second oxidative peak was detected at -250mV in these MFCs after 15days, and a reductive peak at -300mV. It is interesting to note that after 10 days an oxidative peak can be observed in MFC0, MFC330 and MFC1000 of the experiment a or b during the back sweeping of the cyclic voltammetry. This profile can be observed for direct EET for some proteins [143].

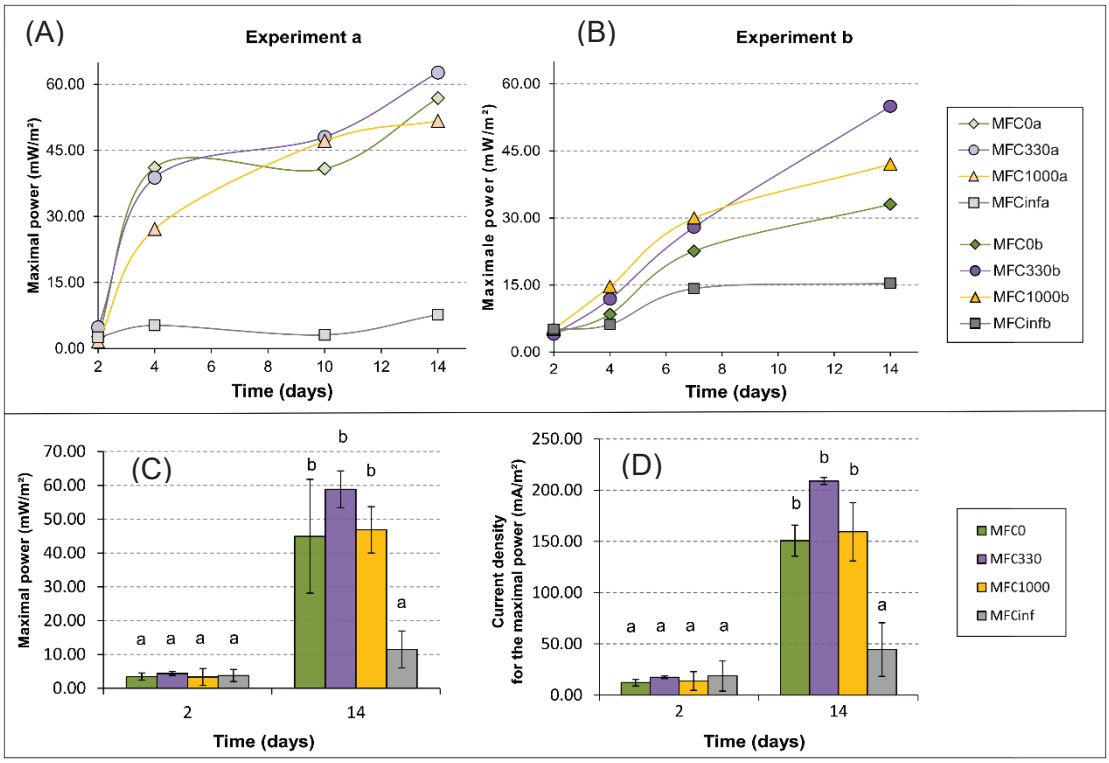

Figure 3.5. Electricity production as a function of time. (A) Maximal power density of the experiment a as a function of time. (B) Maximal power density of the experiment b in function of the time. (C) Maximal power density mean of the experiments a and b. The error bars are the standard error. The letters a and b indicate significantly different groups after a Wilcoxon test at a p-value< 0.01. (D) Current density means of the experiments a and b corresponding to the maximal power. The letters a and b indicate significantly different groups after a Wilcoxon test at a p-value< 0.01. The error bars are the standard error.

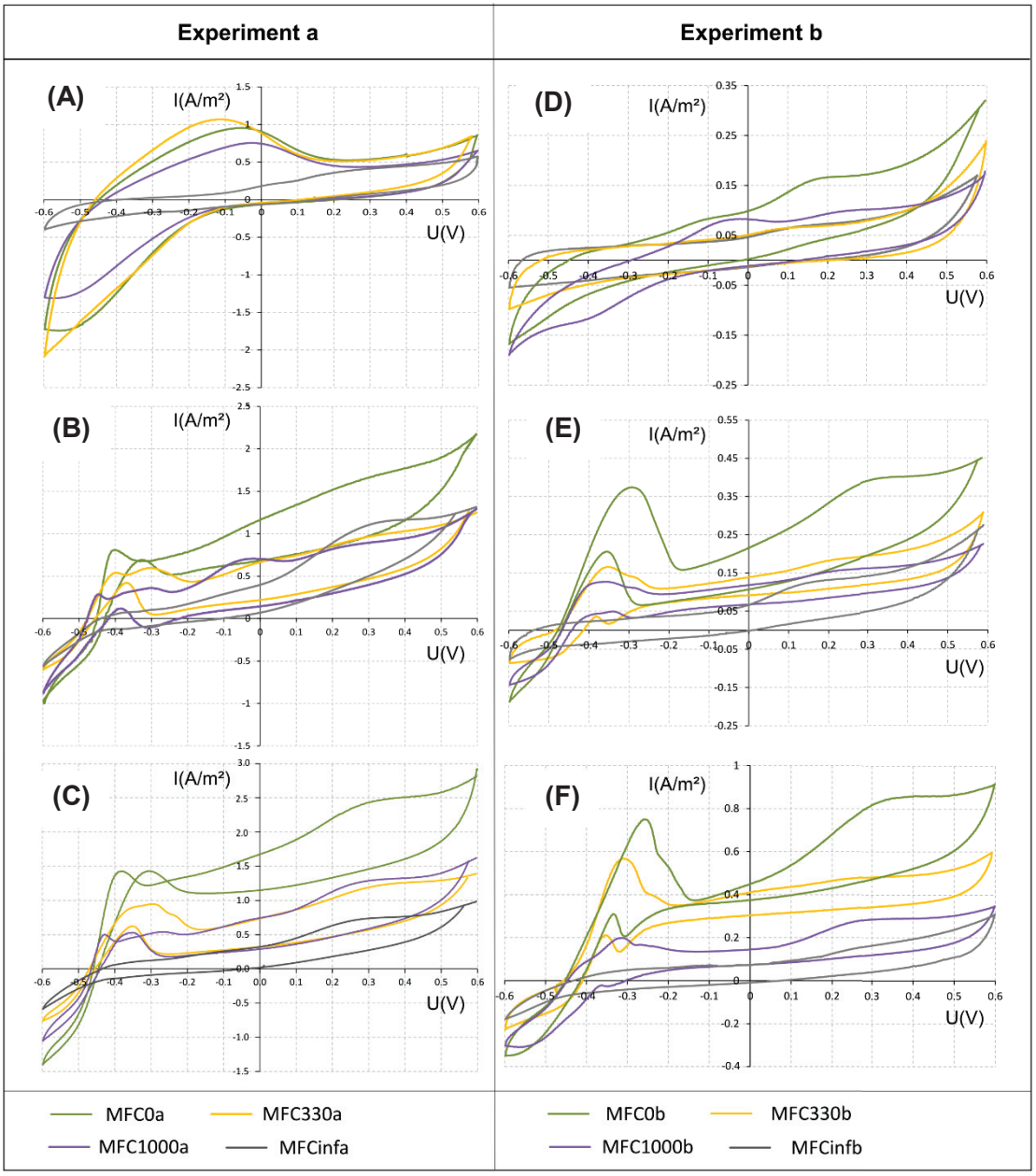

Figure 3.6. Cyclic voltammetry analysis. Cyclic voltammetry measurements were done at different time points in a three electrode system: the anode as the working electrode, the cathode as the auxiliary electrode and an Ag/AgCl electrode as the reference electrode. The electrochemical anodic potentials were expressed *versus* the electrochemical potential of the reference electrode Ag/AgCl (+198mV). The cycle rate was 10mV/s. (A) and (D) were measured after 2 days. (B) and (E) were measured after 10 days. (C) and (F) were measured after two weeks.

3.3.2. **Growth of biofilms**

The biofilm formation was followed as a function of the time by fluorescence microscopy in all eight MFCs (Figures 3.7 and 3.8). During the first two days, the biofilm growth on the anode is low, with a total coverage percentage of 17.44 ± 5.25 % in the experiment a, and 8.11 ± 1.90 % in the experiment

b after 2 days (Figure 3.7). After 4 days, the coverage percentage became stable with a total coverage percentage of about 40% in the experiment a and 20% in the experiment b. However, the images (F) and (G) of the Figure 3.8 show that even if the coverage percentage stayed stable, the biofilms thickened between 4 and 15 days.

3.3.3. Evolution of the bacterial communities

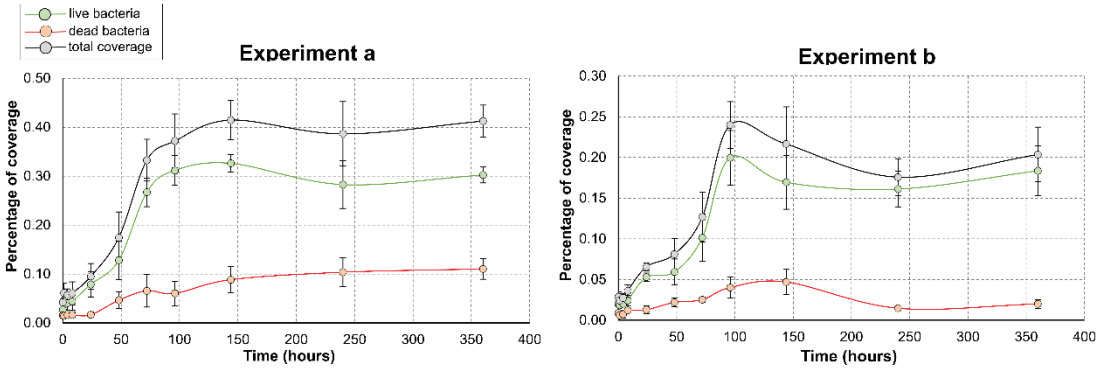

Figure 3.7. Surface coverage percentage of the anode as a function of time. The coverage percentage was determined by image analysis from microscopy observations of biofilms, previously labelled with a LIVE/DEAD kit. The coverage percentage of live bacteria is in green, dead bacteria in red and the total biofilm coverage is in black. Points represents the mean at each time of the four MFCs for the experiment a and the four for experiment b. The error bars represent the standard error calculated from eight different images.

In order to know the bacterial community dynamic for the anode colonization, DNA was extracted at different times and the 16S rRNA gene was sequenced by MiSeq Illumina paired-end sequencing. The sequences were annotated using the RDP databases [140], [144]. From annotated sequences, two major communities were identified: EAB specifically adapted to EET using a direct EET as *Geobacteraceae*, and EAB nonspecifically adapted to EET using mainly an indirect EET and which could use diverse other soluble electron acceptors as *Pseudomonodaceae* (Figure 3.9). The relative abundance of nonspecific EAB increased very quickly until reaching over 80% at the second day in every MFC. Then, from the 4th day onward, their relative abundance decreased until reaching 24.19, 20.78, 31.35, and 40.51% for MFC0, MFC330, MFC1000 and MFCinf, respectively. The major genus present of the nonspecific EAB were *Pseudomonas*, *Acinetobacter*, and *Comamonas*. The relative abundance of specific EAB increased from the 4th day onward in MFCs producing electricity (*i.e.*, MFC0, MFC330, and MFC1000), and more in MFCs with a higher electricity production (MFC0 and MFC330). After two weeks, the relative abundance of specific EAB was 51.61, 39.61, 30.37, and 8.74% in MFC0, MFC330, MFC1000 and MFCinf, respectively. The major genus of specific EAB were *Geobacter* and *Desulfuromonas*.

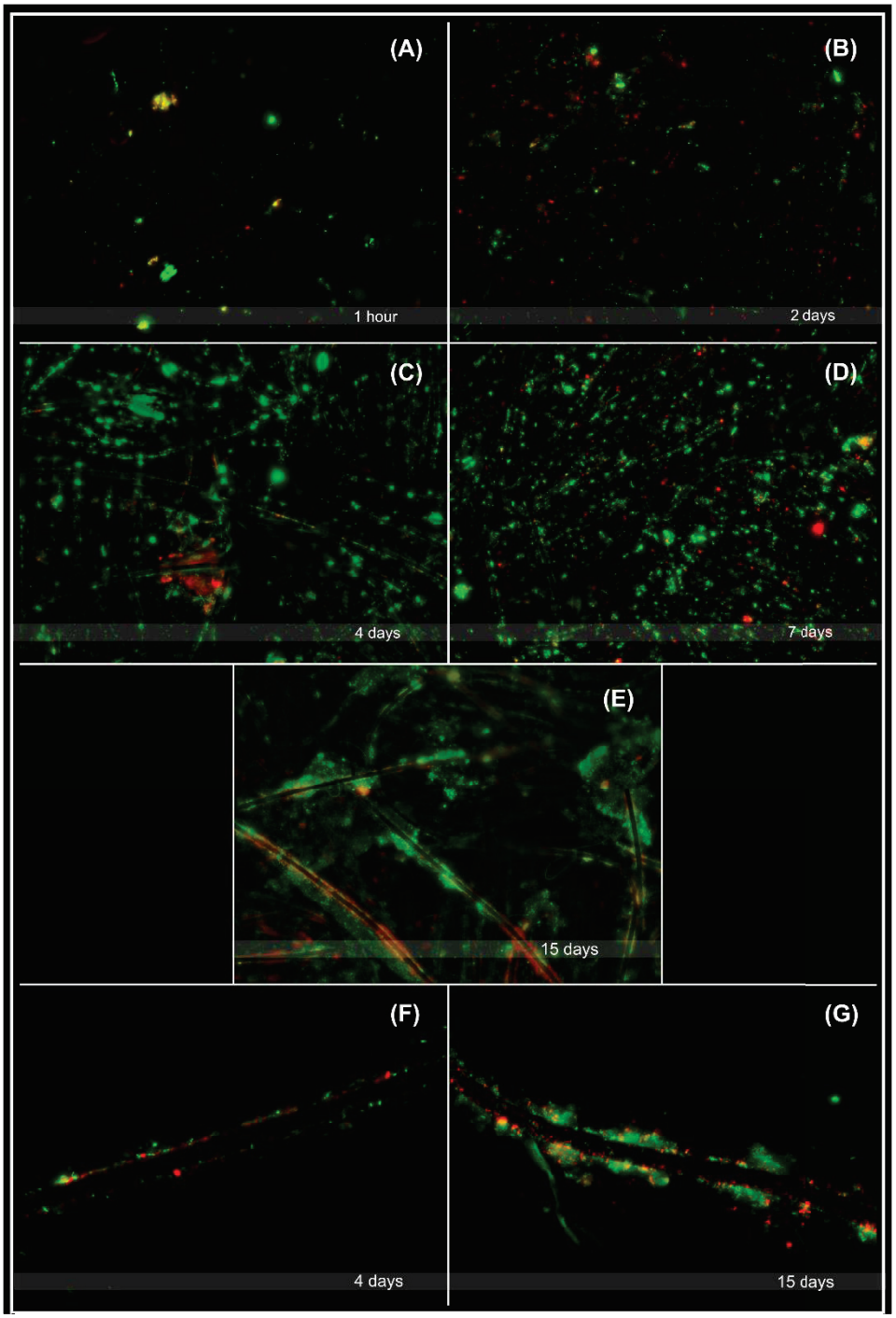

Figure 3.8. Anodic biofilm growths. Biofilms were observed in fluorescence microscopy using a focus x200 (A-E) or x500 (F and G). Biofilms were labelled using a LIVE/DEAD Bactlight viability kit. Dead bacteria with damaged membrane are red, whereas bacteria with an undamaged membrane are green. Presented images are biofilms from the MFC0a taken at different times: after 1 hour (A), 2 days (B), 4 days (C and F), 7 days (D) and 15 days (E and G).

In order to know if the EAB selection was mirrored in the liquid medium, samples from the liquid medium were taken and the 16S rRNA genes were sequenced over time. We observed a similar increase in the relative abundance of nonspecific EAB in the liquid medium until the 4th day (around 80%), followed by a decrease in the relative abundance of this community as in the anodic samples. Contrary to anodic samples, the specific EAB did not increase in the liquid medium. After 2 weeks, the

relative abundance of specific EAB was only 11.40, 14.32, and 11.44% in MFC0, MFC330, and MFC1000, respectively. Their relative abundance in the MFCinf was 9.03%. So, the EAB increase was not observed in the liquid medium. In conclusion, two steps were observed, a first step where the relative abundance of nonspecific EAB increased in the liquid medium and in the anodic biofilm and a second step where specific EAB increased in the anodic biofilm.

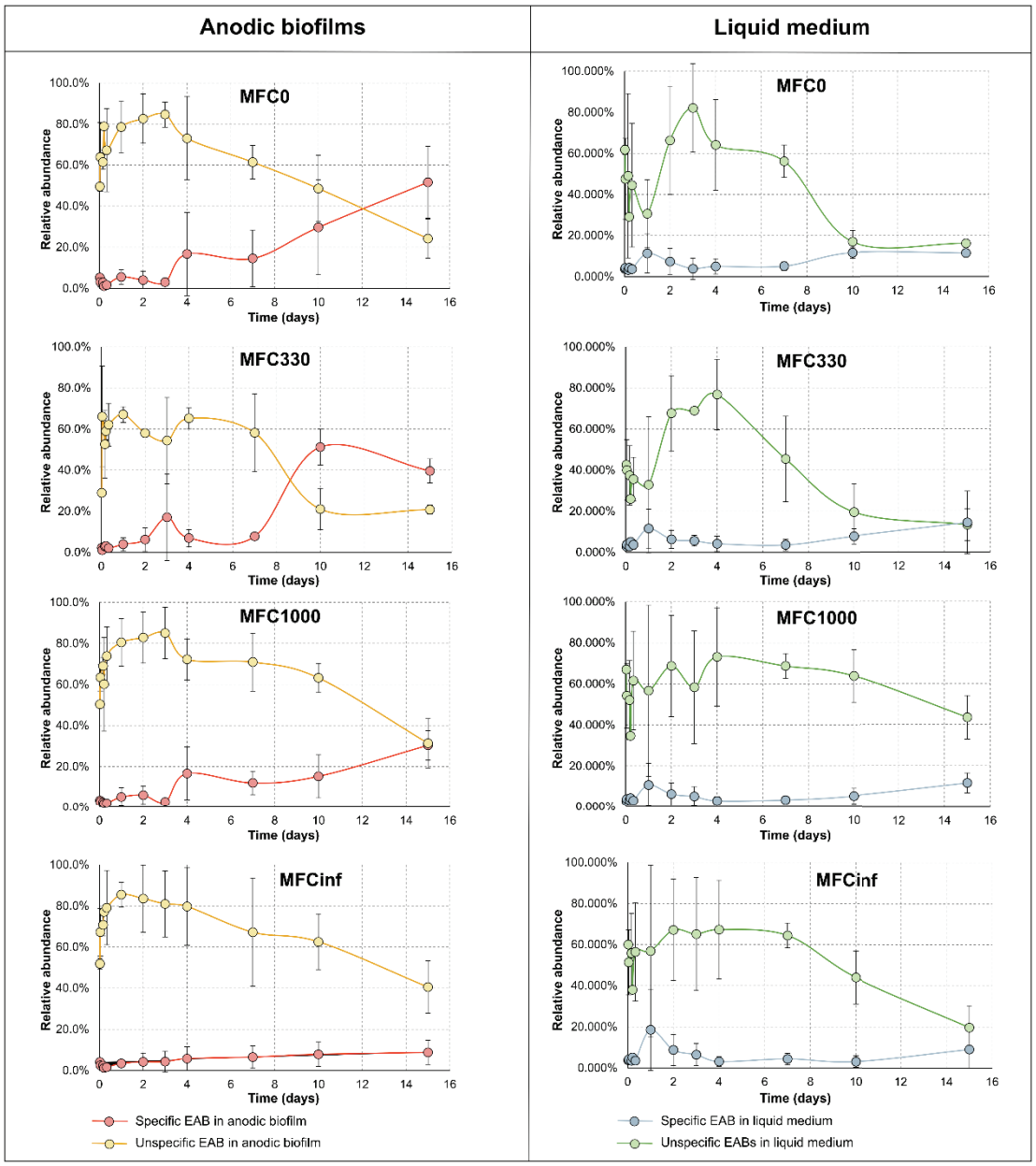

Figure 3.9. Relative abundance of two bacterial communities: specific EAB and nonspecific EAB. The relative abundance of these communities is represented as a function of time for biofilm (left column) and liquid medium (right column). The points represent the means of samples from the experiments a and b. The error bars represent the standard errors of samples from the experiments a and b.

3.3.4. Evolution of the biofilm diversity

A decrease of the biofilm diversity was an indicator of specialization of an environment. The first group, A, represents the microbial communities in the initial state. Two other groups were defined as a function of the dynamic communities previously described in the paragraph 3.3.3 above: a group, B, consisting of anodic biofilms from day 1 to day 4 and a group, C, consisting of anodic communities from the 4th to the 15th day. For these three groups, the number of genus was calculated as an indicator of the richness of the microbial community and the Shannon index was also calculated as an indicator of richness and evenness of the microbial diversity. A strong decrease of the number of genus was observed after one day. The median of the genus number was 232.88 in the group A and only 95.20 and 114.91 respectively in the group B and C (Figure 3.10). So an estimated difference of 126.4 ± 12.5 genus between the group A and B, and of 115.8 ± 9.1 genus between the group A and C was observed. No difference was observed before and after 4 days (group B and C), with an estimated difference between both groups of 10.7 ± 15.2 genus.

The Shannon index decreased after one day. The median was 2.836 in the group A and 1.526 in the group B, presenting difference with a p value = 2.0 10^{-6} (Table 3.1). Although the number of genus did not increase after 4 days, the Shannon index increased to 2.168 after 4 days. In conclusion, the diversity decreased strongly in the anodic biofilms during the first days in terms of richness and evenness and then the richness stayed low while the evenness increased again.

Shannon index			
	Group A/B	**Group A/C**	**Group C/B**
p value	5.0E-02	6.2E-01	1.7E-02
estimated difference	0.658 [0.264 - 1.052]	0.125 [-0.221 - 0.471]	0.533 [0.292 - 0.774]

Number of Genus			
	Group A/B	**Group A/C**	**Group C/B**
p value	2.0E-06	3.9E-07	3.8E-01
estimated difference	126.4 [113.9 - 138.9]	115.8 [106.7 - 124.8]	10.7 [-5.5 - 26.8]

Table 3.1. Statistical paired Student test from diversity data. The groups correspond to means of samples from each MFC before day 1 (Group A), after one day and before 4 days (Group B), and after 4 days (Group C). Normality conditions were previously tested using a Shapiro-Wilk test. The difference between paired data was tested between the three groups. P value, estimated difference and the interval of confidence at 80% of this estimated difference are presented in this table.

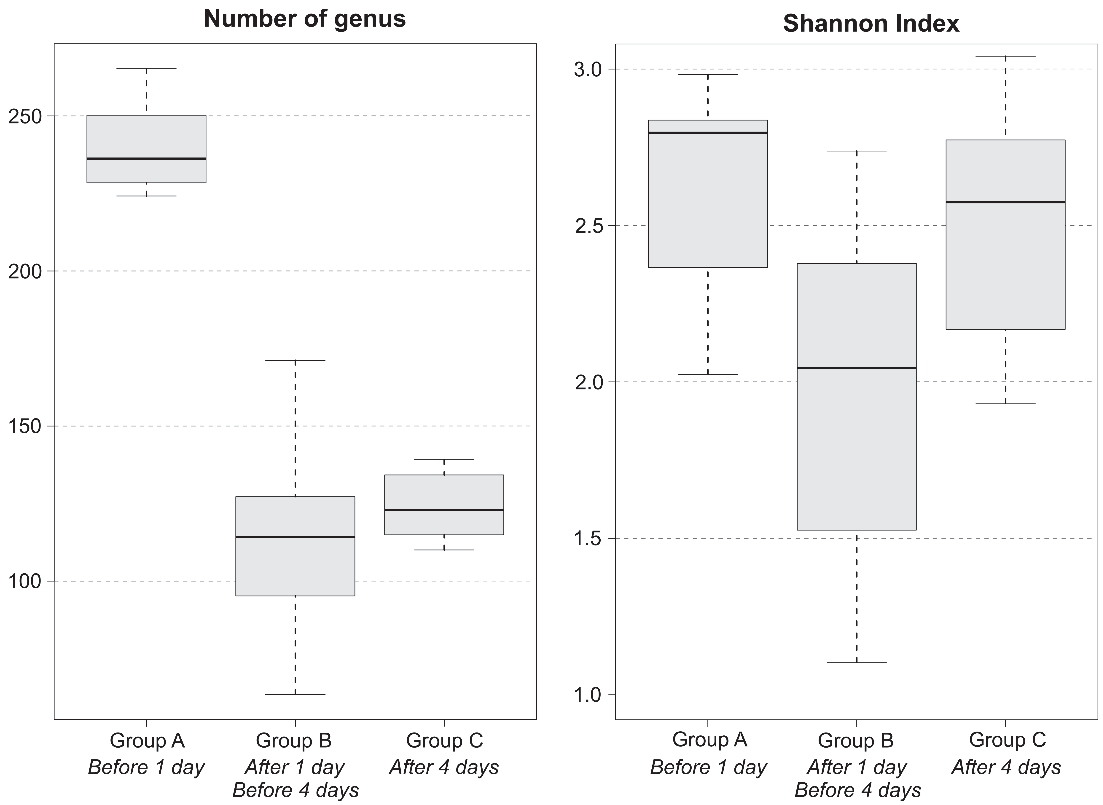

Figure 3.10. Evolution of the biofilm diversity. Boxplot of the means of genus number and Shannon index in function of time. Three groups were formed in function of time from biofilm samples: samples before day 1 (Group A), samples from between day 1 and day 4 (Group B), and samples after 4 days (Group C). Means were calculated for each MFC. Resulting data were three groups of 8 values.

3.4 Discussion

3.4.1. Specialization of the anodic biofilms

The goal of this study was to understand when and how the selection of EAB happens in the anodic biofilm formation. The results showed that there are two steps in the biofilm formation. First, the richness and the evenness of the diversity decreased during the first four days. Nonspecific EAB, using mainly indirect EET grew. They can use a large diversity of carbon source and electron acceptors. In our study, *Pseudomonas* was the major genus of this group as shown previously [129]. Bacteria identified in the cathodic community were *Acinetobacter* also as observed previously [42], [145], [146]. During this phase, the electricity production began but stayed relatively low. We hypothesized that this community used other electron acceptors such as oxygen and nitrate to grow quickly. Since they used soluble electron acceptors, they grew on both the anode and in the liquid medium. They probably secreted redox molecules for EET to the anode, but maybe also to communicate for the biofilm formation as *Pseudomonas* is known to use quorum sensing during biofilm formation [132], [133]. In addition, quorum sensing could favor the electroactivity in mixed biofilm community [147]. The cell voltage was low and the electrochemical potential of the anode was relatively high at this stage (Table3.2. . We hypothesized that electrons could be taken up by bacteria usually present in the cathodic community. In conclusion, this community might use EET to communicate and grow, and the electron flux would evolve progressively from a chaotic flux to a directional flux. This step would occur in all the MFC regardless of the external resistance or electrical conditions.

Experiment a

Time	MFC0a	MFC330a	MFC1000a	MFCinfa
2	-40.25	-60.25	64.75	-490.25
4	-200.25	-435.25	-504.25	-577.25
7	-430.50	-479.25	-460.25	-511.00
15	-266.25	-458.25	-435.25	-461.25

Experiment b

Time	MFC0b	MFC330b	MFC1000b	MFCinfb
2	36.75	56.75	19.75	-254.25
4	-28.73	-70.41	-82.34	-420.76
10	-299.25	-367.25	-385.25	-437.25
15	-488.25	-475.25	-496.25	-526.25

Table3.2. Anodic potential in mV for the 8 MFCs and at different time. The results are expressed *versus* Ag/AgCl

During the second step, the relative abundance of nonspecific EAB decreased, potentially due to the decrease of the other electron acceptors such as oxygen and nitrogen. The electrochemical potential of the anode decreased. Specific EAB that are more dependent on EET for their growth increased. *Geobacter* and *Desulfuromonas* were the major genus of this community in our study. The microbial richness stayed low but the microbial evenness increased. The electricity production increased in terms of current density and maximal power density (Figure 3.11). The growth of specific EAB was more dependent of electricity production. Their relative abundance increases as a function of the maximal power density with a Spearman correlation coefficient of 0.79 (p-value<0.001). On the other hand, nonspecific EAB were negatively correlated with the maximal power density (Figure 3.11). The Spearman coefficient correlation was -0.72 (p-value<0.001). So, this step could not happen in the MFCinf. For this reason, this community can only grow on the anode and not in the liquid medium.

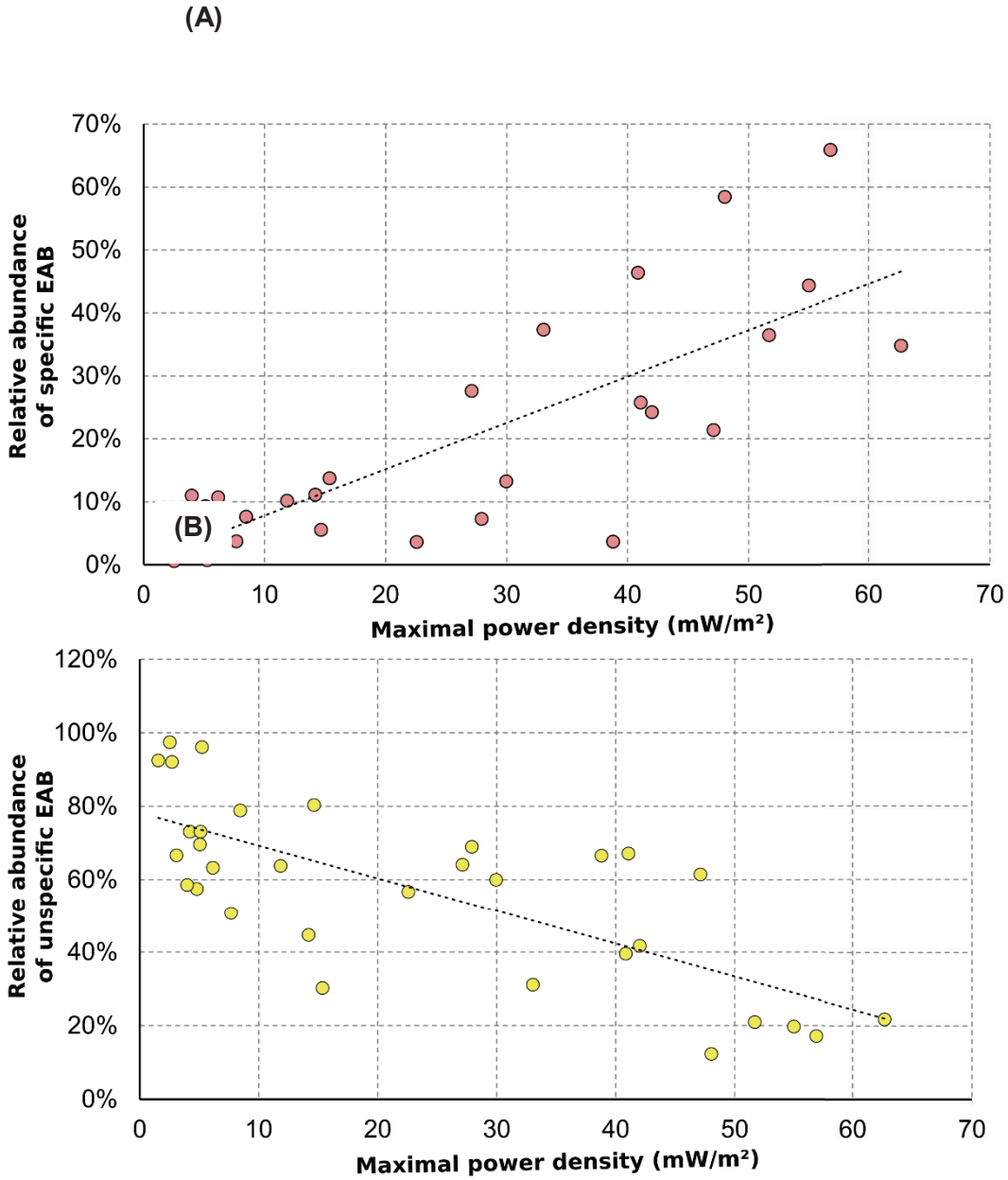

Figure 3.11. Correlation between the maximal power density and (A) specific EAB, and (B) nonspecific EAB. The points represent the experimental data and the line represents the linear tendency function.

3.4.2. Bacterial competition/colonization in the anode biofilm

Different competition happened during anode colonization. First, there was a competition between nonspecific and specific EAB. Nonspecific EAB colonized the anode first, because their growth was faster, and because they could use soluble electron acceptors that are energetically more favorable, such as oxygen and nitrate. They grew fast but the anode coverage percentage was still low after 4 days. After the consumption of soluble electron acceptors, specific EAB became more competitive and colonized the anode (as there was still plenty of available anodic surface). During the second step, the space for the anode colonization decreased and there was competition between different specific EAB (*e.g.*, the major bacteria in the specific EAB community) as observed in the 20 samples where the relative abundance of specific EAB was higher than nonspecific EAB. When *Geobacteriaceae* increased, the relative abundance of *Desulfuromonodaceae* decreased (Figure 3.12). The Spearman coefficient correlation was -0.735 with a p-value< 0.001. If there was no competition between these two families, these groups should have increase simultaneously. However, it difficult to know if this competition is due to anode accessibly or to the carbon source.

3.4.3. Effect of external resistance on the bacterial community

Several studies have examined the effect of external resistance on electricity production [148]–[151]. In our study, no significant difference of maximal power density was observed for MFCs with resistances of 0, 330 and 1000 ohms. However, the bacterial communities (measured by the relative abundance of EAB, genus numbers, and Shannon index) were different as a function of external resistance. After two weeks, the relative abundance of specific EAB was lower when the external resistance was higher (51.61±17.53, 39.61±5.89, 30.37±7.12 and 8.74±5.87% for MFC0, MFC330, MFC1000 and MFCinf, respectively). After two weeks, the genus number and the Shannon index increased when the external resistance was higher (genus number: 123.3±8.5, 127.5±9.0, 137.7±17.5

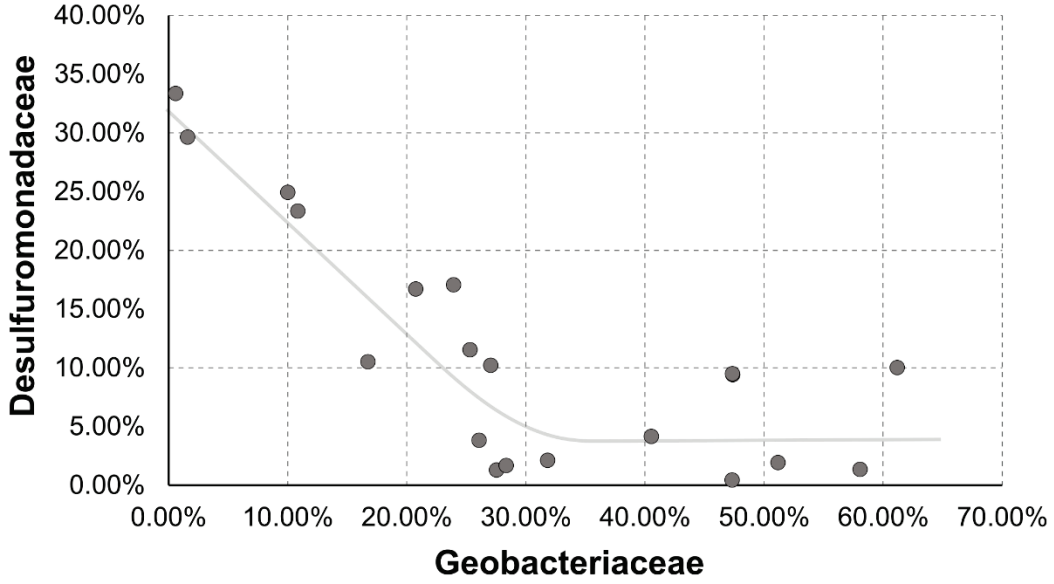

Figure 3.12. Bacterial competition between EAB. The relative abundance of *Desulfuromonadaceae* is drawn in function of the relative abundance of *Geobacteriaceae*. Only the 20 samples where the relative abundance of specific EAB were higher than nonspecific EAB were used.

and 162.7±13.1 for MFC0, MFC330, MFC1000 and MFCinf, respectively; the Shannon index: 2.09±0.40, 2.54±0.12, 2.76±0.40, 3.20±0.23 for MFC0, MFC330, MFC1000 and MFCinf, respectively). Previous studies showed the effect of external resistance on bacterial communities and electricity production, but without identifying the bacterial populations [148].

3.4.4. **Conclusion**

Our major results show a two-step process in the biofilm formation. The first is the selection for nonspecific EAB with their flexible metabolism and ability to use indirect EET to grow in all MFCs whether they are producing electricity or not. The second step is the selection of specific EAB adapted to direct EET only in MFCs producing electricity and their growth corresponded to an exponential increase in electricity production. Also, the results showed competition between different specific EAB, especially between *Geobacter* and *Desulfuromonas* during the second step, although it did not seem to affect electricity production. These results could be used to understand and control biofilm formation. An inhibition of the first step should decrease the competition between nonspecific and specific EAB during the anode colonization and potentially increase the electricity production.

Abstract: Chapter 4

The attachment of bacteria to a surface is often considered as a critical step for biofilm formation and could be a key step for the selection of electroactive bacteria (EAB). The hydrodynamic forces and more specifically the shear forces, strongly influence bacterial adhesion. We hypothesized that the shear stress could select EAB on the anode during the adhesion step by detaching non EAB. MFC reactors with a shear stress chamber that created specific shear stress on the anode were designed and built. Then, the evolution of the adhesion under different shear stress conditions (1, 10 and 50 mPa) were compared. The control was a classical MFC without shear stress. The microbiological structure was studied by 16S RNA gene (*rrs*) sequencing and the biofilm coverage percentage was studied by fluorescence microscopy. This study showed that the relative abundance of specific EAB, such as *Geobacter*, was higher (up to 30.14%) under a high shear stress than under low shear stress (1%). In addition, the shear stress decreased the biofilm coverage percentage on the anodic surface and is consistent with the increase in the relative abundance of specific EAB occurs by detaching other bacteria. Thus, the shear stress could be used to select specific EAB to increase the electroactivity of the anodic biofilms. More studies are necessary to understand the effect of the shear stress on mature biofilms.

Chapter 4.

Adhesion of electroactive bacteria under flow conditions

4.1 Introduction

Biofilm formation is a major process that leads to a stable, mature, resistant and resilient biofilm. Five stages are involved in biofilm formation: reversible adhesion, irreversible adhesion, microcolony formation, maturation and dispersion. In natural environments and in industrial reactors, microbial biofilms are structured in part by hydrodynamic forces. The hydrodynamic forces, especially shear forces, strongly influence bacterial adhesion. The shear stress can be defined by the equation (1.19). The stress is dependent on the velocity gradient and the fluid viscosity:

$$\tau = \mu \frac{\partial V}{\partial y} \qquad (4.1)$$

with τ as the shear stress in Pa, μ is the dynamic viscosity in Pa.s, v is the velocity in m/s of the fluid at the distance y from the surface, and y the distance to the surface in meters. The forces and torques applied on a particle are (i) the hydrodynamic drag F_p (1.21), (ii) the hydrodynamic torque M_t (4.3), and (iii) the lift F_t (4.4):

$$F_p = 32\tau r^2 \qquad (4.2)$$

$$M_t = 12.16\tau r^3 \quad (4.3)$$

$$F_t = \frac{9.26\tau^2 r^4}{\mu v} \qquad (4.4)$$

where *r* is the bacterial radius in m, v the kinematic viscosity in $m^2.s^{-1}$ and F_p the drag force in N. The bacterial radius is small, so the high order terms, M_t and F_t, are negligible. The drag force (which can vary from few to hundreds pN [110]) is opposite of the adhesion force, and so a high shear stress can induce a slow-down of the anode colonization by preventing bacterial adhesion. Thomen *et al.* [111] observed an increase in the lag time as a function of the shear stress between 0.42 and 10 mPa. If the shear stress could detach some specific bacteria, it might be used to select EAB that could grow and colonize the anode without competition from other bacteria.

Few papers study the impact of the shear stress on bacterial communities [114], [118], [119]. Rochex *et al.* [114] observed a decrease in diversity after one week when the shear stress increased (from 55 to 270 mPa), but the analysis of bacterial diversity was done using the PCR-single strand conformation polymorphism (SSCP) technique that does not identify bacteria and only compares gel band diversity. Opposite results were found for smaller shear stresses when Fang *et al.* [119] observed that the diversity increased when the shear stress increased from 2.79 to 21.2 mPa. Their 16S rRNA gene analysis revealed different bacterial composition under the different shear stress conditions.

A few studies have investigated the effect of the shear stress on MFC performances [115], [121]–[123]. Pham *et al* [115] observed an increase in the power production under a shear rate of 120 s^{-1} (about 120m Pa) in comparison to a shear rate of 0.3 s^{-1} (about 0.3 mPa). The thickness and the density of the biofilm were higher under a high shear stress than a low shear stress. The studies of Oliveira *at al.* [121] and Ajayi *et al.* [122] use the Reynolds number as an indicator of the rotation speed and, thus,

the hydrodynamic force. They showed an increase in electricity production at a higher Reynolds number: Ajayi *et al.* observed a higher electrical current for Re=4900 than for Re=900 and Oliveira *et al.* observed a higher power density for Re=22317 than for Re=2236 and Re=11152. However, no study explained the effect of shear stress on bacterial adhesion and bacterial composition of the biofilm.

We hypothesized that shear stress plays a major role in the bacterial adhesion and the selection of EAB on the anode. MFC reactors with a shear stress chamber that created specific shear stress on the anode were designed and built. Then, the evolution of the adhesion under different shear stress conditions (1, 10 and 50 mPa) was compared. The control was a classical MFC without shear stress. The microbiological structure was studied by 16S RNA gene (*rrs*) sequencing and the coverage percentage was studied by fluorescence microscopy.

4.2 Materials and methods

4.2.1. MFC set-up under no flow conditions

Single-chamber batch MFCs in 250mL Wheaton bottles were set up in the laboratory at ambient temperature. The anode consisted of one (10 x 15 cm) piece of carbon cloth. The carbon cloth was cut to have 25 (0.5 x 8 cm) pieces as described in the Chapter 3. The cathode was prepared with PTFE coating and 5% of platinum catalyst as described by Cheng *et al.* [124]. The MFCs were filled with 250mL of primary effluent and 1g of dehydrated sludge from a Grand Lyon domestic wastewater treatment plant (Lyon, France) and fed with 1g/L of sodium acetate. The experiment was done in duplicate (a and b). The anode was connected to the cathode by an external resistance of 1000ohms (M1000a, M1000b). Two MFCs were started without external resistance and were used as negative controls (MFCcta and MFCctb). The MFC voltage was recorded every 5 minutes with a precision of 1µV. For each time point (0.5, 1, 4, and 8 hours), two anodic samples (0.5 x8) cm were taken in each MFC. One part of the anode (0.5 x 6 cm) was used for DNA extraction and one part (0.5 x 2 cm) was used for microscopic observations.

4.2.2. MFC set-up under flow conditions

Reactor design

Three specific MFCs were designed and built to control the shear stress applied on the anodic surface. The configuration of the shear stress flow chamber was chosen for improved quality control and the homogeneity of the shear stress field. Each reactor (Figure 4.1) consisted of (i) one upper PMMA plate B (500x240x20 mm), (ii) one bottom PMMA plate A (500x240x20 mm) with different openings for fluid to enter and exit and for the electrodes, and (iii) one hollowed PTFE plate shim (500x240x0.5 mm) to channel the fluid flow. The plates were held together by 70 screws and bolts. The electrodes were a graphite rod (ø24x50mm) for the anode and an air cathode (ø24mm). A plastic piece held each electrode and was easily removed by removing the two screws. An O-ring maintained the seal around the electrode.

The hydrodynamic characterization of this configuration was done previously by Lorthois *et al.* [125], [126] and the forces applied on a particle for this configuration were given by O'Neil [127]. The thickness of the channel was small (0.5 mm) in comparison to the width of the channel (10 mm). In such a channel, the flow is theoretically a two-dimensional Poiseuille flow. A diverging-converging channel at the entrance of the fluid ensures a homogenous shear stress in the channel. The shear stress was uniform except near a confined part near the channel side walls. In this configuration, the shear stress can be expressed by the following equation (2.2):

$$\tau = \frac{3\mu Q}{4w^2 t} \qquad (4.5)$$

where *w* is the half width of the channel in meters and *t* is the half thickness of the channel in meters. The drag force *D* applied on an isolated bacteria on a surface can be expressed as a function of the shear stress by the equation (2.3):

$$D = 32\tau r^2 \qquad (4.6)$$

with *r* as the bacterial radius in m (about 1.10^{-6} m).

Experimental set-up

MFCs were started under three different shear stresses (1, 10 and 50 mPa) within hydrodynamic characteristics are presented in the Table 4.1. An external resistance of 1000 ohms was used for all channels. The voltage of each channel was recorded every 5 min. A phosphate buffer was used as medium amended with 1g/L of sodium acetate. Dehydrated active sludge from wastewater treatment plant was added to the medium at a concentration of 4g/L. The pumps were syringe pumps to ensure a homogenous fluid flow as a function of time. A loss of head was added at the outlet to ensure an equal fluid flow in each channel.

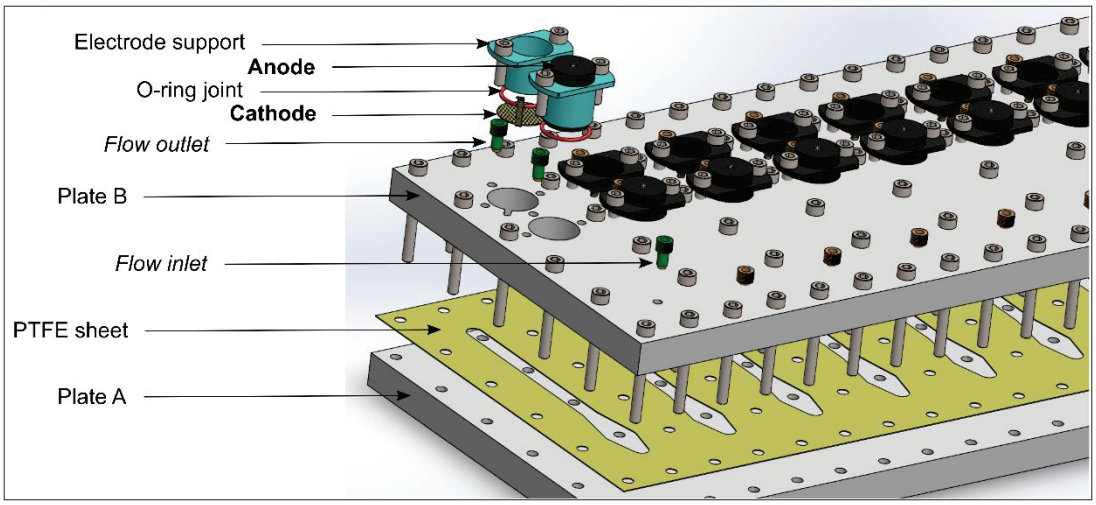

Figure 4.1. Schematic of a multichannel MFC configuration

τ (mPa)	Q (mL.h^{-1})	Re	D (pN)
1.0	0.75	0.021	0.032
10.0	7.50	0.208	0.320
50.0	37.50	1.042	1.600

Table 4.1. Reynolds number, shear stress and drag force as a function of the fluid flow.

4.2.3. Microscopic observations

The anodic biofilms were observed by fluorescence microscopy. The samples were labelled using a solution of SYBR green diluted to 1/50. Five µL of SYBR green were mixed in 2mL of sterile NaCl 0.8%. Then, 200µL were deposed on each sample. Samples were incubated for 15 min in the dark before observations. Four images were taken per sample using a z-stack of one image per 10 µm and a focus x 200. The image size was 1388 x 1040 pixels with a resolution of 150 ppp.

The biofilm coverage percentage was determined using the ImageJ software [135]–[137]. In the order to remove the out-of-focus signal recorded for each individual image, different filters were applied. First, a 3D median filter was applied, then the background was subtracted with a rolling ball radius of 50 pixels. Then, the maximal intensity z-projection was applied. Finally, a threshold was applied for

each channel. The number of white pixels of each channel divided by the total number of pixels was calculated and used as the coverage percentage.

4.2.4. **16S rRNA gene sequencing**

For each sample (0.5 x 6 cm²), DNA was extracted using the Nucleospin Soil kit. The solution SL1 was used for the cell lysis and DNA was eluted using 2 x 25µL of the elution solution. Then, the region V3-V4 of 16S rRNA gene was amplified using Platinum Taq DNA Polymerase of ThermoFisher Scientific. The forward primer sequence was:
5' TCGTCGGCAGCGTCAGATGTGTATAAGAGACAGCCTACGGGNGGCWGCAG 3',
and the reverse primer sequence was:
5' GTCTCGTGGGCTCGGAGATGTGTATAAGAGACAGGACTACHVGGGTATCTAATCC. The PCR program was 95°C for 3 minutes, 25 cycles of 95°C for 30 seconds, 55°C for 30 seconds and 72°C for 30 seconds, then a final step of 72°C for 5 minutes. The resulting amplicon size is about 550 bp. Then the library preparation was performed in respect of the Illumina protocol [128]. The amplicons were sequenced by a paired-end MiSeq sequencing using the technology V3 of Illumina with 2 x 300 cycles. The adapter sequences were removed by internal Illumina software at the end of the sequencing (forward overhang 5'TCGTCGGCAGCGTCAGATGTGTATAAGAGACAG and reverse overhang 5'GTCTCGTGGGCTCGGAGATGTGTATAAGAGACAG).
To remove the low base quality at the end of the read 2, the read 2 sequences were cut at the 200th base using the command *–fastq_filter* and the option *–fastq_trunclen* of USEARCH [138]. Then, Pandaseq [139] was used to link read 1 and 2 using a minimal and maximal length of 430 and 490bp, a minimal and maximal overlap of 30 and 60bp, and a quality threshold of 0.9. Other parameters were left at default values. The resulting sequences (length mean: 465bp) were annotated by RDP classifier [140] using the RDP database and an assignment confidence cutoff of 0.8. In the bacterial community analysis, family rank was chosen as a good compromise between the precision of the taxonomic rank and the annotation percentage. Two bacterial communities were particularly researched: nonspecific adapted EAB (composed of *Pseudomonadaceae*, *Comamonadaceae*, and *Moraxellaceae*), and specific adapted EAB (composed of *Geobacteraceae*, *Desulfuromonadaceae*, *Clostridiaceae*, and *Desulfovibrionaceae*).

4.2.5. **Statistical analysis**

The diversity analysis was done at the genus level using R software [141] and the R package vegan [142]. 200 subsamples of 10000 sequences were repetitively taken in each sample, in order to compare the diversity between samples. The mean of the number of genus and the mean of the Shannon index was calculated for each sample from these 200 subsamples. Statistical tests were done using R software too. Normal distribution of data was tested using the function *shapiro.test*. If data fit a normal distribution, parametric tests (*t.test*) were used. If data did not fit a normal distribution, non-parametric tests were used (*wilcox.test*). In order to compare the adhesion rates, linear models using the R function *lm* were built and compared. Linear models were of type y = Ax. The coefficients A were compared using a student test. This test was calculated using the following equation (4.7):

$$T = \frac{|A_1 - A_2|}{\sqrt{Sd_1^2 + SD_2^2}} \quad (4.7)$$

where A_1 and A_2 are the coefficients of the model 1 and 2, Sd_1 and Sd_2 are the standard errors of A_1 and A_2.

4.3 Results

4.3.1. Anodic biofilm coverage

The coverage percentage of the anode was determined from microscopic observations during the first hours of the biofilm formation. Under static conditions, there was no significant difference in the biofilm coverage between MFC1000 and MFCct (Figure 4.2). The coverage percentage was respectively 0.54±0.16% and 0.35±0.20% after a half hour for MFC1000 and MFCct. After one hour, there was no significant change, but after 4 hours, the coverage percentage increased and was 1.27±0.15% and 1.44±0.28% for MFC1000 and MFCct, respectively. After 8 hours, the coverage was 1.45±0.16 and 1.66±0.20%, respectively.

The coverage percentage was measured also under flow conditions under three different shear stresses: 1, 10 and 50 mPa. After a half hour, the coverage percentage was 2.37±0.71%, 1.14±0.23% and 0.53±0.19% for 1, 10 and 50 mPa, respectively. After 8 hours, the difference was higher between the different conditions with the coverage percentage at 7.50±1.69%, 6.38±1.02% and 2.15±0.59% for 1, 10 and 50 mPa, respectively. In order to compare the coverage rates for the different shear stresses, linear models of type $y=Ax$ were built (Figure 4.3), where y is the coverage percentage, x the time and A the linear coefficient. The three linear models fit a high proportion of the coverage variability with a $R^2>0.7$ and were significant with a p-value$<10^{-4}$. The coefficients A were 1.11±0.12%, 0.77±0.06% and 0.27±0.04% for 1, 10 and 50 mPa, respectively. A student test between the coefficients A was performed showing significant difference between coefficients at a p-value<0.01. So, the adhesion rates under shear stresses of 10 mPa and 50 mPa were respectively 1.44 and 4.11 times slower than under a shear stress of 1 mPa.

4.3.2. Selection of bacteria under shear stress conditions

The bacterial composition of the biofilms was determined in order to know if shear stress selects EAB. There was no statistical difference between MFC1000 and MFCct without shear stress (Figure 4.4). No evolution of specific EAB as a function of time was observed. From a half-hour to 8 hours, the relative abundance of specific EAB was 1.02±0.44% on average. So there was no specific EAB selection during bacterial adhesion. The relative abundance of nonspecific EAB increased as a function of time from 61.16±17.26% after a half hour to 79.40±12.71% after 8 hours. So under static conditions, nonspecific EAB were selected (p-value< 0.05).

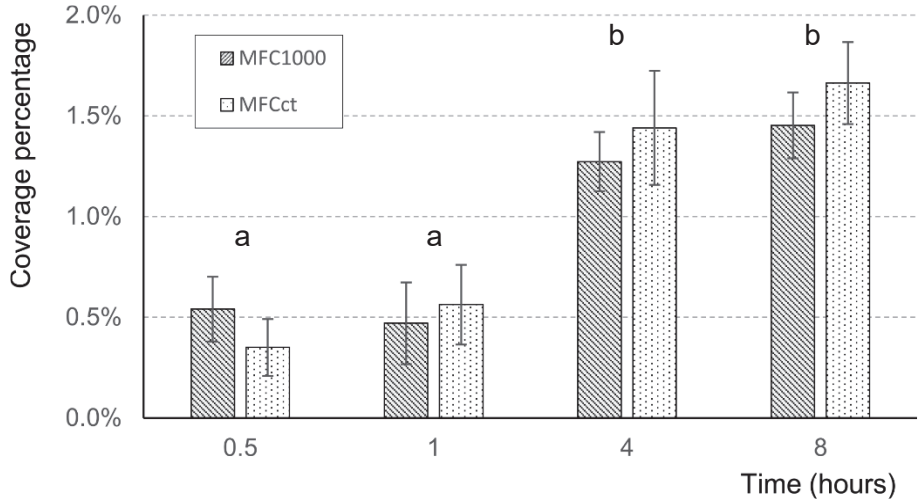

Figure 4. 2. Anodic coverage percentage as a function of time under static conditions. The coverage percentage was calculated from 8 fluorescence microscopic images taken at a focus x200. The error bars represent the error deviation. The letters correspond to statistical group after a Wilcoxon test at a p-value<0.05.

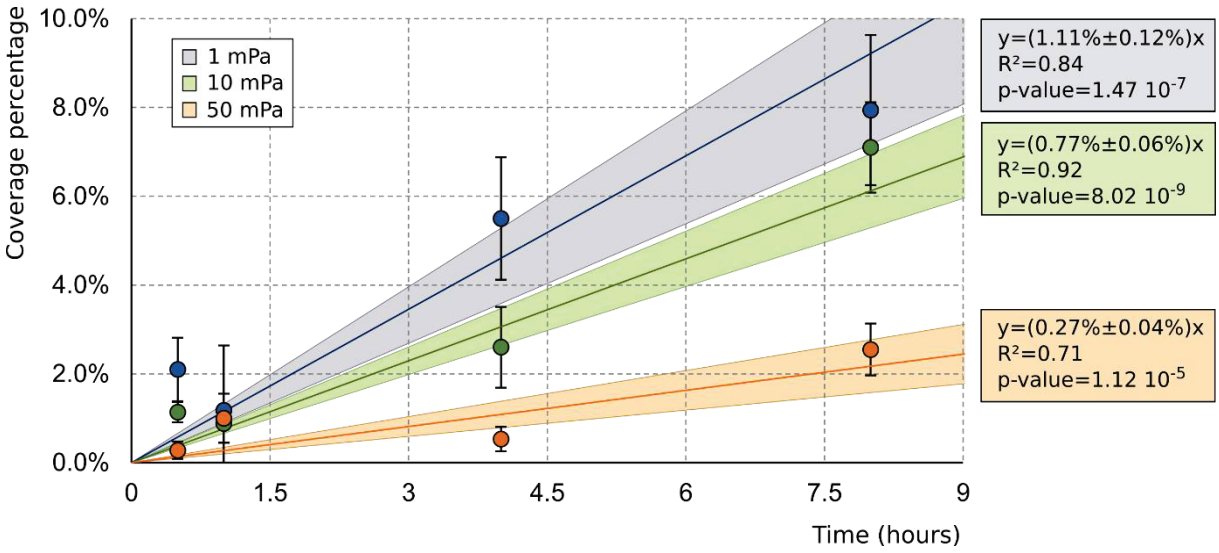

Figure 4..3 Coverage kinetic models. The models are linear and of the type y=Ax. Three models were built corresponding to three shear stress conditions: 1 mPa (blue), 10 mPa (green), and 50 mPa (red). The lines represent the linear models. The points represent the experimental data. The coverage percentage was calculated from 4 fluorescence microscopic images taken at a focus x200. The error bars are the error deviations. The colored area is the confidence interval at 90% of predicted values.

The relative abundance of EAB was also measured under different flow conditions creating shear stresses of 1, 10 and 50 mPa (Figure4.4). There was no significant difference of specific EAB between a shear stress of 1 mPa and 10 mPa. The relative abundances were between 0.09% and 0.69%. So, there was no specific EAB selection under shear stresses of 1 and 10 mPa during bacterial adhesion. Under a shear stress of 50 mPa, the relative abundance of specific EAB was significantly different than

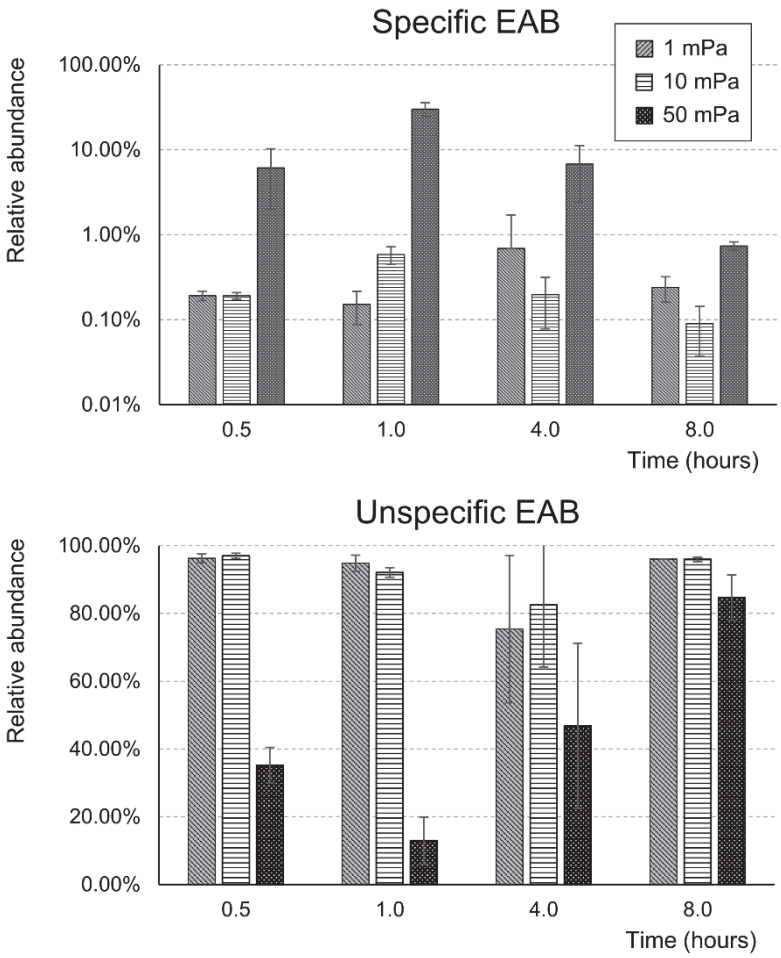

Figure4.2. The relative abundance of EAB under shear stress conditions. The error bars represents the standard deviations.

under a shear stress of 1 mPa (p-value<10^{-3}) and or of 10 mPa (p-value<10^{-4}). Globally, there were 61 and 38 times more specific EAB under a shear stress of 50 mPa than under a shear stress of 1 and of 10 mPa, respectively. The high shear stress selected specific EAB. *Geobacteriaceae*, *Desulfuromonodaceae*, *Peptostreptococcaceae* and *Clostridiaceae* were the major families selected during the adhesion phase under a shear stress of 50 mPa (Figure 4.5). In addition, this selection happened during the first hour, when the relative abundance increased from 6.13% after a half hour to 30.14% after 1 hour. The relative abundance of specific EAB decreased to 6.79% after 4 hours and 0.74% after 8 hours. After 8 hours, no difference was detected between a shear stress of 50 mPa, 1, and 10 mPa.

Nonspecific EAB were not different between a shear stress of 1 and 10 mPa at any times. The values ranged between 75.39% and 96.99%. On the other hand, under a shear stress of 50 mPa, the relative abundances of nonspecific EAB were lower than under stresses of 1 mPa (p-value<0.01, mean of differences = 50.39%) and of 10 mPa (p-value<0.01, mean of differences = 50.37%). These counter selections happened during the first hours as the relative abundance decreased from 35.23±5.23% to 12.96±6.96%. After four hour, the relative abundance increased again to 46.83±24.36%. After 8 hours,

the relative abundance of nonspecific bacteria was similar under all stress conditions (96.0±50.05%, 95.94±0.64% and 84.71±6.71% under a shear stress of 1, 10 and 50 mPa, respectively).

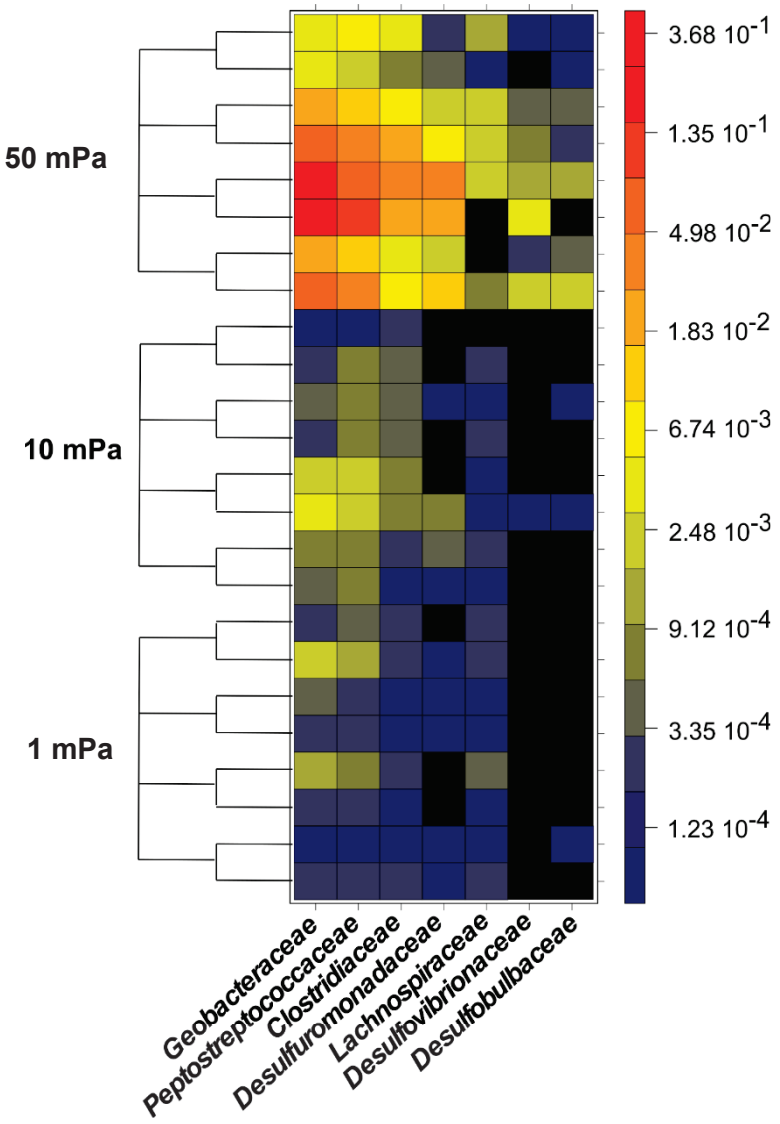

Figure4.3. Relative abundance of each family considered as specific EAB present in the anodic biofilms

4.3.3. Evolution of bacterial diversity

The diversity was calculated for each sample under static and different flow conditions (Figure 4.6). The number of genus was higher on the anode under static conditions than under any shear stress conditions. Genus numbers were 262.0 genus after a half hours and 204 after 8 hours under static conditions. However, under a shear stress of 1 and 10 mPa, the number of genus was lower at 55.6 and 50.9 genus were detected after a half hour under a shear stress of 1 and 10 mPa, respectively and 63.1 and 69.2 after 8 hours, respectively. When the shear stress was 50 mPa, the number of taxon was higher than under other stress conditions but lower than under static conditions. Under shear stress

of 50 mPa, there was 142 genus after a half hour and 139 after 8 hours. After 8 hours, the Shannon index was 2.12, 086, 0.90 and 1.35 under shear stresses of 0, 1, 10 and 50 mPa, respectively.

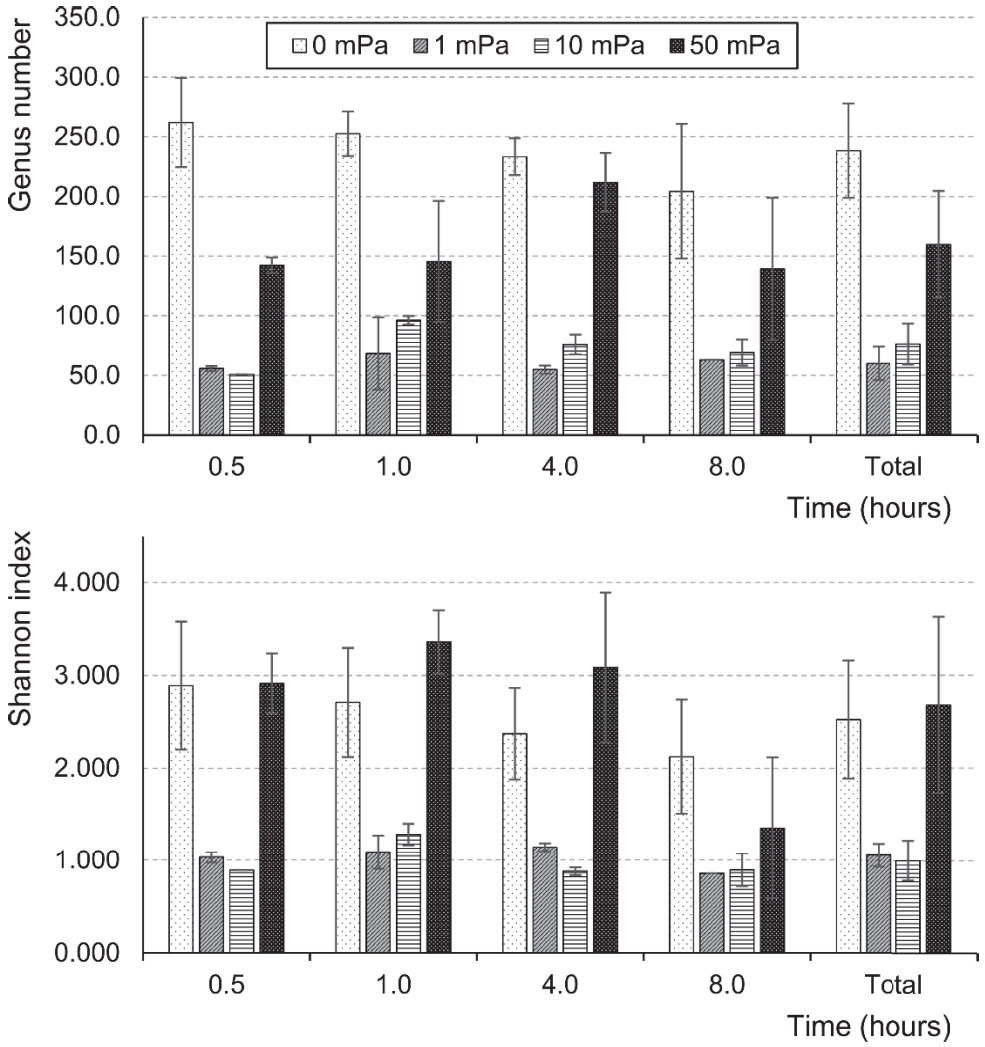

Figure 4.4. Evolution of the diversity as a function of time for shear stresses of 1, 10 and 50 mPa. The genus number (richness) and the Shannon index (richness and evenness) are represented.

4.4 Discussion

4.4.1. Complex effect of the shear stress on bacterial adhesion

In our study, the coverage rate decreased as a function of the shear stress. The coverage percentage was modeled by a linear equation of type y=Ax. The coefficient A was 1.11±0.12%, 0.77±0.06% and 0.27±0.04% for a shear stress of 1, 10 and 50 mPa, respectively. This rate led to a coverage percentage after 8 hours of 7.50±1.69%, 6.38±1.02% and 2.15±0.59% under a shear stress of 1, 10 and 50 mPa, respectively. In contrast to detachment experiments where bacteria attach to the surface without shear stress during the adhesion [152], [153], the adsorption force is not the only one involved in adhesion. The flow velocity modifies the probability that the bacteria will contact the surface. The effect of the shear stress is even more important if the bacterial load is taken into account. The flow rates were 0.75, 7.5 and 37.5 mL.h^{-1} corresponding to a shear stress of 1, 10 and 50 mPa, respectively. After 8 hours, the cumulative volume through the reactors was 6, 60 and 300 mL for the 1, 10 and 50 mPa shear stresses, respectively. The higher volume put more bacteria in contact with the surface.

The sedimentation force can also influence the bacterial adhesion that is dependent on the residence time of bacteria inside the reactor. The residence times inside the reactor were about 176.0, 17.6 and 3.5 minutes for a reactor volume of 2.2 mL. The sedimentation velocity can be estimated at 5.45 10^{-5} mm.s^{-1} using the Stokes equation (4.8):

$$v_s = \frac{2r^2 g \Delta\rho}{9\mu} \qquad (4.8)$$

with r is the particle radius estimated for a bacteria to 0.5 µm, g is the gravitational acceleration of 9.81 m.s^{-2}, $\Delta\rho$ is the volume density difference between the fluid (estimated to 1000 kg.m^{-3}) and the bacteria (estimated to 1100 kg.m^{-3} [154]) and μ is the dynamic viscosity of the fluid (10^{-3} kg.m^{-1}.s^{-1}). The characteristic sedimentation time for a distance of 500 µm (the channel height) is 152.9 minutes. The sedimentation favors the adhesion by increasing the contact probability only under the shear stress of 1 mPa but not under the other shear stresses, where the residence time is too fast in comparison to the characteristic sedimentation time. Other forces, such as the shear gradient lift force or the Magnus force, could modify the contact probability but in the case where the particle is not buoyant, these forces are considered as negligible [155]–[157].

4.4.2. Specificity of electroactive bacteria adhesion

In our study, a higher shear stress selected specific EAB up to 30.14% relative abundance after 1 hour under a shear stress of 50 mPa and selected less than 1% EAB relative abundance under shear stresses of 1 and 10 mPa. *Geobacteriaceae* was the major family selected. This bacterium has a better adhesion to the surface than other bacteria. These results can be explained by the fact that in natural environment, specific EAB, such as *Geobacter*, use insoluble metal oxide particles as electron acceptors. Under these conditions, this bacterium has to adhere more competitively then other bacteria to these particles to survive and grow. This capacity can be due to (i) the hydrophilic/hydrophobic membrane characteristics, (ii) the membrane potential and/or (iii) the membrane proteins. The extended DLVO theory [98] includes three forces: the Van der Waals force, the electrostatic force and the Lewis acid/base force. The Van der Waals force is not dependent of

bacterial membrane proprieties and so can be not responsible of a differential adhesion force between bacterial species. On the other hand, the electrostatic force is dependent of bacterial membrane potential and the Lewis acid/base force is dependent of hydrophilic membrane characteristics of the bacterium. So, these forces could be responsible for a better adhesion of *Geobacter*. The production of some membrane proteins could also explain the higher adhesion. The nanowires and other specific proteins could help the metal-reducing bacteria to adhere strongly to the surface.

After 8 hours, the relative abundance of specific EAB was not statistically different under a high shear stress than under a low shear stress. This can be explain by the (i) first bacteria create a more favorable surface for the adhesion of other bacteria and/or (ii) the growth of other bacteria is faster than specific EAB. For example, with two bacteria, one with a double time of 1h and one with a double time of 10h, the first bacterium will multiplied its concentration by 256 and the other by only 1.07 after 8 hours.

4.4.3. **Potential impact on MFC performances**

The shear stress could be a way to increase the current density in MFCs by favoring a high density of specific electroactive bacteria in the anodic biofilms. This study shows that after one hour under a shear stress of 50 mPa, the percentage of specific EAB was 30% and less than 1% under a shear stress of 1 and 10 mPa. On the other hand, a high shear stress decreased the coverage percentage. Some studies suggested that the power density was correlated to the coverage percentage [158], [159]. Li *et al.* showed a correlation between the current density and the biomass density on the anode. A high shear stress could become negative if it prevented the biofilm formation with a high anodic coverage. More investigations are necessary to understand the effect of the shear stress over a longer period. In addition, the percentage of specific EAB after 8h was not significantly different between MFCs at different shear stresses. A study of the biofilm formation during several days would be necessary to confirm the selection of specific EAB under a high shear stress.

Abstract: Chapter 5

In natural environments and in industrial reactors, microbial biofilms are structured by hydrodynamic forces. The hydrodynamic forces, especially shear forces, strongly influence the microbial and physical structure of biofilms. We hypothesized that the shear stress could be a tool to control biofilm formation on the anode in MFCs. The goal of this work was to study the effect of the shear stress on the microbial selection during biofilm growth. We hypothesized that under increased shear stress conditions, bacteria with a higher interaction with the anode would be selected and, thus, lead to an increase in EAB that mediate direct EET. MFC reactors with a shear stress chamber that created specific shear stress on the anode were designed and fabricated. Then, the evolution of the biofilm growth under different shear stress conditions (1, 5 and 10 mPa) were compared. The taxonomic and functional structure was studied by 16S rRNA gene and metagenomic sequencing, and the physical biofilm characteristics were measured via fluorescence microscopy. These results support the conclusion of Chapter 4 that specific EAB are selected under different shear stress conditions. Initially (first 10 days), the anodic biofilms growing under 10mPa had a higher relative abundance of specific EAB (35.78±6.70%) dominated by *Geobacteriaceae* as compared to the anodic biofilms growing under 1mPa (EAB=16.20±3.14%). In addition, the shear stress decreased the biofilm development rate. After 10 days, no difference of coverage percentage or thickness was observed. This was probably due to the relative low range of shear stress used. However, the shear stress modified the proportion of live and dead bacteria in the biofilm. The biofilms growing under a shear stress of 5 mPa had a lower proportion of dead bacteria than at lower shear stress, which did not cause the detachment of dead matter, and than at higher shear stress, which appeared to inhibit bacteria. This work demonstrated the role shear stress can play in biofilm formation. Applying a shear stress could be a way to control the selection of EAB and the quantity of dead matter in anodic biofilms.

Chapter 5.

Electroactive biofilms developed under flow conditions

5.1 Introduction

Currently, one of the critical steps in MFC start-up is the initial colonization of the anode by EAB as this step affects the bacterial community and the physical structure of the mature biofilm and, thus, the overall electron transfer rate. In natural environments and in industrial reactors, microbial biofilms are structured by hydrodynamic forces. The hydrodynamic forces, especially shear forces, strongly influence the microbial and physical structure of biofilms. We hypothesized that the shear stress could be a tool to control the biofilm formation on the electrodes in MFCs.

Recently, few studies investigated the effect of the shear stress on MFC performances [115], [121]–[123]. Pham *et al* [115] observed an increase in power production under a shear stress of about 120m Pa (120 s^{-1}) in comparison to a shear stress of about 0.3 mPa (0.3 s^{-1}). The thickness and the density biofilm were higher under a high shear stress than a low shear stress. Oliveira *at al.* [121] and Ajayi *et al.* [122] used the Reynolds number as an indicator of the rotation speed and thus the hydrodynamic force. They showed an increase in electricity production at higher Reynolds numbers. However, no study has explained the effect of the shear stress on the bacterial composition in anodic biofilms. In addition, the bacterial composition in the other MFC studies is often measured by 16S RNA gene sequencing, which is only useful for evaluating the taxonomic structure. The composition of functional genes should provide insight into the biofilm potential activity, which is critical for evaluating how the biofilm responds under shear stress. Two of the rare studies that described the potential functional capabilities of microorganisms in the anodic biofilm were done recently with metagenomic data annotated sequences to genes known for enzymes potentially involved in the extracellular electron transfer [160], [161]. In these studies, the authors highlighted the differences of metabolic pathways in different MFCs.

The goal of this work was to study the effect of the shear stress on the microbial selection during biofilm growth. We hypothesized that under increased shear stress conditions, bacteria with a higher interaction with the anode would be selected and ,thus, lead to an increase in EAB that mediate direct EET. MFC reactors with a shear stress chamber that created specific shear stress on the anode were designed and fabricated. Then, the evolution of the biofilm growth under different shear stress conditions (1, 5 and 10 mPa) were compared. The taxonomic and functional structure was studied by 16S rRNA gene and metagenomic sequencing, and the physical biofilm characteristics were measured via fluorescence microscopy.

5.2 Materials and methods

5.2.1. MFC set-up under flow conditions

Reactor design

In order to control the shear stress applied to the anodic surface, three specific MFCs were designed and built. The configuration of a shear stress flow chamber was chosen because of the quality control and the homogeneity of the applied shear stress. See Chapter 2 and the Section 4.2.1 of the Chapter 4 for more information.

Experimental set up

The MFCs were started with three different shear stress (1, 5 and 10 mPa) with the hydrodynamic characteristics presented in Table 4.1. An external resistance of 1000 ohms was used for all the channels between anode and cathode. The voltage of each channel was recorded every 5 min. A phosphate buffer was used as medium and amended with 1g/L of sodium acetate. Dehydrated (25% humidity) active sludge from wastewater treatment plant was added to the medium at a concentration of 4g/L. The pump was a HPLC pump to ensure a homogenous fluid flow as a function of time. A head loss was added at the outlet to ensure equal fluid flow in each channel.

τ (mPa)	Q (mL.h^{-1})	Re	T (min)
1.0	0.75	0.021	176.0
5.0	3.75	0.114	35.2
10.0	7.50	0.208	17.6

Table 5.1. Reynolds number, shear stress and residence time as a function of the fluid flow.

5.2.2. Electrochemical measures

The polarization curves of the MFCs were measured at different time points by measuring the cell voltage as a function of the external resistance. The current density was calculated using Ohm's law ($I = \frac{R}{U}$), and the power density was calculated as $P = U.I$.

5.2.3. Microscopic observations

The anodic biofilms were observed by fluorescence microscopy. The samples were labelled using LIVE/DEAD *BacLight* Bacterial viability kit of Invitrogen. SYTO9 (1.5µL) and propidium iodide (1.5µL) were mixed in 2mL of a sterile NaCl solution (0.8%). Then, 200µL were deposed on each sample. Samples were incubated 15 min in the dark before observations. Two images were taken per sample using a z-stack of one image per 1 µm and a focus x 500. The image size was 1388 x 1040 pixels, with a resolution of 150 ppp.

The coverage percentage and the proportion of active and inactive bacteria, were determined using the ImageJ software [135]–[137]. The green and red channels were treated separately. In the order to remove the out-of-focus signal recorded for each individual image, different filters were applied. First, a 3D median filter was applied. Then the background was subtracted with a rolling ball radius of 50 pixels. Then, the maximal intensity z-projection was applied. Finally, a threshold was applied for each channel. The number of white pixels for each channel divided by the total number of pixels was used to determine the coverage percentage of active and inactive bacteria. In order to determine the thickness of the biofilms, the z-stacks of active and inactive bacteria were added. The thickness of the biofilm was determined by the observation of the light intensity as a function of the z-axis. The total anodic coverage was determined by applying a threshold on the Z-projection of the maximal intensity.

5.2.4. **Metagenomic sequencing and bioinformatics**

For each sample (0.5 x 2 cm^2), DNA was extracted using the Nucleospin Soil kit. The solution SL1 was used for the cell lysis and DNA was eluted using 2 x 25µL of the elution solution. Then, the metagenomic library was prepared following the Illumina protocol of the Nextera XT DNA library prep kit [162]. One ng of DNA was tagmented according to Illumina instructions. Then, the indexes were added during 12 PCR cycles. The libraries were purified and normalized using AMPure XP beads. The fragments were sequenced by a paired-end MiSeq sequencing using the technology V3 of Illumina with 2 x 300 cycles. The reads 1 and 2 were trimmed as a function of the base quality using the command *–fastq_filter* and the option *–fastq_trunqual* of USEARCH [138]. The sequences were trimmed in order to have no base with a quality value, Q, below 20. A minimal sequence length of 50 bp was imposed using the option *–fastq_minlen*. The metagenomic DNA sequences were assigned using the non-redundant protein (nr) database from NCBI using a BLASTx with Diamond software [163]. Only the matches with a percentage of identity higher than 40 % and a p-value less than 10^{-5} were kept. The best assignments were kept for each sequence. In order to study the relative abundance of genes involved in the extracellular electron transfer, specific functions associated with cytochrome, hydrogenase, shuttles, acetate and adhesion functions were recovered by using these keywords in the BLASTx output files. Statistical analyses were performed using the R environment.

5.3 Results

5.3.1. Electrical performances

The cell voltage was recorded as a function of time during the experiments. The current density was deduced using Ohm's law (Figure 5.1). Under a shear stress of 1 mPa, the electricity production increased linearly to about 5 µA/cm² from 0 and 4 days (increasing at 1.25 µA/cm² per day). After 4 days, an increase of the electricity production was observed, followed by stable electricity production with a current of about 23 µA/cm² of anode (Figure 5.1). Under a shear stress of 5 mPa, the current density also increased linearly as a function of the time during the experiment, but without any exponential phase. The current density after 10 days was about 20 µA/cm² (increasing by 2 µA/cm² per day). Under a shear stress of 10 mPa, the current density did not increase during the first three days, then increased and tended to become stable at about 14 µA/cm² after 7 days (increasing at about 3.5 µA/cm² per day between day 3 and 7). While the electricity production during the first few days seemed relatively similar, the current density after 8 days decreased as a function of the shear stress. The mean of the current density from both replicates between 8 and 10 days (n=4) decreased with increasing shear stress (Figure 5.2). The current density was different (at $p < 0.05$) under the three conditions: 22.61±4.98, 17.12±2.36 and 13.15±2.01 µA/cm² under a shear stress of 1, 5 and 10 mPa, respectively.

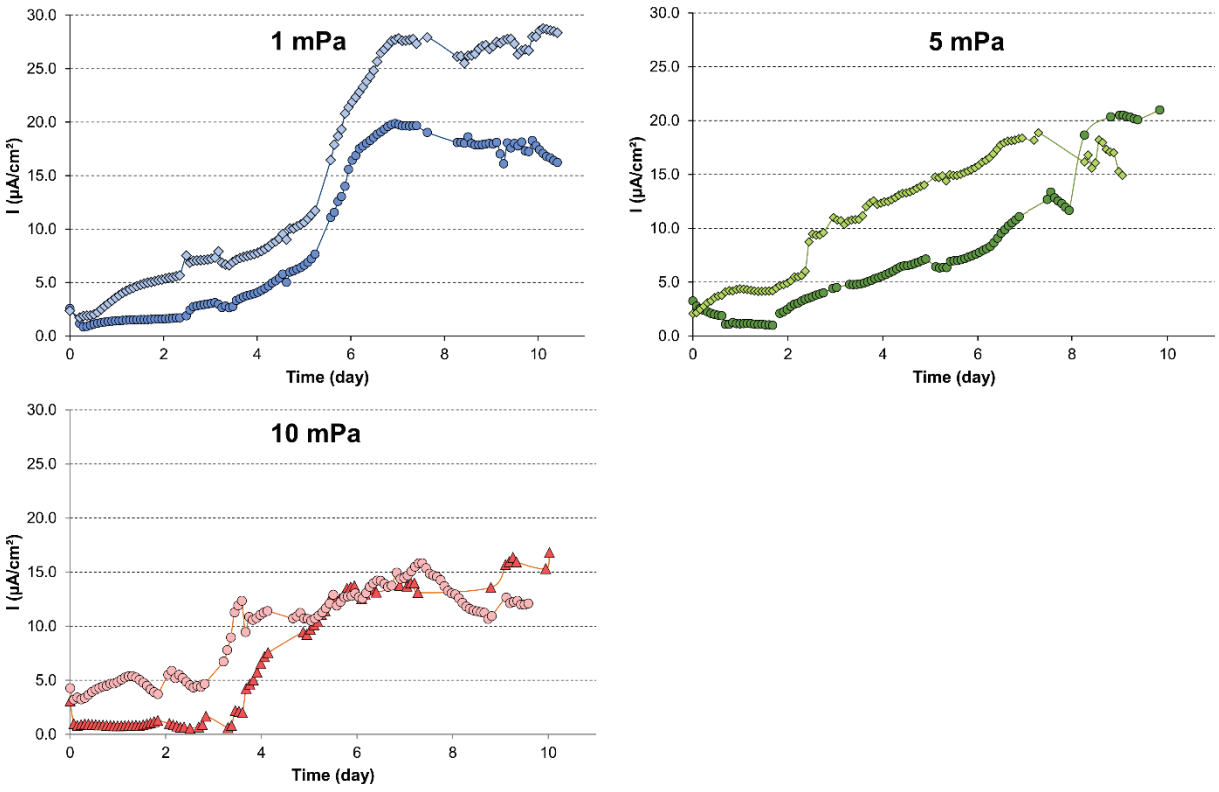

Figure 5.1. Current density produced in function of the time. Two replicate were done for each shear stress condition.

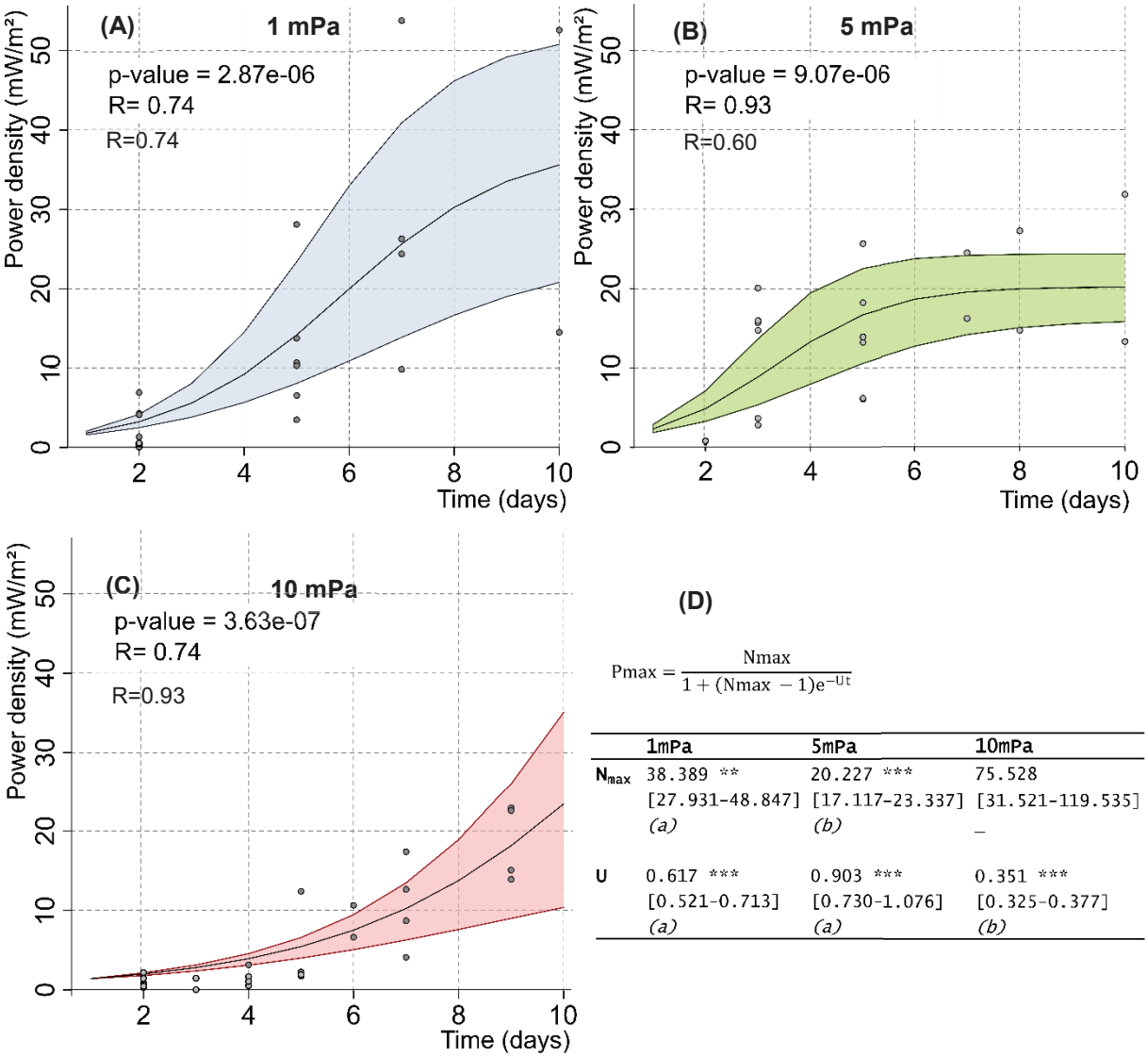

	1mPa	5mPa	10mPa
N_{max}	38.389 **	20.227 ***	75.528
	[27.931-48.847]	[17.117-23.337]	[31.521-119.535]
	(a)	*(b)*	_
U	0.617 ***	0.903 ***	0.351 ***
	[0.521-0.713]	[0.730-1.076]	[0.325-0.377]
	(a)	*(a)*	*(b)*

Figure 5.2. Maximal power density as a function of time under three different shear stress coditions. The maximal power was modeled by a bacterial growth function. A non-linear model of type $\boldsymbol{P_{max}} = \frac{N_{max}}{1+(N_{max}-1)e^{-Ut}}$ was built. The panels A, B and C represents the power density models. The points represent the experimental data. The dark line is the model values. The color area represents the confidence interval at 80% of the model. The parameter R is the Pearson correlation coefficient between the predicted data and the experimental data. The panel D describes the statistical data. The table contains the value of the parameters Nmax and U of the three different model fittings and their confidence interval at 95%. The stars at the right of the parameters value correspond to the p-value associated to the parameters (***: p-value<0.001, **: p-value<0.01). The letters represent the statistical groups based on p-value <0.05 with the Student t-test).

The maximal power density was measured at different times (Figure 5.3). In order to compare the evolution of the maximal power density under the three conditions, models were built and the parameters were compared. Since electricity production generally follows bacterial growth, a model based on bacterial growth models was used (5.1):

$$P_{max} = \frac{N_{max}}{1+(N_{max}-1)e^{-Ut}} \quad (5.1)$$

with N_{max} the limited maximal power density that the MFC can produce, and U the kinetic parameter. The three fittings to the model were significant at p-value<0.001. The parameter R is the Pearson correlation coefficient between the predicted and the experimental data. R was greater than 0.5 for the three fittings. The N_{max} parameter was higher under a shear stress of 1 mPa than 5 mPa, 38.39±10.46 mW/m² and 20.23±3.11 mW/m², respectively. Under a shear stress of 10 mPa, the maximal power never stabilized and so the N_{max} parameter was not applicable. The U parameter was similar between the results for the MFCs at 1 and 5 mPa shear stresses. The maximal power density under both these conditions increased at similar rates: 0.617±0.096 and 0.903±0.173 mW.m^{-2}.day^{-1}, respectively. Under a shear stress of 10 mPa, the power density increased more slowly: 0.351±0.026 mW.m^{-2}.day^{-1}. In conclusion, under a shear stress of 5 mPa, the power density increased somewhat faster than under 1 mPa of shear stress, but became stable at a lower value. Under 10 mPa of shear stress, the maximal power density increased slowly and a stable phase was not observed during the experiment. The shear stress modified the evolution of the power density as a function of time. The mean of the power density between 7 and 10 days was similar in the three conditions: 30.24±18.80, 22.63±7.72 and 22.07±6.74 mW/m² respectively under 1, 5 and 10 mPa.

5.3.2. **Physical structure of biofilms**

In order to know if the difference of electricity production is due to the percentage coverage, the thickness or the active percentage of the biofilm, fluorescent microscopic observations were done at different times.

Anodic coverage kinetics

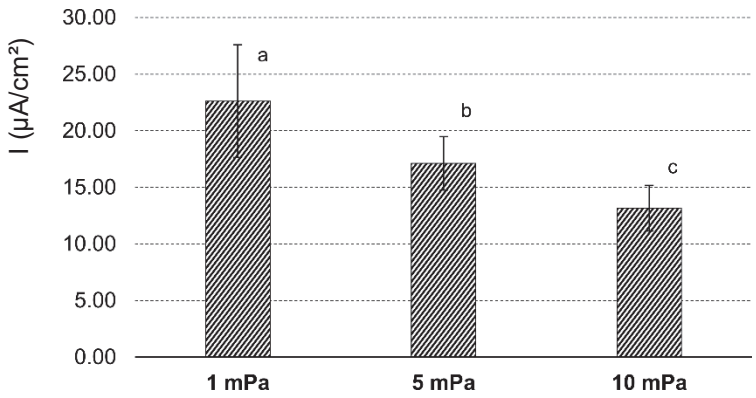

Figure 5.3. Current density between 8 and 10 days. The graphic represents the mean of the current density from both replicates between 8 and 10 days. The error bars represent the standard errors. The letters indicate the significant statistical group (p-value < 0.05 after a student test).

The anodic coverage kinetics are presented in the Figure 5.4.(A). Under a shear stress of 1 mPa, the coverage increased slowly until 5 days (9.68±3.09%), then an exponential phase was observed until 7 days (48.68±17.79%) and became stable. Under 5 mPa, the coverage percentage increased faster: after 5 days, the coverage percentage was of 22.25±8.36%. No stable phase was observed, and it was of 52.46±5.54% after 10 days. Under 10 mPa, the anodic coverage kinetic was slower. It was only of 11.13±7.56% after 6 days. But after 10 days, the value was of 51.15±9.84% and was similar than under 1 or 5 mPa. In conclusion, the shear stress modified the anodic coverage rate as a shear stress of 5 mPa increased the rate relative to the 1mPa shear stress, but a higher shear stress of 10 mPa decreased the rate. After 10 days, the coverage was similar at around 50% under the three conditions.

Thickness of biofilms

The biofilm thickness increased linearly as a function of time under the three conditions (Figure 5.4B). Under 5 mPa, it seems that the thickness increased faster during the first days of the experiment. The biofilm thickness was of 3.25±1.27µm after two days under 1 mPa shear stress, 4.08±1.13µm after three days under 10 mPa and 7.67±2.19µm after two days under 5 mPa. After 10 days, less difference was observable as the thickness was 10.33±2.02µm, 13.25±2.44µm and 13.56±1.31µm under 1, 5 and 10 mPa shear stress, respectively. Under 10 mPa shear stress, the power density continued to increase after 10 days.

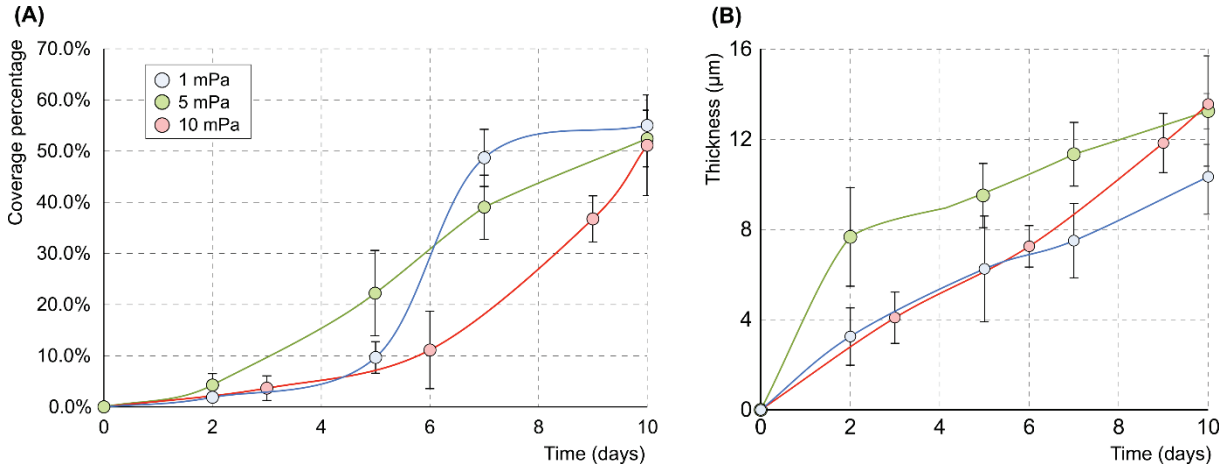

Figure 5.4. Coverage (A) and thickness (B) of the biofilms as a function of time. The points represent the mean of the coverage percentage and biofilm thickness from fluorescent microscopy observations (2 observations per sample). A threshold was applied on a Z-projection of the maximal intensity using imageJ. The error bars represent the standard error.

Active and Inactive biofilm percentage

The active and inactive microbial fraction was determined by the analysis of fluorescent microscopy biofilm labelled using the Live/Dead kit. The proportion of active bacteria between 7 and 10 days was 72.30±16.28%, 86.17±4.71% and 58.13±11.65% under 1, 5 and 10 mPa shear stress, respectively (Figure 5.5). A medium shear stress of 5 mPa increased the proportion of active bacteria by 13.87% relative to the 1mPa shear stress, but the shear stress of 10 mPa decreased this proportion by 14.17%.

5.3.3. **Bacterial community analysis**

In order to know if the shear stress could select EAB, the bacterial community was identified from metagenomic data annotated with the *nr* database from NCBI (Figure 5.6 and 5.7). The mean of the sequence number per sample was of 230783.2±183325.3 sequences. The mean of the annotated sequence percentage in each sample was 59.7±10.7%. The relative abundance of specific EAB that were mainly from the *Geobacteriaceae* family increased strongly with the shear stress (Figure 5.7). The

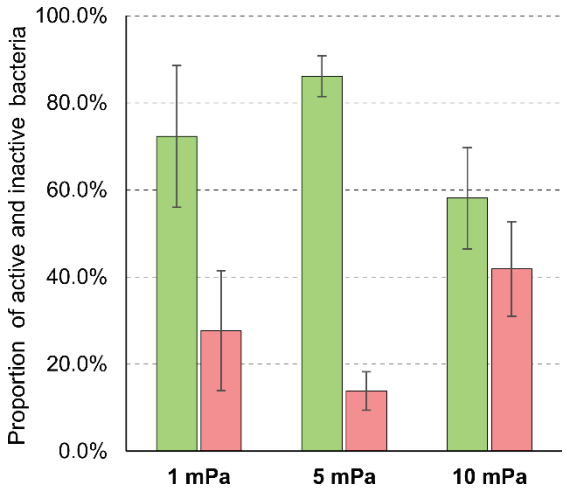

Figure 5.5. Percentage of active and inactive bacteria after 7-10 days. The graphic represent the mean of the active and inactive bacteria percentage from microscopy observations of samples between 7 and 10 days. Green bars are active and pink bars are inactive microorganisms. The error bars represent the standard error.

percentage was only of 2.37±0.34% (within 0.34±0.13% of *Geobacteriaceae*) in the inoculum and it was of 16.20±3.14% (within 11.46±2.32% of *Geobacteriaceae*), 20.40±8.56% (within 16.06±7.20% of *Geobacteriaceae*) and 35.78±6.70% (within 28.41±5.49% of *Geobacteriaceae*) under a shear stress of 1, 5 and 10 mPa, respectively. Unspecific EAB, which were mainly *Pseudomonas* and *Comamonas*, decreased as a function of the shear stress with 2.44±0.38%, 8.95±2.45%, 6.20±2.05% and 1.77±0.37% in the inoculum and under 1, 5 and 10 mPa shear stress conditions, respectively. In conclusion, a high shear stress modified the competition between specific and unspecific EAB. It favored the growth of specific EAB in the biofilm and mainly the *Geobacteriaceae* family.

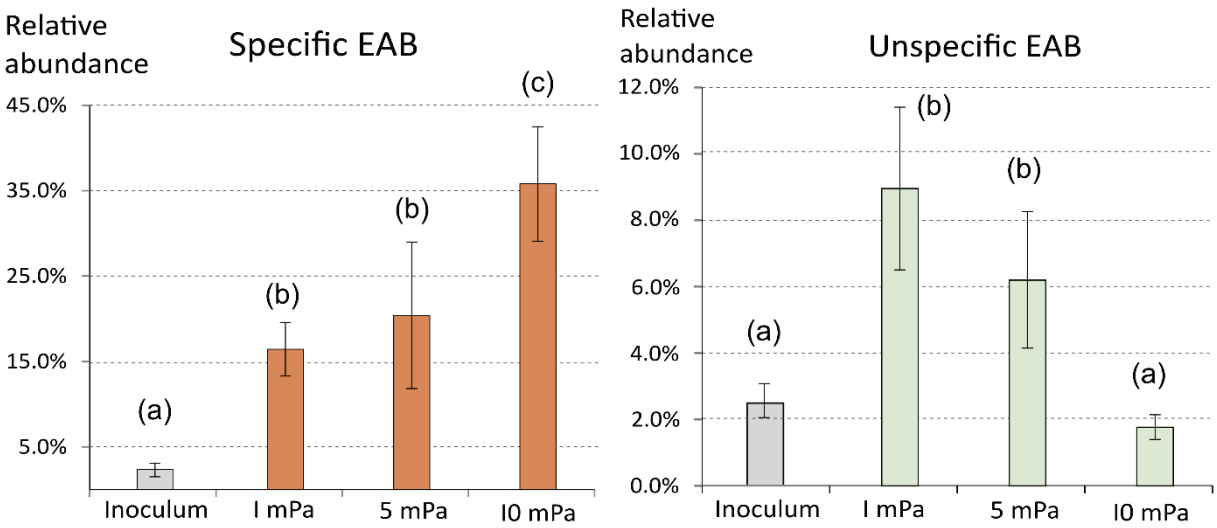

Figure 5.6. Relative abundance of specific and unspecific EAB in the inoculum and after 5 days under different shear stress in the MFCs. The error bars represent the standard errors. Data presented here are from metagenomic sequencing annotated against the nr database from NCBI. The bars represent the mean of samples after 5 days under each shear stress. The letters indicate statistical groups based on p-value<0.05 after a Wilcoxon test.

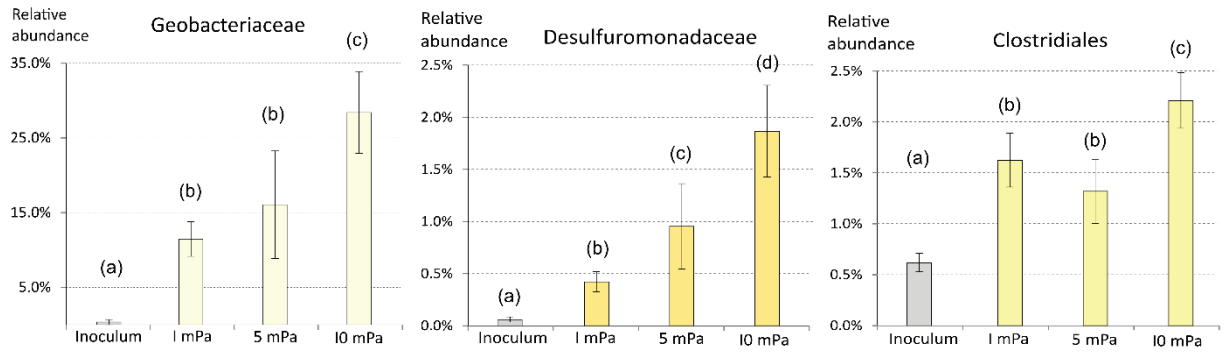

Figure 5..7. Relative abundance of some specific EAB in the inoculum and after 5 days under different shear stress conditions. The error bars represent the standard errors. Data presented here are from metagenomic sequencing annotated again the *nr* database from NCBI. The histogram bars represent the mean of samples after 5 days under each shear stress. The letters indicate statistical groups based on p-value<0.05 after a Wilcoxon test.

5.3.4. **Functional analysis**

In order to know if an applied flow favored direct EET over an indirect EET by redox mediators, the relative abundance of the genes associated to this functions were compared between 7 and 10 days (Figure 5.8 and Figure 5.9). The cytochromes C are ubiquitous proteins involved in the microbial respiration. Here, the only cytochrome C gene detected was not evidence of direct EET, however outer-membrane cytochrome C is a key protein for a direct EET. The relative abundance of genes coding for cytochromes C was higher in the biofilms than in the inoculum. More specifically, the genes coding for cytochromes C from specific EAB which used mostly a direct EET, were statistically more abundant in the biofilms than in the inoculum, and increased all the more as the shear stress increased: respectively 0.01±0.01%, 0.27±0.06%, 0.37±0.18 and 0.51±0.07% for the inoculum and after one week under 1, 5 and 10 mPa. So, an increase of the shear stress seems favor a direct EET. On the other hand, the relative abundance of genes associated with redox shuttles was lower in the biofilms after 7 days than in the

inoculum (2.65±0.20%, 1.80±0.10%, 2.02±0.12% and 2.65±0.20% for the inoculum and after one week under 1, 5 and 10 mPa, respectively). These results confirm that this function was not specifically involved in the EET. In addition, the relative abundance of the redox mediator genes increased with the shear stress, which suggest that fluid flow does not reduce redox shuttles. The main genes coding for proteins involved in shuttles were genes coding for the production of the flavin family (1.89±0.20%, 1.11±0.05%, 1.28±0.11% and 1.41±0.05% for the inoculum and after one week under 1, 5 and 10 mPa, respectively). The other genes were relatively less abundant and coded for the production of quinone and phenazine families.

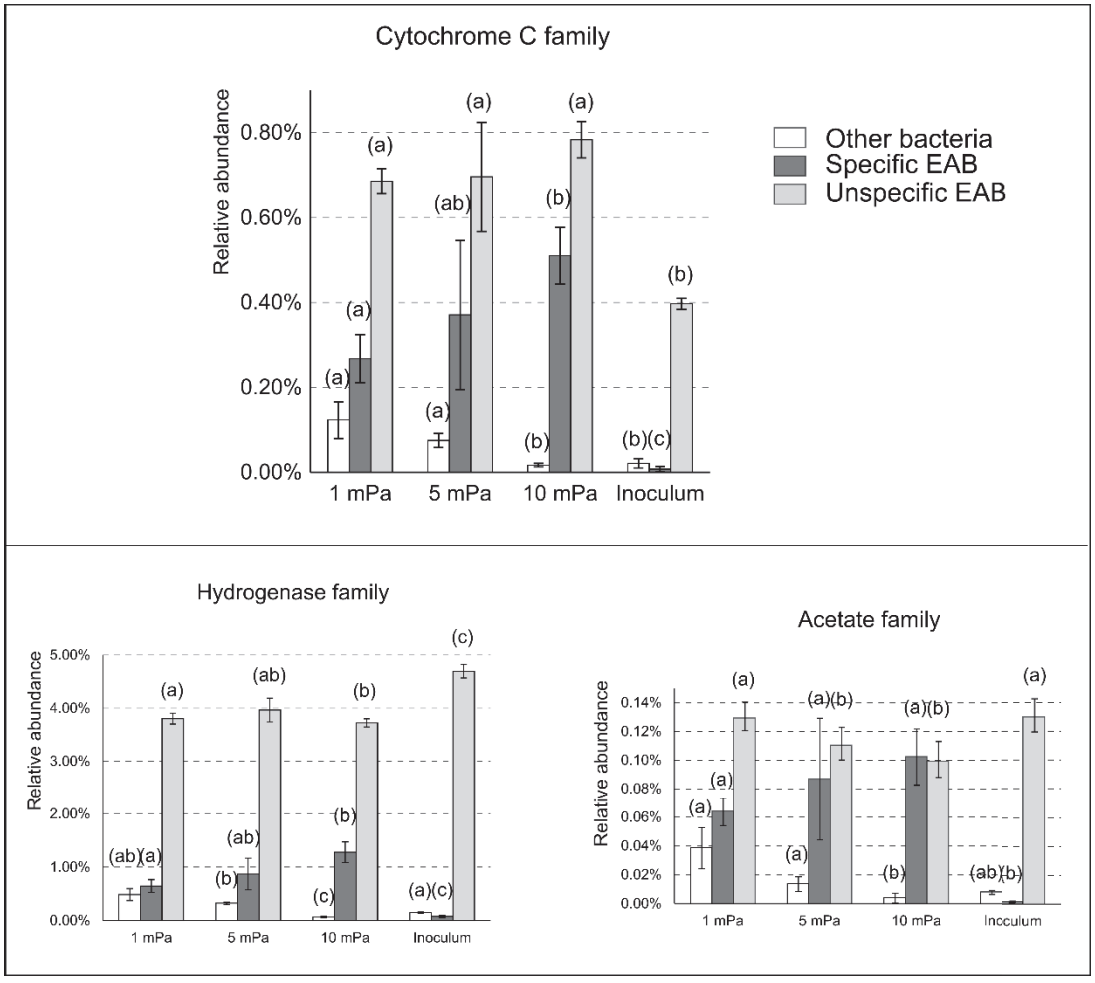

Figure 5.8. Relative abundance of genes coding for major functions of the electron flux between 7 and 10 days: functions associated to cytochromes C, hydrogenases and acetate consumption family. For each function the relative abundance of functions belonging to specific EAB (dark gray), unspecific EAB (white) and to the other bacteria (gray) is indicated. The error bars represent the standard error. The letters represent the statistical group (p-value < 0.05 after a Wilcoxon test).

In order to know if a shear stress selects genes coding for bacterial adhesion, the relative abundance of genes coding for the production of pili was (Figure 5.10). The relative abundance of these genes was higher in biofilms growing under shear stress conditions than in the inoculum (0.33±0.04%, 0.52±0.05%, 0.46±0.02% and 0.52±0.01% for the inoculum and after one week under 1, 5 and 10 mPa shear stress, respectively). The relative abundance of genes coding for pili in the biofilm under 10 mPa was similar to that for the biofilm under 1 mPa.

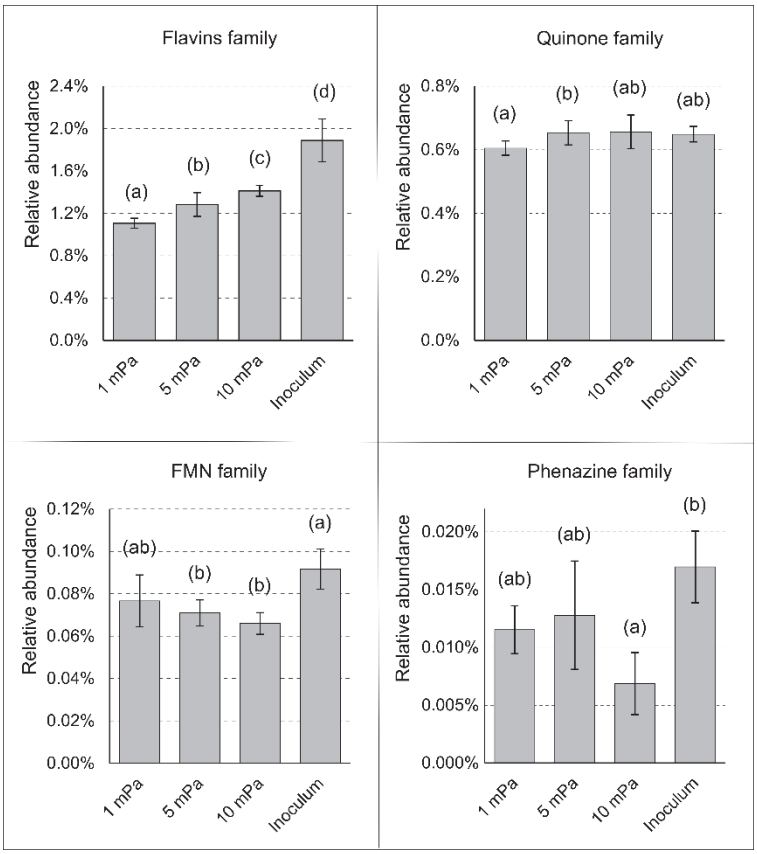

Figure 5.9. Relative abundance of genes coding for major functions of electron shuttles between 7 and 10 days: functions associated to the production of flavin, FMN (FlavoMonoNucleotid), quinone and phenazine family. The error bars represent the standard error. The letters represent the significant statistical group (p-value < 0.05 after a Wilcoxon test).

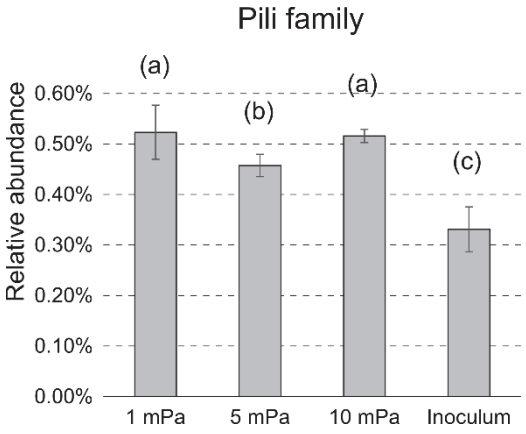

Figure 5.10. Relative abundance of genes coding for major functions of adhesion between 7 and 10 days: functions associated to the production of pili. The error bars represent the standard error. The letters represent the statistical group (p-value < 0.05 after a Wilcoxon test).

5.4 Discussion

5.4.1. Anodic coverage vs EAB selection for electricity production

This study shows that the selection of specific EAB increased as a function of shear stress after 5 days. The power density was not correlated to the relative abundance of specific (R^2 = 0.35) or unspecific EAB (R^2=-0.04),but, it was linearly correlated to the coverage percentage (R^2 = 0.95) (Figure 5.11). Two hypotheses could explain these results: (i) other bacteria were not taken into account in this study and are also involved directly or indirectly in electricity production and/or (ii) the power density was limited by other factors such as mass transport or electrochemical conditions and not microbiological factors. For the first hypothesis, other bacteria might be needed to provide essential nutrients to EAB. For the second hypothesis, the mass transport might be limiting due to the low Reynolds numbers in microfluidic system. However, the initial concentration in acetate, the residence time and the fact that the power density was not higher under conditions where the Reynolds number was higher, make this hypothesis unlikely. The electrochemical conditions such as the electrochemical anodic potential seems a more probable hypothesis. The reactor design should be adapted to include the insertion of a reference electrode to verify this parameter during the biofilm development.

5.4.2. Limits of the functional metagenomic analysis

Functional metagenomic analyses provide access to useful information about the mechanisms involved in EET in electroactive biofilms. The genes involved in EET in *Geobacter* and *Shewanella* are

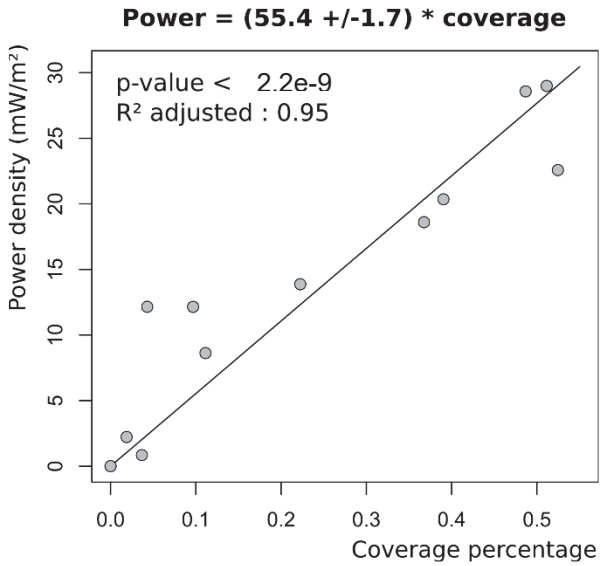

Figure 5..11. Linear model of the power density in function of the coverage percentage of the anode. Points: mean of the power density in function of mean of coverage percentage from MFC under the three shear stress and from all the time points. Line: associated linear model of type y = ax.

relatively well known, but those in other bacteria are not. Both bacteria have high numbers of c-cytochromes type genes. Sturn *et al.* [62] analyzed the number of c-cytochromes in 483 proteo-bacterial genomes. The average number was 13 whereas *S. oneidensis* MR-1 has 41 putative c-type cytochromes and *Geobacter sulfurreducens* has more than one hundred [96]. EAB could be adapted to a large insoluble electron acceptor with a large surface potential by using a large diversity of c-cytochromes with different redox catalytic sites. Some correlation between the number of cytochromes and the ability to EET has been shown [14]. Yet, *Shewanella denitrificans* has 14 c-cytochromes and is unable to mediate EET. However, some other bacteria, such as *Bradyrhizobium japonicum*, have a higher number of cytochromes and are also unable to mediate EET. Other bacteria, such as *Escherichia coli*, have a lower number of c-cytochromes and are able to mediate EET. So, a genetic marker of direct EET does not yet exist.

Genetic markers for indirect EET are less ambiguous. For example, the presence of genes coding for the synthesis of flavins involved the bacterial capacity of an indirect EET. But, the production of flavin or phenazine family (within the function is present in a large diversity of taxon) has other role than EET in bacteria such as the intercellular communication, the *quorum sensing* [132], [133]. So, if the presence of genes involved in the synthesis of redox shuttles predicates the capacity of indirect EET, the real activity of an indirect EET cannot be concluded. For this reasons, functional analysis on the DNA level is limited and should be coupled to a metaproteomic analysis (see Appendix 1). The sequencing of proteins had been planned (*i.e.*, proteins were extracted) and making possible this approach in the future.

5.4.3. **Conclusion**

These results support the conclusion of the Chapter 4: specific EAB are selected under shear stress conditions. Three shear stress were tested in this study: 1, 5 and 10 mPa. The anodic biofilms growing under 10mPa presented a relative abundance of specific EAB of 35.78±6.70% (within 28.41±5.49% of *Geobacteriaceae*), in opposite to the anodic biofilms growing under 1mPa which presented a relative abundance of 16.20±3.14% (within 11.46±2.32% of *Geobacteriaceae*).

In addition, the shear stress decelerates the kinetic of biofilm development. But after 10 days, no difference of coverage percentage or thickness was observed. It was probably due to the relative low range of shear stress used. However, the shear stress modified the proportion of live and dead bacteria in the biofilm. The biofilms growing under a shear stress of 5 mPa had the lower proportion of dead bacteria: a lower shear stress did provoke the detachment of dead matter and a higher shear stress was probably harmful for bacteria. More analyses are necessary to observe the density of the biofilm and the spatial repartition of live and dead bacteria in the biofilms.

This work demonstrated the major role of the shear stress in the biofilm formation and should be taken into account for the architecture of reactors. Applying a shear stress could be a way to control the selection of EAB and the quantity of dead matter in anodic biofilms.

Abstract : Chapter 6

Hydrodynamic conditions play a major role in the biofilm formation. They impact the bacterial composition of the biofilm, their activities and the physical structure of the biofilm by a control of the substrate and product transport outside and inside the biofilm. They control also the forces applied to the surface, the shear stress, which impact the biofilm formation in terms of density, thickness or dead mass proportion. Mass transport and shear stress are both dependent of the fluid velocities. For this reasons, it is difficult to study the effect of the shear stress independently to the mass transport and the residence time. In order to resolve this problem, a MFC with a Taylor reactor configuration was designed and build. The Taylor reactors have the advantages to be studied in different domains, so the hydrodynamic conditions are well known. It is composed of two cylinders: an inner rotating cylinder and an outer fixed cylinder. The liquid medium is present between this two cylinders. Different flow types can be observed in function of the reactor dimensions and the rotation velocity of the inner cylinder. From a critical Reynolds number, Taylor vortices can be observed between cylinders. This work presents the configuration characteristics and preliminary experiments to test the MFC with a Taylor configuration and the electricity production.

The reactor was composed of two cylinders: a rotating inner cylinder (ø160 x 380 mm) on which a carbon cloth anode was fixed covering the whole surface (1909.12 cm^2), and a fixed outer cylinder (ø189x380 mm) on which 12 air cathodes (ø 40mm) were inserted (cathode surface: 150.80 cm^2). The volume between cylinders was 3.02 L. The distance between cylinders, and so between electrodes was 14.5 mm. In this configuration, the shear stress is not homogenous on the anodic surface and the variation were described and should be taken into account for the choice of the rotation velocity and the sampling strategy. Under a shear stress between 76.9 and 131.8 mPa, corresponding to a rotation velocity of 80 rpm, the MFC had a maximal power of 4.52 mW/m^2 after 25 days and a substrate flow of 1.29 $g.L^{-1}.day^{-1}$. The MFC degraded 63% of the BOD, that to say an activity of 0.32 $g.L^{-1}.day^{-1}$. The resistances of the MFC after 25 days were 14.97±0.38 ohms for the ohmic resistance, 5.85±0.35 ohms for the resistance linked to the cathode and 12.04 ohms for the resistance linked to the anode. The biofilm growth was very long, due firstly to a limit of substrate concentration and maybe due to a high shear stress.

The Taylor configuration seems a good solution to study independently the shear stress and the mass transport in MFC which are major parameters for the scale-up of MFCs. More experiments at different shear stress and different residence times are necessary and should give more information about the optimization of hydrodynamic parameters for the scale-up of MFC.

Chapter 6.

Study of a MFC with a Taylor reactor configuration

6.1 Introduction

Hydrodynamic conditions play a major role in the biofilm formation and their activities [113], [114], [164]–[168]. They impact the bacterial composition of the biofilm, their activities and the physical structure of the biofilm by a control of the substrate and product transport outside and inside the biofilm. They control also the forces applied to the surface, the shear stress, which impacts the biofilm formation in terms of density, thickness or dead mass proportion. Mass transport and shear stress are both dependent of the fluid velocities. For this reasons, it is difficult to study the effect of the shear stress independently to the mass transport and the residence time.

In order to resolve this problem, a MFC with a Taylor reactor configuration was designed and build. The Taylor reactors have the advantages to be studied in different domains such as cellular culture and fluidic dynamic [114], [169]–[174], so the hydrodynamic conditions such as shear forces but also mass transport are well known in this type of reactor. It is composed of two cylinders: an inner rotating cylinder and an outer fixed cylinder. The liquid medium is present between this two cylinders. Different flow types can be observed in function of the Taylor number which is a one dimension value determining the flow type. It is calculated by the following equation (6.1) [175]:

$$Ta = 4.Re^2.\frac{r_{ext}-r_{int}}{r_{ext}+r_{int}} = 4.\left(\frac{\Omega}{\nu}\right)^2.r_{int}^2.\frac{(r_{ext}-r_{int})^3}{r_{ext}+r_{int}} \qquad (6.1)$$

with $Re = \Omega.r_{int}.\frac{r_{ext}-r_{int}}{\nu}$ (6.2)

where r_{int} and r_{ext} are the inner and outer cylinder radii in m, *Re* the Reynolds number, *v* the cinematic viscosity of water in $m^2.s^{-1}$, and *Ω* the rotation velocity in $rad.s^{-1}$. For $Re_c < 134.57$, the flow is tangential and laminar (a Couette flow). Then there is a formation of Taylor vortices ($Re_c>134.57$). The flow is first still laminar ($134.57<Re_c<955.45$) and after become turbulent keeping unstable vortex structure.

In MFC domain, several studied are interested by mass transport [176], but no study takes care precisely of both mass transport and shear stress. The MFC with a Taylor configuration was designed for this goal. This work presents the characteristics of the reactor and preliminary experiments to test the MFC and the electricity production.

6.2 Materials and methods

6.2.1. Reactor configuration and setting up

The Taylor reactor configuration was described in the Figure 6.1. It was composed of two cylinders: a rotating inner cylinder (ø160 x 380 mm) on which a carbon cloth anode was fixed covering the whole surface (1909.12 cm²), and a fixed outer cylinder (ø189x380 mm) on which 12 air cathodes (ø 40mm) were inserted (cathode surface: 150.80 cm²). The cathodes were built by following previous protocol [124], [177]. The volume between cylinders was 3.02 L. The distance between cylinders, and so between electrodes was small (14.5 mm), decreasing the ohmic resistance. The anode and the cathode were connected by an external resistance of 1000 ohms. The motor driving the inner cylinder was controlled by the Biostat B control unity. A rotation velocity of 80 rpm was applied during the whole experiment, corresponding to a Taylor number of 4137, a Reynolds number of 9718 (turbulent flow) and a shear stress of 50 mPa. A peristaltic pump controlled by the Biostat B control unity, applied an axial flow through the reactor, controlling the residence time in the reactor. The dimensions of the reactor were determined in order to have a Taylor vortex regime for small rotated velocities and a shear stress lower than 100 mPa.

The medium was wastewater from a wastewater plant station (Feyssine, Lyon, France) amended with 1.2 g/L (20mM) of sodium acetate. The biochemical oxygen demand (BOD)5 was only of 16 mg/L before the amendment. The bacterial concentration was of 3.2 10^3 cells/mL, and was measured by direct counting using a Malassi cell. The pH was 7.66 and the conductivity was 2.25 mS/cm. They were measured using electrochemical probes. The cell voltage was reordered every 10 minutes.

Shear stress calculation

The shear stress mean was calculated with the following approximation [114]:

$$\tau = 2.13 \frac{\left(\frac{r_{int}}{\delta + r_{int}}\right)^{\frac{3}{2}}}{\left(\frac{\delta}{\delta + r_{int}}\right)^{\frac{7}{4}}} Re^{1.445} \frac{\rho \nu^2}{2\pi r_{int}} \quad \text{for Re} > 800 \quad (6.3)$$

$$\tau = 0.113 \frac{\left(\frac{r_{int}}{\delta + r_{int}}\right)^{\frac{3}{2}}}{\left(\frac{\delta}{\delta + r_{int}}\right)^{\frac{7}{4}}} Re^{1.764} \frac{\rho \nu^2}{2\pi r_{int}} \quad \text{for Re} > 10\,000 \quad (6.4)$$

with $$Re = \frac{\Omega \delta r_{int}}{\nu} \quad (6.5)$$

where r_{int} is the inner cylinder radius in m, δ is the distance between cylinders in m, ρ the liquid density in kg.m^{-3}, ν the cinematic viscosity in m^2.s^{-1}, and Ω the rotation velocity in rad.s^{-1}.

6.2.2. Residence time distribution

The residence time distribution was measured by pulse experiment using a solution of E122-Azorubine as marker. Its maximal wave length was at 515 nm. The absorbance at 515 nm was 0.523 for a

concentration of 1mL/L. 3.02 mL were injected in the reactor (volume: 3.02L) in order to have a maximal concentration of 1mL/L. After the injection, the absorbance in the output was measured every minutes during the first 10 minutes, then every 3 minutes until 30 minutes, and finally every 5 minutes until 110 minutes. The results are expressed in relative absorbance as a function of the time. The applied flow was 28mL/min, and the rotated velocity was 80 rpm.

6.2.3. BOD5 measures

The BOD5 is measured after 5 days of incubation with microorganisms at 20°C. It was measured using an OxiTop. The BOD5 was measured in output of the reactor in order to determine the carbon consumption percentage and the coulombic efficiency defined by the equation (6.6):

$$EC = \frac{i}{F.n.Q.\Delta BOD5} \qquad (6.6)$$

where *EC* is the coulombic efficiency, *i* the current in A, *F* the faraday constant of 96485 C.mol^{-1}, *n* the number of electrons produced per mole of substrate (8 electrons per mole of acetate), *Q* the fluid flow in mL.s^{-1}, and *ΔBOD5* the difference of substrate concentrations in mol.mL^{-1}.

6.2.4. Electrochemical analysis

The maximal power density was measured by linear voltammetry using a Voltalab potentiostat. A two electrode configuration was used: the anode as working electrode and the cathode as auxiliary electrode. The potential scanning started from the cell voltage in open circuit to 0 mV, with a rate of 1

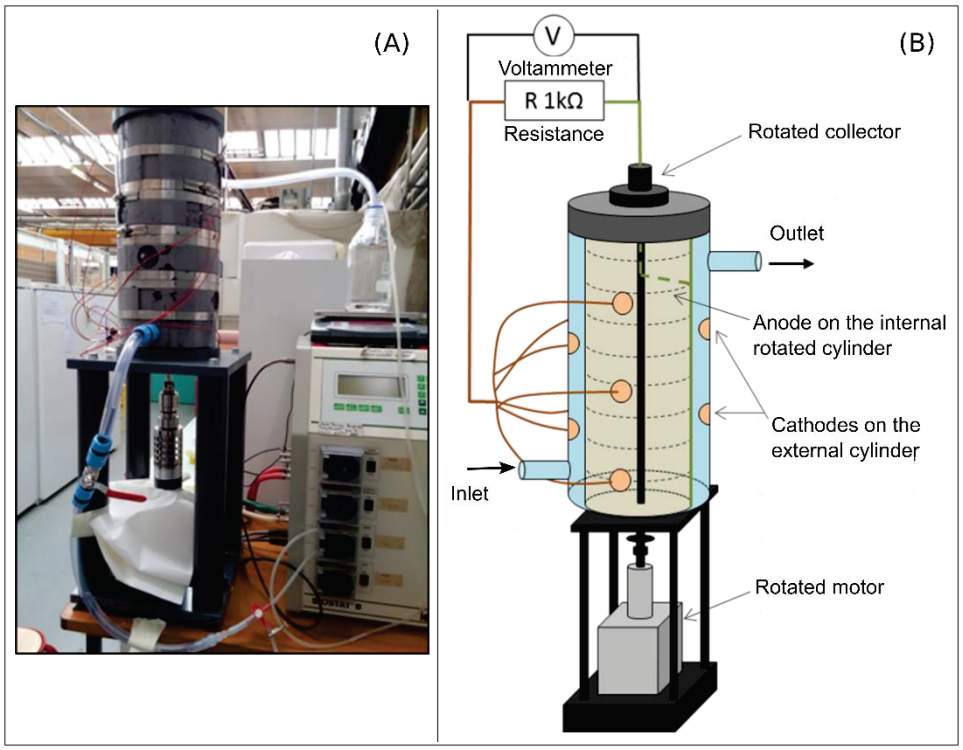

Figure 6.1. (A) Photography of the Taylor reactor. (B) Schematic of the Taylor reactor.

mV/s. This measures were done with a rotation of 80 rpm. The power density was calculated from the following equation (6.7):

$P=UI$ (6.7)

where *P* is the power density in W/m², *U* the cell voltage in V, and *I* the current density in A/m²

Impedance spectroscopy was also measured in order to determined different resistances: the anodic and cathodic resistances of charge transfer and the ohmic resistance. The resistances were determined by fitting the results against a circuit model described in the Figure 6.2. The scanning was of 10mV around the cell voltage in open-circuit, with frequencies from 1000 Hz to 100 mHz. Because of a too important noise due to the cylinder rotation, the measures were done without rotation of the inner cylinder.

6.2.5. **Model**

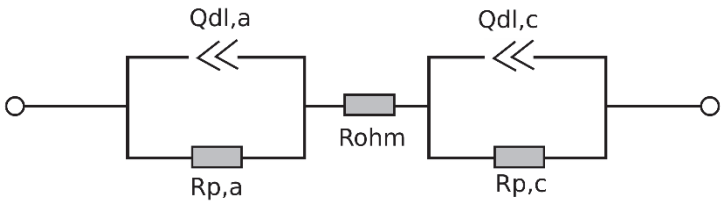

Figure 6.2. Circuit model for impedance spectroscopy studies. Rohm corresponds to the ohmic resistances, Rp,a and Rp,c to the charge transfer resistances of respectively the anode and the cathode.

A model was built using Comsol to verify the fluidic regimes in function of the rotated velocity and to observe the repartition of the shear stress on the anodic surface. Thanks to the reactor geometry, an axis symmetric hypothesis was used to simplify the three dimensional geometry into two dimensional one. The space between cylinders was then represented by a rectangular area (0.0145x0.380 m²), composed one mobile wall for the inner cylinder and one fixed wall for the outer cylinder. The mesh was built from recommended parameters of Comsol and was refined closed to the walls to take account of boundary layers. The flow inlet and outlet were neglected. The model was ran for different rotation velocities. The liquid medium was considered as water with a density of 1000 $kg.m^3$ and a

dynamic viscosity of 0.001 Pa.s. The model resolved the incompressible Newtonian Navier-Stokes equations, and turbulences were modeled by a RANS k-ε model.

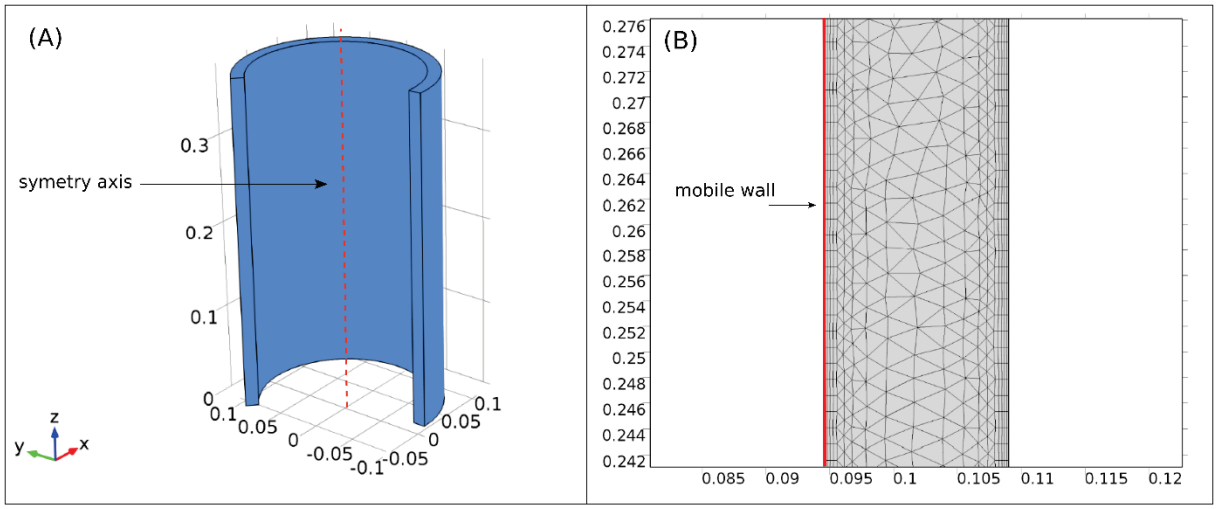

Figure6.3. Model geometry of the Taylor reactor. (A) 3D schematic of the reactor. The symmetry axis is represented in red and is the origin of the x and y axis. The xyz dimensions are in meter. (B) The 2D model of the reactor. The space between the cylinders is represented by a rectangular area with a mobile wall. The mesh is represented. The axis are the dimensions x and y in meter.

6.3 Results

6.3.1. Model

The rotation velocity of the model was between 20 and 125 rpm. The Table 6.3 shows the Reynolds and Taylor number calculated by the equation (6.1) and (6.2), and the flow regime theoretically associated at each rotation velocity. In order to verify that the model described correctly the flow regime of the Taylor reactor, the normed velocity was observed (Figure 6.5 and Figure 6.4). Taylor vortices were observed at each rotation velocity even in turbulent regime. The reactor was modeled to describe the distribution of the shear stress on the anodic surface. The modeled shear stress was closed to the theoretically shear stress calculated from the equations, (6.4), (6.4), (6.5) (Figure 6.7). The repartition of shear stress on the anodic surface is represented in the Figure 6.6, and follow the vortex formations. In opposite to microfluidic channels, the shear stress is not perfectly homogenous on the anodic surface. The shear stress can vary between 76.9 and 131.8 mPa (standard error = 15.8 mPa) on a distance y of about 3 cm. This information should be considered in the future if anode samples are taken.

Rotation velocity (rpm)	Reynolds	Taylor	flow regime
10.0	1214.7	517.2	*Taylor vortex*
20.0	2429.5	1034.3	*Taylor vortex*
30.0	3644.2	1551.5	*Taylor vortex*
40.0	4859.0	2068.6	*Taylor vortex*
50.0	6073.7	2585.8	*Taylor vortex*
60.0	7288.5	3103.0	*Taylor vortex*
70.0	8503.2	3620.1	*Taylor vortex*
80.0	9718.0	4137.3	*Taylor vortex*
90.0	10932.7	4654.4	*Taylor vortex*
100.0	12147.5	5171.6	*Turbulent*
125.0	15184.4	6464.5	*Turbulent*

Table 6.3. Characteristics of the flow regime as a function of the rotation velocity (rpm). Reynolds and Taylor number were calculated with the equations (6.1) and (6.2). The flow regime was determined from Reynolds numbers.

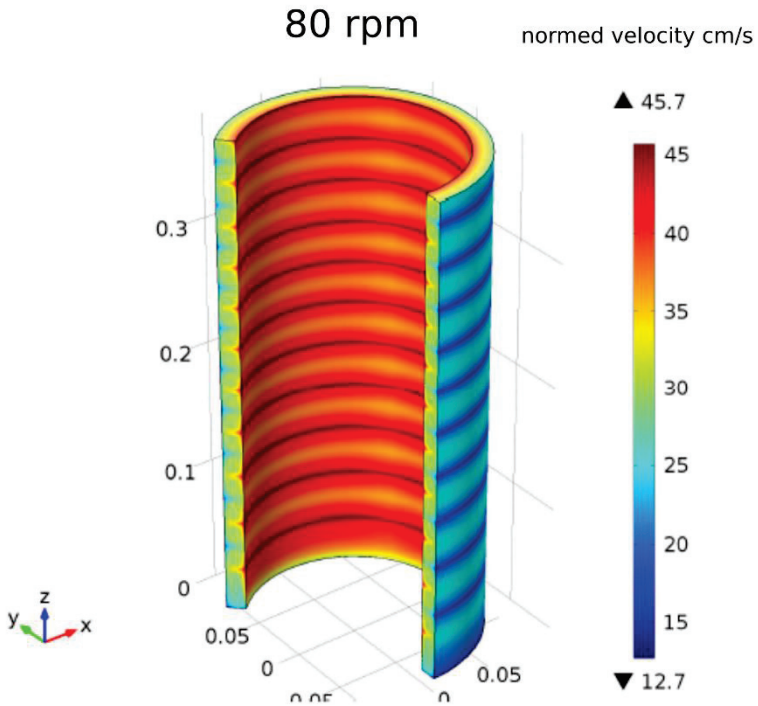

Figure 6.5. Flow regime at 80 rpm. The 3D graphic represents the normed velocity in cm.s^{-1}. Taylor vortex can be observed at 80 rpm.

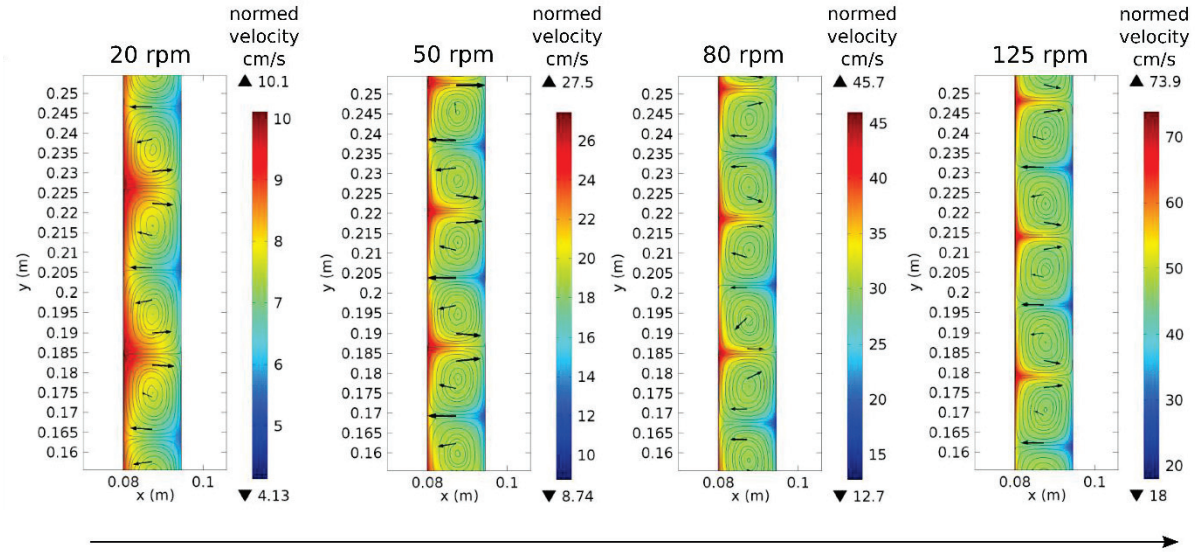

Figure 6.4. Evolution of the flow regime as a function of the rotation velocity. The colors represent the normed velocities in cm.s^{-1}.

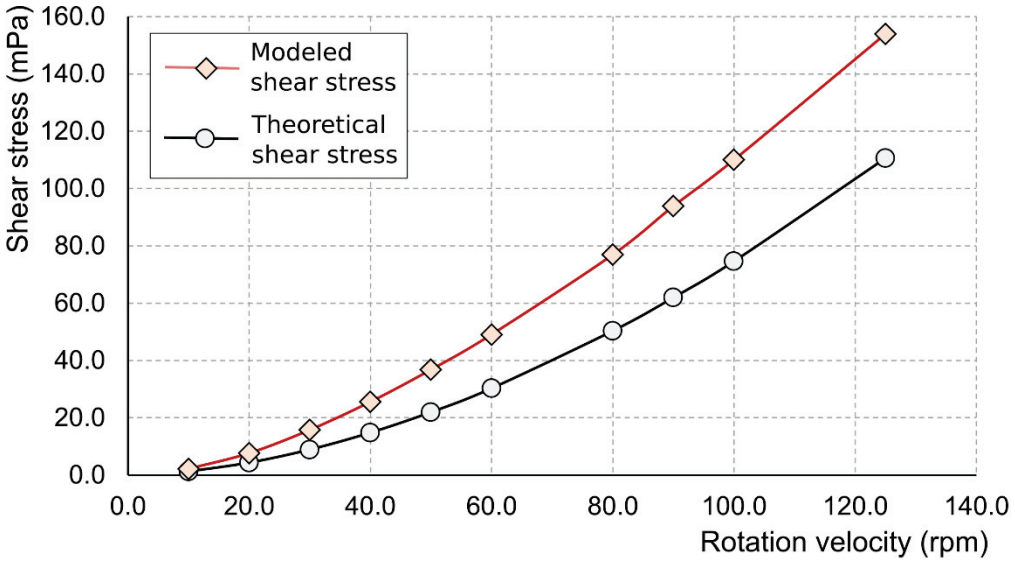

Figure 6.7. Shear stress in mPa on the anodic surface as a function of the rotation velocity. The dark curve represents the theoretical shear stress calculated by the equations (6.3), (6.4) and (6.5). The red curve is the shear stress measured using the model.

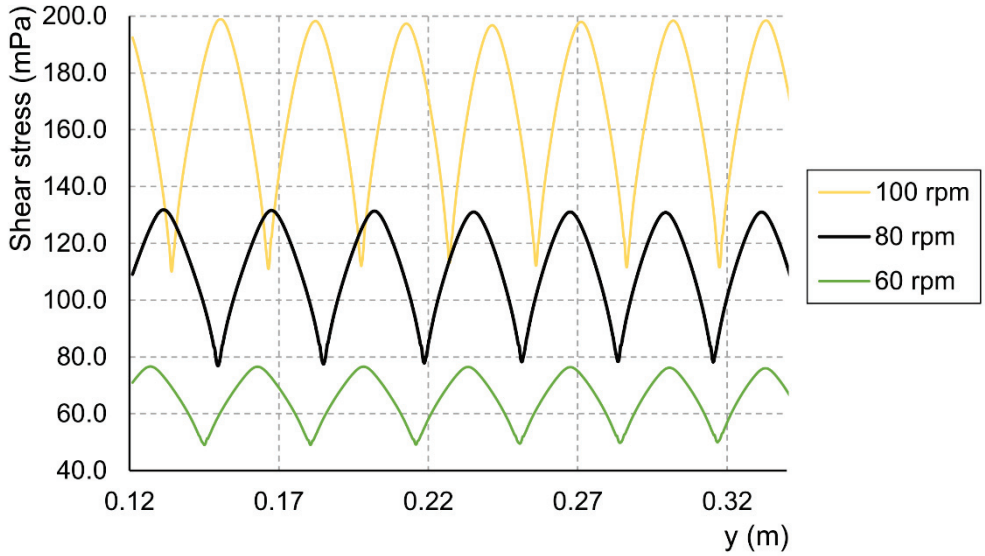

Figure 6.6. Shear stress in mPa in function of the y axe for a rotation velocity of 60, 80 or 100 rpm.

6.3.2. **Residence time distribution**

In a perfect mixed reactor, the concentration evolution of an injected marker by pulse experiment in function of the time is defined by the equation (6.8):

$$C = C_0 e^{-t/\bar{t}} \quad (6.8)$$

where *C* is the marker concentration in the output flow, C_0 the maximal concentration of the marker, $\bar{t}$ the residence time mean, and *t* the residence time. In this study, the maximal relative absorbance is 1 and the residence time mean is theoretically given by the equation (6.9):

$$\bar{t} = \frac{V}{Q} = \frac{3.019}{0.028} = 107.14\ min \leftrightarrow \frac{1}{\bar{t}} = 0.009\ \mathrm{min}^{-1} \qquad (6.9)$$

where *V* is the reactor volume of 3 liters and Q the fluid flow in L/min^{-1}. The Figure 6.8 shows the marker concentration in the fluid output in function of the time for experimental measures and theoretical distribution. The residence time mean was very smaller than theoretical residence time mean (6.10):

$$\frac{1}{\bar{t}} = 0.018 \leftrightarrow \bar{t} = 55.6\ min \qquad (6.10)$$

This results demonstrate that there is a dead volume of 1.46L in the reactor. Raguin L.G. *and al.* [169] showed that the matter transfer is preferentially between the vortices than inside the vortices. The vortex centers could be considered as dead volume. This effect can be observed in the Figure 6.9 showing the x and y normed velocity. The velocity in the vortex centers was only of 0.15 cm.s^{-1}, while the velocity outer the vortices was 7.31 cm.s^{-1}. The Figure 6.9 shows also a low velocity of 0.5 cm.s^{-1} between the vortices where a dead volume can exist too.

6.3.3. Electricity production

The Figure 6.11 shows the cell voltage in function of the time. Firstly, the fluid flow was 88.8mL.h^{-1} ($\bar{t} = 1.42\ day$), but the cell voltage stayed low (less than 180mV) after two weeks. So the fluid flow had been increased until 136.0 mL.h^{-1} ($\bar{t} = 0.93\ day$) the 18th days. Immediately after this change, the cell

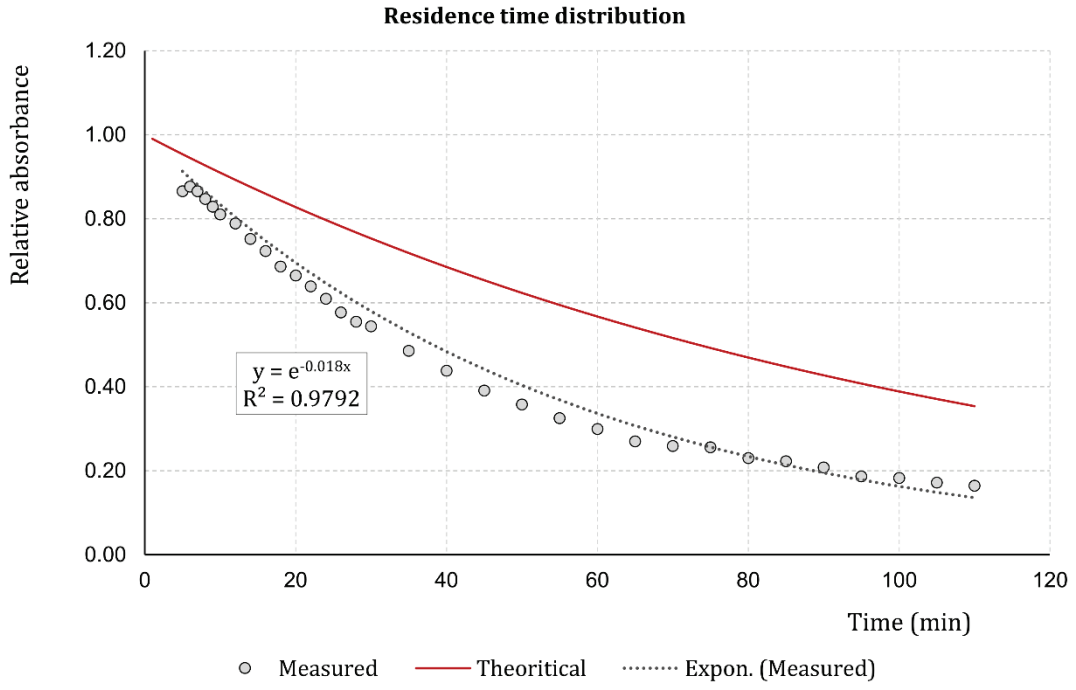

Figure 6.8. Residence time distribution. The red curve represents the theoretical distribution in a perfect mixed reactor. The points represent the experimental measured and the dotted curve represents the tendency curve from experimental points.

voltage increased from the 18th day to 524 mV the 30th day corresponding to a current density of 2.75 mA/m² and a power density of 1.44 mW/m².

The maximal power density was measured after 17 and 25 days (Figure 6.11). After 17 days, the cell voltage was 153.5 mV and the maximal power density was 0.91 mW/m² at a current density of 12.43 mA/m². After 25 days the cell voltage was 350.4 mV and the maximal power density increased until 4.52 mW/m² at a current density of 27.47 mA/m².

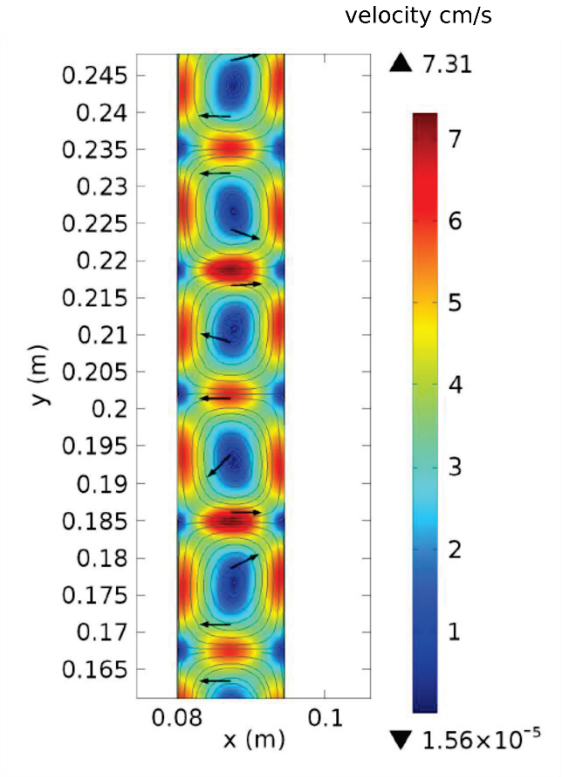

Figure 6.9. Flow normed velocity in x and y axis at 80 rpm

6.3.4. **BOD consumption**

The BOD consumptions were measured the 17th and the 25th day. The initial BOD5 was 1241.67 ± 58.45 $mg.L^{-1}$. After 17 days, the BOD5 was of 120.00±69.28 $mg.L^{-1}$, corresponding to a consumption of 90.34% of the BOD and to an activity of 0.19 $g.L^{-1}$. Day^{-1}. At the 25th day, the BOD5 was 458.89±81.92 $mg.L^{-1}$ corresponding to a consumption of 63.04% of the BOD and to an activity of 0.32 $g.L^{-1}.day^{-1}$ of BOD. The mixing inside the reactor allows a good consumption of the organic matter but lead also to a very low columbic efficiency. It was 0.4 10^{-3} at the 17th day and 0.2.10^{-3} at the 25th day.

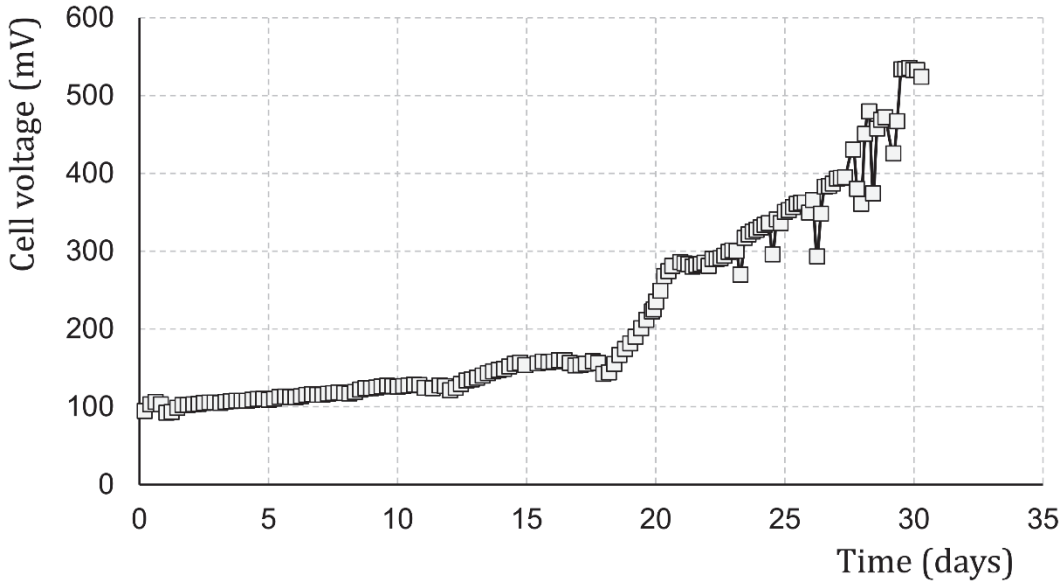

Figure 6.11. Evolution of the cell voltage in function of the time. An external resistance of 1000 ohms was used during whole the experience.

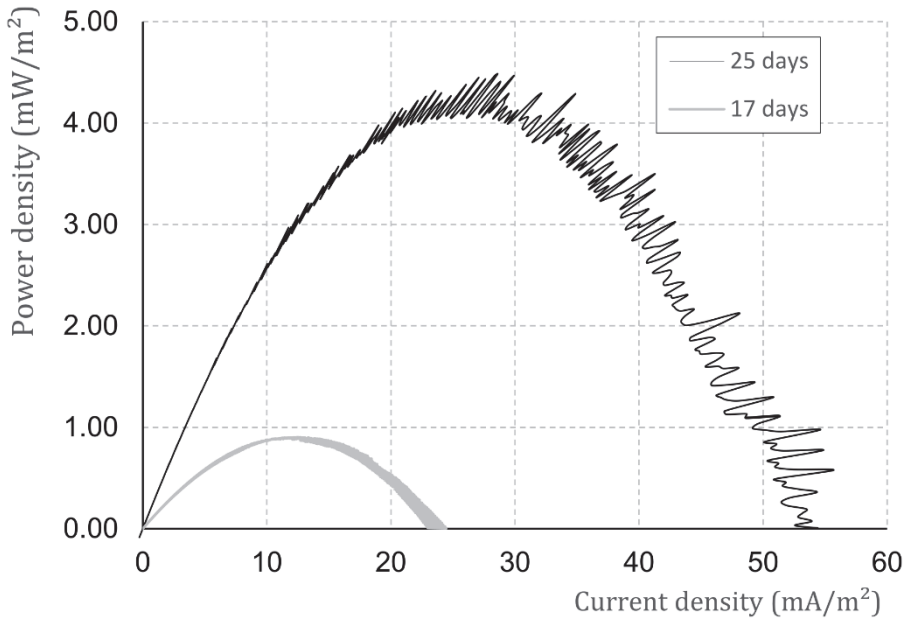

Figure 6.10. Power density in function of the current density after 17 and 25 days

6.3.5. **Impedance**

The impedance spectrometry was measured in order to determine the anodic charge transfer resistance. The Figure 6.12 shows the Nyquist graphic from the impedance spectrometry measures after 17 and 25 days. The ohmic resistance was similar at 17 and 25 days and it was 14.97±0.38 ohms. The resistance at the cathode was also similar at 17 and 25 days and it was 5.85±0.35 ohms. However the anode resistance evolved in function of the time. It was difficult to determine the anode resistance at 17 days but it was superior to 700 ohms. After 25 days, the resistance can be measured and it was only of 12.04 ohms.

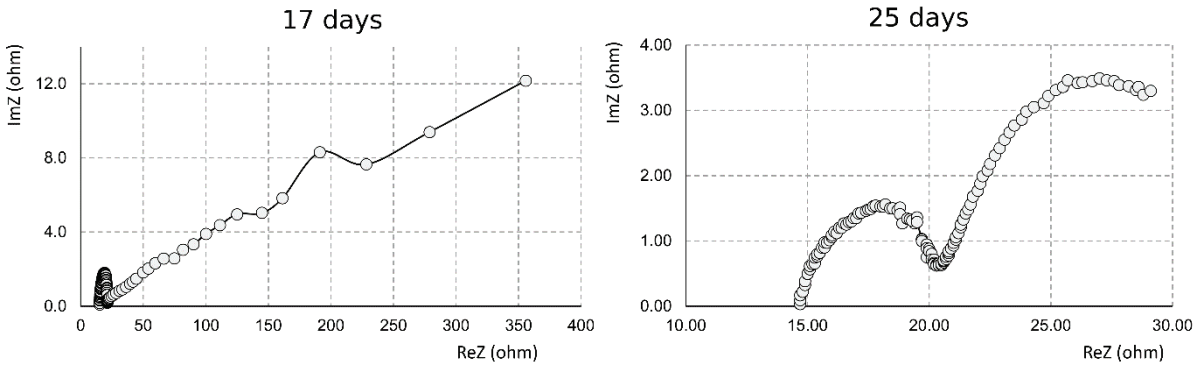

Figure 6.12. Impedance spectrometry at 17 and 25 days (Nyquist graphic).

6.4 Discussion

6.4.1. Microfluidic vs Taylor reactors

The hydrodynamic conditions influence dependently different parameters: the shear stress, the residence time, the mass transport in the liquid medium but mostly at the biofilm surface and inside the biofilm. The MFCs with a configuration of a laminar flow chamber were designed to observe the biofilm formation under flow conditions. It should be used to observe the mass transport inside the biofilm under different flow. Several studies modeled mass transport in MFCs [101], [106], [178]–[181]. Picioreanu C. *et al.* in 2010 [106] and Marcus A. K. *et al.* in 2011 [182] studied the limits of protons transport as a limiting factor of the biofilm growth. However, it is difficult to compare this models to experimental data. For that microfluidic reactors coupled to fluorescence microscopy seem unavoidable.

However, it is not possible with this reactors to study independently the shear stress and the residence time or the mass transport. For that a MFC with a Taylor configuration was designed, built and set up in the Chapter 6. This reactor was built as an intermediate step towards scaling-up. The Taylor reactors is well studied in different domains such as cellular culture and fluidic dynamic [170]–[172], [172], [183], so the hydrodynamic conditions are well known. The knowledge in hydrodynamic conditions (mass transport, shear stress and residence time) should lead the choice of architecture and parameters of applied MFCs, particularly for MFCs with a 3D anode such as carbon granule or foam. Indeed, the researches show a particular interest this last years for 3D anodes which offer a larger active surface than plane anode. The knowledges about the effect of the shear stress and the mass transport inside the biofilm should lead the choice of the size of interstices in the anodes.

The optimization of hydrodynamic conditions is a major lock for the MFC development that can be unbolted by a unique approach but the association of different methods: (i) microfluidic coupled to microscopy to study the biofilm formation (kinetics, density, thickness…) and the mass transport inside the biofilm, (ii) scaled up MFCs with a well-known architecture model for process engineering studies and evaluation of the organic charge abatement, coulombic efficiency and electrical performances, (iii) pilot building.

6.4.2. Conlusion

The Taylor configuration seems a good solution to study independently the shear stress and the mass transport in MFC which are major parameters for the scale-up of MFCs. The shear stress is not homogenous on the anodic surface and the variations were described and should be taken into account for the choice of the rotation velocity and the sampling strategy. Under a shear stress between 76.9 and 131.8 mPa (corresponding to a rotation velocity of 80 rpm), the MFC had a maximal power of 4.52 mW/m² after 25 days and a substrate flow of 1.29 $g.L^{-1}.day^{-1}$. The MFC degraded 63% of the BOD in 0.93 days, that to say an activity of 0.32 $g.L^{-1}.day^{-1}$. The resistances of the MFC after 25 days were 14.97±0.38 ohms for the ohmic resistance, 5.85±0.35 ohms for the resistance linked to the cathode and 12.04 ohms for the resistance linked to the anode. The biofilm growth was very long, due firstly to a limit of substrate concentration and maybe due to a high shear stress: after 30 day the electricity

production seemed to just starting to be stable. More experiments at different shear stress and different residence times are necessary and should give more information about the optimization of hydrodynamic parameters for the scale-up of MFC.

Conclusion

Through this thesis, different points about the dynamic of bacterial communities during the biofilm formation were highlighted. Based on the work of C. Koch *et al.* [61], special attention was given on specific and non specific EAB. Specific EAB include bacteria living in aerobic or anoxic environment, able to use a large range of electron acceptors and substrates and able to indirect EET such as *Shewanella oneidensis*. In opposite, non specific EAB includes bacteria living in anoxic environment, able to use a low range of electron acceptors and substrates, and able to direct EET, such as *Geobacter sulfurreducens*. The mechanisms involved in the selection of EAB were also a major part of this work.

First, the bacterial successions were studied under stationary conditions and in classical laboratory configurations. Three main results were showed:

- the biofilm formation was divided in two steps : first non specific EAB with a very flexible metabolism and using indirect EET grow in all MFCs producing or not electricity, then specific EAB adapted to direct EET become more competitive and predominant in the biofilm. The second step happened only in MFCs producing electricity and corresponded to an exponential increase of electricity production. In addition, the relative abundance of specific EAB was positively correlated to the maximal power density while the relative abundance of non specific EAB was negatively correlated to the maximal power density.
- The results show also a competition between specific EAB, especially between *Geobacter* and *Desulfuromonas* during the second step, but it did not lead to better or lesser electricity production.
- The selection of specific EAB happened only in the anodic biofilm and not in the liquid medium contrary to non specific EAB.

From this results, we hypothesis that an inhibition of the first step should decreases the competition between non specific and specific EAB during the anode colonization, and favors the growth of specific EAB in the biofilm. We propose to use the shear stress to select specific EAB during the adhesion step by detaching none and non specific EAB. For that MFCs with a configuration of a laminar flow chamber were designed, built and set up. The results demonstrate that under a high shear stress the abundance of specific EAB as *Geobacter* was very higher, until 30.14% in opposite to low shear stress where the relative abundance was lower than 1%. In addition, the shear stress decreases the coverage percentage of the anodic surface, showing that the selection of specific EAB happens by detaching other bacteria. So, the shear stress could be used to select specific EAB.

Finally, the effect of the shear stress on the microbial selection during the biofilm growth was investigated. This results confirm the precedent conclusion: specific EAB are selected under shear stress conditions. The anodic biofilms growing under 10mPa presented a higher relative abundance of specific EAB (35.78±6.70%) dominated by *Geobacteriaceae*, in opposite to the anodic biofilms growing under 1mPa (16.20±3.14%). In addition, the shear stress decelerates the kinetic of biofilm development. But after 10 days, no difference of coverage percentage or

thickness was observed. However, the shear stress modifies the proportion of live and dead bacteria in the biofilm. The biofilms growing under a shear stress of 5 mPa had the lower proportion of dead bacteria: a lower shear stress did not allow the detachment of dead matter, and a higher shear stress was certainly harmful for bacteria. This work demonstrates the major role of the shear stress in the biofilm formation, and should be taken into account for the architecture of reactors. Applying a shear stress could be a way to control the selection of EAB and the quantity of dead matter in anodic biofilms.

References

[1] A. S. Mathuriya and J. V. Yakhmi, “Microbial fuel cells – Applications for generation of electrical power and beyond,” *Critical Reviews in Microbiology*, vol. 42, no. 1, pp. 127–143, Jan. 2016.

[2] K. Rabaey and R. A. Rozendal, “Microbial electrosynthesis — revisiting the electrical route for microbial production,” *Nat Rev Micro*, vol. 8, no. 10, pp. 706–716, Oct. 2010.

[3] M. Di Lorenzo, T. P. Curtis, I. M. Head, and K. Scott, “A single-chamber microbial fuel cell as a biosensor for wastewaters,” *Water Research*, vol. 43, no. 13, pp. 3145–3154, Jul. 2009.

[4] J. D. Jang, J. P. Barford, Lindawati, and R. Renneberg, “Application of biochemical oxygen demand (BOD) biosensor for optimization of biological carbon and nitrogen removal from synthetic wastewater in a sequencing batch reactor system,” *Biosensors and Bioelectronics*, vol. 19, no. 8, pp. 805–812, Mar. 2004.

[5] M. Kim *et al.*, “Practical field application of a novel BOD monitoring system,” *J. Environ. Monit.*, vol. 5, no. 4, pp. 640–643, Jul. 2003.

[6] I. Ieropoulos, J. Greenman, and C. Melhuish, “Imitating metabolism: Energy autonomy in biologically inspired robots,” in *Proceedings of the AISB*, 2003, vol. 3, pp. 191–4.

[7] S. Wilkinson, “‘Gastrobots’—Benefits and Challenges of Microbial Fuel Cells in FoodPowered Robot Applications,” *Autonomous Robots*, vol. 9, no. 2, pp. 99–111, Sep. 2000.

[8] C. Melhuish, I. Ieropoulos, J. Greenman, and I. Horsfield, “Energetically autonomous robots: Food for thought,” *Auton Robot*, vol. 21, no. 3, pp. 187–198, Nov. 2006.

[9] C. Bettin, “Applicability and feasibility of incorporating microbial fuel cell technology into implantable biomedical devices,” The Ohio State University, 2006.

[10] T. Song, Y. Xu, Y. Ye, Y. Chen, and S. Shen, “Electricity generation from terephthalic acid using a microbial fuel cell,” *J. Chem. Technol. Biotechnol.*, vol. 84, no. 3, pp. 356–360, Mar. 2009.

[11] H. Pham, N. Boon, M. Marzorati, and W. Verstraete, “Enhanced removal of 1,2-dichloroethane by anodophilic microbial consortia,” *Water Res.*, vol. 43, no. 11, pp. 2936–2946, Jun. 2009.

[12] J. M. Morris, S. Jin, B. Crimi, and A. Pruden, “Microbial fuel cell in enhancing anaerobic biodegradation of diesel,” *Chemical Engineering Journal*, vol. 146, no. 2, pp. 161–167, Feb. 2009.

[13] J. M. Morris and S. Jin, “Feasibility of using microbial fuel cell technology for bioremediation of hydrocarbons in groundwater,” *J Environ Sci Health A Tox Hazard Subst Environ Eng*, vol. 43, no. 1, pp. 18–23, Jan. 2008.

[14] K. B. Gregory, D. R. Bond, and D. R. Lovley, “Graphite electrodes as electron donors for anaerobic respiration,” *Environmental Microbiology*, vol. 6, no. 6, pp. 596–604, Jun. 2004.

[15] A. Xue, Z.-Z. Shen, B. Zhao, and H.-Z. Zhao, “Arsenite removal from aqueous solution by a microbial fuel cell–zerovalent iron hybrid process,” *Journal of Hazardous Materials*, vol. 261, pp. 621–627, Oct. 2013.

[16] E. Y. Ryu, “Characterization of Microbial Fuel Cells Enriched Using Cr(VI)-Containing Sludge,” *Journal of Microbiology and Biotechnology*, vol. 21, no. 2, pp. 187–191, Feb. 2011.

[17] S. A. Patil *et al.*, “Electricity generation using chocolate industry wastewater and its treatment in activated sludge based microbial fuel cell and analysis of developed microbial community in the anode chamber,” *Bioresource Technology*, vol. 100, no. 21, pp. 5132–5139, Nov. 2009.

[18] S. Venkata Mohan, G. Mohanakrishna, and P. N. Sarma, “Composite vegetable waste as renewable resource for bioelectricity generation through non-catalyzed open-air cathode microbial fuel cell,” *Bioresour. Technol.*, vol. 101, no. 3, pp. 970–976, Feb. 2010.

[19] Y. Feng, X. Wang, B. E. Logan, and H. Lee, “Brewery wastewater treatment using air-cathode microbial fuel cells,” *Appl Microbiol Biotechnol*, vol. 78, no. 5, pp. 873–880, Apr. 2008.

[20] M. Sun, L.-F. Zhai, W.-W. Li, and H.-Q. Yu, “Harvest and utilization of chemical energy in wastes by microbial fuel cells,” *Chemical Society Reviews*, vol. 45, no. 10, pp. 2847–2870, 2016.

[21] B. E. Logan, “Exoelectrogenic bacteria that power microbial fuel cells,” *Nat Rev Micro*, vol. 7, no. 5, pp. 375–381, May 2009.

[22] “Cadre réglementaire - Réglementation française des déchets,” *ADEME*. [Online]. Available: http://www.ademe.fr/expertises/dechets/elements-contexte/politique-vigueur/dossier/cadre-reglementaire/reglementation-francaise-dechets. [Accessed: 27-Oct-2017].

[23] M. C. Potter, “Electrical Effects Accompanying the Decomposition of Organic Compounds,” *Proceedings of the Royal Society of London. Series B, Containing Papers of a Biological Character*, vol. 84, no. 571, pp. 260–276, 1911.

[24] J. B. Davis and H. F. Yarbrough, “Preliminary Experiments on a Microbial Fuel Cell,” *Science*, vol. 137, no. 3530, pp. 615–616, Aug. 1962.

[25] M. Del Duca and J. Fuscoe, “Thermodynamics and applications of bioelectro-chemical energy conversion systems,” 1964.

[26] J. Canfield, B. Goldner, and R. Lutwack, “Utilization of human wastes as electrochemical fuels,” *NASA Technical Report, Magna Corporation, Anaheim CA. p*, vol. 63, pp. 615--616, 1963.

[27] H. P. Bennetto, J. L. Stirling, K. Tanaka, and C. A. Vega, “Anodic reactions in microbial fuel cells,” *Biotechnology and bioengineering*, vol. 25, no. 2, pp. 559–568, 1983.

[28] J. L. Stirling *et al.*, “Microbial fuel cells,” *Biochemical Society Transactions*, vol. 11, no. 4, pp. 451–453, Aug. 1983.

[29] S. D. Roller, H. P. Bennetto, G. M. Delaney, J. R. Mason, J. L. Stirling, and C. F. Thurston, “Electron-transfer coupling in microbial fuel cells: 1. comparison of redox-mediator reduction rates and respiratory rates of bacteria,” *Journal of Chemical Technology and Biotechnology*, vol. 34, no. 1, pp. 3–12, 1984.

[30] G. M. Delaney, H. P. Bennetto, J. R. Mason, S. D. Roller, J. L. Stirling, and C. F. Thurston, “Electron-transfer coupling in microbial fuel cells. 2. performance of fuel cells containing selected microorganism—mediator—substrate combinations,” *Journal of Chemical Technology and Biotechnology*, vol. 34, no. 1, pp. 13–27, 1984.

[31] B. H. Kim, H. J. Kim, M. S. Hyun, and D. H. Park, “Direct electrode reaction of Fe (III)-reducing bacterium, Shewanella putrefaciens,” *THE KOREAN SOCIETY FOR APPLIED MICROBIOLOGY*, vol. 9, pp. 127–131, 1999.

[32] B. H. Kim *et al.*, “Electrochemical activity of an Fe(III)-reducing bacterium, Shewanella putrefaciens IR-1, in the presence of alternative electron acceptors,” *Biotechnology Techniques*, vol. 13, no. 7, pp. 475–478, Jul. 1999.

[33] H. S. Park *et al.*, “A Novel Electrochemically Active and Fe(III)-reducing Bacterium Phylogenetically Related to Clostridium butyricum Isolated from a Microbial Fuel Cell,” *Anaerobe*, vol. 7, no. 6, pp. 297–306, Dec. 2001.

[34] D. R. Bond and D. R. Lovley, “Electricity Production by Geobacter sulfurreducens Attached to Electrodes,” *Appl. Environ. Microbiol.*, vol. 69, no. 3, pp. 1548–1555, Jan. 2003.

[35] H. J. Kim, H. S. Park, M. S. Hyun, I. S. Chang, M. Kim, and B. H. Kim, “A mediator-less microbial fuel cell using a metal reducing bacterium, Shewanella putrefaciens,” *Enzyme and Microbial Technology*, vol. 30, no. 2, pp. 145–152, Feb. 2002.

[36] Y. A. Gorby *et al.*, “Electrically conductive bacterial nanowires produced by Shewanella oneidensis strain MR-1 and other microorganisms,” *Proceedings of the National Academy of Sciences*, vol. 103, no. 30, pp. 11358–11363, 2006.

[37] G. Reguera, K. P. Nevin, J. S. Nicoll, S. F. Covalla, T. L. Woodard, and D. R. Lovley, “Biofilm and Nanowire Production Leads to Increased Current in Geobacter sulfurreducens Fuel Cells,” *Appl. Environ. Microbiol.*, vol. 72, no. 11, pp. 7345–7348, Jan. 2006.

[38] E. Afkar, G. Reguera, M. Schiffer, and D. R. Lovley, “A novel Geobacteraceae-specific outer membrane protein J (OmpJ) is essential for electron transport to Fe (III) and Mn (IV) oxides in Geobacter sulfurreducens,” *BMC Microbiology*, vol. 5, p. 41, Jul. 2005.

[39] H. Richter, K. P. Nevin, H. Jia, D. A. Lowy, D. R. Lovley, and L. M. Tender, “Cyclic voltammetry of biofilms of wild type and mutant Geobacter sulfurreducens on fuel cell anodes indicates possible roles of OmcB, OmcZ, type IV pili, and protons in extracellular electron transfer,” *Energy & Environmental Science*, vol. 2, no. 5, pp. 506–516, 2009.

[40] O. Bretschger *et al.*, “Current Production and Metal Oxide Reduction by Shewanella oneidensis MR-1 Wild Type and Mutants,” *Applied and Environmental Microbiology*, vol. 73, no. 21, pp. 7003–7012, Nov. 2007.

[41] Z. He and L. T. Angenent, “Application of Bacterial Biocathodes in Microbial Fuel Cells,” *Electroanalysis*, vol. 18, no. 19–20, pp. 2009–2015, Oct. 2006.

[42] K. Rabaey *et al.*, “Cathodic oxygen reduction catalyzed by bacteria in microbial fuel cells,” *The ISME Journal*, vol. 2, no. 5, pp. 519–527, May 2008.

[43] M. Tandukar, S. J. Huber, T. Onodera, and S. G. Pavlostathis, “Biological Chromium(VI) Reduction in the Cathode of a Microbial Fuel Cell,” *Environ. Sci. Technol.*, vol. 43, no. 21, pp. 8159–8165, Nov. 2009.

[44] A. ter Heijne, H. V. M. Hamelers, and C. J. N. Buisman, “Microbial Fuel Cell Operation with Continuous Biological Ferrous Iron Oxidation of the Catholyte,” *Environ. Sci. Technol.*, vol. 41, no. 11, pp. 4130–4134, Jun. 2007.

[45] L. Huang, X. Chai, X. Quan, B. E. Logan, and G. Chen, “Reductive dechlorination and mineralization of pentachlorophenol in biocathode microbial fuel cells,” *Bioresource Technology*, vol. 111, pp. 167–174, May 2012.

[46] B. Min, S. Cheng, and B. E. Logan, “Electricity generation using membrane and salt bridge microbial fuel cells,” *Water Research*, vol. 39, no. 9, pp. 1675–1686, May 2005.

[47] S.-E. Oh and B. E. Logan, “Proton exchange membrane and electrode surface areas as factors that affect power generation in microbial fuel cells,” *Appl Microbiol Biotechnol*, vol. 70, no. 2, pp. 162–169, Mar. 2006.

[48] B. Logan, S. Cheng, V. Watson, and G. Estadt, “Graphite Fiber Brush Anodes for Increased Power Production in Air-Cathode Microbial Fuel Cells,” *Environ. Sci. Technol.*, vol. 41, no. 9, pp. 3341–3346, May 2007.

[49] K. Scott, G. A. Rimbu, K. P. Katuri, K. K. Prasad, and I. M. Head, “Application of Modified Carbon Anodes in Microbial Fuel Cells,” *Process Safety and Environmental Protection*, vol. 85, no. 5, pp. 481–488, 2007.

[50] Z. He, N. Wagner, S. D. Minteer, and L. T. Angenent, “An Upflow Microbial Fuel Cell with an Interior Cathode: Assessment of the Internal Resistance by Impedance Spectroscopy†,” *Environ. Sci. Technol.*, vol. 40, no. 17, pp. 5212–5217, Sep. 2006.

[51] S. Cheng, H. Liu, and B. E. Logan, “Increased Power Generation in a Continuous Flow MFC with Advective Flow through the Porous Anode and Reduced Electrode Spacing,” *Environ. Sci. Technol.*, vol. 40, no. 7, pp. 2426–2432, Apr. 2006.

[52] H. Liu, S. Cheng, and B. E. Logan, “Power Generation in Fed-Batch Microbial Fuel Cells as a Function of Ionic Strength, Temperature, and Reactor Configuration,” *Environ. Sci. Technol.*, vol. 39, no. 14, pp. 5488–5493, Jul. 2005.

[53] B. Min and B. E. Logan, “Continuous Electricity Generation from Domestic Wastewater and Organic Substrates in a Flat Plate Microbial Fuel Cell,” *Environ. Sci. Technol.*, vol. 38, no. 21, pp. 5809–5814, Nov. 2004.

[54] M. A. Rodrigo, P. Cañizares, J. Lobato, R. Paz, C. Sáez, and J. J. Linares, “Production of electricity from the treatment of urban waste water using a microbial fuel cell,” *Journal of Power Sources*, vol. 169, no. 1, pp. 198–204, Jun. 2007.

[55] H. Rismani-Yazdi, A. D. Christy, B. A. Dehority, M. Morrison, Z. Yu, and O. H. Tuovinen, “Electricity generation from cellulose by rumen microorganisms in microbial fuel cells,” *Biotechnol. Bioeng.*, vol. 97, no. 6, pp. 1398–1407, Aug. 2007.

[56] B. E. Logan *et al.*, “Microbial Fuel Cells: Methodology and Technology†,” *Environ. Sci. Technol.*, vol. 40, no. 17, pp. 5181–5192, Sep. 2006.

[57] H. Liu and B. E. Logan, “Electricity Generation Using an Air-Cathode Single Chamber Microbial Fuel Cell in the Presence and Absence of a Proton Exchange Membrane,” *Environmental Science & Technology*, vol. 38, no. 14, pp. 4040–4046, Jul. 2004.

[58] M. Stern and A. L. Geary, “Electrochemical polarization I. A theoretical analysis of the shape of polarization curves,” *Journal of the electrochemical society*, vol. 104, no. 1, pp. 56–63, 1957.

[59] O. F. Devereux, “Polarization Curve-Fitting by Computer Modelling,” *CORROSION*, vol. 35, no. 3, pp. 125–129, Mar. 1979.

[60] N. S. Malvankar, T. Mester, M. T. Tuominen, and D. R. Lovley, “Supercapacitors Based on c-Type Cytochromes Using Conductive Nanostructured Networks of Living Bacteria,” *ChemPhysChem*, vol. 13, no. 2, pp. 463–468, Feb. 2012.

[61] C. Koch and F. Harnisch, “Is there a Specific Ecological Niche for Electroactive Microorganisms?,” *ChemElectroChem*, vol. 3, no. 9, pp. 1282–1295, Sep. 2016.

[62] G. Sturm, K. Dolch, K. Richter, M. Rautenberg, and J. Gescher, “Metal Reducers and Reduction Targets. A Short Survey About the Distribution of Dissimilatory Metal Reducers and the Multitude of Terminal Electron Acceptors,” *SpringerLink*, pp. 129–159, 2013.

[63] A. S. Commault, G. Lear, and R. J. Weld, “Maintenance of Geobacter-dominated biofilms in microbial fuel cells treating synthetic wastewater,” *Bioelectrochemistry*, vol. 106, Part A, pp. 150–158, Dec. 2015.

[64] S. Jung and J. M. Regan, “Comparison of anode bacterial communities and performance in microbial fuel cells with different electron donors,” *Appl Microbiol Biotechnol*, vol. 77, no. 2, pp. 393–402, Nov. 2007.

[65] D. Ki, J. Park, J. Lee, and K. Yoo, “Microbial diversity and population dynamics of activated sludge microbial communities participating in electricity generation in microbial fuel cells,” *Water Science & Technology*, vol. 58, no. 11, p. 2195, Dec. 2008.

[66] J. P. Stratford, N. J. Beecroft, R. C. T. Slade, A. Grüning, and C. Avignone-Rossa, “Anodic microbial community diversity as a predictor of the power output of microbial fuel cells,” *Bioresource Technology*, vol. 156, pp. 84–91, Mar. 2014.

[67] Y. Sun, J. Wei, P. Liang, and X. Huang, “Electricity generation and microbial community changes in microbial fuel cells packed with different anodic materials,” *Bioresource Technology*, vol. 102, no. 23, pp. 10886–10891, Dec. 2011.

[68] M. D. Yates *et al.*, “Convergent development of anodic bacterial communities in microbial fuel cells,” *ISME J*, vol. 6, no. 11, pp. 2002–2013, Nov. 2012.

[69] D. M. Hodgson *et al.*, “Segregation of the Anodic Microbial Communities in a Microbial Fuel Cell Cascade,” *Front. Microbiol.*, vol. 7, 2016.

[70] A. Paitier, A. Godain, D. Lyon, N. Haddour, T. M. Vogel, and J.-M. Monier, “Microbial fuel cell anodic microbial population dynamics during MFC start-up,” *Biosensors and Bioelectronics*, vol. 92, no. Supplement C, pp. 357–363, Jun. 2017.

[71] S. Falkow, E. Rosenberg, K.-H. Schleifer, and E. Stackebrandt, *The Prokaryotes: Vol. 2: Ecophysiology and Biochemistry*. Springer Science & Business Media, 2006.

[72] G. Sezonov, D. Joseleau-Petit, and R. D’Ari, “Escherichia coli Physiology in Luria-Bertani Broth,” *J. Bacteriol.*, vol. 189, no. 23, pp. 8746–8749, Jan. 2007.

[73] D. E. Holmes *et al.*, “Molecular Analysis of the In Situ Growth Rates of Subsurface Geobacter Species,” *Appl. Environ. Microbiol.*, vol. 79, no. 5, pp. 1646–1653, Jan. 2013.

[74] C. I. Torres, A. K. Marcus, P. Parameswaran, and B. E. Rittmann, “Kinetic Experiments for Evaluating the Nernst−Monod Model for Anode-Respiring Bacteria (ARB) in a Biofilm Anode,” *Environ. Sci. Technol.*, vol. 42, no. 17, pp. 6593–6597, Sep. 2008.

[75] J. Wei, P. Liang, X. Cao, and X. Huang, “A New Insight into Potential Regulation on Growth and Power Generation of Geobacter sulfurreducens in Microbial Fuel Cells Based on Energy Viewpoint,” *Environ. Sci. Technol.*, vol. 44, no. 8, pp. 3187–3191, Apr. 2010.

[76] F. Kracke, I. Vassilev, and J. O. Krömer, “Microbial electron transport and energy conservation – the foundation for optimizing bioelectrochemical systems,” *Front Microbiol*, vol. 6, Jun. 2015.

[77] J. M. Dantas *et al.*, “Rational engineering of Geobacter sulfurreducens electron transfer components: a foundation for building improved Geobacter-based bioelectrochemical technologies,” *Front. Microbiol.*, vol. 6, 2015.

[78] T. C. Santos, M. A. Silva, L. Morgado, J. M. Dantas, and C. A. Salgueiro, “Diving into the redox properties of Geobacter sulfurreducens cytochromes: a model for extracellular electron transfer,” *Dalton Trans*, vol. 44, no. 20, pp. 9335–9344, May 2015.

[79] C. E. Levar, C. L. Hoffman, A. J. Dunshee, B. M. Toner, and D. R. Bond, “Redox potential as a master variable controlling pathways of metal reduction by Geobacter sulfurreducens,” *ISME J*, vol. 11, no. 3, pp. 741–752, Mar. 2017.

[80] D. R. Bond, S. M. Strycharz-Glaven, L. M. Tender, and C. I. Torres, “On Electron Transport through Geobacter Biofilms,” *ChemSusChem*, vol. 5, no. 6, pp. 1099–1105, Jun. 2012.

[81] C. H. Chan, C. E. Levar, F. Jiménez-Otero, and D. R. Bond, “Genome Scale Mutational Analysis of Geobacter sulfurreducens Reveals Distinct Molecular Mechanisms for Respiration and Sensing of Poised Electrodes versus Fe(III) Oxides,” *J. Bacteriol.*, vol. 199, no. 19, pp. e00340-17, Jan. 2017.

[82] L. A. Zacharoff, D. Morrone, and D. R. Bond, “Geobacter sulfurreducens extracellular multiheme cytochrome PgcA facilitates respiration to Fe(III) oxides but not electrodes,” *bioRxiv*, p. 172775, Aug. 2017.

[83] C. E. Levar, C. H. Chan, M. G. Mehta-Kolte, and D. R. Bond, “An inner membrane cytochrome required only for reduction of high redox potential extracellular electron acceptors,” *MBio*, vol. 5, no. 6, p. e02034, Nov. 2014.

[84] L. Zacharoff, C. H. Chan, and D. R. Bond, “Reduction of low potential electron acceptors requires the CbcL inner membrane cytochrome of Geobacter sulfurreducens,” *Bioelectrochemistry*, vol. 107, pp. 7–13, Feb. 2016.

[85] J. R. Lloyd *et al.*, “Biochemical and genetic characterization of PpcA, a periplasmic c-type cytochrome in Geobacter sulfurreducens,” *Biochemical Journal*, vol. 369, no. 1, pp. 153–161, Jan. 2003.

[86] N. S. Malvankar *et al.*, “Structural Basis for Metallic-Like Conductivity in Microbial Nanowires,” *mBio*, vol. 6, no. 2, pp. e00084-15, Jan. 2015.

[87] D. E. Holmes, Y. Dang, D. J. F. Walker, and D. R. Lovley, “The electrically conductive pili of Geobacter species are a recently evolved feature for extracellular electron transfer,” *Microbial Genomics*, vol. 2, no. 8, Aug. 2016.

[88] C. Leang, X. Qian, T. Mester, and D. R. Lovley, “Alignment of the c-Type Cytochrome OmcS along Pili of Geobacter sulfurreducens,” *Appl. Environ. Microbiol.*, vol. 76, no. 12, pp. 4080–4084, Jun. 2010.

[89] K. P. Nevin *et al.*, “Anode Biofilm Transcriptomics Reveals Outer Surface Components Essential for High Density Current Production in Geobacter sulfurreducens Fuel Cells,” *PLOS ONE*, vol. 4, no. 5, p. e5628, May 2009.

[90] E. D. Brutinel and J. A. Gralnick, “Shuttling happens: soluble flavin mediators of extracellular electron transfer in Shewanella,” *Appl. Microbiol. Biotechnol.*, vol. 93, no. 1, pp. 41–48, Jan. 2012.

[91] D. Coursolle and J. A. Gralnick, “Modularity of the Mtr respiratory pathway of Shewanella oneidensis strain MR-1,” *Molecular Microbiology*, vol. 77, no. 4, pp. 995–1008, Aug. 2010.

[92] D. E. Ross, J. M. Flynn, D. B. Baron, J. A. Gralnick, and D. R. Bond, “Towards Electrosynthesis in Shewanella: Energetics of Reversing the Mtr Pathway for Reductive Metabolism,” *PLoS ONE*, vol. 6, no. 2, 2011.

[93] J. A. Gralnick, “On conducting electron traffic across the periplasm,” *Biochem. Soc. Trans.*, vol. 40, no. 6, pp. 1178–1180, Dec. 2012.

[94] S. Pirbadian *et al.*, “Shewanella oneidensis MR-1 nanowires are outer membrane and periplasmic extensions of the extracellular electron transport components,” *PNAS*, vol. 111, no. 35, pp. 12883–12888, Feb. 2014.

[95] N. J. Kotloski and J. A. Gralnick, “Flavin Electron Shuttles Dominate Extracellular Electron Transfer by Shewanella oneidensis,” *mBio*, vol. 4, no. 1, pp. e00553-12, Jan. 2013.

[96] B. A. Methé *et al.*, “Genome of Geobacter sulfurreducens: Metal Reduction in Subsurface Environments,” *Science*, vol. 302, no. 5652, pp. 1967–1969, Dec. 2003.

[97] E. J. W. Verwey, “Theory of the stability of lyophobic colloids.,” *The Journal of Physical Chemistry*, vol. 51, no. 3, pp. 631–636, 1947.

[98] M. Hermansson, “The DLVO theory in microbial adhesion,” *Colloids and Surfaces B: Biointerfaces*, vol. 14, no. 1–4, pp. 105–119, Aug. 1999.

[99] A. Kato Marcus, C. I. Torres, and B. E. Rittmann, “Conduction-based modeling of the biofilm anode of a microbial fuel cell,” *Biotechnology and Bioengineering*, vol. 98, no. 6, pp. 1171–1182, Dec. 2007.

[100] H. V. M. Hamelers, A. ter Heijne, N. Stein, R. A. Rozendal, and C. J. N. Buisman, “Butler–Volmer–Monod model for describing bio-anode polarization curves,” *Bioresource Technology*, vol. 102, no. 1, pp. 381–387, Jan. 2011.

[101] C. Picioreanu, I. M. Head, K. P. Katuri, M. C. M. van Loosdrecht, and K. Scott, “A computational model for biofilm-based microbial fuel cells,” *Water Research*, vol. 41, no. 13, pp. 2921–2940, Jul. 2007.

[102] R. P. Pinto, B. Srinivasan, M.-F. Manuel, and B. Tartakovsky, “A two-population bio-electrochemical model of a microbial fuel cell,” *Bioresource Technology*, vol. 101, no. 14, pp. 5256–5265, Jul. 2010.

[103] C. I. Torres, A. K. Marcus, and B. E. Rittmann, “Kinetics of consumption of fermentation products by anode-respiring bacteria,” *Appl. Microbiol. Biotechnol.*, vol. 77, no. 3, pp. 689–697, Dec. 2007.

[104] A. Torrents, N. Godino, F. J. del Campo, F. X. Muñoz, and J. Mas, “Influence of pH and Carbonate Buffering on the Performance of a Lactate Microbial Fuel Cell.”

[105] C. I. Torres *et al.*, “Selecting Anode-Respiring Bacteria Based on Anode Potential: Phylogenetic, Electrochemical, and Microscopic Characterization,” *Environ. Sci. Technol.*, vol. 43, no. 24, pp. 9519–9524, Dec. 2009.

[106] C. Picioreanu, M. C. M. van Loosdrecht, T. P. Curtis, and K. Scott, “Model based evaluation of the effect of pH and electrode geometry on microbial fuel cell performance,” *Bioelectrochemistry*, vol. 78, no. 1, pp. 8–24, Apr. 2010.

[107] A. E. Franks, K. P. Nevin, H. Jia, M. Izallalen, T. L. Woodard, and D. R. Lovley, “Novel strategy for three-dimensional real-time imaging of microbial fuel cell communities: monitoring the inhibitory effects of proton accumulation within the anode biofilm,” *Energy Environ. Sci.*, vol. 2, no. 1, pp. 113–119, Dec. 2008.

[108] N. S. Malvankar, M. T. Tuominen, and D. R. Lovley, “Biofilm conductivity is a decisive variable for high-current-density Geobacter sulfurreducens microbial fuel cells,” *Energy & Environmental Science*, vol. 5, no. 2, p. 5790, 2012.

[109] N. S. Malvankar, J. Lau, K. P. Nevin, A. E. Franks, M. T. Tuominen, and D. R. Lovley, “Electrical Conductivity in a Mixed-Species Biofilm,” *Applied and Environmental Microbiology*, vol. 78, no. 16, pp. 5967–5971, Aug. 2012.

[110] A. Persat *et al.*, “The Mechanical World of Bacteria,” *Cell*, vol. 161, no. 5, pp. 988–997, May 2015.

[111] P. Thomen, J. Robert, A. Monmeyran, A.-F. Bitbol, C. Douarche, and N. Henry, “Bacterial biofilm under flow: First a physical struggle to stay, then a matter of breathing,” *PLoS ONE*, vol. 12, no. 4, p. e0175197, 2017.

[112] M. Lemos, F. Mergulhão, L. Melo, and M. Simões, “The effect of shear stress on the formation and removal of Bacillus cereus biofilms,” *Food and Bioproducts Processing*, vol. 93, no. Supplement C, pp. 242–248, Jan. 2015.

[113] Y. Liu and J.-H. Tay, “Metabolic response of biofilm to shear stress in fixed-film culture,” *Journal of Applied Microbiology*, vol. 90, no. 3, pp. 337–342, Mar. 2001.

[114] A. Rochex, J. Godon, N. Bernet, and R. Escudie, “Role of shear stress on composition, diversity and dynamics of biofilm bacterial communities,” *Water Research*, vol. 42, no. 20, pp. 4915–4922, Dec. 2008.

[115] H. T. Pham *et al.*, “High shear enrichment improves the performance of the anodophilic microbial consortium in a microbial fuel cell,” *Microbial Biotechnology*, vol. 1, no. 6, pp. 487–496, 2008.

[116] P. S. Stewart, “Mini-review: convection around biofilms,” *Biofouling*, vol. 28, no. 2, pp. 187–198, 2012.

[117] A. Park, H.-H. Jeong, J. Lee, K. P. Kim, and C.-S. Lee, “Effect of shear stress on the formation of bacterial biofilm in a microfluidic channel,” *BioChip J*, vol. 5, no. 3, p. 236, Sep. 2011.

[118] U. Risse-Buhl *et al.*, “The role of hydrodynamics in shaping the composition and architecture of epilithic biofilms in fluvial ecosystems,” *Water Research*, vol. 127, no. Supplement C, pp. 211–222, Dec. 2017.

[119] H. Fang, Y. Chen, L. Huang, and G. He, “Analysis of biofilm bacterial communities under different shear stresses using size-fractionated sediment,” *Scientific Reports*, vol. 7, 2017.

[120] N. Islam, Y. Kim, J. M. Ross, and M. R. Marten, “Proteomic analysis of Staphylococcus aureus biofilm cells grown under physiologically relevant fluid shear stress conditions,” *Proteome Science*, vol. 12, no. 1, p. 21, Apr. 2014.

[121] V. Oliveira, T. Carvalho, L. Melo, A. Pinto, and M. Simões, “Effects of hydrodynamic stress and feed rate on the performance of a microbial fuel cell,” vol. 15, pp. 2497–2504, Jan. 2016.

[122] F. F. Ajayi, K.-Y. Kim, K.-J. Chae, M.-J. Choi, and I. S. Kim, “Effect of hydrodymamic force and prolonged oxygen exposure on the performance of anodic biofilm in microbial electrolysis cells,” *International Journal of Hydrogen Energy*, vol. 35, no. 8, pp. 3206–3213, Apr. 2010.

[123] J. R. Kim *et al.*, “Porous anodes with helical flow pathways in bioelectrochemical systems: The effects of fluid dynamics and operating regimes,” *Journal of Power Sources*, vol. 213, no. Supplement C, pp. 382–390, Sep. 2012.

[124] S. Cheng and W. Liu, “How to make Cathodes with a diffusion layer for single-chamber microbial fule cells.” 2008.

[125] S. Lorthois, P. Schmitz, D. Houi, and E. Angles-cano, “Experimental Study of Fibrin Embolization Under Shear Flow,” *The Journal of Adhesion*, vol. 72, no. 2, pp. 229–239, Mar. 2000.

[126] S. Lorthois, P. Schmitz, and E. Anglés-Cano, “Experimental Study of Fibrin/Fibrin-Specific Molecular Interactions Using a Sphere/Plane Adhesion Model,” *Journal of Colloid and Interface Science*, vol. 241, no. 1, pp. 52–62, Sep. 2001.

[127] M. E. O’Neill, “A sphere in contact with a plane wall in a slow linear shear flow,” *Chemical Engineering Science*, vol. 23, no. 11, pp. 1293–1298, Nov. 1968.

[128] Illumina, “16S Sample Preparation Guide.” https://www.illumina.com.

[129] T. H. Pham, N. Boon, K. D. Maeyer, M. Höfte, K. Rabaey, and W. Verstraete, “Use of Pseudomonas species producing phenazine-based metabolites in the anodes of microbial fuel cells to improve electricity generation,” *Appl Microbiol Biotechnol*, vol. 80, no. 6, pp. 985–993, Aug. 2008.

[130] E. Marsili, D. B. Baron, I. D. Shikhare, D. Coursolle, J. A. Grainick, and D. R. Bond, “Shewanella secretes flavins that mediate extracellular electron transfer,” *PNAS*, vol. 105, no. 10, pp. 3968–3973, 2008.

[131] H. von Canstein, J. Ogawa, S. Shimizu, and J. R. Lloyd, “Secretion of Flavins by Shewanella Species and Their Role in Extracellular Electron Transfer,” *Appl. Environ. Microbiol.*, vol. 74, no. 3, pp. 615–623, Jan. 2008.

[132] T. R. De Kievit, “Quorum sensing in Pseudomonas aeruginosa biofilms,” *Environmental Microbiology*, vol. 11, no. 2, pp. 279–288, Feb. 2009.

[133] L. E. P. Dietrich, A. Price-Whelan, A. Petersen, M. Whiteley, and D. K. Newman, “The phenazine pyocyanin is a terminal signalling factor in the quorum sensing network of Pseudomonas aeruginosa,” *Molecular Microbiology*, vol. 61, no. 5, pp. 1308–1321, Sep. 2006.

[134] L. S. Thomashow and D. M. Weller, “Role of a phenazine antibiotic from Pseudomonas fluorescens in biological control of Gaeumannomyces graminis var. tritici.,” *J. Bacteriol.*, vol. 170, no. 8, pp. 3499–3508, Jan. 1988.

[135] J. Schindelin, C. T. Rueden, M. C. Hiner, and K. W. Eliceiri, “The ImageJ ecosystem: An open platform for biomedical image analysis,” *Mol. Reprod. Dev.*, vol. 82, no. 7–8, pp. 518–529, Jul. 2015.

[136] C. A. Schneider, W. S. Rasband, and K. W. Eliceiri, “NIH Image to ImageJ: 25 years of image analysis,” *Nat Meth*, vol. 9, no. 7, pp. 671–675, Jul. 2012.

[137] J. Schindelin *et al.*, “Fiji: an open-source platform for biological-image analysis,” *Nat Meth*, vol. 9, no. 7, pp. 676–682, Jul. 2012.

[138] R. C. Edgar, “Search and clustering orders of magnitude faster than BLAST,” *Bioinformatics*, vol. 26, no. 19, pp. 2460–2461, Oct. 2010.

[139] A. P. Masella, A. K. Bartram, J. M. Truszkowski, D. G. Brown, and J. D. Neufeld, “PANDAseq: paired-end assembler for illumina sequences,” *BMC Bioinformatics*, vol. 13, p. 31, Feb. 2012.

[140] Q. Wang, G. M. Garrity, J. M. Tiedje, and J. R. Cole, “Naïve Bayesian Classifier for Rapid Assignment of rRNA Sequences into the New Bacterial Taxonomy,” *Appl. Environ. Microbiol.*, vol. 73, no. 16, pp. 5261–5267, Aug. 2007.

[141] R Development Core Team, “R: A Language and Environment for Statistical Computing,” *R Foundation for Statistical Computing, Vienna, Austria*, 2008.

[142] J. Oksanen *et al.*, “vegan: Community Ecology Package,” vol. R package version 2.3-5, 2016.

[143] F. A. Armstrong, H. A. Heering, and J. Hirst, “Reaction of complex metalloproteins studied by protein-film voltammetry,” *Chemical Society Reviews*, vol. 26, no. 3, pp. 169–179, 1997.

[144] J. R. Cole *et al.*, “Ribosomal Database Project: data and tools for high throughput rRNA analysis,” *Nucleic Acids Res*, vol. 42, no. D1, pp. D633–D642, Jan. 2014.

[145] S. Freguia, S. Tsujimura, and K. Kano, “Electron transfer pathways in microbial oxygen biocathodes,” *Electrochimica Acta*, vol. 55, no. 3, pp. 813–818, Jan. 2010.

[146] S. Parot *et al.*, “Catalysis of the electrochemical reduction of oxygen by bacteria isolated from electro-active biofilms formed in seawater,” *Bioresource Technology*, vol. 102, no. 1, pp. 304–311, Jan. 2011.

[147] S. Chen, X. Jing, J. Tang, Y. Fang, and S. Zhou, “Quorum sensing signals enhance the electrochemical activity and energy recovery of mixed-culture electroactive biofilms,” *Biosensors and Bioelectronics*, vol. 97, no. Supplement C, pp. 369–376, Nov. 2017.

[148] D. Y. Lyon, F. Buret, T. M. Vogel, and J.-M. Monier, “Is resistance futile? Changing external resistance does not improve microbial fuel cell performance,” *Bioelectrochemistry*, vol. 78, no. 1, pp. 2–7, Apr. 2010.

[149] K. P. Katuri, K. Scott, I. M. Head, C. Picioreanu, and T. P. Curtis, “Microbial fuel cells meet with external resistance,” *Bioresource Technology*, vol. 102, no. 3, pp. 2758–2766, Feb. 2011.

[150] H. Rismani-Yazdi, A. D. Christy, S. M. Carver, Z. Yu, B. A. Dehority, and O. H. Tuovinen, “Effect of external resistance on bacterial diversity and metabolism in cellulose-fed microbial fuel cells,” *Bioresource Technology*, vol. 102, no. 1, pp. 278–283, Jan. 2011.

[151] L. Zhang, X. Zhu, J. Li, Q. Liao, and D. Ye, “Biofilm formation and electricity generation of a microbial fuel cell started up under different external resistances,” *Journal of Power Sources*, vol. 196, no. 15, pp. 6029–6035, Aug. 2011.

[152] G. Guillemot, S. Lorthois, P. Schmitz, and M. Mercier-Bonin, “Evaluating the Adhesion Force Between Saccharomyces Cerevisiae Yeast Cells and Polystyrene From Shear-Flow Induced Detachment Experiments,” *Chemical Engineering Research and Design*, vol. 85, no. 6, pp. 800–807, Jan. 2007.

[153] J. E. Duddridge, C. A. Kent, and J. F. Laws, “Effect of surface shear stress on the attachment of Pseudomonas fluorescens to stainless steel under defined flow conditions,” *Biotechnol. Bioeng.*, vol. 24, no. 1, pp. 153–164, Jan. 1982.

[154] W. W. Baldwin, R. Myer, N. Powell, E. Anderson, and A. L. Koch, “Buoyant density of Escherichia coli is determined solely by the osmolarity of the culture medium,” *Arch. Microbiol.*, vol. 164, no. 2, pp. 155–157, Aug. 1995.

[155] J. M. Martel and M. Toner, “Inertial Focusing in Microfluidics,” *Annu Rev Biomed Eng*, vol. 16, pp. 371–396, Jul. 2014.

[156] C. Gutfinger, D. Pnueli, L. Moldavsky, K. Shuster, and M. Fichman, “Particle Motion in Simple Shear Flow with Gravity,” *Aerosol Science and Technology*, vol. 37, no. 10, pp. 841–845, Oct. 2003.

[157] J. Zhang *et al.*, “Fundamentals and applications of inertial microfluidics: a review,” *Lab Chip*, vol. 16, no. 1, pp. 10–34, Dec. 2015.

[158] N. Li, R. Kakarla, and B. Min, *Effect of influential factors on microbial growth and the correlation between current generation and biomass in an air cathode microbial fuel cell*, vol. 41. 2016.

[159] J. A. Cornejo *et al.*, “Surface Modification for Enhanced Biofilm Formation and Electron Transport in Shewanella Anodes,” *J. Electrochem. Soc.*, vol. 162, no. 9, pp. H597–H603, Jan. 2015.

[160] L. Kiseleva *et al.*, “Taxonomic and functional metagenomic analysis of anodic communities in two pilot-scale microbial fuel cells treating different industrial wastewaters.,” *Journal of integrative bioinformatics*, vol. 12, no. 1, p. 273, 2015.

[161] Y. Zhang, J. Jiang, Q. Zhao, K. Wang, and H. Yu, “Analysis of functional genomes from metagenomes: Revealing the accelerated electron transfer in microbial fuel cell with rhamnolipid addition,” *Bioelectrochemistry*, vol. 119, pp. 59–67, Feb. 2018.

[162] Illumina, “Nextera XT DNA Library Prep Kit - Reference Guide.” Illumina, Apr-2017.

[163] “Fast and sensitive protein alignment using DIAMOND | Nature Methods.” [Online]. Available: https://www.nature.com/articles/nmeth.3176. [Accessed: 21-Nov-2017].

[164] Y. S. Cao and G. J. Alaerts, “Influence of reactor type and shear stress on aerobic biofilm morphology, population and kinetics,” *Water Research*, vol. 29, no. 1, pp. 107–118, Jan. 1995.

[165] Y. Liu and J.-H. Tay, “The essential role of hydrodynamic shear force in the formation of biofilm and granular sludge,” *Water Research*, vol. 36, no. 7, pp. 1653–1665, Apr. 2002.

[166] B. E. Rittman, “The effect of shear stress on biofilm loss rate,” *Biotechnol. Bioeng.*, vol. 24, no. 2, pp. 501–506, Feb. 1982.

[167] B. M. Peyton and W. G. Characklis, “A statistical analysis of the effect of substrate utilization and shear stress on the kinetics of biofilm detachment,” *Biotechnol. Bioeng.*, vol. 41, no. 7, pp. 728–735, Mar. 1993.

[168] B. M. Peyton, “Effects of shear stress and substrate loading rate on Pseudomonas aeruginosa biofilm thickness and density,” *Water Research*, vol. 30, no. 1, pp. 29–36, Jan. 1996.

[169] L. G. Raguin, M. Shannon, and J. G. Georgiadis, “Dispersion radiale et axiale dans les écoulements tourbillonnaires de Taylor–Couette et Poiseuille: Radial and axial dispersion in Taylor–Couette and Poiseuille vortex flows,” *International Journal of Heat and Mass Transfer*, vol. 44, no. 17, pp. 3295–3306, Sep. 2001.

[170] G. Baier, M. D. Graham, and E. N. Lightfoot, “Mass transport in a novel two-fluid taylor vortex extractor,” *AIChE journal*, vol. 46, no. 12, pp. 2395–2407, 2000.

[171] S. J. Curran and R. A. Black, “Oxygen transport and cell viability in an annular flow bioreactor: Comparison of laminar Couette and Taylor-vortex flow regimes,” *Biotechnol. Bioeng.*, vol. 89, no. 7, pp. 766–774, Mar. 2005.

[172] B. Haut, H. Ben Amor, L. Coulon, A. Jacquet, and V. Halloin, “Hydrodynamics and mass transfer in a Couette–Taylor bioreactor for the culture of animal cells,” *Chemical Engineering Science*, vol. 58, no. 3, pp. 777–784, Feb. 2003.

[173] R. J. Campero and R. D. Vigil, “Axial dispersion during low Reynolds number Taylor-Couette flow: intra-vortex mixing effects,” *Chemical Engineering Science*, vol. 52, no. 19, pp. 3303–3310, Oct. 1997.

[174] N. Barbouche, *Réponse biologique de cellules animales à des contraintes hydrodynamiques : simulation numérique, expérimentation et modélisation en bioréacteurs de laboratoire*. Vandoeuvre-les-Nancy, INPL, 2008.

[175] Y. Takeda, “Quasi-periodic state and transition to turbulence in a rotating Couette system,” *Journal of Fluid Mechanics*, vol. 389, pp. 81–99, Jun. 1999.

[176] C.-T. Wang, “Flow Control in Microbial Fuel Cells,” *Pr. Chin-Tsan Wang (Ed.)*, 2014.

[177] S. Cheng, H. Liu, and B. E. Logan, “Power Densities Using Different Cathode Catalysts (Pt and CoTMPP) and Polymer Binders (Nafion and PTFE) in Single Chamber Microbial Fuel Cells,” *Environ. Sci. Technol.*, vol. 40, no. 1, pp. 364–369, Jan. 2006.

[178] E. A. Zielke, “Numerical analysis of a one dimensional diffusion equation for a single chamber microbial fuel cell using a linked simulation optimization (LSO) technique,” *Advanced Numerical Methods E*, vol. 521, p. 2006, 2006.

[179] C. Picioreanu, K. P. Katuri, M. C. M. van Loosdrecht, I. M. Head, and K. Scott, “Modelling microbial fuel cells with suspended cells and added electron transfer mediator,” *Journal of Applied Electrochemistry*, vol. 40, no. 1, pp. 151–162, Jan. 2010.

[180] C. Picioreanu, M. C. M. van Loosdrecht, K. P. Katuri, K. Scott, and I. M. Head, “Mathematical model for microbial fuel cells with anodic biofilms and anaerobic digestion,” *Water Science & Technology*, vol. 57, no. 7, p. 965, Apr. 2008.

[181] K. J. Martin, C. Picioreanu, and R. Nerenberg, “Multidimensional modeling of biofilm development and fluid dynamics in a hydrogen-based, membrane biofilm reactor (MBfR),” *Water Research*, vol. 47, no. 13, pp. 4739–4751, Sep. 2013.

[182] A. K. Marcus, C. I. Torres, and B. E. Rittmann, “Analysis of a microbial electrochemical cell using the proton condition in biofilm (PCBIOFILM) model,” *Bioresource Technology*, vol. 102, no. 1, pp. 253–262, Jan. 2011.

[183] S. Dong, “Direct numerical simulation of turbulent Taylor–Couette flow,” *Journal of Fluid Mechanics*, vol. 587, pp. 373–393, Sep. 2007.

Résumé de l'Annexe 1

Les piles à combustible microbiennes, en tant que biotechnologie potentiellement durable, peuvent assurer la conversion directe de la matière organique des eaux usées en électricité en utilisant des biofilms bactériens comme biocatalyseurs. L'un des points critiques dans les biopiles microbienne est de comprendre quelles bactéries électroactives (EAB) et quels mécanismes sont impliqués dans le transfert d'électrons extracellulaires vers l'anode. Le but de cette étude était d'évaluer comment une tension appliquée entre l'anode et la cathode influence la structure et l'activité de la communauté bactérienne anodique. Deux biopiles ont été exploitées avec une résistance externe de 1000 ohms. L'une a été soumise à une tension électrique appliquée de 500 mV pendant les quatre premiers jours de formation du biofilm et l'autre a été démarrée sans tension appliquée supplémentaire. Lorsque la production d'électricité était stable, l'ADN total et les protéines ont été extraits et séquencés. L'approche couplée métaprotéomique/métagénomique montre que lorsqu'une tension était appliquée pendant l'étape de colonisation, un transfert direct d'électrons via les cytochromes C, était le mécanisme majeur détecté et principalement réalisé par *Geobacter sp.* Dans l'autre biopile, une plus grande diversité de bactéries, telles que *Pseudomonas* et *Aeromonas*, semble être impliquée dans la production d'électricité en utilisant le transfert d'électrons via des navettes redox de la famille des flavines

Abstract: Appendices 1

Microbial fuel cells (MFCs), as a potentially sustainable biotechnology, can mediate the direct conversion of organic matter from wastewater into electricity using bacterial biofilms as biocatalysts. One of the critical points in MFCs is to understand which electroactive bacteria (EAB) and which mechanisms are involved in the extracellular electron transfer to the anode. The goal of this study was to evaluate how an applied voltage between anode and cathode influences the anodic bacterial community structure and activity. Two MFCs were operated with an external resistance of 1000 ohms. One was submitted to an applied electrical voltage of 500 mV during the first four days of biofilm formation and the other was started without additional applied voltage. When the electricity production was stable, both total DNA and total protein were extracted and sequenced. The combined metaproteomic / metagenomic approach shows that when a voltage was applied during the colonization step, a direct electron transfer via cytochrome c was the major mechanism detected and mainly mediated by *Geobacter* sp. With the other MFC, a higher diversity of bacteria, such as *Pseudomonas* and *Aeromonas*, seemed to be involved in the electricity production using mediated electron transfer via flavin family members when no voltage was applied during the colonization step.

Metaproteomic and metagenomic coupled approach to investigate microbial response to electrochemical conditions in Microbial Fuel Cell

A1. INTRODUCTION

Microbial fuel cells (MFCs) have been recognized as a potentially sustainable biotechnology that involves the direct conversion of organic matter from wastewater into electricity using bacterial biofilms as biocatalysts [1]–[3]. Electroactive bacteria (EAB) use organic matter as electron donors and are capable of extracellular electron transfer to the anode. Over the last 10 years, reported MFC power densities have increased up to 6.9 W per m^2 of anode [4]. Currently, one of the critical steps in MFCs start-up is the initial colonization of the anode by EABs as this step affects the bacterial community structure of the mature biofilm, and thus, the overall electron transfer rate. In order to control this step, a better understanding of the EAB community involved in the extracellular electron transfer and the mechanisms used by these bacteria to transfer their electrons is needed. Many bacteria use redox shuttles such as Flavin- (*Shewanella*) or phenazine- (*Pseudomonas*) type molecules. Another mechanism is a direct electron transfer via c-type cytochrome as in *Clostridium*, *Geobacter* or *Shewanella* [5], [6]. The electrons can be transferred directly from c-type cytochrome to the anode or through nanowires as in *Geobacter* or *Shewanella* [6].

Different methods have been proposed to favor the development of EABs on the anode. Different substrates have been tested to see if some bacteria could be preferentially selected on the anode and several studies have shown that the addition of acetate favors the growth of *Geobacter* [7], [8]. This use of acetate selects the acetotroph bacteria *Geobacter*, which is an electroactive bacterium and, thus, leads to an increased electricity production. However, the chemical nature of the electron donor might not be the only parameter that affects the selection of bacteria in MFCs. Electrical and electrochemical parameters might play major roles in selecting the type and level of anodic respiration. Two electrochemical parameters have been extensively studied: the electrochemical anodic potential and the external resistance. Some studies have shown the influence of the anodic potential on microbial community structure and electrical performances of MFCs [9]–[13]. Wang *et al.* [12] reported that the MFC start-up could be accelerated by the application of an anode potential of 200mV (vs Ag/AgCl), but the bacterial community analysis was not performed. In addition, Wei *et al.* [13] showed that a positive anode potential (vs Ag/AgCl) decreased the start-up time and increased the current generation for *G. sulfurreducens*. On the other hand, Alterman *et al.* [9] reported that a negative anode potential (-200mV vs Ag/AgCl) improved current

generation and did not influence the start-up time. Torres *et al.* [11] reported that a negative anode potential selected *Geobacter* and that a positive anode potential produced a diverse bacterial community. The external resistance also appears to have an impact on electrical performance and the selected bacterial communities. Alterman *et al*. [14] and Zhang *et al*. [15] concluded that the external resistance needed to be the lowest possible but close to the internal resistance to produce a better power density. Lyon *et al.* [16] reported that differences in the external resistance induced different bacterial communities on the anode. While the influence of electrochemical anodic potential and the external resistance have been widely studied, other parameters such as the potential between anode and cathode have not been studied. The potential between the anode and the cathode should influence the anodic bacterial community of the MFC by creating an electromotive force during start-up, and thus, this potential should favor the movement of microorganisms to the anode. Therefore, the voltage between anode and cathode might modify the taxonomic and functional characteristics of the anodic biofilm. Environmental EABs belong to diverse taxononomic groups such as Firmicutes (*Clostridium*), Betaproteobacteria (*Rhodoferax*), Deltaproteobacteria (*Geobacter*), Epsilonproteobacteria (*Arcobacter*), or Gammaproteobacteria (*Shewanella*) [5], [17]–[21]. The MFCs with a high relative abundance of *Geobacter* often have the best electrical performances [22]. However, mixed-cultures often generated higher power than pure cultures. Recently, some studies have investigated the taxonomic diversity and structure of mixed-species anodic biofilms [22]–[29]. The major taxa varied from one study to another as Deltaproteobacteria [27], [28], Betaproteobacteria [22], and Bacteroidetes [25] were all observed to be the major bacteria present. Stratford *et al.* [26] investigated the relation between different parameters of diversity and power production. They showed that the Shannon index (representative of richness and evenness) was positively correlated with power production. In other studies, MFCs with higher power production had lower Shannon indices [27]. One of the rare studies that described the potential functional capabilities of microorganisms in the anodic biofilm was done recently with metagenomic data annotated sequences to genes known for enzymes potentially involved in the extracellular electron transfer [30]. Unfortunately, the presence of these genes represents only the microbial potential and not their activity. A functional analysis based on both metaproteomics and metagenomics would provide both. Metaproteomics has been recognized as a promising method to access bacterial ecosystem function [31]. Leary *et al.* used metaproteomics to investigate the impact of the cathodic electrochemical potential on gene expression in the cathodic biofilm [32]. To our knowledge, studies applying metaproteomics to anodic biofilms have not been reported. The goal of this study was to investigate how an applied voltage between anode and cathode influences the bacterial community structure and activity using a combined metaproteomics / metagenomics approach.

A2. MATERIALS AND METHODS

A2.1. MFC setting up

Single-chamber batch MFCs in 250mL Wheaton bottles were set up in the laboratory at ambient (24°C) temperature. The anode consisted of two 3 x 5 cm pieces of carbon cloth. The cathode consisted of carbon cloth (designation B) 2.5 cm in diameter. It was prepared with PTFE coating and 5 % platinum catalyst as described by Cheng *et al*. [33]. The MFCs were filled with 250mL of primary effluent from a domestic wastewater treatment plant (Lyon, France) and fed with 1g/L sodium acetate every 2 days. The anode and cathode were connected to a generator and were polarized with a direct current voltage of 0.5V. The voltage was applied for 4 days (MFC4d). After 4 days, the polarization in the MFC4d was stopped. The external circuit was closed with an external resistance of 1000 ohms. A classical MFC without initial polarization and with an external resistance of 1000 ohms was used as the control (CtrlMFC). The evolution of the voltage was measured every 30 min using Hewlett Packard 3456A Digital Voltmeter combined with Agilent 34970A Data acquisition/Switch Unit in both MFCs over 20 days.

A2.2. Polarization Curve Analysis and Cyclic Voltammetry

After the electricity production stabilized (after 17 days), the polarization curves of the MFCs were measured. A variable external resistance and voltmeter were used. The surface current was determined with the following equation (1)

$$I = \frac{U}{R}.\frac{1}{S} \quad (1)$$

where U is the voltage of the cell, R the external resistance and S the surface of the anode. The power density was calculated with the following equation (2)

$$P = UI \quad (2)$$

The cyclic voltammetry (CV) spectra of the anodes was performed with a potentiostat (Voltalab) using a three electrode arrangement consisting of the working electrode (anode), a saturated Ag/AgCl reference electrode, and a platinum wire serving as the counter electrode. The CV measurement scanned the potential range from -0.8 V to 1V vs Ag/AgCl with a rate of 10m V/s.

A2.3. **DNA extraction and Sequencing**

After 17 days, two 1 cm^2 pieces of anode were cut and placed into 1 mL 0.8 % sterile NaCl solution with 1 sterile ceramic bead (MP Biomedicals, Illkirch, France). The pieces of anode were then bead-beaten using a FastPrep machine (MP Biomedicals) at a speed of 6 m/s for 20s. Five hundred microliters of the suspension were used for total DNA extraction using a modified Genomic DNA from Tissue kit (Macherey-Nagel GmbH and Co. KG, Duren, Germany). The manufacturer's instructions were followed except that the pre-lysis incubation was performed by first incubating the centrifuged sample with 180 µL T1 and 25 µL of proteinase K for 5 min at room temperature, then vortexed and incubated for 10 min at 70°C. The reaction was stopped by exposing the tubes to 95°C for 5 min. The metagenomic DNA was sequenced with the 454 technology. The 16S ribosomal RNA gene amplicons were sequenced with the Illumina MiSeq System. The region V3-V4 of the 16S rRNA gene (*rrs*) was amplified by the forward primer 5' TCGTCGGCAGCGTCAGATGTGTATAAGAGACAGCCTACGGGNGGCWGCAG 3' and the reverse primer 5' GTCTCGTGGGCTCGGAGATGTGTATAAGAGACAGGACTACHVGGGTATCTAATCC 3' (amplicon size: 460bp).

A2.4. **Proteins Extraction and Sequencing**

Each cell pellet was lysed, denatured, and reduced in a solution of 6 M guanidine and 10 mM DTT in 50 mM Tris buffer (pH 7.6) and shaken overnight at 37°C. The solution was diluted 6-fold with 50 mM Tris buffer 10mM CaCl2 (pH 7.6), the proteins were digested into peptides with 1/100 (wt/wt) sequencing grade trypsin (Promega, Madison, WI) and the insoluble cellular material was removed by centrifugation (2000 g for 10 min). Peptides were desalted off-line by C18 solid phase extraction (Waters, Milford, MA), concentrated, filtered and aliquoted as previously described by Verberkmoes *et al.* [34]. Two-dimensional nano-LC MS/MS analysis of each sample was carried out on a LTQ-Orbitrap hybrid mass spectrometer (Thermo Fisher, San Jose, CA) as described elsewhere [19]. In brief, chromatographic separation of the tryptic peptides was conducted over a 22 hour period of increasing (0-500 mM) pulses of ammonium acetate followed by a 2 hr aqueous to organic solvent gradient. The LTQ was operated in a data-dependent manner as follows: MS/MS on top five ions detected in full scan, two microscans for both, full and MS/MS scans, centroid data for all scans, and dynamic exclusion set at 1.

Proteomic data for each sample can be found at the following links:

https://compbio.ornl.gov/mspipeline/vogel/dtaselect_Sample_Set_050208_Sample33_tryp_JMM_S33.html

https://compbio.ornl.gov/mspipeline/vogel/dtaselect_Sample_Set_050208_Sample35_tryp_C02_S35.html

Quantitative value for proteins sequences is reported in NSAF (normalized spectral abundance factor). The NSAF is based on spectral counts detected for peptides belonging to a given protein. A correction factor is applied to account for the higher probability of detecting a longer protein (due to it yielding more peptides) and is normalized to total spectral count for the run.

A2.5. **Sequence Analyses**

1. 16S Ribosomal RNA Gene Amplicon Sequence Analysis

The sequences were joined with Pandaseq [35] with a minimal overlap of 50bp and a final sequence length between 500 and 600bp. Then, the OTUs were defined arbitrarily at 97 % of identity with QIIME [36] using the pick – closed – reference.py script. The associated taxonomy was assigned using the Greengene database. The number of sequences for all the samples was adjusted to the same number of sequences of the smallest sample. The Shannon index was calculated on a pseudo-genus level by the following equation (3):

$$H' = -\sum p_i . ln(p_i) \quad (3)$$

where p_i is the proportion of the OTUi considered to belong exclusively to the annotated genus. The relative abundance of the major genus present in the samples was analyzed. Bacterial genus considerate as potential EABs were *Geobacter*, *Arcobacter*, *Desulfovibrio*, *Clostridium*, *Pseudomonas*, *Shewanella*, *Streptomyces*, *Bacillus*, *Aeromonas*, *Rhodoferax*, *Escherichia*.

2. Metagenomic and Metaproteomic Sequence Analysis

The metagenomic DNA sequences were assigned using the non-redundant protein (nr) database from NCBI using a BLASTx with Diamond software [37]. For the metaproteomic data analysis, only the proteins matching with the metagenomic sequences from the MFCs were kept. This step was done using R software [38] with the package seqinr [39]. The metaproteomic sequences were assigned with the database from each specific MFC using a BLASTp of Diamond software [37]. Only the matches with a percentage of identity higher than 40 % were kept. The best assignments were kept for each sequence. Then, the NSAF of sequences were added for each assignment. The results were analyzed with Megan software [8] and STAMP [40]. The gi map was used to analyze taxonomic structure. The SEED

classification with RefSeq map was used to analyze the functional genes. In order to study the relative abundance of genes and proteins involved in intracellular and extracellular electron transfer, data were also BLASTed against different functional-specific databases. The databases were created from the Bacteria RefSeq database of NCBI by research of key words. Five specific databases were created with proteins associated with cytochrome function, hydrogenase function, shuttles function, acetate function and adhesion function. The databases can be found at genomenviron.org. Only the matches with a percentage of identity higher than 40% were kept. The better assignment was kept for each sequence. Then, the number of sequences and the relative abundance for each assignment were calculated. In order to study the functional diversity, a Shannon index was calculated using RefSeq protein identifier as the unit for metagenomic and metaproteomic data.

A3. RESULTS

A3.1. Effect of the Applied Voltage on Electricity Production

The exponential phase of the electrical current production started within one day after the applied voltage was stopped in MFC4d (Fig. 1), so after 4.5 days total time. On the other hand, the exponential phase started after 8 days from the start-up point for the control MFC (CtrlMFC). The MFC4d also had a higher voltage (50% greater than the control) after reaching the stationary phase (between 450 and 500mV) than the CtrlMFC, which had a maximum voltage of about 340mV. The applied voltage for 4 days appeared to decrease the latency phase and increase the voltage of the stationary phase. The maximal power for MFC4d and CtrlMFC was 38.2 and 29.5 mW/m^2 with a density current of 150.0 and 134 mA/m^2 and an open circuit voltage of 545 and 554mV, respectively (Supplementary Data Fig. S1). Despite the fact that MFC4d had a higher voltage, the maximum power density was similar to that for the CtrlMFC. For both MFCs, the cyclic voltammetry spectrum from each MFC showed one unique peak of oxidation (Supplementary Data Fig. S2). The peak was

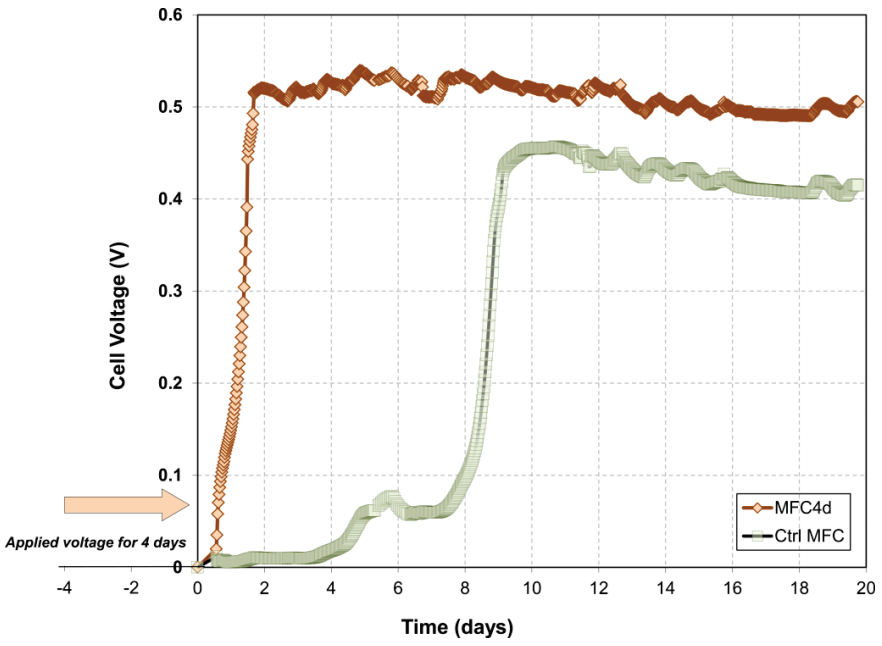

Figure.1. Evolution of the microbial fuel cell voltage as a function of time after the applied voltage (MFC4d) and without preceding phase of applied voltage (CtrlMFC). The external resistance was set at 1000 Ohms.

observed at 300mV vs Ag/AgCl for MFC4d and at 450mV vs Ag/AgCl for CtrlMFC. This difference might explain in part the difference in the voltage between theMFCs.

A3.2. **Bacterial Composition of Biofilms**

The 16S ribosomal gene (*rrs*) sequences of V3-V4 region were annotated to determine the bacterial community structure (Fig. 2). There were 122 834 sequences for the CtrlMFC (sequence length: 457.07 +/- 11.14 bp; 59.18 % annotated), and 52 901 for the MFC4d (sequence length: 463.30 +/-6.55 bp, 59.61 % annotated). The number of observed OTUs was respectively of 289 and 316. However, the Shannon index was higher for the CtrlMFC than for the MFC4d (2.38 and 1.84, respectively). The major taxa in the CtrlMFC were Epsilonproteobacteria (30.24%), which was 100% *Arcobacter*; Deltaproteobacteria (18.64%), which was 98.50% *Geobacter*; Betaproteobacteria (15.38%); Gammaproteobacteria (13.24%); and Flavobacteria (13.16 %). Some minor taxa included Bacteroidia (3.82%), Alphaproteobacteria (2.35%) and Clostridia (2.67%). For the MFC4d, the *Geobacter* genus itself was the highest abundant taxon (58.86%). The other major taxa

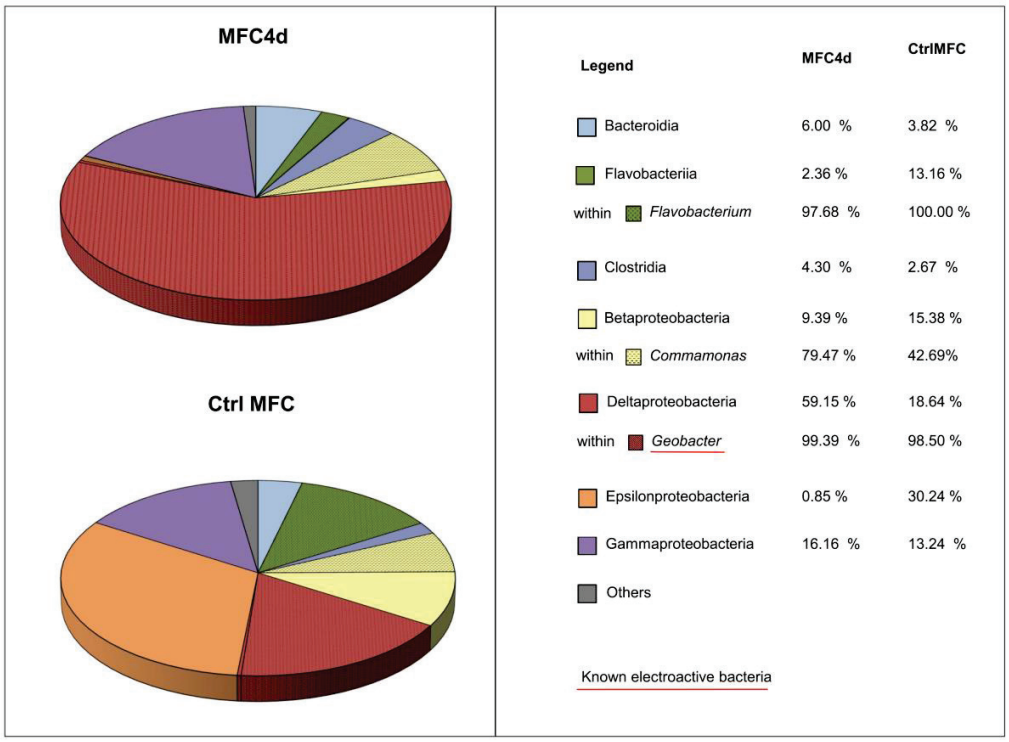

Figure 2. Bacterial community structure. The relative abundance of major classes and genus are represented for CtrlMFC and MFC4d samples

were Gammaproteobacteria (16.16%), Betaproteobacteria (9.39%), Bacteroidia (6.00%) and Clostridia (4.30%). However, Flavobacteria represented only 2.36%. The relative abundance of total putative electroactive bacteria (EAB) was 69.0% in MFC4d and 56.6% in CtrlMFC. The development of *Geobacter* on the anode appears to have been favored in MFC4d by the application of a voltage during the colonization step. *Geobacter* appeared to be the major genus responsible for electricity production in the MFC4d. However, in the CtrlMFC, *Arcobacter* seemed to be the major genus putatively responsible for electricity production.

A3.3. **Comparison of Functional Gene Expression**

DNA extracted from CtrlMFC and MFC4d samples were sequenced by pyrosequencing and proteins extracted for both CtrlMFC and MFC4d were sequenced by LC-MS-MS. The number of DNA sequences was 251 718 (sequence length: 239.79 +/- 37.30 bp) and 201 041 (sequence length: 239.42 +/- 41.57 bp), respectively. The number of unique peptide sequences (with variable abundances) was 3443 (sequence length: 77.08 +/- 12.06 aa) and 2348 (sequence length: 77.54 +/- 13.22 aa), respectively (Supplementary Data Fig. S3). These metagenomic and metaproteomic sequences were BLASTed against the non-redundant protein database from NCBI and analyzed with Megan and STAMP software (Supplementary Data Fig. S4 and Table S1). Then, the electron transfer function was more effectively targeted by BLASTing metagenomic and metaproteomic data against specific databases (Fig. 3, 4 and 5) (the data are available at www.genomenviron.org). Hydrogenases

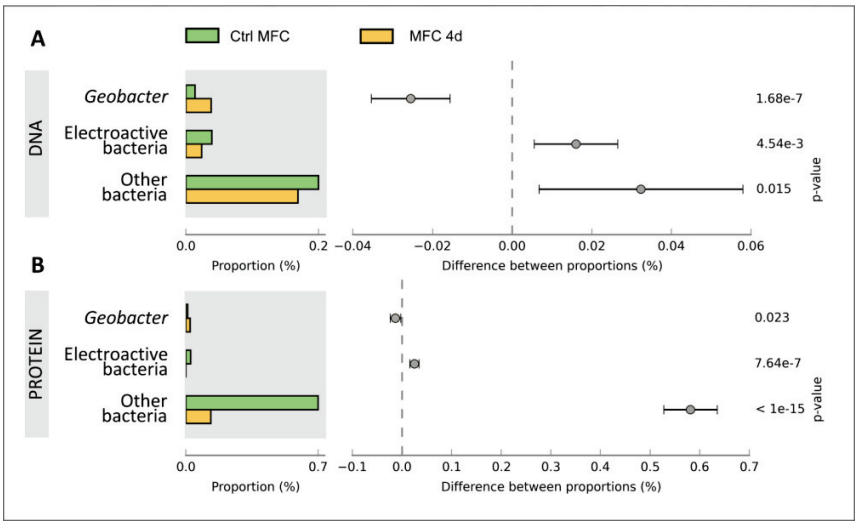

Figure.3. Acetate uptake function in microbial fuel cell communities. Proportion of sequences annotated as acetate uptake and difference between proportion of CtrlMFC and MFC4d in Panel A: metagenomic data and Panel B: metaproteomic data. Error bars are the 95 % confidence intervals and were calculated with STAMP software.

and proteins associated with acetate and linked to electron donors and cytochrome c oxidase were the proteins involved putatively in direct electron transfer mechanisms. *Geobacter* proteins were more abundant in MFC4d than CtrlMFC for each of these functions. In addition, about 95% of cytochrome c oxidases identified in MFC4d were assigned to *Geobacter* (only 18% of cytochrome c oxidases in CtrlMFC were assigned to *Geobacter*). This result implicated *Geobacter* as a major player in the electron transfer in MFC4d. Overall acetate uptake proteins were lower in the MFC4d than in the CtrlMFC. Since the hydrogenase proteins were higher in the MFC4d, acetate might not have been as important a source of electrons as hydrogen for the dominant *Geobacter* in the MFC4d.

To explore which bacteria might be involved in the electricity production in the CtrlMFC, the functions associated with other EABs were evaluated. The EAB include members of the genus *Bacillus*, *Pseudomonas*, *Shewanella*, *Desulfovibrio*, *Aeromonas*, *Arcobacter*, *Streptomyces*, *Clostridium*, and *Rhodoferax*. Although there was three times more cytochrome c oxidase from EABs in the CtrlMFC than from those in the MFC4d, the relative abundance of these proteins was still relatively low. Since many EABs use shuttles to transfer their electrons to the anode, the relative abundance of proteins and genes associated with shuttle production was evaluated (Fig. 6). The relative abundance of the genetic sequences associated with electron shuttle production were approximately the same for both MFCs. However, the relative abundance of proteins associated with electron transfer shuttles was four-times higher in the CtrlMFC than in the MFC4d (0.0056 and 0.0014, respectively). The

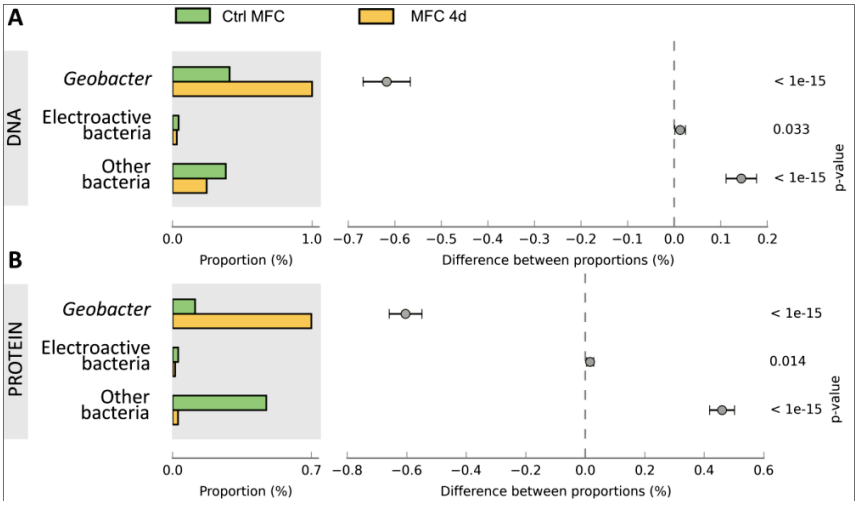

Figure 4. Cytochrome c oxidase function in microbial fuel cell communities. Proportion of sequences annotated as cytochrome c and difference between proportion of CtrlMFC and MFC4d in Panel A: metagenomic data and Panel B: metaproteomic data. Error bars are the 95 % confidence intervals and were calculated with STAMP sofware.

relative abundance of proteins associated with FMN (FlavoMonoNucleotide) was also higher in the CtrlMFC than in the MFC4d (0.0014 and 0.0001, respectively). In the CtrlMFC, about 87% of these proteins were assigned to *Pseudomonas* and 13% to Bacillus. The proteins annotated as flavins were not detected in the MFC4d and their relative abundance was 0.0014 in the CtrlMFC. All flavins were assigned to *Pseudomonas* and identified as flavin reductases. Flavoproteins were the most abundant proteins in the CtrlMFC (0.020) and were assigned to *Streptomyces*. Finally, the relative abundance of proteins associated with riboflavins was 0.0050 in the CtrlMFC and 0.0003 in the MFC4d. In the CtrlMFC, riboflavin proteins were identified as riboflavin biosynthase and assigned to *Aeromonas*. So, the electricity production in the CtrlMFC seemed to be the result of redox mediators belonging to a more diverse bacterial community than those in the MFC4d.

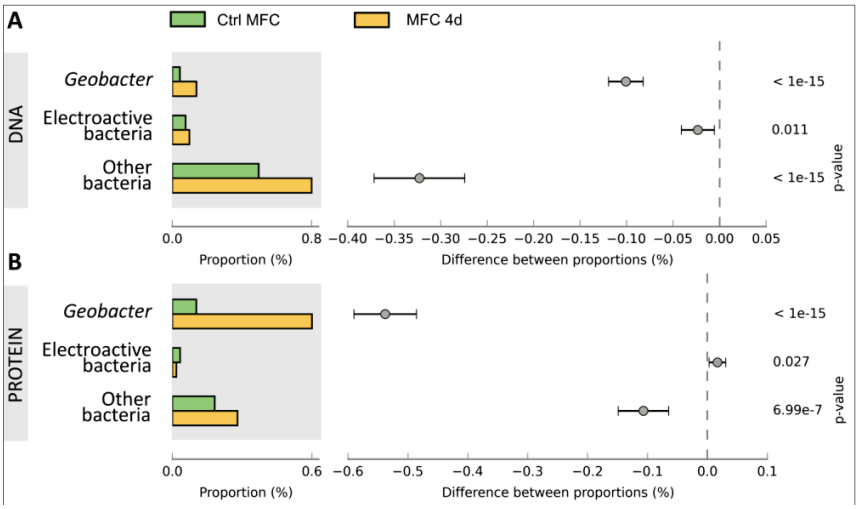

Figure.5. Hydrogenase function in microbial fuel cell communities. Proportion of sequences annotated as hydrogenase and difference between proportion of CtrlMFC and MFC4d in Panel A: metagenomic data and Panel B :metaproteomic data. Error bars are the 95 % confidence intervals and were calculated with STAMP software.

In order to evaluate the impact of the applied voltage on functional diversity and selection pressure, the Shannon index was calculated using the RefSeq protein identifier (Table 1). The Shannon index was similar for cytochrome c oxidase, hydrogenase and acetate functions at the gene level. However, the Shannon index was lower for these functions in MFC4d than in the CtrlMFC at the protein level. So, the applied voltage appeared to increase the production of more specific proteins for these functions in the MFC4d. On the other hand, the Shannon index was higher in the CtrlMFC than in the MFC4d at both the gene and protein level for the electron shuttle function. Thus, the protein diversity was different between MFC4d and CtrlMFC (Fig. S1).

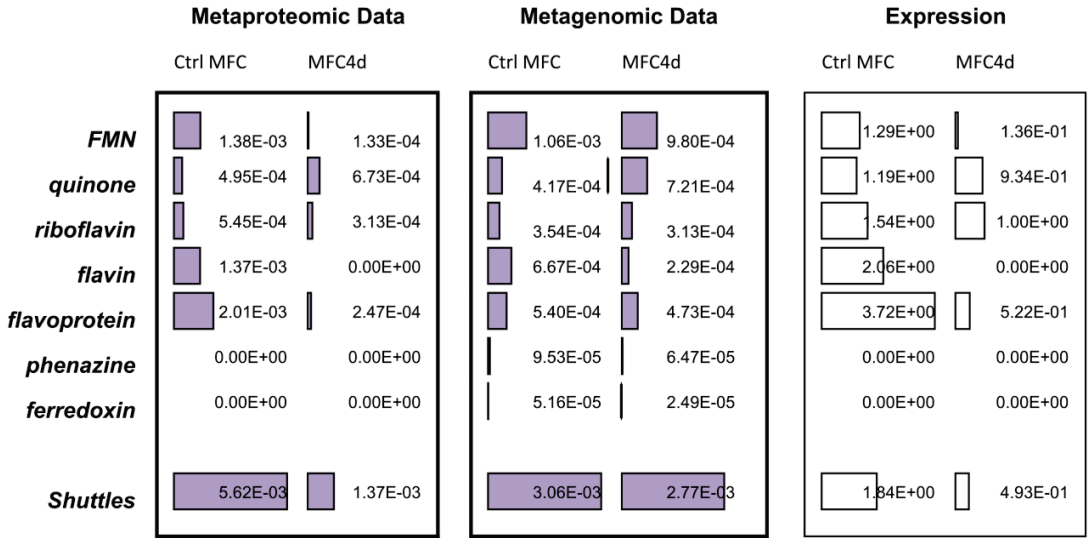

Figure 6. Shuttles Function. The relative abundance of functional gene and proteins is represented by the bar graph with the corresponding values for Ctrl MFC and MFC4d samples.

	Metaproteomic Data		Metagenomic Data	
Functions	Crtl MFC	MFC 4d	Crtl MFC	MFC 4d
Cytochrome c oxidase	2.575	1.602	5.836	5.277
Hydrogenase	2.457	1.944	5.517	5.439
Function associated to acetate	2.862	1.661	4.613	4.477
Shuttles	3.310	2.656	6.125	5.453

Table.1. Functional diversity. Shannon index calculated with individual enzyme for Ctrl MFC and MFC4d samples and for metaproteomic and metagenomic data.

A4. DISCUSSION

A4.1. Electron transfer mechanisms in the biofilms

The apparent mechanisms for electron transfer in both biofilms were different. In the MFC4d, the high abundance of *Geobacter* and *Geobacter* proteins annotated as cytochrome c is consistent with *Geobacter* as the major bacteria responsible for the observed electricity production. *Geobacter* is known to use a direct electron transfer via the cytochrome c [6]. In addition, the low relative abundance of proteins associated with electron shuttles was interpreted as an indication that this mechanism of electron transfer was not the primary one responsible for electricity production in the MFC4d. So, the direct electron transfer was probably the mechanism driving electricity production in the MFC4d. *Geobacter* is able to produce nanowires, but the protein PilA involved in the nanowires formation were not observed in either MFCs (Supplementary data, Fig. S5). This lack of detection should not be due to the detection limit as *Geobacter* was abundant in the MFC4d and nanowires are composed of many PilA proteins. *Geobacter* can (and in this case might have) transfer their electrons directly from cytochrome c to the anode and not via nanowires.

In the CtrlMFC, the production of proteins associated with redox shuttles was higher than in the MFC4d. There was a relatively high abundance of FMN reductases and of flavin reductases from Pseudomonas. Pseudomonas has been reported to transfer their electrons via shuttles, but the reported shuttles were phenazines [21], which were not detected in either sample. On the other hand, Pseudomonas might have played a key role in the electricity production using flavin family proteins to transfer their electrons in the CtrlMFC. The presence of riboflavin biosynthase protein from Aeromonas in the CtrlMFC indicated that Aeromonas might have also participated in the electron transfer via flavin family. Aeromonas is known to be an EAB. The formulated hypothesis for the mechanism for the electron transfer was cytochrome c, but no experiment has shown that yet [20]. The role of flavoprotein reductases from Streptomyces is more debatable. Streptomyces is capable of electricity production [41], but the electron transfer mechanism is unknown. Flavoprotein reductases are involved in its respiratory chain, but the role of flavoproteins in the extracellular electron transfer has not been established for Streptomyces. Streptomyces was active based on the protein analysis and might be involved in the electricity production in the CtrlMFC. While cytochrome c is an important enzyme involved in extracellular electron transfer, few of these proteins associated with Geobacter were observed in the CtrlMFC. The resulting conclusion that Geobacter is relatively inactive in the CtrlMFC is further supported

by the lower expression of cytochrome and hydrogenase genes in the CtrlMFC than in the MFC4d. About 47% of cytochrome c proteins in the CtrlMFC were from Acidovorax. Acidovorax was found in several samples from anodic [42] and cathodic biofilms [43]. So these bacteria might play a role in the electron transfer.

A4.2. **Taxonomic and Functional Diversity in Microbial biofilm**

The impact of the applied voltage on taxonomic and functional diversity was evaluated by calculating the Shannon index. The Shannon index was chosen because this index includes both richness and evenness. Stratford *et al*. reported that the Shannon index was the best correlation between taxa and power density in MFC [26]; the power density was higher when the taxonomic diversity was higher. Unlike Stratford *et al*., Sun *et al*. observed that MFCs with higher power density had lower taxonomic diversity [27]. In our study, an imposed voltage for 4 days induced the selection of *Geobacter* in the anodic biofilm (59 % in the MFC4d and 18 % in the CtrlMFC) and reduced the diversity. The taxonomic diversity was much lower for the MFC that had the start-up phase with the voltage applied (Shannon index: 1.84 for the MFC4d and 2.38 for the CtrlMFC) and much higher for the operating electrical production (500mV versus 340mV at 1000 Ohms). The measured maximum power density was the same for both system, but as this could be due to cathode limitations, the electricity production during normal operations was also determined. At the gene level, the functional diversity was relatively similar for cytochrome c oxidases, hydrogenase and acetate functions between the MFC4d and the CtrlMFC. This could be explain by the relatively high proportion of the *Geobacter* genus, which has a high relative diversity of cytochrome c oxidases and hydrogenases [44], [45]. For example, Butler *et al*. compared six genomes of *Geobacter* and reported that *Geobacter* has on average 76 genes coding for cytochromes. Contrary to the functional gene diversity, the protein diversity for cytochrome c oxidases, hydrogenases and acetate functions decreased in the MFC that had the voltage applied. The functional diversity for shuttle functions was higher at the gene and protein level in the CtrlMFC than in the MFC4d. Indeed, these functions are very common in bacteria but absent in the *Geobacter* genome(s) and are involved in other cellular processes than extracellular electron transfer, such as quorum sensing. This bacterial communication can control different process as biofilm formation [46], [47]. The start-up applied voltage appeared to induce the production of more specific proteins for the electron transfer activity and to select for the *Geobacter* genus and the production of more specific proteins for the extracellular electron transfer.

A4.3. **Effects of the Applied Voltage on *Geobacter* selection**

We showed that an applied voltage between anode and cathode during the colonization step influenced the bacterial communities that grew on the anode. The functional expression and the electron transfer mechanisms were different, too. In addition, an applied voltage decreased the time of the start-up phase. One hypothesis is that the imposed voltage favored the activity of anodic respiration of *Geobacter* by the presence of electromotive force during the start-up phase. To study if the metabolic regulation of *Geobacter* was different in the CtrlMFC and MFC4d MFCs, the ratio of the relative abundance of proteins to the relative abundance of the corresponding gene was calculated (Fig.7). The expression of cytochrome c was higher in the MFC4d than in the CtrlMFC (0.69 and 0.27, respectively). This ratio for hydrogenase was also higher in the MFC4d than in the CtrlMFC (4.43 and 2.43, respectively). Therefore, the applied voltage increased the long-term (after the voltage was stopped) electron transfer gene expression of *Geobacter*. *Geobacter* cannot use a large diversity of soluble electron acceptors contrary to other EABs, such as *Shewanella*. Initially in CtrlMFC, there was no electromotive force. Therefore, the first bacteria on the anode could not use anodic respiration to grow and might have used soluble electron acceptors. Over time, the voltage of MFC increased and an electromotive force might have been created and favored anodic respiration in the control. This could explain the higher diversity of bacteria in CtrlMFC with less specific adaptation to extracellular electron transfer than *Geobacter*. More experiments studying the impact of soluble electron acceptors on anodic bacterial community development are needed. In the MFC4d, an electromotive

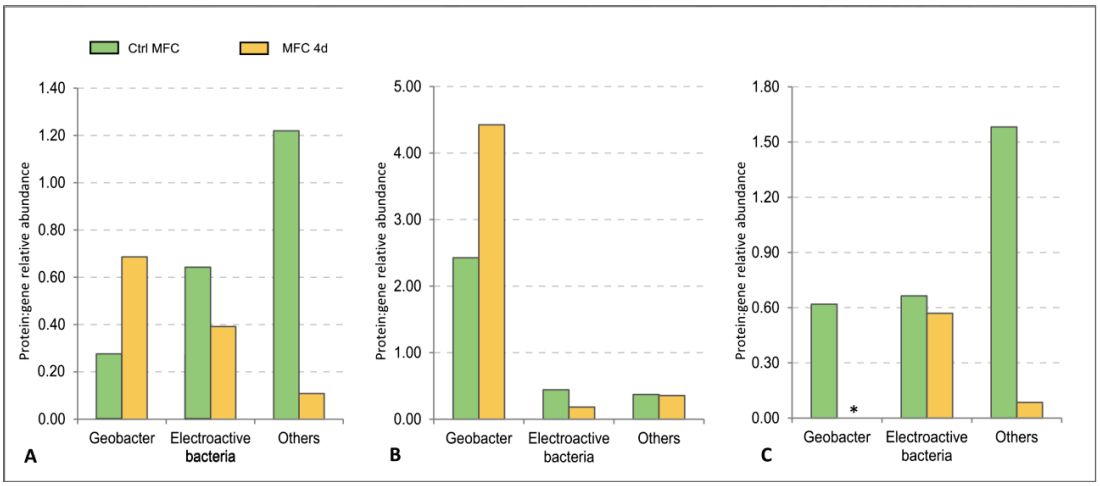

Figure 7. Ratio of relative abundance of proteins to genes for different functions A: cytochrome oxidase, B: hydrogenase, C: acetate uptake.

force probably favored the electron transfer on the anodic surface. So, the growth of *Geobacter* was possible earlier. The competitivity of *Geobacter* might have been better than other EABs in the MFC4d for two reasons. First, the choice of acetate as substrate favored acetotroph bacteria such as *Geobacter*. Secondly, *Geobacter* might be more competitive using a direct electron transfer that involved less energetic losses during the extracellular electron transfer than bacteria that use shuttle mediated electron transfer [48].

A4.4. **Advantages and Limits of Metaproteomic Analysis**

The metaproteomic approach appeared to evaluate the microbial community activity better than just metagenomic approaches. We use it to answer the question who does what in a microbial ecosystem [31], [32]. The LC/MS/MS approach has a higher sensitivity for the detection and identification of proteins than the 2D-page analysis [49]. However, the number of identified sequences is much lower than the number of sequences in the metagenomic dataset. So, the comparison of the metagenomic and metaproteomic data was limited. In this study, we compared the protein relative abundance versus gene relative abundance as an indicator of gene expression, but this comparison cannot be considered as a direct measurement of gene expression. In addition, the protein annotation process is more complex than that for the metagenomic database and by consequence, generic metagenomic databases cannot be used for assigning proteins. By annotating proteins on the same samples' metagenomic dataset, errors of identification can be reduced [31]. In spite of that, the more complex an environmental sample is, the less robust the identification is. MFCs have lower diversity than some environments, such as soils, and therefore, provide favorable conditions to investigate functional expression and to link function and taxonomy in microbial ecosystem. However, one of the difficulties in investigating the functional expression of electron transfer in MFCs is the ubiquity of the functions themselves.

Supporting Information

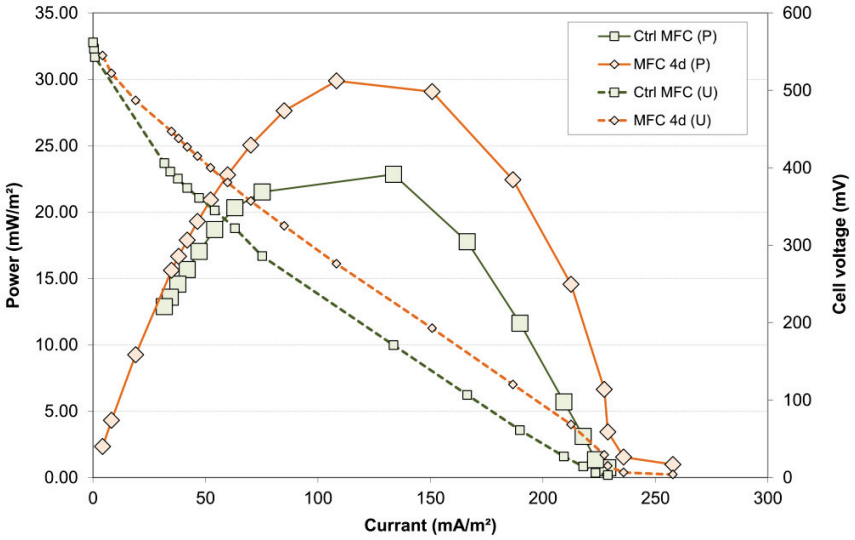

Figure S1. Polarization curves and power density.

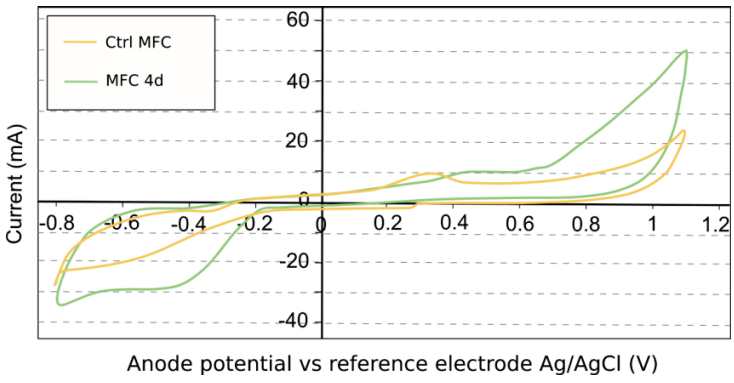

Figure S2. Cyclic Voltametry curves. CVs of MFC4d and Ctrl MFC

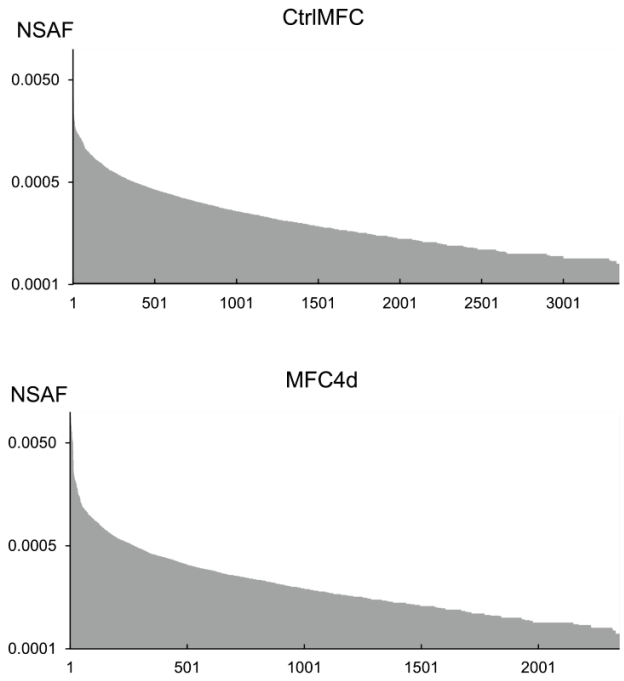

Figure S3. Normalized spectral abundance factor (NSAF) for each protein sequence in A: MFC4d and B: CtrlMFC

		Samples		non_redundant		acetate	
		nb_seq	filtred	nb_seq _db	%seq	nb_seq _db	%seq
DNA	Ctrl MFC	251718	-	96063464	82.48%	12168	0.26%
	MFC 4d	201041	-	96063464	77.49%	12168	0.24%
Protein	Ctrl MFC	112308	3522	96063464	99.36%	198	0.76%
	MFC 4d	104383	3232	96063464	97.74%	161	0.16%

		hydrogenase		cytochrome		pili	
		nb_seq _db	%seq	nb_seq _db	%seq	nb_seq _db	%seq
DNA	Ctrl MFC	60977	2.08%	351535	5.96%	115382	3.20%
	MFC 4d	60977	2.64%	351535	5.90%	115382	3.10%
Protein	Ctrl MFC	1001	0.35%	3953	1.33%	1543	0.32%
	MFC 4d	954	0.98%	2649	1.48%	1159	0.24%

Table S1. Functional Gene Structure. The relative abundance of functional gene and the difference between proportion are represented for Ctrl MFC and MFC4d samples in function of SEED classification. The error bar are the 95 % confidence interval and were calculated with STAMP software.

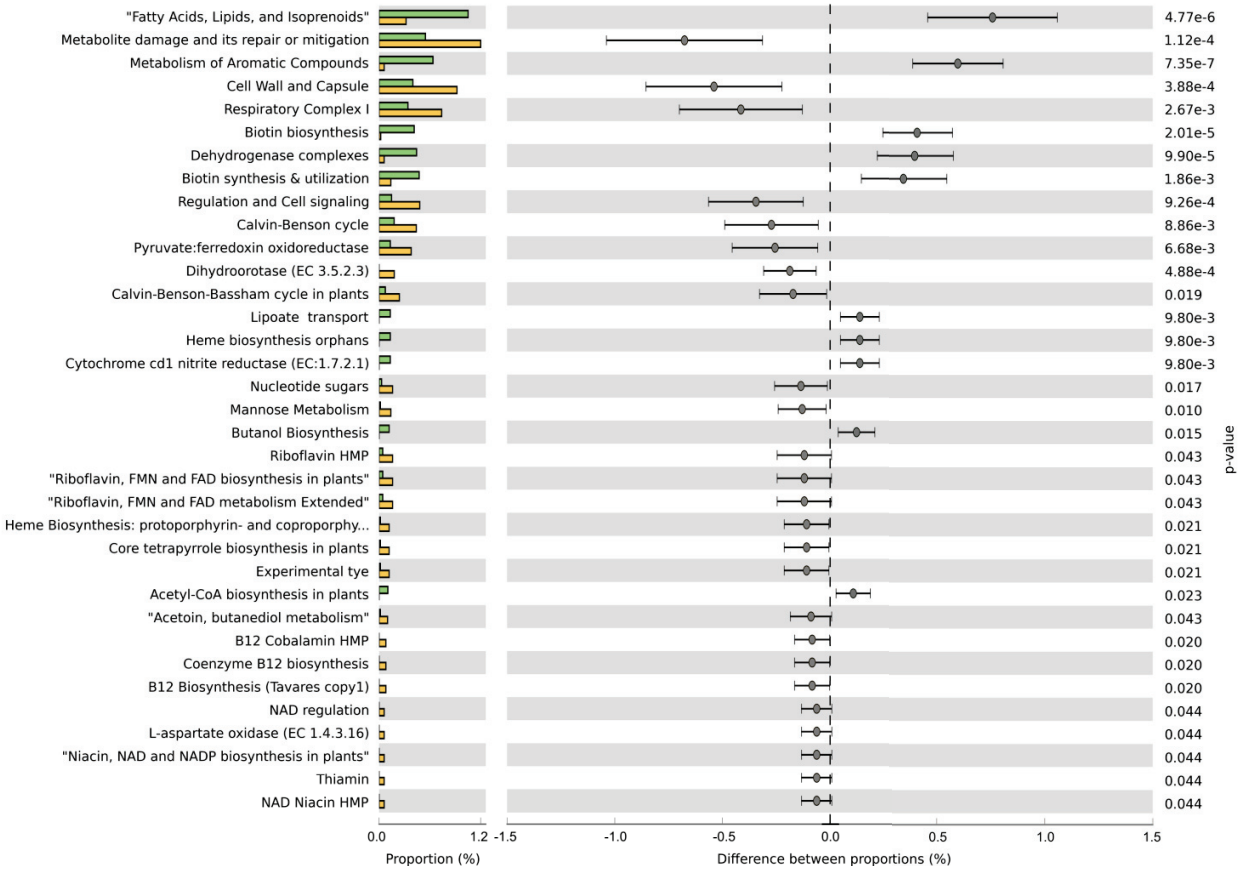

Figure S4. Functional Proteins Structure. The relative abundance of proteins and the difference between proportion are represented for Ctrl MFC and MFC4d samples in function of SEED classification. The error bar are the 95 % confidence interval and were calculated with STAMP software.

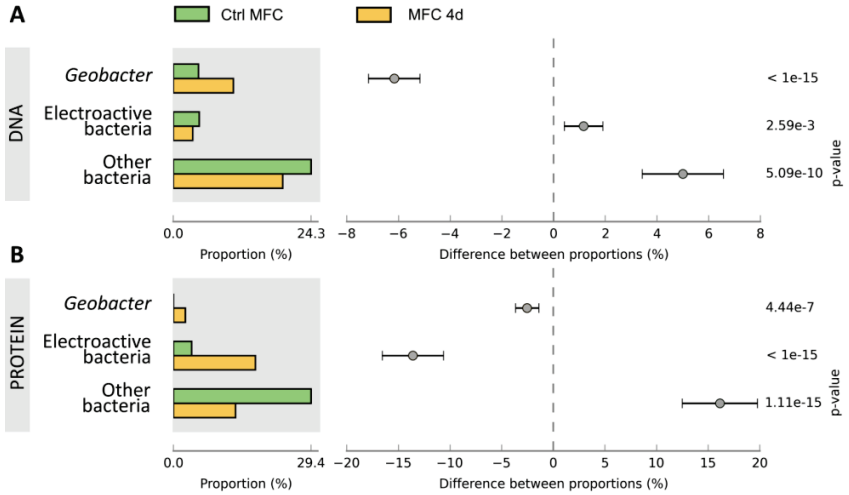

Figure S5. Pili function in microbial fuel cell communities. Proportion of sequences annotated as pili and difference between proportion of CtrlMFC and MFC4d in A:metagenomic data and B:metaproteomic data. Error bars are the 95 % confidence interval and were calculated with STAMP software.

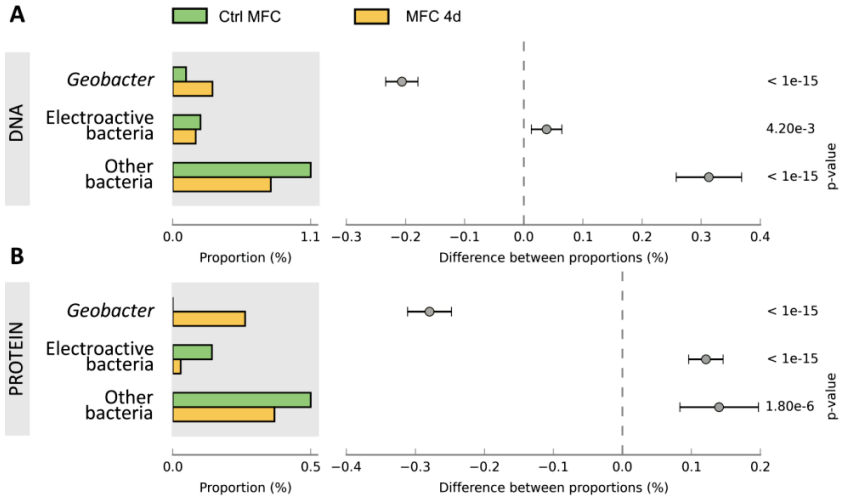

Figure S6. Cytochrome function in microbial fuel cell communities. Proportion of sequences annotated as cytochrome c and difference between proportion of CtrlMFC and MFC4d in A:metagenomic data and B:metaproteomic data. Error bars are the 95 % confidence interval and were calculated with STAMP software.

References

[1] K. Rabaey and W. Verstraete, “Microbial fuel cells: novel biotechnology for energy generation,” *Trends in Biotechnology*, vol. 23, no. 6, pp. 291–298, Jun. 2005.

[2] Z. Du, H. Li, and T. Gu, “A state of the art review on microbial fuel cells: A promising technology for wastewater treatment and bioenergy,” *Biotechnology Advances*, vol. 25, no. 5, pp. 464–482, Sep. 2007.

[3] B. E. Logan *et al.*, “Microbial Fuel Cells: Methodology and Technology†,” *Environ. Sci. Technol.*, vol. 40, no. 17, pp. 5181–5192, Sep. 2006.

[4] B. E. Logan, “Exoelectrogenic bacteria that power microbial fuel cells,” *Nat Rev Micro*, vol. 7, no. 5, pp. 375–381, May 2009.

[5] H. S. Park *et al.*, “A Novel Electrochemically Active and Fe(III)-reducing Bacterium Phylogenetically Related to Clostridium butyricum Isolated from a Microbial Fuel Cell,” *Anaerobe*, vol. 7, no. 6, pp. 297–306, Dec. 2001.

[6] Y. A. Gorby *et al.*, “Electrically conductive bacterial nanowires produced by Shewanella oneidensis strain MR-1 and other microorganisms,” *Proceedings of the National Academy of Sciences*, vol. 103, no. 30, pp. 11358–11363, 2006.

[7] K.-J. Chae, M.-J. Choi, J.-W. Lee, K.-Y. Kim, and I. S. Kim, “Effect of different substrates on the performance, bacterial diversity, and bacterial viability in microbial fuel cells,” *Bioresource Technology*, vol. 100, no. 14, pp. 3518–3525, Jul. 2009.

[8] D. H. Huson *et al.*, “MEGAN Community Edition - Interactive Exploration and Analysis of Large-Scale Microbiome Sequencing Data,” *PLOS Computational Biology*, vol. 12, no. 6, p. e1004957, Jun. 2016.

[9] P. Aelterman, S. Freguia, J. Keller, W. Verstraete, and K. Rabaey, “The anode potential regulates bacterial activity in microbial fuel cells,” *Applied Microbiology and Biotechnology*, vol. 78, no. 3, pp. 409–418, Mar. 2008.

[10] D. A. Finkelstein, L. M. Tender, and J. G. Zeikus, “Effect of Electrode Potential on Electrode-Reducing Microbiota,” *Environ. Sci. Technol.*, vol. 40, no. 22, pp. 6990–6995, Nov. 2006.

[11] C. I. Torres *et al.*, “Selecting Anode-Respiring Bacteria Based on Anode Potential: Phylogenetic, Electrochemical, and Microscopic Characterization,” *Environ. Sci. Technol.*, vol. 43, no. 24, pp. 9519–9524, Dec. 2009.

[12] X. Wang *et al.*, “Accelerated start-up of two-chambered microbial fuel cells: Effect of anodic positive poised potential,” *Electrochimica Acta*, vol. 54, no. 3, pp. 1109–1114, Jan. 2009.

[13] J. Wei, P. Liang, X. Cao, and X. Huang, “A New Insight into Potential Regulation on Growth and Power Generation of Geobacter sulfurreducens in Microbial Fuel Cells Based on Energy Viewpoint,” *Environ. Sci. Technol.*, vol. 44, no. 8, pp. 3187–3191, Apr. 2010.

[14] P. Aelterman, M. Versichele, M. Marzorati, N. Boon, and W. Verstraete, “Loading rate and external resistance control the electricity generation of microbial fuel cells with different three-dimensional anodes,” *Bioresource Technology*, vol. 99, no. 18, pp. 8895–8902, Dec. 2008.

[15] L. Zhang, X. Zhu, J. Li, Q. Liao, and D. Ye, “Biofilm formation and electricity generation of a microbial fuel cell started up under different external resistances,” *Journal of Power Sources*, vol. 196, no. 15, pp. 6029–6035, Aug. 2011.

[16] D. Y. Lyon, F. Buret, T. M. Vogel, and J.-M. Monier, “Is resistance futile? Changing external resistance does not improve microbial fuel cell performance,” *Bioelectrochemistry*, vol. 78, no. 1, pp. 2–7, Apr. 2010.

[17] V. Fedorovich, M. C. Knighton, E. Pagaling, F. B. Ward, A. Free, and I. Goryanin, “Novel Electrochemically Active Bacterium Phylogenetically Related to Arcobacter butzleri, Isolated from a Microbial Fuel Cell,” *Appl. Environ. Microbiol.*, vol. 75, no. 23, pp. 7326–7334, Jan. 2009.

[18] H. J. Kim, H. S. Park, M. S. Hyun, I. S. Chang, M. Kim, and B. H. Kim, “A mediator-less microbial fuel cell using a metal reducing bacterium, Shewanella putrefaciens,” *Enzyme and Microbial Technology*, vol. 30, no. 2, pp. 145–152, Feb. 2002.

[19] J. Niessen, U. Schröder, and F. Scholz, “Exploiting complex carbohydrates for microbial electricity generation – a bacterial fuel cell operating on starch,” *Electrochemistry Communications*, vol. 6, no. 9, pp. 955–958, Sep. 2004.

[20] C. A. Pham *et al.*, “A novel electrochemically active and Fe(III)-reducing bacterium phylogenetically related to Aeromonas hydrophila, isolated from a microbial fuel cell,” *FEMS Microbiology Letters*, vol. 223, no. 1, pp. 129–134, Jun. 2003.

[21] T. H. Pham, N. Boon, K. D. Maeyer, M. Höfte, K. Rabaey, and W. Verstraete, “Use of Pseudomonas species producing phenazine-based metabolites in the anodes of microbial fuel cells to improve electricity generation,” *Appl Microbiol Biotechnol*, vol. 80, no. 6, pp. 985–993, Aug. 2008.

[22] S. A. Patil *et al.*, “Electricity generation using chocolate industry wastewater and its treatment in activated sludge based microbial fuel cell and analysis of developed microbial community in the anode chamber,” *Bioresource Technology*, vol. 100, no. 21, pp. 5132–5139, Nov. 2009.

[23] A. S. Commault, G. Lear, and R. J. Weld, “Maintenance of Geobacter-dominated biofilms in microbial fuel cells treating synthetic wastewater,” *Bioelectrochemistry*, vol. 106, Part A, pp. 150–158, Dec. 2015.

[24] S. Jung and J. M. Regan, “Comparison of anode bacterial communities and performance in microbial fuel cells with different electron donors,” *Appl Microbiol Biotechnol*, vol. 77, no. 2, pp. 393–402, Nov. 2007.

[25] D. Ki, J. Park, J. Lee, and K. Yoo, “Microbial diversity and population dynamics of activated sludge microbial communities participating in electricity generation in microbial fuel cells,” *Water Science & Technology*, vol. 58, no. 11, p. 2195, Dec. 2008.

[26] J. P. Stratford, N. J. Beecroft, R. C. T. Slade, A. Grüning, and C. Avignone-Rossa, “Anodic microbial community diversity as a predictor of the power output of microbial fuel cells,” *Bioresource Technology*, vol. 156, pp. 84–91, Mar. 2014.

[27] Y. Sun, J. Wei, P. Liang, and X. Huang, “Electricity generation and microbial community changes in microbial fuel cells packed with different anodic materials,” *Bioresource Technology*, vol. 102, no. 23, pp. 10886–10891, Dec. 2011.

[28] M. D. Yates *et al.*, “Convergent development of anodic bacterial communities in microbial fuel cells,” *ISME J*, vol. 6, no. 11, pp. 2002–2013, Nov. 2012.

[29] A. Paitier, A. Godain, D. Lyon, N. Haddour, T. M. Vogel, and J.-M. Monier, “Microbial fuel cell anodic microbial population dynamics during MFC start-up,” *Biosensors and Bioelectronics*, vol. 92, no. Supplement C, pp. 357–363, Jun. 2017.

[30] L. Kiseleva *et al.*, “Taxonomic and functional metagenomic analysis of anodic communities in two pilot-scale microbial fuel cells treating different industrial wastewaters.,” *Journal of integrative bioinformatics*, vol. 12, no. 1, p. 273, 2015.

[31] P.-A. Maron, L. Ranjard, C. Mougel, and P. Lemanceau, “Metaproteomics: A New Approach for Studying Functional Microbial Ecology,” *Microb Ecol*, vol. 53, no. 3, pp. 486–493, Mar. 2007.

[32] D. H. Leary *et al.*, “Metaproteomic evidence of changes in protein expression following a change in electrode potential in a robust biocathode microbiome,” *Proteomics*, vol. 15, no. 20, pp. 3486–3496, Oct. 2015.

[33] S. Cheng and W. Liu, “How to make Cathodes with a diffusion layer for single-chamber microbial fule cells.” 2008.

[34] N. C. VerBerkmoes *et al.*, “Determination and Comparison of the Baseline Proteomes of the Versatile Microbe Rhodopseudomonas palustris under Its Major Metabolic States,” *J. Proteome Res.*, vol. 5, no. 2, pp. 287–298, Feb. 2006.

[35] A. P. Masella, A. K. Bartram, J. M. Truszkowski, D. G. Brown, and J. D. Neufeld, “PANDAseq: paired-end assembler for illumina sequences,” *BMC Bioinformatics*, vol. 13, p. 31, Feb. 2012.

[36] J. G. Caporaso *et al.*, “QIIME allows analysis of high-throughput community sequencing data,” *Nat Methods*, vol. 7, no. 5, pp. 335–336, May 2010.

[37] “Fast and sensitive protein alignment using DIAMOND | Nature Methods.” [Online]. Available: https://www.nature.com/articles/nmeth.3176. [Accessed: 21-Nov-2017].

[38] R Development Core Team, “R: A Language and Environment for Statistical Computing,” *R Foundation for Statistical Computing, Vienna, Austria*, 2008.

[39] D. Charif and J. R. Lobry, “SeqinR 1.0-2: A Contributed Package to the R Project for Statistical Computing Devoted to Biological Sequences Retrieval and Analysis,” in *Structural Approaches to Sequence Evolution*, Springer, Berlin, Heidelberg, 2007, pp. 207–232.

[40] D. H. Parks, G. W. Tyson, P. Hugenholtz, and R. G. Beiko, “STAMP: statistical analysis of taxonomic and functional profiles,” *Bioinformatics*, vol. 30, no. 21, pp. 3123–3124, Nov. 2014.

[41] S. H. A. Hassan, Y. S. Kim, and S.-E. Oh, “Power generation from cellulose using mixed and pure cultures of cellulose-degrading bacteria in a microbial fuel cell,” *Enzyme and Microbial Technology*, vol. 51, no. 5, pp. 269–273, Oct. 2012.

[42] A. P. Borole, C. Y. Hamilton, T. Vishnivetskaya, D. Leak, and C. Andras, “Improving power production in acetate-fed microbial fuel cells via enrichment of exoelectrogenic organisms in flow-through systems,” *Biochemical Engineering Journal*, vol. 48, no. 1, pp. 71–80, Dec. 2009.

[43] Y. Sun, J. Wei, P. Liang, and X. Huang, “Microbial community analysis in biocathode microbial fuel cells packed with different materials,” *AMB express*, vol. 2, no. 1, p. 21, 2012.

[44] J. E. Butler, N. D. Young, and D. R. Lovley, “Evolution of electron transfer out of the cell: comparative genomics of six Geobacter genomes,” *BMC Genomics*, vol. 11, p. 40, 2010.

[45] M. V. Coppi, “The hydrogenases of Geobacter sulfurreducens: a comparative genomic perspective,” *Microbiology*, vol. 151, no. 4, pp. 1239–1254, 2005.

[46] M. B. Miller and B. L. Bassler, “Quorum sensing in bacteria,” *Annual Reviews in Microbiology*, vol. 55, no. 1, pp. 165–199, 2001.

[47] C. M. Waters and B. L. Bassler, “Quorum sensing: cell-to-cell communication in bacteria,” *Annu. Rev. Cell Dev. Biol.*, vol. 21, pp. 319–346, 2005.

[48] C. I. Torres, A. K. Marcus, H.-S. Lee, P. Parameswaran, R. Krajmalnik-Brown, and B. E. Rittmann, “A kinetic perspective on extracellular electron transfer by anode-respiring bacteria,” *FEMS Microbiology Reviews*, vol. 34, no. 1, pp. 3–17, Jan. 2010.

[49] R. J. Ram *et al.*, “Community Proteomics of a Natural Microbial Biofilm,” *Science*, vol. 308, no. 5730, pp. 1915–1920, Jun. 2005.